Model Predictive Control with Performance-Driven Parameter Tuning using Bayesian Optimisation for Type-1 Diabetes

Hong Yang Lee

Master of Science Thesis

TU Delft Delft University of Technology

Delft Center for Systems and Control

Model Predictive Control with Performance-Driven Parameter Tuning using Bayesian Optimisation for Type-1 Diabetes

Master of Science Thesis

For the degree of Master of Science in Systems and Control at Delft University of Technology

Hong Yang Lee

August 26, 2024

Faculty of Mechanical Engineering (ME) · Delft University of Technology





Copyright © Delft Center for Systems and Control (DCSC)
All rights reserved.

Abstract

Over the years, the conventional open-loop *basal-bolus* regiment has proven to be inadequate for long-term glucose management of Type-1 diabetes mellitus (T1DM) patients. The 'artificial pancreas (AP)', which is characterized by a closed-loop control system that typically relies solely on subcutaneous glucose measurements as a feedback to deliver insulin corrections, is widely regarded as a viable alternative to the former approach. An earlier literature survey showed that model predictive control (MPC) and proportional-integral-derivative (PID) control are the two most commonly employed approaches in APs to treat T1DM, especially the former in recent years, due to its ability to incorporate flexible safety-critical constraints and account for inherent system delays. With most state-of-the art MPC controllers designed to exert direct control on insulin corrections over the patient however, the extent to which closed-loop performance can be maximised greatly depends on how accurately the plant is modelled. In addition to the immense difficulty in identifying certain physical parameters and non-linearities that describe an individual patient's insulin-glucose pharmacokinetics, practical challenges arising from the collection of open-loop data from the patient hinder the identification process of a prediction model. The resulting model-plant mismatch is detrimental to the closed-loop performance, especially during postprandial periods when hypoglycemic episodes are most likely to occur. As a countermeasure for the model-plant mismatch, insulin delivery rates are often tightly enforced, which may increase robustness of the MPC controller but comes at a price of reduced, sub-optimal performance due to worse-case conservative assumptions.

This thesis presents a dual-layer control scheme: a lower layer comprising of a control architecture that regulates the rate of insulin delivery for corrections against disturbances, and an upper layer that represents a performance-driven tuning framework using Bayesian Optimisation (BO). The proposed control architecture is hierarchical, consisting of an inner-loop PID controller and an MPC which serves as the outer-loop controller that governs the reference input signal to the inner-loop control system. The upper layer tuning framework is implemented in two stages, the first on a set of clinical-related parameters, and the second a controller and model parameter, as part of the individualized control objective. In both stages, the BO framework optimises the parameters via a daily query of one parameter set and its corre-

sponding performance value, which is computed based on experimental data. The proposed control scheme is designed and evaluated using a cohort of 10 adult virtual patients of the U.S. Food & Drug Administration (FDA)-accepted University of Virginia/Padova simulator through several *in silico* scenarios. Numerical evaluation and results show that the proposed hierarchical controller outperforms its baseline counterpart, and that glycaemic performance of all the tested subjects improved using the proposed tuning approach compared to under nominal settings. Notwithstanding the absence of a probabilistic safety-critical constraint in the BO problem, the employment of a barrier-like penalty in the objective function, subjected to a deterministic domain-based constraint that is augmented using a rule-based approach, demonstrated to be an efficient safeguard against hypoglycaemia during the parameter tuning process.

Table of Contents

Acknowledgements **ix**

1 Introduction **1**

1-1 Background and Motivation 1

1-2 Research Question and Objectives 2

1-3 Thesis Outline 2

2 Literature Review and Preliminaries **5**

2-1 Fundamentals of Glucose-Insulin Dynamics, and Insulin Management 5

2-1-1 Glucose-Insulin Dynamics 8

2-1-2 Insulin Management Tools 12

2-2 Automated Insulin Delivery ('Artificial Pancreas') — Preliminaries 14

2-2-1 State-of-the-art Hybrid and Fully AID Systems 15

2-2-2 Glucose Prediction Models 17

2-2-3 Performance Metric and Safety-Critical Constraints 22

2-3 Control Methodologies and Analysis 25

2-3-1 PID Controller 26

2-3-2 Model Predictive Control Analysis 30

2-4 Bayesian Optimisation 35

2-4-1 Introduction 35

2-4-2 Performance Analysis in T1DM Applications 37

2-4-3 Bayesian Optimisation in Other Applications 37

2-5 Discussion and Research Gap 40

2-5-1 Discussion 40

2-5-2 Research Gap and Directions 42

3 Proposal of Control System **45**
3-1 High-fidelity Model for Numerical Simulations . . . 45
3-2 Control Architecture . . . 48
3-2-1 PID Controller Parameterization . . . 49
3-2-2 Prediction Model Parameterization . . . 53
3-2-3 Safety Regulation Unit . . . 60
3-2-4 Model Predictive Control . . . 66
3-3 Performance-Driven Parameter Tuning . . . 71

4 Performance and Results **77**
4-1 Analysis of MPC Design Choices . . . 77
4-1-1 Performance in Announced Meal Scenario . . . 78
4-1-2 Performance in Unannounced Meal Scenario . . . 80
4-2 Performance Analysis of Bayesian Optimisation Tuning . . . 83
4-2-1 Stage 1: Clinical-related Parameters . . . 84
4-2-2 Stage 2: Tuning of Model and Control-related parameters . . . 89
4-3 Performance Analysis of Tuned Controller in Different Meal Scenarios . . . 94

5 Discussion **105**

6 Conclusion and Future Work **109**
6-1 General Conclusion . . . 109
6-2 Recommendations for Future Work . . . 112

A Supplementary materials for Chapter 2 **115**
A-1 Glossary . . . 115
A-1-1 State Variables . . . 115
A-1-2 Model Parameters and Process Variables . . . 116
A-1-3 Input and Output variables . . . 118
A-2 Insulin Guide . . . 119
A-2-1 Insulin Characteristics . . . 119

B Supplementary materials for Chapter 3 **121**

Bibliography **123**

Glossary **145**
List of Acronyms . . . 145
List of Symbols . . . 146

List of Figures

2-1 Variations of CVGA plots. 24

2-2 Example of insulin-on-board (IOB) curves adapted from [67] corresponding to the different insulin clearance times τ_{IOB} (h). Θ_{IOB} represents the fraction of the insulin infused that is still working up till τ_{IOB} after which at least approximately 95% of it has been cleared, depending on the IOB curve used. 25

2-3 Illustration of the aDOBO framweowrk for optimizing the dynamical model for a given cost using the computed cost values. Credits to Bansal *et al.* [17] 38

3-1 Block diagram of the control architecture. 48

3-2 Comparative plots of PID controller response to a perturbed measurement output y_{CGM} of Patient 14 for different values of $N_{D,\mathcal{K}}$. 52

3-3 Validation (top) and step (bottom) plot of identified model for each adult virtual patient. 58

3-5 Block diagram of the *linear* control architecture, including the contributions of d. Since the latter is omitted in the MPC control scheme, the blocks and notations corresponding to it are given a faded depiction. 59

3-4 Comparative validation plots of all patient models with respect to the validation data of Patient 14. 59

4-1 Post-prandial performance analysis of AP controller with vs without $Q_{(\Delta y)_+}$ in the respective single MPC strategies during a 70 g carbohydrates (CHO) announced meal scenario. 79

4-2 Post-prandial performance analysis of AP controller with varying zonal bound or set-point tracking values vs fixed values employed in the respective single MPC strategies, during a 70 g CHO announced meal scenario. 80

4-3 Post-prandial performance analysis of zone model predictive control (Z-MPC) only vs set-point tracking model predictive control (SP-MPC) only strategy for two different unannounced CHO sizes. 81

4-4 Post-prandial performance analysis of the proposed switching MPC-strategy vs Z-MPC only and SP-MPC only strategy during two independent unannounced meal scenarios. 82

4-5 Performance analysis of proposed controller with proportional insulin limits dependent on announced CHO size vs without, during a 100 g CHO announced meal scenario. 82

4-6 *In silico* performance analysis of minimum performance cost after each iteration for the first stage of BO tuning. 86

4-7 *In-silico* performance analysis for all three virtual patients when initial parameter settings $(\mathbf{w}, \mathbf{o}) = (\mathbf{w}_0, \mathbf{o}_0)$ are used vs tuned parameters after BO Stage 1 tuning $(\mathbf{w}, \mathbf{o}) = (\mathbf{w}_{\text{opt}}, \mathbf{o}_0)$, across a 48-h time span starting from 6 am. The ensemble means and 95% confidence intervals of the sensor glucose (SG), insulin delivery rate u and IOB u_{IOB} across the 10 runs for each subject using $\mathbf{w} = \mathbf{w}_{\text{opt}}$ (see Table 4-2) are presented. 89

4-8 Minimum cost performance vs iterations for Stage 1 BO tuning. 90

4-9 Objective function model plot after 13 iterations for Patient 14. 90

4-10 Objective function model plot after 13 iterations for Patient 15. 91

4-11 *In-silico* performance analysis for all three virtual patients when initial parameter settings $(\mathbf{w}, \mathbf{o}) = (\mathbf{w}_0, \mathbf{o}_0)$ are used vs after Stage 1 BO tuning settings $(\mathbf{w}, \mathbf{o}) = (\mathbf{w}^*, \mathbf{o}_0)$ vs after Stage 2 BO tuning settings $(\mathbf{w}, \mathbf{o}) = (\mathbf{w}^*, \mathbf{o}_{\text{opt}})$, across a 48-h time span starting from 6 am. The ensemble means and 95% confidence intervals of the SG, insulin delivery rate u and IOB u_{IOB} corresponding to $\mathbf{o}_{\text{opt}}$ across the 10 runs (see Table 4-4) are presented. 93

4-12 *In silico* visual analysis comparing the performances among the different experimental protocols used in Section 4-3, across a 48-h time span starting from 6 am. 98

4-13 *In silico* performance visual analysis for Protocol D (unannounced meals) when $Q_{\zeta+} = 0.1$ (before augmentation) vs $Q_{\zeta+} = 1$ (after augmentation) for Range 3 (Z-MPC), across a 48-h time span starting from 6 am. 103

4-14 Extended minimum cost performance after each iteration in the Stage 2 BO tuning scheme for Patient 15. Refer to Figure 4-6c for non-extended plot. 104

List of Tables

2-1 Core continuous glucose monitor (CGM) metrics formulated by the international consensus [55], commonly used in AP studies 7

2-2 Summary of the hybrid/fully closed-loop automated insulin delivery (AID) system characteristics and references to the control algorithm and randomised clinical trials. Adu — Adults, Ado — Adolescents, Chd — Children 16

2-3 Summary of PID controller methodologies discussed in Section 2-3. 29

2-4 Summary of MPC methodologies discussed in Section 2-3. (LO — Luenberger Observer, KF — Kalman Filtering) 34

2-5 Glossary of penalizing weights in Table 2-4 and the MPC formulations in Section 3-2. 35

2-6 Summary of safety enforcements applied in the works discussed in Table 2-7. . . 38

2-7 Summary of works discussed in Section 2-4 that employed Bayesian Optimisation for T1DM applications. 39

3-1 UVa/Padova metabolic S2008 variables from (3-1). 47

3-2 UVa/Padova metabolic S2008 model parameters. 47

3-3 Calculated K_P for $\tau_c = 120$ min using (3-9). 52

3-4 Chosen parameter values of PID controller (3-3). 52

3-5 Parameter and constant values from Section 3-2-2 60

3-6 Nominal weights of the Set-point MPC for different y_{CGM} (sensor glucose level (SGL)) ranges 70

3-7 Nominal weights of the Zone MPC for different y_{CGM} (SGL) ranges 71

3-8 Initial and training parameter vectors used in Stage 1 (top) and Stage 2 (bottom) BO parameter tuning for a run r. CR_0 represents the empirically calculated patient-specific carbohydrate-to-insulin ratio (CR) using eq. (2-21b), and $\mathcal{T}_{\mathrm{bolus},0}$ refers to the nominal insulin bolus decay length that is *a priori*-determined. 74

4-1 Initial and training parameter sets for BO parameter tuning. 84

4-2 *In silico* results corresponding to the 10 optimum parameter vectors of $\mathbf{w}_{\mathrm{opt}}$ and the initial settings $\mathbf{w}_0$. BO cost is evaluated during the tuning process prior to the 48-h protocol. 87

4-3 Final parameter vector after the dual-stage BO parameter tuning process. 91

4-4 *In silico* results corresponding to the 10 optimum parameter vectors of $\mathbf{o}_{\text{opt}}$ and the initial settings $\mathbf{o}_0$. BO cost is evaluated during the tuning process prior to the 48-h protocol 92

4-5 *In silico* results of all four protocol experimental settings performed on each of the three virtual patients, across a 48-h time span starting from 6 am. 99

4-6 *In silico* results of all four protocol experimental settings performed on each of the three virtual patients after the augmentation of $Q_{\zeta+}$, across a 48-h time span starting from 6 am. Results in brackets refer to those before augmenting $Q_{\zeta+}$, as presented in Table 4-5. 101

4-7 Performance comparison with adaptive Z-MPC strategy proposed in [163]. The percentages in brackets denote the fractions of correctly calculated insulin boluses that were delivered to the subjects for a given meal size. 103

5-1 $\mathbf{o}_{\text{opt}}$ values corresponding to each Stage 2 BO-tuning run for Patients 14 after 13 iterations. 107

5-2 $\mathbf{o}_{\text{opt}}$ values corresponding to each Stage 2 BO tuning run for Patients 15 after 22 iterations. 107

A-1 Symbol definition of glucose-insulin simulation model discussed in Section 2-1. . 115

A-2 Symbol chart from Section 2-1 denoting the equivalent notations used in [53, 54]. 119

A-3 Characteristics of the different insulin types. 120

Acknowledgements

"Knowledge is power". This proverb, often attributed to the English philosopher, Sir Francis Bacon (1597), ignited a learning principle that resonates deeply with me, that is, to value newly acquired knowledge for the purpose of spurring positive developments in life. Throughout the course of my study and thesis research at TU Delft, I experienced a strong and steep learning curve, having faced challenges that seemed mountainous and often vexatious. Overcoming these hurdles allowed me to learn from my mistakes and reflect on my strengths and weaknesses simultaneously. It also made me realise the value of perseverance as well as the need to adapt accordingly to changes. I enjoyed every aspect of my thesis research, even when the subject matter felt initially daunting. This invaluable and eye-opening experience broadened my knowledge, and will no doubt be an asset to my future endeavours.

My journey at TU Delft could not have happened without the generosity of the university's Education and Student Affairs (ESA) department, who were willing to accept my belated enrolment request that was made only days before the beginning of the new academic year. I managed to avoid a study delay in the process and for that, I would like to express my sincere thanks to the relevant personnel and the university.

The completion of this thesis project marks the conclusion of my Master study after nearly seven years as a student in the Netherlands. I am thoroughly grateful for the opportunity to study at TU Delft, and it is an honour and privilege to be graduating with a Master of Science (MSc) degree in Systems & Control (S&C) Engineering from this wonderful institution. It goes without saying that I am indebted to many individuals for their contribution to making this incredible milestone possible.

First and foremost, I would like to express my sincere appreciation to dr. Azita Dabiri for her supervision during the course of my thesis project. Her guidance and feedback were valuable in shaping the direction of my research. I am profoundly thankful to dr. Mohammad Khosravi for his much valued assistance and tutorship that imparted key insights to my research approach. He was always available for my questions and invested considerable amount of his time to attend to my queries. The help and feedback that I received sometimes transcended my thesis work, extending to opportunities that aided my personal development. His critical mindset and enthusiasm for learning and control research motivated me to push myself hard to strive for and deliver the best possible results within my reach. The countless hours of discussions that have taken place were instrumental to the outcomes of this project and I could not have asked for a better team of supervisors.

Next, this master study was made possible primarily because of my parents, whose unconditional encouragement and support have been paramount to my well-being during my time away from Singapore. I want to specially thank them for allowing me to pursue my dreams and ambitions.

It is difficult to fully express my thoughts of gratitude towards my awesome friends, who showed me their unwavering care and support during my time in Delft. The achievement of this thesis is specially dedicated to them, without whom I would not have succeeded. In particular, I want to show my utmost gratitude and appreciation to Karolis Navikas for his companionship, Brigitte de Graaf for her warm-hearted acts of friendship, and Nino van Wering, my S&C partner with whom I worked together on numerous group assignments and courses, as well as other friends for assisting me with the help I needed along the way.

Last but not least, I would like to thank members of the thesis committee for taking the time to review my thesis, and hope that readers find it insightful.

Delft, University of Technology Hong Yang Lee
August 26, 2024

Chapter 1

Introduction

1-1 Background and Motivation

Globally, according to the International Diabetes Federation (IDF) [145], it was estimated based on a finding in 2021 that as many as 536.6 million people are living with diabetes, of which 8.4 million individuals had been known to be suffering from the Type-1 diabetes mellitus (T1DM) disease. In a separate finding by Lancelet Diabetes & Endochrinology [91], a 60 to 107% increase in prevalent cases is expected by 2040. T1DM is a chronic autoimmune disease characterized by the destruction of pancreatic insulin-producing β-cells, resulting in lifelong complete insulin deficiency [107]. A lack of insulin inevitably leads to chronic hyperglycemia, that is, high blood glucose level (BGL), which if left untreated, can lead to microvascular and macrovascular complications such as limb loss, blindness, ischemic heart disease, as well as end-stage renal disease [45]. Patients suffering from T1DM therefore require lifelong insulin supplement and management therapy to manage hyperglycemia from the time of diagnosis.

Driven by the growing demand for T1DM treatments and the inherent shortcomings associated with conventional insulin therapies, a viable solution that not only reduces T1DM patients' mean blood glucose (BG), but also the glycaemic variability and maximises the duration for which glycaemic levels lie within the bounds of a medically-defined target range, is required. In recent years, advancements in glucose sensing and insulin delivery technologies have spurred developments of automated insulin delivery (AID) systems, also known as the artificial pancreas (AP). An AP is mainly characterized by its automated computation of insulin correction doses with the employment of a closed-loop control algorithm, typically using blood glucose measurements as the feedback variable. Since the introduction of AID systems in clinical trials and their commercial availability, improved glycemic performance among T1DM patients have been overwhelming attributed to the use of AID systems. This ascendancy has thus provided a compelling argument for increased AP research in the control systems domain, and in the process, fueling its growth and popularity. Research on AP has garnered significant attention in the control systems domain where proportional-integral-derivative (PID) and model predictive control (MPC) form two of the most commonly studied

control methodologies. Numerous clinical trials involving APs based on the latter two, have demonstrated superior glycemic performance among T1DM patients to other existing insulin therapies. The studies showed the continued relevance of patient-specific clinical parameters such as the total daily insulin dose (TDD), carbohydrate-to-insulin ratio (CR) and correction factor (CF) as well as the patient's body weight in shaping closed-loop control policies, such as insulin limits, feedforward meal bolus insulin corrections and model gain personalization.

1-2 Research Question and Objectives

Driven by the aforementioned issues and demands for an individualized glucose management therapy, this thesis seeks to exploit the merits of both the PID and MPC, in conjucture with exploring a novel adaptive tuning framework of control and model-related parameters using Bayesian Optimization. Drawing inspiration from [149], this thesis aims at developing a novel controller design that moves away from the conventional single-loop control system approach, one that includes an inner-loop controller to stabilize the plant, and an outer-loop controller serving as a reference governor that is capable of boosting the performance of the inner-loop control system. In view of this aim, the following research question is conceived:

Can a dual-loop control scheme supported by an iterative Bayesian Optimisation parameter tuning framework yield a satisfactory glycaemic performance in T1DM?

Deriving a conclusive answer to this question entails a comprehensive analysis on the established PID and MPC controller methodologies, the feasibility of Bayesian Optimisation (BO)-based tuning strategies in a T1DM setting, as well as safety-critical constraints, which demands a basic understanding of the underlying clinical practices adopted in conventional insulin therapies. In order to facilitate these developments and address the research question, the research objectives are formulated as follows:

- Assess the effectiveness of a dual-loop control scheme with limited adaptation of its inner-loop system parameter settings;
- Determine alternative measures that can increase the time-in-range (TIR) without compromising on patient safety;
- Validate the applicability of the *Identification for Control (I4C)* approach in T1DM treatment;
- Evaluate the robustness of the AP controller under miscalculated meal bolusing and unannounced meal scenarios.

The realisation of these goals forms the crux of this research, and will be addressed in subsequent chapters of this paper as outlined in Section 1-3.

1-3 Thesis Outline

This paper is structured as follows:

Chapter 2 provides readers with a basic understanding of the subject matter and introduces to the reader the state-of-the-art research pertaining to glucose-insulin glycaemic control in T1DM. A literature survey is presented in which different aspects of the research are analysed. The chapter concludes with the research gap that will set up a basis for the proposed control strategy.

Chapter 3 begins with a summarised version of the insulin-glucose dynamics employed in the virtual metabolic simulator which will be used to assess the performance of the proposed strategy. Subsequently, a comprehensive, systematic explanation on the key features of both the lower-layer control architecture and upper-layer parameter tuning scheme are detailed.

Chapter 4 presents an in-depth performance analysis on the results obtained for the different scenarios in order to rigorously assess the capabilities of the proposed AP controller.

In Chapter 5, key findings from the results and performance presented in Chapter 4 are assessed, followed by Chapter 6, in which a general conclusion is provided to the thesis. Here, the main contributions of this thesis are outlined which are used to assess the research objectives defined in order to derive a conclusive answer to the research question, thereby fulfilling the goals of this thesis project. In the same chapter, some recommendations that may be worth studying in future works are also presented.

Chapter 2

Literature Review and Preliminaries

This chapter provides an in-depth overview of the established state-of-the-art literature and research pertaining to glucose-insulin glycaemic control in Type-1 diabetes mellitus (T1DM) patients. Section 2-1 presents the relevant dynamical laws and models found in the literature using a maximal physiological model that describes the effects of insulin and food intakes on blood glucose (BG) concentrations. An introduction of the common metrics and phenomena adopted by the various diabetes organisations is presented to familiarise readers with the terminologies that are often used in the current research. Subsequently, Section 2-2 introduces the paradigms employed in an artifical pancreas system (APS) to inform readers on the crucial aspects of artificial pancreas (AP) design considerations. Hereafter in Section 2-3, the various control methodologies and frameworks focusing on proportional-integral-derivative (PID) control and model predictive control (MPC) are analysed, followed by an introduction and an analysis of Bayesian Optimisation (BO) and its applications in T1DM. Lastly, Section 2-5 discusses the key findings and offers a critical assessment of the examined literature, where the research gaps are simultaneously identified. Chapter 2 concludes with an insight on the possible directions that can be taken to tackle these gaps, thereby setting up a basis for the proposed frameworks described in Chapter 3.

2-1 Fundamentals of Glucose-Insulin Dynamics, and Insulin Management

Pharmacokinetic models have been proposed and studied in the past few decades, as far back as the 1960s [28]. Broadly classified into two classes, that is, minimal (coarse-grained) and maximal (fine-grained), these models are used for three main purposes: to support physiology studies, to perform simulations, and to be implemented as part of a model-based closed-loop controller design. Minimal physiological models provide a simplified description concerning the key components of the system functionality [47]. They are usually linear, sometimes with subtle non-linear features that are often limited only to the plasma glucose state response, such as the case in [147]. Further details and analyses on minimal model structures are outlined in Section 2-2. As opposed to the lower order nature of minimal models, a maximal

model is generally large, nonlinear and of high order. Its conceivement aims to provide a comprehensive representation of a diabetic individual's body physiology using existing knowledge so as to facilitate experiments involving simulations with *virtual* (*in silico*) patients. Some of the well-known maximal models include the Sorensen [165], Hovorka (Cambridge) [100][99], and Dalla Man/Cobelli [54] models, where the latter forms the basis of the established UVA/-Padova simulator. These three maximal models, developed by Sorensen *et al.*, Hovorka *et al.* and Dalla Man *et al.* respectively, were conceived using known physiology and metabolic processes, consisting of compartments that correspond to the various organs and tissues and are described by mass-balance equations. Each model primarily composes of two sub-system models that describe the glucose kinetics and insulin action, with single or multi-compartment models used to represent the sub-system models. For interested readers, a comprehensive review on the three maximal glucose-insulin models can be found in the works of Wilinska *et al.* [190, 191], Pompa *et al.* [151] and Colmegna *et al.* [50].

In insulin management of T1DM patients, the goal is to meet the standard glycemic targets laid out by diabetes organisations such as the American Diabetes Association (ADA) so as to avoid life-threatening risks as presented in Chapter 1. According to the ADA [15], these targets include achieving a glycated hemoglobin (HbA1c) level of $< 7\%$ (53 mmol/mol) for most non-pregnant adult patients, which can be realised by limiting the patient's peak postprandial plasma glucose concentration (i.e. blood glucose level (BGL)) to < 180 mg/dL and preprandial glucose concentration to within the range of 80 to 130 mg/dL [11]. For the reader's understanding, the measure of HbA1c is expressed as a percentage of total hemoglobin concentration in the patient's blood sample [14]. The estimated average BG (eGA) and HbA1c can be described by the relation [12]

$$\text{eGA} = 28.7\ \text{HbA1c} - 46.7\ \ [\text{mg/dL}] \tag{2-1a}$$

or

$$\text{eGA} = \frac{28.7\ \text{HbA1c} - 46.7}{10}\ \ [\text{mmol/L}] \tag{2-1b}$$

Regarded as the only prospectively evaluated tool for evaluating long-term diabetic complication risks [18], the HbA1c reflects a patient's mean BGL over the last 2 to 3 months, with measurements taken from blood samples every three to six months [74]. Attaining a HbA1c level of $< 7\%$ approximately translates to an estimated mean BGL that is below 154 mg/dL (8.6 mmol/L) [15]. These tests, however, do not provide sufficient information on acute glycemic excursions and acute complications of hypo- and hyperglycemia, not to mention glycemic variability. In spite of its limitation, the relevance of HbA1c measurements and their significance are not overlooked, but rather, other assessment methods have been proposed to complement the latter. One of such examples is the time-in-range (TIR), which refers to percentage time spent in the target range (euglycemia) in a day. Analyses conducted by Vigersky *et al.* [183] and Beck *et al.* [19] showcased a correlation between TIR and HbA1c, and also the effect of TIR on diabetic complications. This led to the TIR forming one of the core continuous glucose monitor (CGM) metrics established by an international panel of expert clinicians and researchers [55] in 2017, some of which are pivotal to the evaluation of AP control performance. These metrics are summarised in Table 2-1. The terminologies describing the glycemic conditions associated with the different BGL ranges of a diabetic patient, also according to the panel, are defined as follows [55]:

Metric	Unit	Definition
Mean BGL	mg/dL	Average blood glucose level
Glucose CV	%	Glycemic coefficient of variation
TAR(2) — (> 250 mg/dL)	%	Time above target range (2) (Severe hyperglycemia)
TAR(1) (> 180 mg/dL)	%	Time above target range (1) (Hyperglycemia)
TIR (70 – 180 mg/dL)	%	Time in target range (Euglycemia/Normoglycemia)
TBR(1) (< 70 mg/dL)	%	Time below target range (1) (Hyperglycemia)
TBR(2) (< 54 mg/dL)	%	Time below target range (2) (Severe hyperglycemia)
LBGI/HBGI [114]	-	Low/High Blood Glucose Index

Table 2-1: Core CGM metrics formulated by the international consensus [55], commonly used in AP studies

- Severe hypoglycemia — Low blood glucose level below 54 mg/dL (3.0 mmol/L)
- Hypoglycemia — Low blood glucose level below 70 mg/dL (3.9 mmol/L)
- Normoglycemia or Euglycemia — Normal and healthy blood glucose level between 70 and 180 mg/dL (3.9 – 10.0 mmol/L), or between 70 and 140 mg/dL (3.9 – 7.8 mmol/L)
- Hyperglycemia — High blood glucose level above 180 mg/dL (10.0 mmol/dL)
- Severe hyperglycemia — High blood glucose level above 250 mg/dL (13.9 mmol/dL)

The blood glucose index (BGI) as shown in Table 2-1 is a measure of frequency and extent of low and high BGL readings [112]. Analysis on LGBI and HBGI are detailed among other performance metrics in Section 2-2.

In an effort to draw awareness on the significance of the TIR, a survey was conducted by Runge *et al.* [153] in 2018 on a pool of T1DM patients' to gather their responses pertaining to their level of satisfaction with the existing insulin therapy treatments. From the finding, the authors hypothesised a relationship between effective insulin therapy treatments and improved TIR outcomes by considering the physical, psychological, and social outcomes felt by the surveyed patients during insulin therapy treatments. With the availability of CGMs, this reinforces the primary goal of maximizing the TIR of BGLs while minimizing the time-below-range (TBR) in glucose control developments, particularly the AP [173]. Interested readers may refer to a comprehensive review on insulin therapy concerning T1DM by Janez *et al.* [107] for an in-depth analysis on the various glycemic targets as well as insulin profiles, and [18] by Battelino *et al.* for recommendations on clinical targets for CGM data concerning the TIR.

In this section, only the equations and assumptions from the glucose-insulin maximial model of Dalla Man *et al.* are of interest, as the work of this thesis revolves around the utilisation of the UVa/Padova simulator (S2008 version) [134] for in-silico testing of the proposed

control algorithm. The glucose and insulin pharmacokinetics are described based on the system dynamics of *in silico* subjects from the metabolic simulator, which comprises of various dynamical equations that capture the relevant kinetics. In addition to [135, 54], additional equations that describe the new features of the newer S2013 version of the simulator [53] are also described. These new features include glucagon-related dynamics which are absent from the S2008 version and thus excluded for the purpose of this thesis research.

2-1-1 Glucose-Insulin Dynamics

The glucose-insulin model embedded within the UVa/Padova metabolic simulator is fundamentally described by the glucose and insulin kinetics pertaining to plasma concentrations. In both the glucose and insulin subsystems, there exists a relationship between plasma concentrations and the respective fluxes. For the glucose kinetics, the glucose system is modelled as a 2-compartment model, of which the first represents the plasma and rapidly equilibrating tissues, while the second compartment represents the slowly equilibrating tissues. The glucose flux can be sub-divided into different processes, namely glucose appearance in plasma (**GA**) [52], glucose utilization (**U**), endogenous glucose production (**EGP**) and renal excretion of glucose (**E**). Owing to the use of CGM in taking glucose measurements, subcutaneous glucose [144] kinetics is added to account for the time delay between the measured glucose level and the actual BGL at a given time. The insulin subsystem is also described in a similar fashion with two compartments representing the liver and plasma respectively. The insulin fluxes comprises of the insulin appearance (**IA**) in the subcutaneous tissue, as well as degredation (**D**). A glossary of the symbols and their meanings can be found in Appendix A-1 for reference.

It is worth noting however, that glucagon production may still be present in T1DM patients due to the continued presence of α-cells although they have become dysfunctional [62]. Glucagon pharmacokinetics research in T1DM gained attention only in recent years [25] and it is for this reason that knowledge on glucagon pharmacokinetics is still limited compared to insulin ones, and are therefore not covered extensively in T1DM control research.

Glucose subsystem — Kinetics

The glucose subsystem in [54] is modelled as a 2-compartment model. Dalla Man *et al.* described the glucose subsystem kinetics based on the state responses of the glucose masses per unit body mass in the plasma

$$\begin{aligned}\dot{q}_{\text{pla}}(t) = R_{\mathbf{EGP}}(t) + k_{q2}\ q_{\text{tis}}(t) + R_{\mathbf{GA}}(t) \\ - k_{q1}\ q_{\text{pla}}(t) - R_{\mathbf{U},\text{indep}}(t) - R_{\mathbf{E}}(t),\end{aligned} \tag{2-2a}$$

and in the rapidly evaporating tissues

$$\dot{q}_{\text{tis}}(t) = -R_{\mathbf{U},\text{dep}}(t) + k_{q1}\ q_{\text{pla}}(t) - k_{q2}\ q_{\text{tis}}(t). \tag{2-2b}$$

The blood glucose concentration $C_{q_{\text{pla}}}$, which is synonymous to the BGL, is defined as

$$C_{q_{\text{pla}}}(t) = \frac{1}{V_q}\ q_{\text{pla}}(t). \tag{2-3}$$

According to eqs. (2-2), the state response of q_{pla} is governed by the net glucose production, which takes into account the $R_{\mathbf{EGP}}$ rate, glucose appearance rate in the plasma $R_{\mathbf{GA}}$, as well as the glucose transported into the plasma from the tissues, subtracted by the sum of the independent glucose utilisation rate $R_{\mathbf{U},\text{indep}}$, and renal excretion rate $R_{\mathbf{E}}$, all of which are described in eqs (2-11), (2-6) and (2-14) respectively, as well as a subtraction of the glucose transported from the plasma to the tissue.

Glucose Flux — Endogenous Glucose Production (EGP)

The EGP [135] rate is defined as

$$R_{\mathbf{EGP}}(t) = k_{\mathbf{EGP1}} - k_{\mathbf{EGP2}}\ q_{\text{pla}}(t) - k_{\mathbf{EGP3}}\ C_{m_{\text{liv}},\text{delay}}(t) \tag{2-4}$$

where $k_{\mathbf{EGP1}}$ denotes the extrapolated $R_{\mathbf{EGP}}$ at basal conditions, $k_{\mathbf{EGP2}}$ the rate parameter of liver glucose effectiveness and $k_{\mathbf{EGP3}}$ the parameter governing the insulin concentration in the liver.

The dynamics associated with the EGP comprises of the responses of the actual insulin concentration in the liver $C_{m_{\text{liv}}}$, and the perceived insulin concentration by the liver as a result of a signal delay, $C_{m_{\text{liv}},\text{delay}}$. The responses are governed by the following expressions:

$$\dot{C}_{m_{\text{liv}}}(t) = -k_{\mathbf{EGP}m}\ (C_{m_{\text{liv}}}(t) - C_{m_{\text{pla}}}(t)) \tag{2-5a}$$

$$\dot{C}_{m_{\text{liv}},\text{delay}}(t) = -k_{\mathbf{EGP}m}\ (C_{m_{\text{liv}},\text{delay}}(t) - C_{m_{\text{liv}}}(t)). \tag{2-5b}$$

$C_{m_{\text{pla}}}$ denotes the plasma insulin concentration

$$C_{m_{\text{pla}}}(t) = \frac{1}{V_m}\ m_{\text{pla}}(t), \tag{2-5c}$$

where V_m is the distributed volume of insulin.

Glucose Flux — Glucose Appearance (GA)

The ingested carbohydrates (CHO) (or glucose) first reaches the stomach in solid form, and is followed by a process of grinding into liquid form before getting emptied to the small intestines (gut), and finally absorbed into the bloodstream. This accounts for the glucose rate of appearance in the plasma

$$R_{\mathbf{GA}}(t) = \frac{k'_{\mathbf{GA}1} k_{\mathbf{GA}1}\ Q_{\text{gut}}(t)}{W_{\text{body}}}. \tag{2-6}$$

The accompanying dynamics associated with **GA** process are governed by the response of glucose mass present in the stomach in solid state $Q_{\text{sto},s}$, liquid state $Q_{\text{sto},l}$ as well as in the small intestines Q_{gut}, as described in eqs. (2-7):

$$\dot{Q}_{\text{sto},s}(t) = -k_{\mathbf{GA}2}\ Q_{\text{sto,s}}(t) + R_{Q_{\text{in}}}(t) \tag{2-7a}$$

$$\dot{Q}_{\text{sto},l}(t) = -k_{\mathbf{GA}3}(Q_{\text{sto}}(t))\ Q_{\text{sto,l}}(t) + k_{\mathbf{GA}2}\ Q_{\text{sto,s}}(t) \tag{2-7b}$$

$$\dot{Q}_{\text{gut}}(t) = -k_{\mathbf{GA}1}\ Q_{\text{gut}}(t) + k_{\mathbf{GA}3}(Q_{\text{sto}}(t))\ Q_{\text{sto},l}(t), \tag{2-7c}$$

where the parameters $k_{\mathbf{A}1}$ and $k_{\mathbf{A}2}$ are rate constants associated with the intestinal absorption and gastric grinding. Combining $Q_{\text{sto},s}$ and $Q_{\text{sto},l}$ yields the total glucose present in the stomach given by

$$Q_{\text{sto}}(t) = Q_{\text{sto},s}(t) + Q_{\text{sto},l}(t). \tag{2-8}$$

The rate of gastric emptying parameter

$$k_{\mathbf{GA}3} = \begin{cases} k_{\mathbf{GA4}}(Q_{\text{total}}) & \text{if } 0 < Q_{\text{sto}} < Q_{\text{total}} \\ \overline{k}_{\mathbf{GA}3} & \text{if } Q_{\text{sto}} \in \{0, Q_{\text{total}}\} \end{cases} \tag{2-9}$$

where

$$\begin{aligned} k_{\mathbf{GA4}}(Q_{\text{total}}) = \underline{k}_{\mathbf{GA}3} + \frac{\overline{k}_{\mathbf{GA}3} - \underline{k}_{\mathbf{GA}3}}{2}\ \Big\{&\tanh(k_{\mathbf{GA}3\downarrow}\ \{Q_{\text{sto}} - k'_{\mathbf{GA}3\downarrow}\ Q_{\text{total}}\}) \\ &- \tanh(k_{\mathbf{GA}3\uparrow}\ \{Q_{\text{sto}} - k'_{\mathbf{GA}3\uparrow}\ Q_{\text{total}}\}) + 2\Big\}, \end{aligned}$$

is time-varying and Q_{sto}-dependent such that $\underline{k}_{\mathbf{GA}3} \leq k_{\mathbf{GA}3} \leq \overline{k}_{\mathbf{GA}3}$. Q_{total} represents the sum of the ingested CHO (mg) and the remaining amount of glucose in the stomach at the start of the most recently ingested meal [135]. In eq. (2-9), the variables $k_{\mathbf{GA}3\uparrow}$ (mg^{-1}) and $k_{\mathbf{GA}3\downarrow}$ (mg^{-1}) represent the rate parameters relating to the increase and decrease of $k_{\mathbf{GA}3}$ respectively, given by

$$k_{\mathbf{GA}3\uparrow} = \frac{5}{2(1 - k'_{\mathbf{GA}3\uparrow})\ Q_{\text{total}}}, \tag{2-10a}$$

$$k_{\mathbf{GA}3\downarrow} = \frac{5}{2k'_{\mathbf{GA}3\downarrow}\ Q_{\text{total}}}. \tag{2-10b}$$

Glucose Flux — Glucose Utilization (U)

Glucose utilization ($\mathbf{U}$) comes in two forms, one being insulin-dependent, and the other insulin-independent. The former occurs in the second compartment of the glucose subsystem model, and the latter in the first compartment. The rate of glucose utilization $R_{\mathbf{U}}(t)$ is the sum of the glucose-independent $R_{\mathbf{U},\text{indep}}$ and glucose-dependent $R_{\mathbf{U},\text{dep}}$ variables, where the former is a time-dependant variable, as described in eqs. (2-11) and the former is a constant variable.

$$R_{\mathbf{U}}(t) = R_{\mathbf{U},\text{dep}}(t) + R_{\mathbf{U},\text{indep}} \tag{2-11a}$$

$$R_{\mathbf{U},\text{dep}}(t) = \frac{\overbrace{\left\{k_{\mathbf{U}1} + k_{\mathbf{U}2}\ C_{m_{\text{inter}}}(t)\ \overbrace{\left\{1 + k_{f_{\text{risk}},1}\ f_{\text{risk}}(C_{q_{\text{pla}}})\right\}}^{\text{Risk Factor}}\right\}}^{\text{Glucose transportation rate limit}}\ q_{\text{tis}}(t)}{k_{\mathbf{U}3} + q_{\text{tis}}(t)} \tag{2-11b}$$

The parameter $k_{f_{\text{risk}},1}$ and the hypoglyceamic risk component f_{risk} were introduced in the S2013 simulator to quantify the hypoglycaemic risk factor, and are absent in the S2008 version. The BG risk factor is active in the scenario where $C_{q_{\text{pla}}}$ falls below the defined basal plasma glucose concentration $C_{q_{\text{pla}},\text{b}}$ and is at risk of hypoglycemia. f_{risk} is a time-varying parameter that is dependent on the plasma glucose concentration (BGL) governed by eq. (2-12):

$$f_{\text{risk}} = \begin{cases} 0 & \text{if } C_{q_{\text{pla}}} \geq C_{q_{\text{pla,b}}} \\ 20\ k_{f_{\text{risk}},2}\ \log\left(\frac{C_{q_{\text{pla}}}}{C_{q_{\text{pla,b}}}}\right) & \text{if } \underline{C}_{q_{\text{pla}}} \leq C_{q_{\text{pla}}} < C_{q_{\text{pla,b}}} \\ 20\ k_{f_{\text{risk}},2}\ \log\left(\frac{\underline{C}_{q_{\text{pla}}}}{C_{q_{\text{pla,b}}}}\right) & \text{if } C_{q_{\text{pla}}} < \underline{C}_{q_{\text{pla}}}. \end{cases} \tag{2-12}$$

$\underline{C}_{q_{\text{pla}}}$ is the plasma glucose concentration threshold associated with hypoglycemia and $k_{f_{\text{risk}},2}$ a model parameter corresponding to the risk quantity. Another new feature of the S2013 simulator accounts for the plasma glucose dynamics when BGL of the virtual patient lies within the hypoglycemic range. These corresponding dynamics differ from that of eq. (2-2a) (See eq. (13) in [53]).

As seen in eq. (2-11), the rate of BGL-dependent glucose utlisation is influenced by the response of the interstitial insulin concentration

$$\dot{C}_{m_{\text{inter}}}(t) = -k_{\mathbf{U}m}\ C_{m_{\text{inter}}}(t) + k_{\mathbf{U}m}\ \left(C_{m_{\text{pla}}}(t) - C_{m_{\text{plas,b}}}\right) \tag{2-13}$$

where $C_{m_{\text{plas,b}}}$ refers to the basal insulin concentration in the plasma, and $k_{\mathbf{U}m}$ the rate parameter of insulin action on the peripheral glucose utilisation.

Glucose Flux — Renal Excretion (E)

The renal excretion rate is conditional to the amount of glucose in the plasma q_{pla} relative to $k_{\mathbf{E}2}$, given by

$$R_{\mathbf{E}}(t) = \begin{cases} k_{\mathbf{E}1}\ (q_{\text{pla}} - k_{\mathbf{E}2}) & \text{if } q_{\text{pla}} > k_{\mathbf{E}2} \\ 0 & \text{otherwise} \end{cases} \tag{2-14}$$

where $k_{\mathbf{E}2}$ refers to the renal threshold of the distributed plasma glucose.

Insulin subsystem - Kinetics

Insulin kinetics is defined by the responses of the distributed insulin amount in the liver and plasma respectively:

$$\dot{m}_{\text{liv}}(t) = -\left(k_{m1} + k_{m3}\right)\ m_{\text{liv}}(t) + k_{m2}\ m_{\text{pla}}(t), \tag{2-15a}$$

$$\dot{m}_{\text{pla}}(t) = -\left(k_{m2} + k_{m4}\right)\ m_{\text{pla}}(t) + k_{m1}\ m_{\text{liv}}(t) + R_{\mathbf{IA}}(t), \tag{2-15b}$$

where k_{m1} and k_{m2} are rate parameters corresponding to the insulin transportation from the liver to plasma and plasma to liver respectively. k_{m3} and k_{m4} are those relating to the insulin degradation in the liver and periphery respectively.

In (2-15b), the plasma insulin rate of appearance $R_{\mathbf{IA}}(t)$ is dependent on the exogenous subcutaneous insulin infusion rate, described in eq. (2-18), substituting the insulin secretion rate in a healthy human glucose-insulin system described in [54] (Refer to variable S from eq. (3) in [54]). The absence of a working pancreas affects the modelling of parameter m_3 in (2-15a), which was modelled to be non-linearly related to the pancreatic insulin secretion rate (refer to eqs. (4)-(8) in [54]). m_3 is therefore modelled as a constant parameter assigned using its basal steady-state value. The state responses of m_{liv} and m_{pla} are defined by the net rate of insulin transported to the liver and to the plasma respectively. Insulin transported out of the liver are degraded in the liver while that of the plasma in the periphery.

Insulin Flux — Insulin Appearance and Subcutaneous Tissue Kinetics

Insulin flux behaviour is directly influenced by the exogenous insulin infusion rate $R_{m_{\text{in}}}$, thus affecting the rate of insulin appearance $R_{\mathbf{IA}}$. Insulin appearance is correlated to the dynamical behaviour of the glucose and insulin quantities in the subcutaneous tissues. These kinetics can be described by three compartments: the distributed amounts of non-monomeric $m_{\mathbf{sc},1}$ and monomeric insulin $m_{\mathbf{sc},2}$, and of glucose $q_{\mathbf{sc}}$ in the subcutaneous region. The dynamics of these three compartments are governed by the following expressions:

$$\dot{m}_{\mathbf{sc},1}(t) = -(k_{m_{\mathbf{sc}}3} + k_{m_{\mathbf{sc}}1})\ m_{\mathbf{sc},1}(t) + R_{m_{\text{in}}}(t) \tag{2-16a}$$

$$\dot{m}_{\mathbf{sc},2}(t) = k_{m_{\mathbf{sc}}3}\ m_{\mathbf{sc},1}(t) - k_{m_{\mathbf{sc}}2}\ m_{\mathbf{sc},2}(t) \tag{2-16b}$$

$$\dot{q}_{\mathbf{sc}}(t) = -k_{q_{\mathbf{sc}}}\ q_{\mathbf{sc}}(t) + k_{q_{\mathbf{sc}}}\ q_{\text{pla}}(t), \tag{2-17}$$

where $k_{m_{\mathbf{sc}}1}$ and $k_{m_{\mathbf{sc}}2}$ are rate constants of non-monomeric and monomeric insulin absorption respectively while $k_{m_{\mathbf{sc}}3}$ is the rate constant of insulin dissociation in the subcutaneous tissue. $k_{q_{\mathbf{sc}}}$ denotes the transportation rate between the plasma glucose and the subcutaneous glucose, which accounts for the time delay between the measured glucose by the CGM and the actual BGL. The rate of insulin appearance is thereafter defined as

$$R_{\mathbf{IA}}(t) = k_{m_{\mathbf{sc}}1}\ m_{\mathbf{sc},1}(t) + k_{m_{\mathbf{sc}}2}\ m_{\mathbf{sc},2}(t), \tag{2-18}$$

contributing to the state response of plasma insulin in (2-15b). Conversely, the dynamics of the subcutaneous glucose in (2-17) can be described in concentration terms by utilising the relation

$$C_{q_{\mathbf{sc}}}(t) = \frac{q_{\mathbf{sc}}}{V_q} \tag{2-19}$$

thus following eq. (A17) in [53]. (2-19) serves as the system output, that is, the sensor glucose (SG).

2-1-2 Insulin Management Tools

According to the ADA [14], it takes approximately an hour after the start of a meal for a patient's BGL to reach its peak value before returning to its preprandial levels within 2 to 3 h. Glucose concentrations only begin to rise approximately 10 min from the moment

meal is consumed as a result of the absorption of dietary carbohydrates, with the glucose absorption process lasting for up to around 6 h. Consequently, appropriate measures are taken in conventional open-loop insulin therapy, which is characterised by the intake of basal and bolus insulin as part of the *basal-bolus* regiment. Basal insulin refers to the insulin taken to keep the patient's BGL steady between meals and overnight thus maintaining glycemia, while bolus insulin refers to a single dose of insulin administered at the start of (or prior to) meals in order to curb BGL increase induced by CHO intake [72]. Various types of insulins are available for insulin therapy treatments, ranging from rapid-acting to long-acting insulin, whose characteristics can be found in Appendix A-2. These insulin types differ in terms of the time taken for their infusion to take effect on blood glucose. In the basal-bolus regiment, rapid-acting insulin is taken at meal times (bolus), while long-acting insulin is taken once or twice a day (basal) [72]. The required basal and bolus insulin amounts are dependent on the correction factor (CF), carbohydrate-to-insulin ratio (CR) and insulin-on-board (IOB) [101]. The definitions of the latter three terms are as follows:

- Correction Factor (CF) — Glycemic drop per unit of extra insulin when $R_{m,\text{basal}}$ is correctly set. A commonly-used mathematical rule is the so-called 1700-rule (see eq (2-20)). Also known as the insulin sensitivity factor.
- CHO-to-Insulin Ratio (CR) — Number of grams of CHO that is required to compensate for a unit of insulin (1U), when the basal insulin is correctly set.
- Insulin on Board (IOB) — Remaining insulin in the blood, due to the last insulin injection or infusion applied.

To aid patients in their decision making process regarding insulin management, a pedagogical approach commonly utilised in open-loop intensive insulin therapies known as functional insulin therapy (FIT) was introduced in view of the varying activities in their everyday life such as meals [92][108]. This flexibility diminishes the reliance on direct insulin administration by a physician, and also reduces the feeling of restrain by the patient caused by intensive medical care associated with T1DM.

The CF and CR can be empirically determined using the basal-bolus insulin guidelines laid out by Davidson *et al* [58] and Walsh *et al.* [186], both of which formed the basis of those by the American Association of Clinical Endocrinologists/American College of Endocrinology (AACE/ACE) [97]. The total daily insulin dose (TDD), that is, the total basal and bolus insulin dose delivered to the patient in a day over a 24 h-period in a day, is crucial to the derivation of the aforementioned parameters.

The correction factor can be empirically determined using the 1700-rule [58]:

$$\text{CF} = \frac{1700}{\text{TDI}} \text{ [mg/dL/U]}, \tag{2-20}$$

or the 1800-rule [185] which is also clinically accepted, having been used to shape prediction model parameters, such as [182] and [181].

In elementary terms, the CR is simply the ratio between the amount of ingested CHO and the optimal insulin bolus, that is,

$$\text{CR} = \frac{\text{Ingested CHO, } Q_{in}}{\text{Optimal insulin bolus, } M^*_{\text{bolus}}} \text{ [g CHO/U]} \tag{2-21a}$$

Two empirical methods were outlined by the AACE/ACE to calculate the CR, the first being the "2.8 rule" by Davidson *et al.* [58] given by

$$\mathrm{CR} = \frac{2.8 \times \overbrace{2.20462}^{\text{lbs to kg}} \times \mathrm{W}_{\mathrm{body}}}{\mathrm{TDD}} \text{ [g CHO/kg]} \tag{2-21b}$$

where the value 2.20462 in eq. (2-21c) serves as a conversion factor from pounds (lb), the unit used in [58], to kilograms (kg), and the "450-rule"

$$\mathrm{CR} = \frac{450}{\mathrm{TDD}} \text{ [g CHO/kg]} \tag{2-21c}$$

by Walsh *et al.* [184] for the second. Unlike (2-21b) which is weight-dependent, (2-21c) was conceived using average body weights and regular insulin from an earlier study in 1994. According to Walsh *et al.* [184], the (2-21c) is prone to inaccuracies when applied to a pool of patients with body weight and insulin sensitivity variations [186]. Using either (2-21b) or (2-21b), the recommended insulin bolus amount can thereafter be computed using the estimated CHO intake and the *a priori*-calculated CR.

The IOB is widely employed in insulin therapy due to its ability to prevent the closed-loop system from 'stacking' insulin as a consequence of the delay in the insulin action [171]. The IOB is related to the insulin infused as well as the rate of insulin action. In theory, the IOB is mathematically expressed as [1]:

$$\mathrm{IOB}(t) = \int_0^t u(\tau) - R_{\mathbf{IA}}(\tau)\, d\tau \tag{2-22}$$

where $R_{\mathbf{IA}}$ is the rate of appearance of subcutaneous insulin as defined in (2-18). In practice, however, this quantity cannot be directly measured or calculated, but only approximated. Further details relating to IOB estimations are described in Section 2-2.

The aforementioned tools are however, not only limited to open-loop insulin therapy as they remain relevant to the shaping of AP control policies. Even in APs that employ adaptive functionality, deriving these parameters is a necessity for initializing system settings of the closed-loop controller.

2-2 Automated Insulin Delivery ('Artificial Pancreas') — Preliminaries

Measured using a subcutaneous CGM, BGL is regulated by the delivery of basal and bolus insulin via a continuous subcutaneous insulin infusion (CSII) pump. Before the emergence of CGMs, a commonly-used method for measuring blood glucose levels in diabetes management is the finger-stick procedure, which relies on a small amount of capillary blood obtained by pricking one finger with a lancet. Unlike CGMs, the finger-stick procedure provides the current capillary blood glucose concentration, with little or no time delay. However, information

on glucose trend is absent in this procedure given that significantly less measurements are taken, which could lead to incorrect or sub-optimal treatment decisions. Comprising of a glucose sensor, a transmitter, and a receiver/wireless monitor that can be worn on a belt, the CGM on the other hand takes measurements typically every one to five minutes and is durable, thus facilitating its deployment in portable automated insulin delivery (AID) devices. One significant drawback of the CGM lies with the inherent time delays between the measured and actual BGL values, with a review by Zarkogianni *et al.* [197] reporting a mean time delay of 6.7 s for the majority of CGM sensors. This is in part due to the measurements taken from the subcutaneous space and may occasionally require instant calibration, with the presence of noise measurements adding to the list of disadvantages. Even so, ongoing improvements in precision, accuracy and timeliness of hypo/hyperglycemic alerts of commercial CGM sensors [70] are expected to curb concurrent impediments relating to CGM BGL measurement capabilities, which is key to the realisation of safe and reliable AID systems. Readers may refer to [197] and [70] for detailed reviews on blood glucose monitoring technologies.

Reliance on only BGL measurements in feedback control to maintain blood glucose homeostasis is often insufficient. With meals, exercise, stress and sleep being the major forms of disturbance, a form of feedforward action such as manual meal entries and manual adjustments of insulin infusion rates before eating or engaging in a physical activity is often seen as a necessary feature in AID systems [44]. A myriad of feedback control methods, which could either be model-based or model-free, semi- or fully-automated, have been proposed in the literature. AP design concepts include reinforcement learning [124, 194] and fuzzy logic [16, 61]. Among the control strategies, PID [103][136][167] and MPC [88][82] are of particular interest in this thesis, with both types of control approaches being highly popular and extensively researched and reviewed [46][113], including adaptive ones [98][180], especially in clinical environments [29][33][57][21]. The PID approach has been widely regarded as the first choice among controller designs in many practical applications despite its seemingly primitive or simplistic nature [170]. On the other hand, an advanced control algorithm like the MPC, which computes the optimum insulin dose using BGL predictions from an embedded model and simultaneously enforce critical safety constraints, has demonstrated improved glucose control performance in both *in silico* and *in vivo* evaluations [150], leading to the latter becoming a preferred and more popularly researched approach in recent decades [172], including in randomized clinical trials [109]. Nevertheless, the ongoing debate regarding their respective merits reflects the continued relevance of both control algorithm classes in T1DM glucose management for the years to come [20][167].

In this section, readers will first be introduced to some of the characteristics of commercially available AID systems in order to get acquainted with feasible and clinically-proven methods that would guide the realization of a feasible APS.

2-2-1 State-of-the-art Hybrid and Fully AID Systems

Given the relatively recent launch of the first commercially available AP system in 2016, that is, the Medtronic MiniMed 670G (succeded later by 770G) system [21], only a limited number of such devices exist in the market, with several other systems under development or seeking approval from the U.S. Food & Drug Administration (FDA) and Conformite Europeenne (CE) [148]. As of June 2024, only six hybrid closed-loop AID systems have been approved by the FDA for commercial use:

Artificial Pancreas	Control Algorithm	Parameter Initialisation and Adaptation	Randomized Trials
MiniMed 670G/ 770G	PID with insulin feedback [169, 188, 152]	Initialised with CR, active insulin time. Learning based on TDD, estimated fasting glucose and plasma insulin concentration	Adu – [127, 126, 21, 84] Ado – [127, 126, 21, 84], Chd – [79]
MiniMed 780G	PID + Fuzzy Logic with insulin feedback and model-based glucose prediction [94, 95]	Initialised with CR, active insulin time, BGL set-point. Learning based on TDD, estimated fasting BGL and plasma insulin concentration	Adu – [22, 38, 49] Ado – [22, 38, 49] Chd – [22, 49]
Control-IQ	MPC [132, 146, 177, 102, 112]	Initialised with CR, basal insulin rate, CF. Learning based on TDD and real-time data	Adu – [29, 30, 111, 106], Ado – [29, 111, 106], Chd – [78]
Omnipod 5	MPC [122, 87]	Initialised with CR, CF, active insulin time, BGL set-point. Learning based on TDD and real-time data Learning based on TDD	Adu – [34, 35, 76, 75, 160], Ado – [35, 160], Chd – [35, 75, 160]
iLet	MPC [66, 155, 65]	Initialised with body weight. Learning based on real-time data	Insulin Only: Adu –[120, 96, 154], Ado – [142, 96], Chd – [96, 142], Bihormonal: Adu – [39]

Table 2-2: Summary of the hybrid/fully closed-loop AID system characteristics and references to the control algorithm and randomised clinical trials. Adu — Adults, Ado — Adolescents, Chd — Children

- Medtronic MiniMed 670G/770G — Approved in September 2016 [3]; launched in 2017;
- Medtronic MiniMed 780G — Approved in April 2023 [4], launched in the same year;
- Tandem Control IQ — Approved in December 2019 [5], launched in 2020;
- Insulet Omnipod 5 — Approved in January 2022 [105], launched in the same year;
- Beta Bionic iLet bionic pancreas — Approved in May 2023 [6], launched in late 2023;
- Tidepool Loop — Approved in January 2023 [174], not yet launched.

Among the pool of FDA-approved closed-loop AID devices, only the MiniMed 670G/770G and the 780G systems which were developed by Medtronic Diabetes, utilise the PID as their base control algorithm, while the rest employ an adaptive MPC approach as their primary algorithm. The MiniMed 670G/770G was the first AID system to be made commercially available in 2017, while the Tandem Control IQ was the first FDA-approved hybrid closed-loop AID system that employ a MPC-based algorithm [143], launched in 2020 after the Medtronic 670G. The principle controller characteristics and their respective references to the literature and clinical trials are summarised in Table 2-2, with the exception of the Tidepool Loop. As outlined in Table 2-2, the TDD is a key parameter that influences the workings of the APS. Interested readers may refer to [143] for a review of the AID systems on their glycaemic performance for T1DM patients, and to the consensus recommendations regarding the use of AID technologies in clinical practice by Phillip and colleagues [148]. An examination of the control algorithms pertaining to the above AID devices (with the exception of Tidepool Loop) is treated in subsequent parts of this chapter.

2-2-2 Glucose Prediction Models

Prediction models are fundamentally crucial to the shaping of model-based AP algorithms. In clinical practice, the available data are insulin delivery rate, glucose concentration, and CHO count [187]. Among AP designs in the literature that employ linear prediction models, insulin is usually the sole exogenous input in the model due to inaccurate CHO counts, which cannot be accurately or directly measured and rely on self-estimation by the patient [187]. The models can be roughly distinguished into two categories: grey-box, in particular the minimal physiological models, which are often described in subspace state-space form, and black-box, whose properties are identified using the data-driven approach. First proposed in the early works of Cobelli and Bergman [23] in the late 1970s, minimal models have since been widely used in AP design due to their inherent descriptive ability and parameter interpretability. According to Garcia-Tirado *et al.* [83], some of the most commonly used minimal physiological models include the model developed by Patek *et al.* [147], by Lin *et al.* [125] and by Magdelaine *et al.* [128], whereby the former two are extensions of the *Bergman* [23] minimal model. Linear black box models, having the form of a transfer function or subspace state-space, are identified using time-series or frequency response properties. Conventional linear time-series models employed include the autoregressive with exogenous input (ARX) [93, 187, 196], autoregressive moving-average with exogenous input (ARMAX) [27, 181, 69], and the autoregressive integrated moving-average with exogenous input (ARIMAX) models [27, 181], all of which in addition to the deterministic input-output model component

that describes the relationship between insulin infusion and measured glucose, incorporates a stochastic feature that models the process noise, measurement noise and other unknown variables that affect the CGM measurements. Transfer-function models that comprise of only the deterministic part have also been identified using frequency response properties by means of the output-error parametric model estimation method using data of *in silico* subjects. A notable example is the *control-relevant* model developed by van Heusden and colleagues [182], who sought to conceive a suitable prediction model out of control performance considerations over BGL prediction accuracy.

Deep learning [42, 199, 80] as well as other machine learning-based prediction models [68] have also emerged as candidates of BGL prediction studies in recent years. These models are capable of modelling blood glucose dynamics in both the linear and non-linear settings. Popular machine learning models such as the Recurrent Neural Networks (RNN), Convolution Neural Networks and Long Short Term Memory (LSTM) typically require extensive amount of patient data that are often inaccessible. The OhioT1DM Dataset [138, 139] is a well-known resource that have been used by researchers on machine learning model developments to train and validate their respective models. Considering the computational complexity of these models, machine learning models are not explored in great detail in this study. Interested readers on machine learning analyses may refer to survey papers by Woldaregay *et al.* [192], and on deep learning algorithm by Zhu *et al.* [200] on their discretion.

Comparison of linear models — Physiological and Time-series

Large scale comparative studies in clinical trials have yet to be conducted on the two classes of prediction models [81], at least to the author's knowledge. A general consensus on the preference between of physiological and data-driven control-oriented models has thus not been established. Based on an examination of the prediction model performances across various literature studies, one can observe that the differences between the two model classes lie primarily in their respective model characteristics and thus identification considerations. In the context of T1DM, the complex nature of the human physiology might be oversimplified and therefore not sufficiently captured by the use of minimal models. In spite of their supposed model simplification, many minimal models encounter global parameter identification and state observability issues, as exemplified by the models examined in [83]. These bottlenecks can be overcome by assigning *population* (fixed) values to certain parameters, or employing a model with a reduced number of unknown parameters. In a review by Hoyos *et al.* [101], the bottlenecks were also acknowledged by the authors, who attributed the lack of identifiability to the existence of correlated parameters and non-unique solutions, given a dataset comprising of only CGM measurements, insulin doses and self-reported CHO intakes. Moreover, the authors suggested a method for choices of parameters to be assigned with population values, based on the sensitivities of the measured variable to changes of the parameter. The issue of parameter identification in physiological prediction models nonetheless persists, and have led to arguments that a data-driven approach would be able to overcome this limitation [197].

Unlike physiological models in which certain parameters that are not identifiable or non-measurable must be derived using first principles, time-series models require only historical experimental data for parameter identification as part of the data-driven approach, and do not require much understanding of the underlying physiological principles. In view of intra-patient variability, such as the time-varying circadian variability of a T1DM patient's insulin

sensitivity [2], proponents of time-series models, specifically the parametric ones, have argued in favour of the latter for which online model parameter adaptation using recursive means is applicable [69][181]. After a thorough literature search, ARX models were found to be among the most commonly used time-series prediction models in MPC-based AP works, just like in many other applications due to their simple model structure and calculation [196]. Beyond its model simplicity, an ARX model's parameters are relatively easy to identify compared to other black-box models due to their linear-in-parameter structure while itself is robust to various disturbances [131]. Comparative studies that employed both the ARMAX and ARIMAX time-series models, such as [27] by Boiroux and colleagues, are available. ARIMAX models were reported to be beneficial when a non-negligible, non-stationary disturbance results in a steady-state offset error [181], such as a step disturbance, is present in closed-loop control. In [27], a model-plant mismatch was intentionally introduced by the authors to test the robust capabilities of the ARIMAX-based MPC in rejecting the offset error against those of the ARMAX-based MPC which were not faced with any of such errors. Both models contained only fixed parameters during the initial test. In the scenario where the correct meal bolus was administered at mealtime, the authors reported a higher TIR for the ARIMAX-based MPC in the normoglycemic range, but worse hyperglycemic performance, in which a higher time-above-range (TAR) was reported. In the same scenario, an MPC that employed an adaptive ARMAX model was tested, and outperformed those based on both the non-adaptive ARMAX and ARIMAX models, in terms of the TIR in the normoglycemic range, and the TAR. In a separate scenario when the controllers were tested with half of the correct meal bolus administered, the ARIMAX-based MPC was found to have delivered the best glycemic performance among the three time series model-based controllers, achieving the highest TIR, and lowest TAR and TBR recorded despite the absence of parameter adaptation. The study illustrated, using correctly administered meal bolus settings, the advantages of relying on an adaptive parametric time-series model, and on the other hand, the robustness attributes of an ARIMAX model-based MPC when meal bolus is administered incorrectly (under-bolused). For reference, the ARX, ARMAX and ARIMAX models are denoted by

$$y(k) = \frac{B(z)}{A(z)}u(k) + \frac{1}{A(z)}e(k), \tag{2-23a}$$

$$y(k) = \frac{B(z)}{A(z)}u(k) + \frac{C(z)}{A(z)}e(k), \tag{2-23b}$$

and

$$y(k) = \frac{B(z)}{A(z)}u(k) + \frac{C(z)F(z)}{A(z)}e(k) \tag{2-23c}$$

respectively, where

$$A(z) = 1 + a_1 z^{-1} + \cdots + a_{n_a} z^{-n_a}, \quad (a_1, \cdots, a_{n_a}) \in \mathbb{R} \tag{2-24a}$$

$$B(z) = b_1 z^{-1} + \cdots + b_{n_b} z^{-n_b}, \quad (b_1, \cdots, b_{n_b}) \in \mathbb{R} \tag{2-24b}$$

$$C(z) = c_1 z^{-1} + \cdots + c_{n_c} z^{-n_c}, \quad (c_1, \cdots, c_{n_c}) \in \mathbb{R} \tag{2-24c}$$

$$F(z) = \frac{1 - f_1 z^{-1}}{1 - z^{-1}}, \quad f_1 \in [0, 1]\,. \tag{2-24d}$$

In (2-24), a_i, b_i, c_i are real-valued scalars for $i \in \mathbb{Z}^+$ that denote the coefficients of the polynomials relating to the autoregressive $A(z)$, input $B(z)$ and moving average $C(z)$ parts of the model respectively in the time shift operator z, while n_a, n_b, and n_c denote the orders of the corresponding polynomials, for which $n_b \leq n_a$ and $n_c \leq n_a$. $y(k)$, $u(k)$, and $e(k)$ are the output, input and disturbance, all of which in this case, refer to the predicted BGL, the known insulin infusion rate, and CGM noise. In a classical ARIMAX model, $F(z)$ from (2-24) is an integrator in which the parameter $f_1 = 0$. A non-zero f_1 parameter is useful to eliminate a non-stationary steady-state offset error, but at the expense of introducing a model mismatch, as exemplified in [27].

Model Personalization and System Identification

In view of the large inter-patient variability in body physiology, average or population models, also known as general models, are deemed unsuitable for use by MPC-based APs for achieving good glycemic performance. The need for model personalization can be illustrated by Toffanin *et al.* [175], who compared the performance of two MPC-based controllers subjected to the same configuration and experimental settings, with the difference being the prediction model used. While deriving a personalised model by means of an appropriate system identification method using experimental data from each patient is ideal, its realization is impeded by several obstacles. Firstly, the process of obtaining quantitative data under real-life clinical settings is often time-consuming especially if model personalization involves a large number of patients, thus impractical. A more critical aspect of consideration however, relates to patient safety when an open-loop approach is performed on the patient to obtain *qualitative* data. A common open-loop approach involves the intake of bolus insulin in the absence of CHO intake such as during a fasting period so as to quantify a T1DM patient's glycemic response to only insulin, or feeding persistently-excited insulin quantities to the patient to gather sufficiently rich data. Performing the former could cause an occurrence of hypoglycemia, and the latter discomfort or unforeseen side-effects. These consequences violate the strict safety requirements and constraints imposed on clinical protocols and may consequently endanger the patient [71].

The aforementioned shortcoming can be circumvented by the exploitation of data collected from *in silico* patients using a simulator, as well as empirically-calculated *a priori* clinical information of the patient, such as the FIT tools described in Section 2-1-2. Take for example the control-relevant model by van Heusden and colleagues [182] which was previously introduced, the authors first derived an average insulin-glucose transfer function model based on the output-error parameter estimation approach and also an analysis on the closed-loop bandwidth for each of the ten adult virtual subjects from the UVa/Padova simulator. In the simulation, the authors applied three insulin bolus under fasting conditions across 72 hours, one for each day every 24 h with the number of units of insulin corresponding to the day index from 1 to 3, of the simulation with a time interval of 5 min. It is worth mentioning that the method of applying an insulin bolus impulse to yield a glucose impulse response during fasting conditions is a common technique used to identify a glucose-insulin prediction model in virtual settings among the visited literature. For the identification of output error models corresponding to each virtual patient, van Heusden and colleagues used a window size of 116 samples with a 5 min time interval. The results showed a close proximity in pole locations of the identified output error models across all the patients, with the open-loop systems ex-

hibiting a crossover frequency at approximately 2×10^{-4} rad/s (1.2×10^{-2} rad/min). Having leveraged on the information about the models' pole locations, the authors proceeded by conceiving a personalized model using fixed dynamics but with a varying gain that is dependent on the the correction factor as defined in (2-20) using the 1800-rule, and a pre-defined BGL-dependent safety factor (SF). The transfer function model is expressed as

$$G_i(z^{-1}) = \frac{\mathrm{CF} \cdot \mathrm{SF} \cdot \overbrace{z^{-2}}^{\text{delay}}}{(1-0.98z^{-1})(1-0.965z^{-1})^2} z^{-1}. \tag{2-25}$$

In addition to [182], the control-relevant model is also notable for being deployed in an extensively-researched, personalised zone model predictive control (Z-MPC) strategy by Gondhalekar, Dassau, Doyle and colleagues [89, 86, 87, 88, 162], whose MPC algorithm formed the basis of the first FDA-approved tubeless, on-body AID system: the Omnipod 5 [31]. In addition to *in silico* tests, various clinical trials were conducted to evaluate glycemic performance and safety relating to different purposes, namely the open-loop adjustment and adaptation of basal insulin and CR settings [56][57], unannounced moderate exercise [104], meal insulin bolus challenges [34], technical failures of CGM and insulin pumps [77] among others [35][160]. In addition to the latter, (2-25) has also been employed in H_∞ control [51].

To this end, general considerations on model personalization using the aforementioned approach including the output-error model estimation method have been treated, while the significance of employing a prediction model that can be subjected to a high degree of adaptability and exhibits robust capabilities, such as the parametric time-series models have been outlined. In view of the time-varying insulin sensitivity of T1DM patient's glycemic behaviour, recursive algorithms based on different approaches with respect to the employment of recursive algorithms for model parameter identification of time-series models have been adopted. For time-series models with exogenous inputs, they could either be used to identify the deterministic or stochastic components of the model, or both. For example, in [27, 26], Boiroux and colleagues employed the recursive extended least squares (RELS) to identify the model parameters of only the stochastic part, due to considerations of a potentially unstable system or inaccurate model arising from the coupled effects from administering meals and insulin simultaneously [130]. The disturbance signal was assumed by the authors to be that of a white noise process. The deterministic part, which describes the glucose response model to the exogenous insulin infusion input, is identified *a priori* using *in silico* data from selected virtual patients based on the Hovorka/Cambridge simulator. Other studies that also employed a RELS-based adaptive ARMAX model such as Turksoy *et al.* [181] who proposed an adaptive glucose control approach, Eren-Oruklu *et al.* [69] who , and El-Khatib *et al.* [66] who proposed a bi-hormonal MPC which was employed in the iLet Bionic Pancreas AP device, did so with all the model parameters, using insulin as the sole input for the deterministic model. A forgetting factor was applied in all the studies [27, 26, 181, 69, 66] that places greater emphasis in more recently observed data points. In [69], a time-varying forgetting factor was assigned to the RELS algorithm that is dependent on the size of the disturbance, such as that of measurement noise and food.

Model Validation Methods

Several numerical validation methods are available to validate an identified prediction model. The most commonly used metric is the root-mean-square error (RMSE) and MAE, which can be mathematically expressed as

$$\text{MSE} = \frac{1}{N}\sum_{k=0}^{N-1}(y[k] - \hat{y}[k])^2 \tag{2-26a}$$

and

$$\text{RMSE} = \sqrt{\frac{1}{N}\sum_{k=0}^{N-1}(y[k] - \hat{y}[k])^2} \tag{2-26b}$$

respectively, where $\hat{y}[k]$ represents the model output, and $y(k)$ the actual measurement of the system at time k. N refers to the total number of measurement points that are evaluated in the validation process. The usage of RMSE has been employed to great effect in obtaining a model, and has proven to be a more suitable model for model validation compared to the MAE. This is due to the increased sensitivity to larger errors between the validation dataset and the model's predicted values using the RMSE method, assuming an inconsequential number of outliers in the dataset. The RMSE is however, limited in its efficacy when used for comparing multiple models subjected to different conditions. The *index of fitting* (fit), which normalises the RMSE, is therefore introduced and has been a widely employed tool in APS model development studies [176, 175, 182]. The fit is given by

$$\text{fit} = \frac{1 - ||y(k) - \hat{y}(k)||}{||y(k) - \overline{y}(k)||} \cdot 100\% \tag{2-27}$$

In the presence of noise or disturbances however, the efficacy of fit becomes limited. The Variance accounted for (VAF) is therefore introduced, and has been employed such as in by Cescon *et al.* [41], who developed an adaptive subspace-based prediction model method for T1DM. The VAF takes the normalised variance difference between the prediction model output $\hat{y}$, and the validation data, in this case, the BGL measurements, by diving this difference with the variance of the y, thereby resulting in the model goodness of fit in percentage terms. This can be mathematically expressed as

$$\text{VAF} = \left(1 - \frac{\text{Var}(y - \hat{y})}{\text{Var}(y)}\right) \cdot 100\% \tag{2-28}$$

where the expression $\text{Var}(\cdot)$ denotes the variance of the argument variable. It should be noted that the VAF only assesses the model's behavior and not the actual error between the two datasets, and should only be utilised for a noisy dataset.

2-2-3 Performance Metric and Safety-Critical Constraints

In addition to maximising the TIR and reducing mean BGL, achieving good glycaemic control performance is also subjected to the minimum and maximum BGL across the day, that translates to hyper- and hypoglycaemic risks. Previously, the blood glucose indices (BGI),

comprising of the low (LBGI) and high (HBGI) metrics, was briefly mentioned as one of the key internationally-recognised performance metric in Section 2-1. Using [129] which is based on [114], the LBGI is defined as

$$\text{LBGI} = \frac{10}{N}\sum_{i=1}^{N}\left\{\min\left(0, 0.75\left\{\ln(\text{BG}_i)^{1.44} - 9.02\right\}\right)\right\}^2 \tag{2-29a}$$

and for HBGI

$$\text{HBGI} = \frac{10}{N}\sum_{i=1}^{N}\left\{\max\left(0, 0.75\left\{\ln(\text{BG}_i)^{1.44} - 9.02\right\}\right)\right\}^2 \tag{2-29b}$$

where BG and N in this case refer to the blood glucose measurements and the number of the latter in a given dataset respectively.

Another suitable performance metric is crucial especially for long-term control parameter tuning. In [133, 166], variations of the Control Variability Grid Analysis (CVGA) are proposed [133, 88, 177, 146] as a means of graphically evaluating glucose performance of the respective AP controllers, whereby the respective performances corresponding to each patient are mapped as a function of the minimal and maximum BGL values on the $x-$ and $y-$coordinate, as illustrated in Figures 2-1a and 2-1b. In [133], nine rectangular grid zones are introduced where the gylcaemic performances are rated from A to E. Zone A reflects the safest region of the CVGA as well as the highest levels of control accuracy, and Zone E the most unsafe and highly erroneous control performance. To treat severe hypo- and hyperglycaemia episodes as part of the erroneous control performance category, the second variation of the CVGA proposed by Soru *et al.* [166], in which concentric rings where "upper" and "lower" regions are merged to form a single continuous zone, are introduced representing the four zones from A to D, the latter which is equivalent to zone E in [133]. In addition to its graphical representation, the CVGA has also been used to derive a quantitative performance metric. One such example is the 2-norm of the X_{CVGA} and Y_{CVGA} coordinates [166, 146] given by

$$J = ||X_{\text{CVGA}} \quad Y_{\text{CVGA}}||_2 \tag{2-30}$$

X_{CVGA} and Y_{CVGA} are defined as

$$X_{\text{CVGA}} = \max(\min(110 - \text{BGL}_{\min})) \tag{2-31a}$$

and

$$Y_{\text{CVGA}} = \max(p(\text{BGL}_{\min}), 60), 0) \tag{2-31b}$$

respectively, where

$$p(x) = 2.683 \cdot 10^{-6}\ x^3 - 2.210 \cdot 10^{-3}\ x^2 + 0.754\ x - 59.77$$

is a polynomial that interpolates the points (110,0), (180,20), (300,40) and (400,60).

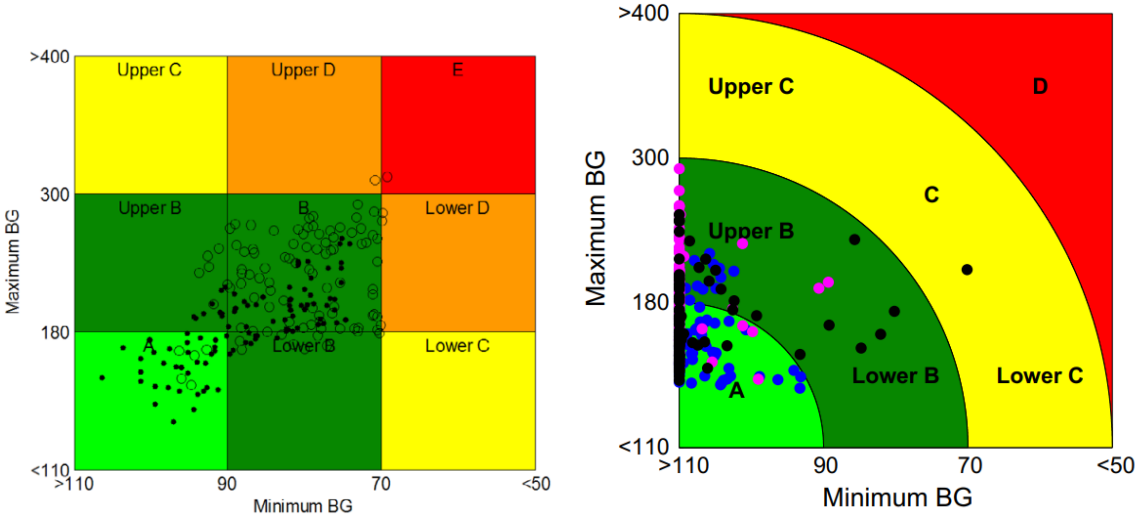

(a) CVGA plot from [133]

(b) CVGA plot from [166].

Figure 2-1: Variations of CVGA plots.

Safety and IOB

Given the extensive attention paid towards the prevention of severe hyper- and hypoglycaemia, safety-critical layers and constraints must be enforced by the APS. Saturating the rate of insulin delivered to a T1DM patient is necessary so as to reduce the likelihood of hypoglycaemia caused by an overly-aggressive control action arising from an inherent plant-model mismatch. Across the examined literature, insulin saturation is primarily influenced by quantities that depend on the CF and IOB. The IOB is a widely used construct in AP design that prevents the closed-loop system from 'stacking' insulin as a consequence of the delay in the insulin action [171]. It provides an approximation of the amount of remaining insulin in the body after the last insulin delivery that has yet to act on the patient's BG.

Ellingsen *et al.* [67] proposed a set of IOB constraints using insulin decay curves of time periods τ_{IOB} between 2 to 8 hours. These curves can be incorporated into rule-based IOB calculations, which are notably utilised in MPC-based AP designs such as in [88] and [146, 177]. A related work by Toffanin *et al.* involves the design of dynamic IOB curves by incorporating the circadian insulin sensitivity variation of T1DM patients [179], differing from those in [67] which were considered to be static. El-Khatib *et al.* proposed another form of IOB computation, which considers the physiological knowledge about the patient's insulin pharmacokinetics, specifically the insulin clearance time and peak effect to model the plasma insulin concentration. In the continuous-time domain, the effects of the fast-acting insulin on the plasma insulin concentration is governed by a bi-exponential model

$$C_{m,\text{pla}}(t) = k_0\, U\ \{\exp(-\tau_1 t) - \exp(-\tau_2 t)\} \tag{2-32}$$

where c_0 is the amplitude of the insulin concentration response, U is the insulin quantity, τ_1 and τ_2 are time constants that influences the time for subcutaneous insulin to peak in blood as well as the time for its (95%) clearance from blood (2-32) (see eq. (18) and SOM Note 3 in the supplementary material of [66]). The accumulated insulin is then calculated by

integrating the plasma insulin concentration function over the time period since the insulin dose was delivered to the patient and . It is worth noting that the length of the accumulated insulin quantity delay curve in (2-32) is related to the 95% clearance time, which functions similarly to the parameter τ_{IOB} that describes the IOB curves in Figure 2-2. The discrete-time equivalent of (2-32) is similar to (2-33b) from Section 2-3.

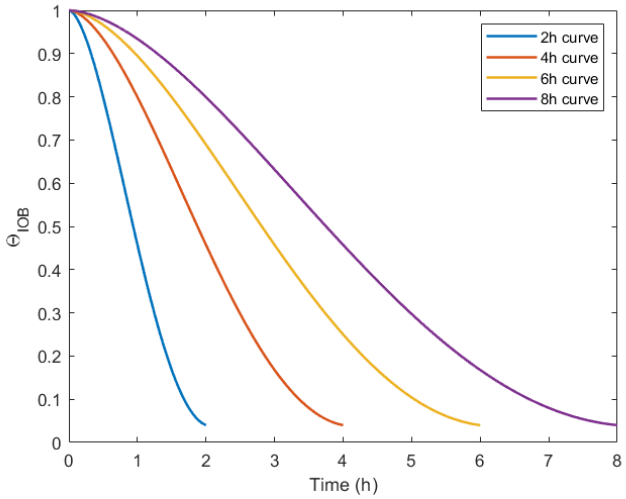

Figure 2-2: Example of IOB curves adapted from [67] corresponding to the different insulin clearance times τ_{IOB} (h). Θ_{IOB} represents the fraction of the insulin infused that is still working up till τ_{IOB} after which at least approximately 95% of it has been cleared, depending on the IOB curve used.

In view of the technological feasibility limitations relating to real measurements of the IOB in a patient's body, novel strategies such as [24] have been proposed in recent years to make theoretical estimates, most often concerning plasma insulin concentration. The strategy designed by Bertachi *et al.* [24] makes use of a dynamic rule-based algorithm for the IOB quantity that is subjected to parameter tuning in a real-world scenario where circadian insulin sensitivity exists. As recent as in 2022, the first clinical trials were conducted by Aiello and colleagues [7] involving an immunosensor capable of measuring plasma insulin concentrations directly from the patient. Subsequently, a state-of-the-art model individualization approach was proposed, involving the use of an Extended Kalman Filter (EKF) that estimates the certain parameters of an insulin pharmacokinetics model from the literature using the immunosensor measurements, as a means to identify a patient-specific model that is capable of estimating plasma insulin concentration and IOB to a higher degree of accuracy.

2-3 Control Methodologies and Analysis

The clinical roles that basal and bolus insulin play in open-loop glucose control in T1DM patients have been outlined in Section 2-1. Basal insulin aims to keep the BGL of a patient at a steady value, while bolus insulin curbs rapid BG hikes using a feedforward fashion, based on prior knowledge of a known disturbance, particularly meal intakes. As opposed

to FIT in which long-acting insulin is injected at various times of the day, basal insulin is delivered continuously during CSII using the fast-acting aspart or lispro, and likewise for insulin bolus. The basal rate is thus treated as a set-point reference input u_{sp} to achieve a certain BGL at steady-state. In the initial literature survey, several PID and MPC works were selected for analysis due to their clinically-validated results. These works include those from research groups who have demonstrated the performance of their respective APs in numerous randomised clinical trials that culminated to the realisation of FDA-approved APS for commercial usage.

In this section, an overview of three PID-based works (see Table 2-3) are considered for analysis, with the remainder dedicated to MPC-based APS control methodologies. It should be noted that establishing an equitable quantitative analysis of the respective controller performance may be challenging for some of the controllers due to differences in the plant model employed in the experiments.

2-3-1 PID Controller

Efforts to model pancreatic insulin secretion of a healthy human body have contributed to the development of PID control in T1DM. A notable example is the works of Steil and colleagues, who drew parallels between the first- and second-phase insulin secretion response of the pancreatic β cells and that of a PID controller [170]. The authors argued in favour of the latter over the modelling of insulin action as an effective countermeasure against BG excursions in the undesirable range, by taking into account the metabolic and mitogenic effects of insulin. It was explained that these effects could pose a safety hazard for impetuous delivery of insulin to the body. Amid the emergence of subcutaneous interaction technology, attempts were made by Steil *et al.* to develop the first PID algorithm [170] that functions in conjuncture with subcutaneous glucose sensing (CGM) and insulin delivery [168] in humans, particularly T1DM patients. Prior observations were included in [170] on studies concerning the insulin secretion constraints imposed on β-cells, which were found to be dependent on the plasma insulin concentrations. Rather than imposing an insulin delivery limit using IOB curves, control action by the PID which sought to emulate that of a β-cell, relied on predicted plasma insulin concentrations that could either be based on a compartment (physiology-based) or autoregressive model, given the absence of real-time insulin measurements [8].

Analysis of PID Methodologies

A successor algorithm to [170] was proposed by Steil *et al.* in [169], in which the most significant difference lies with the introduction of an insulin feedback mechanism, that determines the final deliverable insulin rate given by the expression

$$u_{\text{F}}(k) = (1+\gamma)\ u_{\text{PID}}(k) - \gamma\ C_{m_{\text{pla}}}(k-1) \tag{2-33a}$$

where $C_{m_{\text{pla}}}(k)$ is the plasma insulin concentration at time k which is described by a second-order autoregressive function

$$C_{m_{\text{pla}}}(k) = c_0\ u_{\text{F}}(k-1) + c_1\ C_{m_{\text{pla}}}(k-1) - c_2\ C_{m_{\text{pla}}}(k-2) \cancel{+ c_3\ u_{\text{F}}(k-2)}, \tag{2-33b}$$

γ, c_0, c_1 and c_2 are constant coefficients. The $c_3\ u_{\text{F}}(k-2)$ term is omitted due to $c_3 = 0$.

A similar insulin feedback strategy was also utilised in the PID algorithm of Huyett *et al.* [103], who utilised a non-zero c_3 term in 2-33. Unlike the other two algorithms, Marchetti *et al.*'s [137, 136] however, proposed a time-varying set-point that is rule-based, corresponding to two sensor glucose level (SGL) domains: the first being when the SGL is either ≤ 80 mg/dL, the other > 80 mg/dL, for which in the latter domain, the set-point trajectory changes by an exponential decay relative to the positive deviation of the current SGL from lower bound set-point of 80 mg/dL (see Table 2-3). When SGL increases above 80 mg/dL, the set-point is initiated at y_{sp} and decreases exponentially to 80 mg/dL, which is the lower bound set-point BG that is fixed when the SGL goes below the latter. A switching criteria is implemented such that only after a meal and its corresponding insulin bolus is consumed, the PID controller is initiated when either of the two criteria is satisfied, that is, the BGL reaches its peak value, or that BGL has exceeded 150 mg/dL and the rate of change of glucose increase is more than 15 mg/dl/min.

All three controllers take on the form of a digitalised PID controller in parallel form, but unlike [169] and [136] both of which are in positional form, the velocity form was used in [103]. Another stark difference lies with the operation region of the controller, that is, the intraperitoneal space where insulin is delivered to and glucose sensing takes place in, as opposed to the subcutaneous space. Since system lags are significantly reduced in the intraperitoneal space and thus a faster insulin response, the control problem in [103] can then be confined to one that deals with a standard single-input single-output (SISO) time-series model to facilitate the tuning of PID main parameters which were performed using internal model control (IMC) [164] using the parameters of an average third-order output error glucose-insulin model in discrete-time form, similar to van Heusden *et al.*'s [182]. The PID tuning strategy was adapted from the works of Lee *et al.* [123] who tuned their developed PID controller catered to subcutaneous insulin delivery and glucose measurements, using the parameters from (2-25). Moreover, Huyett *et al.* developed an anti-reset windup strategy that varies the integral gain depends exponentially on the tracking error (i.e. difference between the SG and set-point trajectory) to curb the extent of undershoot caused by a full integral action. This compliments the insulin feedback mechanism in reducing risk of hypoglycaemia, and differs from the technique proposed by Marchetti *et al.* [136] who used a varying set-point without any insulin feedback.

Parameter Tuning

In Steil *et al.*'s PID controller algorithm, the parameters associated with the integral and derivative times were tuned according to prior medical knowledge and *in vivo* trials. The proportional gain K_p is the only one among the three PID parameters which is patient-specific, and is dependent on the subject's TDD and body weight W_{body}. The unknown parameters γ, c_1, c_2 of the insulin feedback model in (2-33) were estimated using the values of the integral time T_i and derivative time T_d. Similarly in [103], K_p is also dependent on the patient's TDD albeit with an additional parameter τ_c, whose value is selected using robust stability and performance considerations.

In [136], the authors assigned two parameters of the PID controller subjected to tuning that achieves the minimum sum of the integral absolute error (IAE) and two exponential terms

relating to the K_p and T_d

$$J = \sum_{k=0}^{k_{\text{inf}}} [\underbrace{y(k) - y_{\text{sp}}}_{\text{IAE}}] + \underbrace{e^{-100(y_{\min} - \overbrace{60}^{\text{Safe minimum}})}}_{\text{Soft constraint } y_{\min}} + \underbrace{e^{-10000(\overbrace{-0.01}^{\text{Upper bound}} - K_p)}}_{\text{Soft constraint } K_p} + \underbrace{e^{-10000(\overbrace{1500}^{\text{Upper bound}} - T_d)}}_{\text{Soft constraint } T_d} \tag{2-34}$$

where $y(k)$ is the measured SGL, y_{sp} is the glucose set-point value and $y_{\min}$ is the minimum observed SGL in the measured dataset of y. $T_d < 1500$ and $K_p < -0.01$ are enforced with soft constraints as described in (2-34). In addition to τ_c, which is subjected to robust stability and performance analysis, the parameters α and γ were subjected to parameter tuning in [103]. These parameters were tuned offline using different values, and analysed based on the post-prandial undershoot.

Performance Analysis

Using nine *in vivo* subjects, Steil *et al.* evaluated their controller performance, with attention paid to the insulin feedback algorithm as well as the effects of the assigned controller parameters, especially K_p. The authors concluded a positive observation from a correlation between the predicted insulin concentration and the measured values, given that that population values, instead of subject-specific ones, of c_1 and c_2 in eq. (2-33) were used, however, they also noted the need to account for intra-patient variability in the subject's pharmacokinetics. In terms of parameter tuning, Steil *et al.* hypothesised that an automated adaptation of K_p would have the most impact on performance, but doing so poses a risk of violating the overall stability of the control system.

Marchetti *et al.*'s control strategy, which was evaluated using the Hovorka model [100] as a virtual patient simulator across a 30-day simulation period, was tested against inaccurate meal estimations. The authors reported an outperformance from their novel control strategy over both the open-loop basal-bolus and PID without the switching criteria and time-varying set-point strategies based on the reported minimum and maximum BGL, as well as shorter setting times. The proposed approach demonstrated its ability to exhibit aggressive settings without sacrificing robustness. Having said, the reported minimum BG for the PID controller was still not within the satisfactory range in the scenario where meal boluses are incorrectly estimated, with BG values reaching below the normoglycaemic threshold of 70 mg/dL.

In [103], the anti-reset windup protection strategy of Huyett *et al.* demonstrated a strong *in silico* TIR performance that is comparable with an MPC approach [122], a control algorithm that is employed in the Omnipod 5 AID device, under the same scenarios when tested using the UVa/Padova metabolic simulator. In addition, the proposed paradigm was shown to have outperformed the subcutaneous insulin delivery-based PD controller developed by Laxminarayan *et al.* [121] under selected scenarios. In a separate study [121], the PD controller of Laxminarayan *et al. et al.* which also employed the same virtual patient simulator, was tested against the performance of Steil *et al.*'s [169] PID controller but under different simulation conditions. The PD controller outperformed the PID controller of Steil *et al.*, and

First Author (Publication)	**PID Characteristics**	***in vivo* Trials**
Steil ([169])	– Fixed SP: 90 (day), 110 (night) $\frac{\text{mg}}{\text{dL}}$ – Fixed K_p, T_i, T_d: • $K_p = \frac{\text{TDD}/\text{W}_{\text{body}}}{135}$, • $T_i = 450$ (day), 150 min (night), • $T_d = 90$ (day), 60 min (night) – Insulin limit: Insulin feedback model (Eq. 2-33)	Yes
Marchetti ([136])	– Varying SP: • 80 $\frac{\text{mg}}{\text{dL}}$ for SGL $\leq$ 80 $\frac{\text{mg}}{\text{dL}}$, • $80 + \text{SGL} - 80\ \exp(\frac{-\text{k}^*}{25})$ otherwise (k^* denotes the relative time from the moment the controller is activated) – Fixed K_p, T_i, T_d: $T_i = 100$ min – Parameter tuning objective: See eq. (2-34) – Tuning parameter: K_p, T_d	No
Huyett ([103])	– Fixed SP: 90 (day), 110 (night) $\frac{\text{mg}}{\text{dL}}$ – Fixed K_p, T_d: • $K_p = \frac{0.023\text{TDD}}{\tau_c+11}$, $T_d = 23.5$ min • Varying $T_i = \frac{273}{K_w}$ min, where $K_w = \exp(-\alpha\lvert e(k)\rvert)$ – Parameter tuning objective: Postprandial undershoot and SGL_{min} – Tuning parameters: τ_c, α, γ – Insulin limit: Insulin feedback model (See eq. (2-33))	No

Table 2-3: Summary of PID controller methodologies discussed in Section 2-3.

one can indirectly infer that the proposed paradigm of Huyett *et al.* would also outperform the latter. It remains however, to be seen if the anti-reset windup strategy when applied to the same PID controller tuning strategy but in the subcutaneous setting [123], can yield comparable results to its intraperitoneal counterpart [103].

2-3-2 Model Predictive Control Analysis

Most state-of-the-art APs that have undergone clinical studies are employ a linear model predictive control (LMPC) approach. The LMPC has shown to be capable of stabilising BGLs, is in spite of the nonlinear property associated with the true dynamics of a T1DM patient. The choice of using a linear prediction model to describe the complex nonlinear glucose-insulin dynamics of diabetic patients is driven by the feasibility of the MPC implementation on a portable AP system, which is characterized by limited battery life and computational power. The LMPC is argued to be sufficiently capable of controlling nonlinear systems using a linear prediction model [187]. In nonlinear MPC (NMPC), the control law is computed by means of solving a non-linear, non-convex optimisation problem. As previously explained, the subcutaneous glucose-insulin pharmacokinetics is highly nonlinear, comprising of multiple compartmental models and other nonlinear phenomena, with some studies advocating for the use of a nonlinear prediction model. Two notable examples are the NMPC developed by Hovorka *et al.* [99] who relied on a nonlinear time varying model whose parameters are adapted online using Bayesian estimation, and in [198], where the authors adapted the prediction model by means of a Recurrent Neural Network. [68]. A major drawback with the employment of the NMPC lies with its expensive computational effort, owing to its inherent high complexity. Given the limited amount of patient-specific parameters or information, as well as the significant inter- and intra-variability among the population of T1DM patients, the use of complex nonlinear models is impeded, rendering its implementation on commercial devices unfeasible from an engineering and safety regulation perspective [130].

Among the MPC methodologies analysed in Table 2-4, those by Gondhalekar *et al.* [88], El-Khatib *et al.* [66] and Patek *et al.* [146] have undergone clinical developments that serve as the primary control algorithms of the Omnipod 5, iLet and Control-IQ AID devices respectively, as summarised in Table 2-2. El-Khatib *et al.*'s insulin-only bionic AP underwent clinical trials of all age groups (adults, children, adolescents) [63, 156, 157]. The extensive randomized clinical trials applied to Patek *et al.*'s AP as well [116, 59, 60, 115, 48, 32]. All except those in [66] and [27, 26] utilised the FDA-approved UVa/Padova Simulator (S2008 and S2013 versions). The Hovorka maximal model was utilised for simulations in [27]. Unlike the other studies, simulations with virtual human patients were not carried out by El-Khatib *et al.* in [66]. Instead, *in vivo* tests involving porcine models of insulin-deficient diabetes were first conducted by the authors, who later established the feasibility of implementation using the same framework with real-life T1DM patients.

Prediction Model

In [146], Patek *et al.* employed model reduction on a linearized version of the nonlinear 13-states UVA/Padova virtual patient model. The linearisation was performed around a certain operating point relating to basal glucose and insulin parameters, with the rest of the

parameters assigned to average values. With model reduction, the resulting model is that of an input-output model, whose states were estimated using past SGL values rather than a state observer. Such a method is arguably inefficient considering that resulting glucose predictions have demonstrated high degrees of plant-model mismatch [175]. Gondhalekar *et al.* utilised a time-series output error model based on van Heusden *et al.*'s control-relevant model (see (2-25), whose input matrix is personalised according to the patient's TDD. Boiroux *et al.* and El-Khatib *et al.* employed an ARMAX glucose-insulin prediction model whose parameters were adapted online using RELS. While Boiroux *et al.* did so only to the stochastic component as explained previously, El-Khatib *et al.* applied teh algorithm to all the parameters of the ARMAX model. Garcia-Tirado *et al.* employed a minimal physiological model based on a modified version of the Bergman minimal model [147] in their proposed MPC design, the RocketAP.

Set-point tracking and Zone MPC

In [93] and [88], both groups of authors utilised a Z-MPC with fixed lower and upper bounds of 80 and 140 mg/dL respectively. Grosman *et al.* also performed an additional experiment with a narrower zonal range between 100 and 120 mg/dL.

For the MPCs that employed the set-point tracking approach, the BGL set point values used during fasting periods ranged between 100 and 130 mg/dL. However, this set-point is not always fixed, and can vary during meal times or follow an exponential decay trajectory across the a given receding horizon, using a similar framework employed by Marchetti *et al.*'s PID-controller reference set-point in [136] that was discussed earlier. Doing so avoids over-delivery of insulin due to delayed reduction in the patient's BGL. In [147], the set-point is fixed at 130 mg/dL in most periods with the exception of a 2 h-interval starting 30 min after the meal is consumed. During that interval, the set-point is set at

$$y_{\text{sp}} = \min(\max(130, y_{\text{CGM}}, 180)) \tag{2-35}$$

during which no penalisation on the the output variable is applied as y_{CGM}, that is, the SGL measurement from the CGM, lingers between the fasting set-point and normoglycaemic range ceiling of 180 mg/dL. Boiroux *et al.* [27] and Garcia-Tirado *et al.* [82] employed an exponential decay function relative decay

$$y_{\text{sp}}(i) = y_{\text{sp0}} + (y_{\text{CGM}} - y_{\text{sp0}}) \exp\left(-\frac{i}{\tau_{\text{sp}}}\right) \tag{2-36}$$

where i denotes the horizon time step, y_{sp0} the nominal set-point, and τ_{sp} the parameter that modulates the rate of approach to the nominal set-point of the controller. Unlike in [82] where the authors only applied (2-36) to SGL values above the nominal set-point of 120 mg/dL, Boiroux *et al.* applied the latter on both positive and negative deviations from the set-point value of 110 mg/dL. The parameters corresponding to the positive and negative deviations (denoted by $\tau_{\text{sp}+}$ and $\tau_{\text{sp}-}$ respectively) are asymmetric, with a smaller value of $\tau_{\text{sp}-}$ than $\tau_{\text{sp}+}$ assigned so as to force the controller to react more aggressively when the SGL falls below the reference value so as to reduce the risks of hypoglycaemia.

Insulin Delivery Actuation

For moments when meals are announced, Gondhalekar *et al.* adopted the two-hour period after the preceding insulin corrections by the MPC when the patient starts consuming food, following the recommendations from endochronologists. This is similar to the strategy adopted by Patek *et al.*, except that the means by which insulin delivery was saturated at the basal rate was enforced by changing the set-point value in Patek *et al.*'s MPC as opposed to in Gondhalekar *et al.*, the insulin limit was enforced as a constraint in the MPC problem. Additionally, Patek *et al.* utilised a rule-based attenuation factor that decreases when the calculated hypoglycaemia risk that is based on the SGL becomes higher. The nominally-calculated insulin is then multiplied by an attenuating factor to yield the final insulin delivery rate.

When there are no meal announcements, for instance during fasting periods or unannounced meal scenarios, it was often the case that the maximum insulin deliverable rate is calculated using the CF described in Section 2-1, and the difference in value between the SGL and the reference value. The mathematical description given by [181]:

$$u_{\max} = \left(0, \frac{y - y_{\text{sp}}}{\text{CF}} \times \frac{60}{T_s} - u_{\text{IOB}}\right) + u_{\text{basal}} \tag{2-37}$$

Parameter Tuning and Adaptation

Online parameter tuning using numerical optimisation methods were not discussed in the selected literature works, with the parameters tuned offline using grid search or trial and error. Having said, adaptable mechanisms were deployed either dependent on the control scenario, or catered to individualised control and modelling. Model parameter adaptation in [64, 66] and [27] have been analysed and will therefore not be treated in this review. Here, only parameters that have been subjected to automatic tuning or adaptation are discussed. Gondhalekar *et al.* designed a velocity-dependent weight that penalises BG excursions above the target zonal range. *Velocity* here refers to the approximation of the rate of change in the output Δy (Refer to Table 2-5 for a glossary of the penalising weight parameters in an MPC controller). The weight Q_{ζ_+} is reduced to a value close to 0 when the MPC senses a negative Δy value. Garcia-Tirado *et al.* proposed an IOB-dependent Q_y strategy in which the penalisation weight decreases to 0 when the IOB crosses a certain threshold, which leaves the rate of change in insulin delivery Δu as the only variable subject to penalisation in the MPC. The authors also introduced a switching, rule-based parameter adaptation scheme for $Q_{\Delta u}$, which is similar to velocity-weighting strategy used in [88], except that it is also dependent on y_{CGM}. In [146], the parameters were tuned to facilitate individualization. Since the cost functions of both MPCs each had only two symmetric weights, only one of the latter is required to be tuned. Patek *et al.* relied on a simple mathematical rule that makes use of a vector of log-transformed clinical parameters (u_{basal}, CR) to tune Q_u. Likewise in [93], Grosman *et al.* who also utilised symmetric weights in their MPC cost function, introduced an automated tuning method for Q_u. Using a simple mathematical-based tuning rule, Q_u was tuned as a function of the settling time of the individualised ARX model when given a step input, and its goodness of fitness, the latter based on (2-27). In a related to study to Patek *et al.*'s [146], the MPC-based AP developed by Toffanin and colleagues [177] underwent testing

with a run-to-run strategy [178] in which the basal insulin delivery rate is adapted at night, and the CR, which relates to the meal bolus calculations, during the day. This tuning strategy employs the TBR and TAR as performance metrics, with both tuning parameters updated using a simple updating law rather than numerical optimization means. The experiment was performed *in silico* using the UVa/Padova S2013 simulator across 8 weeks.

Performance Analysis

In [82], the proposed controller known as the RocketAP, was compared with the state-of-the-art Control-IQ controller whose control algorithm is based on Patek *et al.*'s [146], under scenarios when a CHO intake size of 80 g for dinner was announced and unannounced separately. The RocketAP failed to outperform the baseline controller but rather performed worse in terms of the TIR when dinner was announced (75.7% vs 87.8%). The RocketAP however, did outperform the baseline controller in terms of the TIR in a tighter target range (70 - 140 mg/dL) when the same dinner size was unannounced. This could be attributed to the higher average BGL target set-point of 130 mg/dL as described in (2-35), as opposed to the 120 mg/dL for the RocketAP.

First Author (Publication)	Type	Prediction Model	Cost Function Weights	State Obsv.	Tuned / Adaptable Parameters
Grosman ([169])	Zone (Fixed, 80 – 140, 100 – 120 mg/dL)	ARX (Individualized)	Symmetric: Q_ζ, Q_u	KF	Q_u
Gondhalekar ([88])	Zone (Fixed, 80 – 140)	OE (Individualized using TDD)	Asymmetric: $Q_{\zeta+}$, $Q_{\zeta-}$, Q_{u+}, Q_{u-}, $Q_{(\Delta y)+}$	LO	$Q_{\zeta+}$ (dep. on Δy)
El-Khatib ([64, 66])	Set-point (Fixed, 100 mg/dL)	ARMAX (Online Adaptive) + IOB	Symmetric: Q_y, $Q_{\Delta u}$	KF	Model parameters, Q_y / $Q_{\Delta u}$
Boiroux ([27])	Set-point (Fixed, Exponential)	ARMAX (Online Adaptive)	Symmetric: Q_y, Q_u	KF	Model parameters (Stochastic part)
Garcia-Tirado ([81, 82])	Set-point (Exponential)	Minimal Physiological	Symmetric: Q_y, $Q_{\Delta u}$	KF	Q_y (dep. on IOB), $Q_{\Delta u}$ (dep. on y and Δy)
Patek ([146])	Set-point (Varying)	Input-output derived from linearized physiological maximal model	Symmetric: Q_y, Q_u	—	Q_u

Table 2-4: Summary of MPC methodologies discussed in Section 2-3. (LO — Luenberger Observer, KF — Kalman Filtering)

Variable	Definition
Q_y	Symmetric penalizing weight on SG deviations above and below the target set-point
Q_{y_+}	Symmetric penalizing weight on SG deviations above the target set-point
Q_{y_-}	Symmetric penalizing weight on SG deviations below the target set-point
Q_ζ	Symmetric penalizing weight on SG deviations above and below the upper and lower bound target zones respectively
Q_{ζ_+}	Penalizing weight on SG deviations above the upper bound target zone
Q_{ζ_-}	Penalizing weight on SG deviations below the lower bound target zone
Q_u	Symmetric penalizing weight on insulin infusion deviations above and below the insulin basal (set-point) rate
Q_{u_+}	Penalizing weight on insulin infusion deviations above the insulin basal (set-point) rate
Q_{u_-}	Penalizing weight on insulin infusion deviations below the insulin basal (set-point) rate
$Q_{\Delta u}$	Symmetric penalizing weight on increase and decrease in insulin infusion rate
$Q_{(\Delta y)_+}$	Penalizing weight on increase in SGL
Q_ϵ	Penalizing weight on constraint violations

Table 2-5: Glossary of penalizing weights in Table 2-4 and the MPC formulations in Section 3-2.

2-4 Bayesian Optimisation

2-4-1 Introduction

BO is a sequential model-based approach and statistical method that efficiently models and optimises the computationally expensive so-called "black-box" functions, whose derivatives with respect to the to-be optimised variables cannot be analytically computed. These functions can be treated as an oracle, for which BO makes its computations periodically. Given its recent developments, BO studies on T1DM applications for APs in the literature is limited. Given the possibility that performance function with respect to the parameters may be non-convex, BO can be useful in finding the best parameter values, unlike gradient-based methods, such as policy-gradient, which are local search methods [117]. Five of such studies were found during the literature search by the author and are summarised in Tables 2-6 and 2-7.

The BO framework relies on two primary features [159]:

1. A probabilistic surrogate model, which consists of a prior distribution that describes the assumed behavior of the unknown objective function and an observation model that describes the data generation mechanism. Often, a Gaussian Process (GP) is used to maintain this belief over a certain design space $\mathcal{D}$ [90].

2. A loss function that describes how optimal a sequence of queries are. Loss functions can either take the form of regret, either simple or cumulative in practice. Ideally, the expected loss is minimized to select an optimal sequence of queries.

Additionally, BO makes use of an acquisition function that, according to the authors of [90], expresses the most promising setting for the next experiment, based on the predicted mean and uncertainty of the GP. As noted in [159], the choice of an acquisition function is influenced by the ability to achieve balance between exploration and exploitation. Such acquisitions functions are to be maximised using BO, while considering its non-convexity and complexity. It is therefore imperative to acquire a suitable acquisition function whose variables $\mathbf{w}$ can be analytically optimised compared to the original objective function:

$$\mathbf{w}^* = \arg\max_{w \in \mathcal{W}} f(\mathbf{w}) \tag{2-38}$$

where $\mathcal{W}$ is some design space of interest. The methodological implementation of BO is as follows:

Algorithm 1: Bayesian Optimisation

for $k = 1, 2, \ldots,$ **do**
  select new $\mathbf{w}_{k+1}$ by optimising acquisition function $\doteq \alpha$
    $\mathbf{w_{k+1}} = \arg\max_{\mathbf{w}} \alpha(\mathbf{w}; \mathcal{D}_k)$
  query objective function to obtain y_{n+1}
  augment data $\mathcal{D}_{k+1} = \{\mathcal{D}_k, (\mathbf{w}_{k+1}, y_{k+1})\}$
  update statistical model
end for

in which the subscript k denotes the iteration index. After observing the output of each query of the objective, the prior is updated to produce a more informative posterior distribution over the space of objective functions.

Acquisition function

Many choices for the acquisition functions exists in literature. The common approach to constrained Bayesian optimization is to scale the unconstrained acquisition function with the probability of feasibility, which is simply the cumulative density function of the constraint GP [117]. Although this approach finds the feasible optimum of (3) in [117], it can potentially explore parameter values where the constraints might be violated. While BO is capable of systematically exploring the action space $\mathcal{W}$ in search of a global optimum, it might also pose a problem due to the possibility of violating constraints even in constrained Bayesian optimisation works that handled constraints by scaling the acquisition function with the probability of feasibility (PF) as given in eq. (2) in [118]. Krishnamoorthy and Doyle [118, 119] proposed a safe BO method using interior-point methods that guarantee constraint satisfaction with a sufficiently high probability, in which constraints are enforced by meas of adding log-barrier terms based on the lower confidence bound (LCB) of the constraint GPs to any unconstrained acquisition function. The acquisition function has the form

$$w_k = \arg\min_{w \in W} \alpha^0(w) - \tau \sum_{i=1}^{m} \mathcal{B}_{i,\beta_k}(w) \tag{2-39}$$

where α_0 is the unconstrained acquisition function, $\mathcal{B}_{i,\beta_k}(w) := \ln\left(\mu_{i,k-1} - \sqrt{\beta_{i,k}}\sigma_{i,k-1}(w)\right)$ is the barrier term, and $\tau > 0$ is some smaller user-defined barrier parameter that is reduced iteratively using interior point methods.

2-4-2 Performance Analysis in T1DM Applications

One of the earliest studies that employed BO in T1DM glycaemic control is that by Shi *et al.* [161]. Only a limited number of studies have utilised the optimisation method to treat T1DM. Subsequent studies of the concerned subject matter include those of Cai *et al.* [36] as well as of Krishnamoorthy *et al.* [117, 118, 119] whose works are mainly focused on personalised insulin dose guidance.

In [161], the authors proposed a multivariate BO approach for the purpose of adaptive control in view of the persisting challenges posed on AP adaptation algorithms. One of the BO-tuned parameters that may be relevant to the gylcaemic control problem is the patient-specific CR. Cai *et al.* highlighted a pitfall of relying on CR profiles that could compromised glucose regulation performance, citing the variation of optimal CIR and correction factor (CF) values. The authors instead, employed BO as a means of an insulin bolus regulator, whereby an offline, non-adaptive autoregressive GP model is trained to model the system dynamics. Using asymmetric risk-sensitive cost, insulin bolus amounts, as optimisation variables, are determined using BO. Krishnamoorthy *et al.* [119, 118] on the other hand, similar to Shi *et al.*, sought to employ the BO for tuning the CR, and assumed an unknown cost function that represents a performance metric, modelled using a GP and adopts an online-learning approach. Unlike Shi *et al.* however, the authors did not employ an MPC but rather, they approached the glycaemic control problem as one that follows an open-loop basal-bolus insulin regiment. A single meal of the same CHO size is evaluated per iteration. In another work that was solely proposed by Krishnamoorthy [117], instead of tuning the bolus insulin amount or CR, the author sought to utilise BO for a white-box prediction model learning, and with the employment of an MPC. This is done with prior knowledge of the actual plant which takes on the form of a low-fidelity, minimal physiological model with a dimensionality of 3. The prediction model also takes on the same form, in which Krishnamoorthy intentionally augmented one of its state matrix's model parameter which was subjected to BO tuning. The performance metric is defined by the absolute difference between the average BGL achieved over a 2-h period and a reference BGL value of 81 mg/dL. A similar BO paradigm is employed for all three of these works [119, 118].

2-4-3 Bayesian Optimisation in Other Applications

Several applications have been studied in the literature that pertains to the employment of BO in other applications apart from T1DM, however they do not consider safety in their framework. Piga *et al.* [149] employed the *Identification for Control* (I4C) approach towards a peformance-oriented data-driven MPC design that is used to identify a parameterised subspace prediction model of an inner-loop system controlled with a PID controller for an inverted pendulum application. Shahriari *et al.* [159] reported that the applicability of BO in the field of robotics and reinforcement learning has been successful for the purpose of parameterizing a robot's gait as well as automatic tuning of neural network policy parameters respectively. In view of the increasing complexity caused by perplexing environments, Bansal *et al.* presented a BO-based active learning framework that learns the dynamics in the form of a linear system model achieves the best performance for a given task that is dependent on the observed performance in experiments on the true system. Known as Dynamics Optimization via Bayesian Optimization (aDOBO), the online learning algorithm's working principle resembles

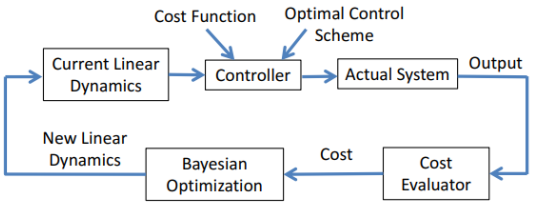

Figure 2-3: Illustration of the aDOBO framweowrk for optimizing the dynamical model for a given cost using the computed cost values. Credits to Bansal *et al.* [17]

that of [149], that is, it places emphasis on identifying a model that yields the best controller performance, thus rendering the need for a highly accurate dynamical model immaterial. A framework of the algorithm can be seen in Figure 2-3.

According to Bansal *et al.*, the tuning of model parameters in adaptive control generally seeks to achieve a good prediction model and does not necessarily maximize the controller performance [17]. This view is similarly shared by Krishnamoorthy [117], who cited the possible negative effects a highly fitted model has on solving optimisation problems in the context of MPC. Having said, implementing BO in medical applications in particular, T1DM, can be an onerous task, since querying the system at an infeasible point may potentially have catastrophic consequences. Such systems require a safe learning framework, whereby safety-critical constraints can be satisfied in the process of finding the optimum performance objective with high probability [117].

First Author (Publication)	**Safety Enforcements**
Shi ([161])	Single parameter tuning at every iteration, Hypoglycaemia risk constraints via $\mathcal{D}_k$ query, Estimated change in performance metric ceiling
Cai ([36])	Monte-Carlo based BO to compute gradient of GP prediction with respect to insulin bolus dosage
Krishnamoorthy [118, 119, 117]	Safe BO using interior-points methods: Log-barrier function added to the lower confidence bound (LCB)-based acquisition function, Lowest postprandial SGL $\geq$ 70 mg/dL

Table 2-6: Summary of safety enforcements applied in the works discussed in Table 2-7.

First Author	Control Approach	Ground Truth	Prediction Model	Performance Metric (BO)	Optimisation Variables
Shi [161]	AP (Zone MPC) [87]	UVa/Padova Simulator Model [53]	Output error model of order 3 [87]	Average BGL throughout day and night	CR, u_{basal}, Q_{u+} tuning
Cai [36]	Open-loop basal + bolus control action using glucose prediction and stochastic optimisation problem (BO)	UVa/Padova Simulator Model [53]	GP regression model (for performance metric computation)	Asymmetric BGL deviation from set-point and bolus insulin penalisation	Insulin Bolus (Control action)
Krishnamoorthy [117]	AP (MPC)	Low fidelity physiological model of order 3 [158]	Same as ground truth except one modified parameter [158]	Absolute difference between mean BGL and 81 mg/dL over 2 h	1 parameter of state matrix
Krishnamoorthy [118]	Open-loop basal-bolus	UVa/Padova Simulator Model [53]	—	Glyceamic Penalty Index [37]	Bolus insulin corresponding to 80 g of CHO intake
Krishnamoorthy [119]	Open-loop basal-bolus	UVa/Padova Simulator Model [53], Hovorka (Cambridge) Simulator Model [189]	—	Maximum Post-prandial BGL increase and +ve deviation from BGL set-point after 6 hours	

Table 2-7: Summary of works discussed in Section 2-4 that employed Bayesian Optimisation for T1DM applications.

2-5 Discussion and Research Gap

2-5-1 Discussion

Prediction Model

Identifiability limitations of several physical parameters and model simplification renders the physiological minimal models tailored to each patient inadequate, even with an extensive individual clinical data of CGM readings, insulin basal-bolus and CHO amounts available for model identification. Factors influencing a patient's pharmacokinetics such as the onset of insulin action, clearance rates, insulin sensitivity, and even gastric emptying vary greatly from patient to patient and also with time, therefore they cannot be directly measured or accurately quantified as parameters of a maximal physiological model. Consequently, BG predictions using a non-adaptive physiological model itself would be insufficient in capturing all the complex biological mechanisms and pathways affecting the blood glucose response behaviour [117]. Moreover, due to the coupling effect between meal insulin bolus and CHO food, the prediction model component representing that of the glucose response to the latter is often omitted. Online adaptation of time-series model parameters does not necessarily yield a set of feasible model parameter solutions where the model's pole locations are restricted to within the unit circle and also a negative insulin gain [27]. A constrained recursive algorithm may be required [180], or by fixing the parameters of the deterministic component like in [27, 26] where only the Kalmain filter gain parameters of the ARMAX model in eq. (2-24c) is adapted recursively.

Alternatively, using simulated data of from a pool virtual patient models representing the variations of pharmacokinetics in the T1DM patient population to obtain an approximate global time-series model in which certain parameters can be individualized, offers a solution to the system identification problem. As demonstrated by Gondhalekar and colleagues [89, 87, 88, 122], the deployment of the control-relevant model [182] whose model gain are adjusted by certain patient-specific clinical parameters, particularly the TDD, in the MPC have proven to be effective, with the AP having undergone clinical validation.

While recent studies [9, 40] that exploited machine learning models with capabilities of modelling non-linear glucose-insulin dynamics rather than linear prediction models can be employed in linear MPC thus facilitating their relevance, in addition to the lack of clinical evidence of their reliability, glycaemic performance in terms of the TIR did not significantly improve compared to conventional linear model-based MPCs like those of [146] and [88], despite evidence of the models demonstrating superior model fitting and prediction accuracy compared to conventional linear models.

Basal rate

Obtaining an accurate value of a T1DM patient's insulin basal delivery rate, which corresponds to a desired BGL steady-state value or set-point can be challenging in practice, due to the circardian variation in insulin sensitivities. In theory, the insulin steady-state value can be determined with a PID controller with sufficient integral action. Due to the relatively slow postprandial response of BGL compared to the time-span between each meal intake however,

observations of the steady-state insulin during the day can be challenging especially with insulin constraints imposed for hypoglycaemia mitigation. As such, parameter tuning of the basal insulin rate tend to be limited to overnight periods, as performed in [161] and [178]. As a result, basal insulin rates tend to be initialised manually by the patient before the use of an AP, using recommendations by a physician.

IOB Settings

In this chapter, two versions of the IOB constraints employed in MPC controllers have been briefly explored, the first based on insulin curves developed by Ellingsen *et al.* [67], and those by El-Khatib *et al.*, which resembles the insulin feedback model deployed in the PID controller paradigm developed by Steil *et al.* [169]. It has been argued by Aiello *et al.* [8] that such insulin estimation methods, which rely on curvilinear or linear decay curves poses an invariance problem when considering intra-patient physiological variations, which led to a novel proposal that involves the use of an EKF and an immunosensor for model identification of insulin pharmacokinetics. While the authors recognise that the concurrent technical limitations associated with the measurements of the immunosensor's novel microneedle sensor, other pitfalls with the proposed approach were not highlighted. Similar to the glucose pharmacokinetics, a more descriptive physiological insulin pharmacokinetics model might not necessarily improve the prediction accuracy of the IOB or overall glycaemic control performance, and the increased dimensionality of the overall model can lead to additional superfluous computation burden.

In [66], El-Khatib *et al.*'s study also demonstrated a large variation in the insulin clearance rate durations across the 11 patients from the *in vivo* trials. This would mean that for every T1DM subject, the length of the IOB delay curves would need to be personalised. However, most of the examined works employed the same set of IOB curves or computation rules for all the patients or virtual subjects that the controllers were tested on. Moreover, in some of the commercial AID devices such as the Medtronic 770G, 780G and Omnipod 5 (see Table 2-2), active insulin time settings is among those that can be manually adjusted by the user [140, 43, 148], suggesting that changes to the insulin decay curve lengths tailored to the patient's specific insulin pharmacokinetics are a necessity.

Parameter and Controller Tuning

Among the discussed literature of AP designs, many have employed heuristics or simple mathematical, rule-based tuning of the parameters within their respective control paradigms. Large volumes of literature have been dedicated to tuning parameters associated with the conventional open-loop insulin therapy, particularly meal boluses and the basal insulin rate in the long-run tuning strategy. Based on the current literature search, the run-to-run approach introduced by Toffanin *et al.*, reinforcement learning by Jafar *et al.* and BO by Shi *et al.* [161] are among the few state-of-the-art works that incorporated the aforementioned two parameter tuning schemes as well as the enforcement of safety constraints into their respective MPC-based AP design frameworks. Through the current literature survey, we have learned that prediction model parameter adaptation catered to specific patient BG needs is key to an effective glycaemic control for model-based control like the MPC. While control adaptation

in T1DM is widely recognised among members from the control community engaged in the research domain, parameter tuning schemes must also take safety into account, which can severely restrict the search freedom of parameters of the algorithm, not to mention the number of evaluations. BO is seen as viable option to circumvent the problem of expensive evaluations, and with the tuning strategy by Shi *et al.* [161] being the only known work that has deployed a BO tuning framework for a personalised MPC-based AP, this leaves room for research avenues in the domain concerning BO.

2-5-2 Research Gap and Directions

In this chapter, the importance of model individualisation, the relevance of enforcing medically-derived safety constraints (e.g. IOB), as well as the need for conventional feedforward meal bolusing before CHO intake in the T1DM glycaemic control problem have been firmly established. We have so far witnessed tuning strategies for the clinical parameter set (e.g. basal rates, CR) and prediction model parameters, but the former is always tuned separately from the latter. Another observation relates to the employment ofCHO intake as a secondary input in the glucose prediction model. This is not considered a viable alternative to feedforward meal boluses, since doing so would require not only relatively accurate dynamical models but also precise information on meal intakes within the various time instances of food consumption. We have considered the significance of varying the IOB decay length tailored to specific patients. So far, no such study were found in the literature to have assigned parameters reflecting the active insulin time in their automated tuning paradigms. While the PID and MPC remain the two most popular controller approaches in the T1DM, to the best of the our knowledge, none from the literature having considered deploying both simultaneously.

Among the MPC topologies examined, the works of Patek *et al.* [146] and Gondhalekar *et al.* [88] are of particular interest. The control architecture of [146] was comprehensively described, comprising of a hierarchy of subsystem layers that prioritises hypoglycaemic preventions, while demonstrating strong TIR performance, in both *in silico* and *in vivo* results. The latter is evidenced by clinical evidence provided by its commercial counterpart, the Control-IQ [106, 141]. In [88], Gondhalekar *et al.* presented an improvement in IOB-defined constraints, where instead of being the curves of specific time lengths (2, 4, 6 and 8 h) proposed in [67], IOB decay curves of arbitrary length can be employed, thus facilitating greater flexibility when it comes to adjustments of the active insulin durations. The Identification for Control (I4C) paradigm proposed by Piga *et al.* presents an opportunity to exploit both the PID and MPC in the proposed control architecture. We also learned in [82], [27] that a time-varying set-point is key to reducing overshoots or undershoots, and even in PID control situations as measure to counter the reset windup effect caused by integral action. Based on the author's knowledge from the encountered literature, the parameter τ_{sp} in (2-36) has thus far been identified either through grid search or other offline methods, especially when it is deployed in the set-point tracking model predictive control (SP-MPC).

In the proposed approach, we can exploit known parameter tuning rules of PID controller parameters, such as the internal model control method, adapted from Lee and Huyett *et al.* [123, 103]. While a complete identification of model parameters is not feasible in a T1DM control task due to patient safety considerations, we can limit the tuning parameters to the input matrix gain, thereby mimicking the concurrent practice of personalising model gain

parameters of time-series models using a single or combination of clinical parameters such as the TDD.

Chapter 3

Proposal of Control System

In the previous chapter, the model structure that governs the pharmacokinetics of Type-1 diabetes mellitus (T1DM) patients in relation to insulin and carbohydrates (CHO) intake effects on blood glucose (BG) concentrations were discussed using the Dalla Man / Cobelli maximal physiological model. Analyses of both conventional and state-of-the-art proportional-integral-derivative (PID) and model predictive control (MPC) approaches brought forth the research gaps presented in Section 2-5. The next step is to adapt concurrent features that are of interest from the literature and incorporate them into the proposed control strategy. In this chapter, a systematic presentation of the research contributions is made, comprising of the various components and algorithms within the artificial pancreas (AP) design along with the key motivations behind each design feature. In Section 3-1, readers are given a mathematical representation of an *in silico* patient that is used for numerical simulations. Section 3-2 introduces the various features of the AP architecture concerning the lower-layer of the control scheme. The Bayesian Optimisation (BO) parameter tuning scheme, which forms the upper-layer of the overall control framework, is discussed in Section 3-3.

3-1 High-fidelity Model for Numerical Simulations

The merits of employing the U.S. Food & Drug Administration (FDA)-approved Uva/Padova model have been broadly highlighted in Section 2-1. In this thesis study, the S2008 version of the metabolic simulator is utilised for *in silico* performance evaluations of the proposed control strategy. Using the parameters corresponding to the cohort of 30 virtual patients (10 adults, 10 adolescents and 10 children) provided by an open-source version of the simulator in Python [193], a MATLAB version was replicated for the purpose of this research. A set of dynamical equations based on the glucose-insulin dynamics and model parameters described in Section 2-1 that governs the pharmacokinetics of the virtual patients are presented as follows:

$$\dot{x}_1 = -k_{\mathbf{GA}2}\ x_1 + d, \tag{3-1a}$$
$$\dot{x}_2 = -k_{\mathbf{GA}3}(x_1, x_2)\ x_2 + k_{\mathbf{GA}2}\ x_1, \tag{3-1b}$$
$$\dot{x}_3 = -k_{\mathbf{GA}1}\ x_3 + k_{\mathbf{GA}3}(x_1, x_2)\ x_2, \tag{3-1c}$$
$$\begin{aligned}\dot{x}_4 = {} & k_{\mathbf{EPG}1} - [k_{\mathbf{EPG}2} + k_{q1}]\ x_4 + k_{q2}\ x_5 - k_{\mathbf{EPG}3}\ x_9 - R_{\mathbf{U},\text{indep}} \\ & - \frac{k'_{\mathbf{GA}1} k_{\mathbf{GA}1}}{W_{\text{body}}}\ x_3 - \max\left(0, k_{\mathbf{E}1}\left[x_4 - k_{\mathbf{E}2}\right]\right),\end{aligned} \tag{3-1d}$$
$$\dot{x}_5 = -\left(\frac{k_{\mathbf{U}1} + k_{\mathbf{U}2}\ x_7}{k_{\mathbf{U}3} + x_5} + k_{q2}\right) x_5 + k_{q1}\ x_4, \tag{3-1e}$$
$$\dot{x}_6 = -(k_{m2} + k_{m4})\ x_6 + k_{m1}\ x_{10} + k_{m_{\mathbf{sc}}1}\ x_{11} + k_{m_{\mathbf{sc}}2}\ x_{12}, \tag{3-1f}$$
$$\dot{x}_7 = -k_{\mathbf{U}m}\ x_7 + k_{\mathbf{U}m}\ \left(\frac{1}{V_m} x_6 - C_{m_{\text{plas,b}}}\right), \tag{3-1g}$$
$$\dot{x}_8 = -k_{\mathbf{EGP}m}\ x_8 - \frac{1}{V_m} x_6, \tag{3-1h}$$
$$\dot{x}_9 = -k_{\mathbf{EGP}m}\ (x_9 - x_8), \tag{3-1i}$$
$$\dot{x}_{10} = -\left(k_{m1} + k_{m3}\right)\ x_{10} + k_{m2}\ x_6, \tag{3-1j}$$
$$\dot{x}_{11} = -(k_{m_{\mathbf{sc}}1} + k_{m_{\mathbf{sc}}3})\ x_{11} + u, \tag{3-1k}$$
$$\dot{x}_{12} = -k_{m_{\mathbf{sc}}2}\ x_{12} + k_{m_{\mathbf{sc}}3}\ x_{11}, \tag{3-1l}$$
$$\dot{x}_{13} = -k_{q_{\mathbf{sc}}}\ x_{13} + k_{q_{\mathbf{sc}}}\ x_4, \tag{3-1m}$$

with an output measured using a subcutaneous continuous glucose monitor (CGM) sensor

$$y_{\text{CGM}} = \frac{x_{13}}{V_q} + v_{\text{CGM}} \tag{3-1n}$$

where v_{CGM} represents the random noise contribution in CGM measurements. Since measurements of y_{CGM} are made every 5 min, we define the parameter that corresponds to the sampling time for the discrete-time control system as $T_s = 5$.

The definitions of the respective model parameters and variables in (3-1) are summarised in Tables 3-1 and 3-2. It is critical to take note of the unit of measurement of the insulin quantity used throughout this thesis. In clinical practice, the conventional unit of measurement of insulin concentration (U/mL) and for the absolute insulin mass (U) are bioefficacy-based, while the Système International (SI) unit of the former and latter are pmol/L and pmol respectively. For the readers' reference, the conversion factor [10] between the conventional and SI unit for human insulin is given by

$$1\ \mu\text{U/mL} = 6.00\ \text{pmol/L}.$$

In the virtual patient model of (3-1), insulin is quantified in terms of its distributed amount with respect to the patient's body mass, expressed in pmol/kg, and for the insulin infusion rate, pmol/kg/min. In conventional practice, the insulin infusion rate is expressed in U/h. One can also utilise the conversion factor from U/h to pmol/kg/min given by

$$1\ \text{U/h} = \frac{100}{W_{\text{body}}}\ \text{pmol/kg/min} \tag{3-2}$$

Symbol	Section 2-1 Notation	Unit
x_1	$Q_{\text{sto},s}$	mg
x_2	$Q_{\text{sto},l}$	mg
x_3	Q_{gut}	mg
x_4	q_{pla}	mg/kg
x_5	q_{tis}	mg/kg
x_6	m_{pla}	pmol/kg
x_7	$C_{m_{\text{inter}}}$	pmol/L
x_8	$C_{m_{\text{liv}}}$	pmol/L
x_9	$C_{m_{\text{liv,delay}}}$	pmol/L
x_{10}	m_{liv}	pmol/kg
x_{11}	$m_{\mathbf{sc},1}$	pmol/kg
x_{12}	$m_{\mathbf{sc},2}$	pmol/kg
x_{13}	$q_{\mathbf{sc}}$	mg/kg

(a) State variables

Symbol	Section 2-1 Notation	Unit
u	$R_{m_{\text{in}}}$	pmol/kg/min
d	$R_{Q_{\text{in}}}$	mg/min

(b) Input variables

Symbol	Section 2-1 Notation	Unit
y_{CGM}	$C_{q_{\mathbf{sc}}}$	mg/dL

(c) Output variable

Table 3-1: UVa/Padova metabolic S2008 variables from (3-1).

Symbol	Unit
$k_{\mathbf{GA}1}$	min^{-1}
$k'_{\mathbf{GA}1}$	-
$k_{\mathbf{GA}2}$	min^{-1}
$k_{\mathbf{EPG}1}$	mg/kg/min
$k_{\mathbf{EPG}2}$	min^{-1}
$k_{\mathbf{EPG}3}$	mg/kg/min per pmol/L
$k_{\mathbf{EGP}m}$	min^{-1}
W_{body}	kg
k_{q1}	min^{-1}
k_{q2}	min^{-1}
V_q	L/kg
k_{m1}	min^{-1}
k_{m2}	min^{-1}
k_{m3}	min^{-1}

Symbol	Unit
k_{m4}	min^{-1}
V_q	dL/kg
$R_{\mathbf{U},\text{indep}}$	mg/kg/min
$k_{\mathbf{E}1}$	min^{-1}
$k_{\mathbf{E}2}$	mg/kg
$k_{\mathbf{U}1}$	mg/kg/min
$k_{\mathbf{U}2}$	mg/kg/min per pmol/L
$k_{\mathbf{U}3}$	mg/kg
$k_{\mathbf{U}m}$	min^{-1}
$C_{m_{\text{pla}},\text{b}}$	pmol/L
$k_{m_{\mathbf{sc1}}}$	min^{-1}
$k_{m_{\mathbf{sc2}}}$	min^{-1}
$k_{m_{\mathbf{sc3}}}$	min^{-1}
$k_{q_{\mathbf{sc}}}$	min^{-1}

(a) UVa/Padova metabolic S2008 model parameter constants as seen in (3-1)

Symbol	Unit
$\bar{k}_{\mathbf{GA}3}$	min^{-1}
$\underline{k}_{\mathbf{GA}3}$	min^{-1}
$k'_{\mathbf{GA}3\downarrow}$	-
$k'_{\mathbf{GA}3\uparrow}$	-

(b) Model parameter constants of $k_{\mathbf{GA}3}$

State	Unit
Q_{sto}	mg
Q_{total}	mg

(c) Time-varying parameters of $k_{\mathbf{GA}3}$

Table 3-2: UVa/Padova metabolic S2008 model parameters.

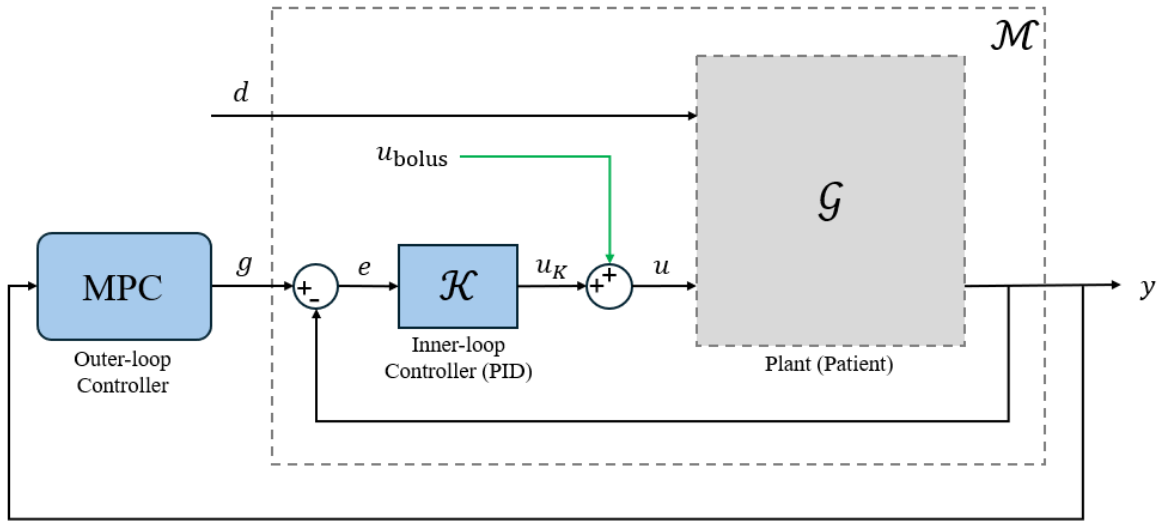

Figure 3-1: Block diagram of the control architecture.

3-2 Control Architecture

In the proposed control architecture, we consider model (3-1) as a *multiple input single output* (MISO) plant $\mathcal{G}$ with dual inputs $\begin{bmatrix} u & d \end{bmatrix}^\top \in \mathbb{R}^2$, with u denoting the insulin infusion rate (U/h) and d (mg/min) the rate at which CHO is consumed by the virtual patient. The former is defined as a controllable input and the latter an uncontrollable input that is treated as a known disturbance. In the hierarchical architecture, the control system comprises of the inner-loop controller which is realised in the form of a discrete-time PID controller $\mathcal{K}$, and an outer-loop controller, that is, an MPC which serves as a reference governor for the inner-loop control system. In control problems where safety is paramount such as T1DM, unconstrained identification of PID controller gains and prediction model parameters is unacceptable. Based on earlier examination of the patients' glucose pharmacokinetics and pole locations [182] in Sections 2-1 and 2-2 respectively, we know however, that $\mathcal{G}$ is exponentially stable, a feature that can be exploited for the proposed paradigm. This obviates the need for the inner-loop controller to be capable of stabilising the plant swiftly [149], so long as *sufficient* stability and safety are guaranteed. By using a PID controller, we seek to achieve improved local linearity in order to be able to employ a linearized prediction model for the MPC and without compromising on the algorithmic computational complexity or output prediction accuracy of the inner-loop model. It is therefore sufficient to tune the PID parameters via empirical means even if their corresponding standalone performance may be sub-optimal.

The MPC on the other hand, as a reference governor, plays a key role in boosting the performance of the inner-loop controller. While increased system linearity might mitigate some of the challenges associated with modelling the non-linear dynamics of $\mathcal{G}$, it does so only partially. Even so, the MPC incorporates insulin-related constraints to address inaccurate insulin delivery rates caused by existential model-plant mismatch, especially in scenarios where significant disturbances are added to the system, such as meal consumption. The insulin limits are not static but dynamic, governed by a Safety Regulation Unit (SRU). In addition,

a MPC switching mechanism involving the zone model predictive control (Z-MPC) and set-point tracking model predictive control (SP-MPC), also governed by the SRU, is introduced as an additional part of our novelty.

During preliminary testing, the *in silico* model of Patient 14 of the virtual simulator model of (3-1) is employed, owing to its high insulin sensitivity, as indicated by the subject's total daily insulin dose (TDD). A high insulin sensitivity implies that there is a higher chance of hypoglycaemic episodes when an over-delivery of insulin occurs. This characteristic is desirable in our controller design scheme, as we strive to robustly challenge the controller's ability to increase the time-in-range (TIR)s of patients without inducing causing hypoglycaemic occurrences.

3-2-1 PID Controller Parameterization

To facilitate the parameter tuning process of the inner-loop system, a continuous-time PID controller is first defined in its standard form, which follows that of establish PID controllers which are designed in digital form [136, 167, 168], given by

$$\mathcal{K}(s) = -K_P \left(1 + \frac{1}{\tau_I\ s} + \frac{\tau_D}{\frac{\tau_D}{N_{D,\mathcal{K}}} + \frac{1}{s}}\right) \tag{3-3}$$

where K_p is the proportional gain (U/h/(mg/dL)), τ_I and τ_D are the integral and derivative time constants respectively. Given that insulin has a negative effect on BG, a negative term is added to model (3-3). Since it is anticipated that noise is inherent in CGM measurements (y_{CGM}), a first-order derivative filter with constant $N_{D,\mathcal{K}}$ is included in the overall PID controller design to mitigate the effects of additive disturbances on control performance.

Procedure

We apply the internal model control tuning approach based on [123], which uses the pole locations of (2-25), to determine the relevant PID parameters. First, the model of (2-25) which has a 5 min sampling interval is converted from discrete- to continuous-time form using the Tustin method, yielding the expression

$$G_c = \frac{0.1308\ k_{G_i}\ (2.5s+1)^3\ e^{-15s}}{(247.5s+1)(140.4s+1)^2} \tag{3-4}$$

where k_{G_i} (mg/dl/(pmol/min)) refers to the model gain parameter of (2-25), which is defined by a product of the correction factor (CF) and safety factor. It is seen in (3-4) that the gain parameter of the model is reduced after the conversion from its discrete-time to continuous time form, with the new gain parameter being

$$k_{G_c} = 0.1308\ k_{G_i}. \tag{3-5}$$

Since the input unit corresponding to the input variable (insulin infusion rate) of model (2-25) used in [182] is pmol/min, a conversion factor to U/h is applied in order to conform to unit consistency. In this chapter, we will use the correction factor calculated using the 1700-rule defined in (2-20). By using the specific patient's TDD value in insulin units (U) instead of

the SI unit (pmol) for the computation of (2-20), this leaves with only the time unit that needs to be mathematically converted. By treating the safety factor as a value of 1, using eq. (3-5), k_{G_c} is expressed as

$$\begin{aligned} k_{G_c} &= 0.1308 \left(\frac{1700}{\text{TDD}}\right) \left[\frac{\text{mg/d}l}{\text{U/min}}\right] \times 60 \text{ [h/min]} \\ &= \frac{1.334\ 10^4}{\text{TDD}} \quad \text{[mg/d}l\text{/(U/h)]}. \end{aligned} \tag{3-6}$$

We reduce (3-4) to a second-order model using Skogestad's half-rule [164], thus giving

$$\widetilde{G}_c = \frac{k_{G_c}\, e^{-\theta_{\tilde{G}_c} s}}{(\tau_{\tilde{G}_c,1} s + 1)(\tau_{\tilde{G}_c,2} s + 1)}, \tag{3-7}$$

where the parameter $\tilde{\theta}_{G_c}$ is calculated using the corresponding pole locations and delay time of G_c

$$\begin{aligned} \tilde{\theta}_{G_c} &= \frac{140.4}{2} + 15 \\ &= 85.2 \\ &\approx 85 \quad \text{[min]}, \end{aligned} \tag{3-8a}$$

$\tau_{G_c,1}$ with the slowest pole:

$$\begin{aligned} \tau_{G_c,1} &= 247.5 \\ &\approx 248 \quad \text{[min]}, \end{aligned} \tag{3-8b}$$

and finally $\tau_{G_c,2}$ using the faster pole:

$$\begin{aligned} \tau_{G_c,2} &= 140.4 + \frac{140.4}{2} \\ &= 210.6 \\ &\approx\ 211 \quad \text{[min]} \end{aligned} \tag{3-8c}$$

Using the calculated parameter values from (3-8), τ_I, τ_D, K_p can be empirically determined by

$$\tau_I = \tau_{G_c,1} + \tau_{G_c,2} \tag{3-9a}$$

$$\tau_D = \frac{\tau_{G_c,1}\tau_{G_c,2}}{\tau_{G_c,1} + \tau_{G_c,2}}, \tag{3-9b}$$

and

$$K_P = \frac{\tau_I}{k_{G_c}\ (\tilde{\theta}_{G_c} + \tau_{\text{c}})} \tag{3-9c}$$

respectively.

The final step of the PID controller formulation procedure involves converting $\mathcal{K}$ from its continous-time form in (3-3) to discrete-time using the zero-order hold (ZOH) method with sampling time $T_s = 5$ min, given by

$$\mathcal{K}(z) = K_P^{(z)} \left(1 + \frac{T_s}{\tau_I^{(z)}\ (z-1)} + \frac{\tau_D^{(z)}}{\frac{\tau_D^{(z)}}{N_{D,\mathcal{K}}} + \frac{T_s}{(z-1)}} \right), \tag{3-10a}$$

or alternatively in its state-space form,

$$\begin{aligned} \xi_{\mathcal{K}}(k+1) &= A_{\mathcal{K}}\ \xi(k) + B_{\mathcal{K}}\ e(k) \\ u_{\mathcal{K}}(k) &= C_{\mathcal{K}}\ \xi(k) + D_{\mathcal{K}}\ e(k). \end{aligned} \tag{3-10b}$$

$K_P^{(z)}$, $\tau_I^{(z)}$, $\tau_D^{(z)}$ are the resulting proportional gain, integral time and derivative time parameters of model (3-10a), and e represents the error tracking variable given by

$$e(k) = y_{\text{sp}}(k) - y_{CGM}(k)$$

in which $y_{\text{sp}}(k)$ is the set-point reference tracking variable.

In the proposed closed-loop control system, a continuous piecetime constant insulin delivery of insulin correction over the time sample T_s is assumed, which follows the approach used in most of the MPCs or other AP-related strategies employed in the literature. It is for this reason that ZOH is employed for the discretization of PID model 3-3 that gave 3-10a, instead of the Tustin method. The Tustin method should be used when emphasis is placed on modelling the dynamic behaviour of the model accurately to yield increased stability margins, such as the case of the discrete- to continous-time conversion of model (2-25) to (3-4) for the design of PID controller parameters.

Assigning the Parameters

As described, τ_I and τ_D can be straightforwardly calculated and assigned as constant parameters of the PID controller (3-3). However with K_P, its value needs to calculated using subject-specific TDD as well as τ_c. In [123], Lee *et al.* experimented on their PID controller under various settings, in which the parameter τ_c was varied between 60 to 300 minutes. The authors deduced that for $\tau_c = 120$, their PID controller achieved the best performance without reported hypoglycaemia events. As such, we will use the same value for τ_C and the *a priori* known TDD quantity to compute the K_P value corresponding all 10 adult *in silico* patients. Table 3-3 summarises the K_P value for each virtual adult patient calculated using eq. (3-9), with the chosen value for τ_c.

Patient Index	K_P ($\tau_c = 120$)
11	8.462×10^{-3}
12	9.713×10^{-3}
13	9.471×10^{-3}
14	5.674×10^{-3}
15	1.147×10^{-2}
16	1.030×10^{-2}
17	7.050×10^{-3}
18	7.180×10^{-3}
19	1.128×10^{-2}
20	1.082×10^{-2}

Table 3-3: Calculated K_P for $\tau_c = 120$ min using (3-9).

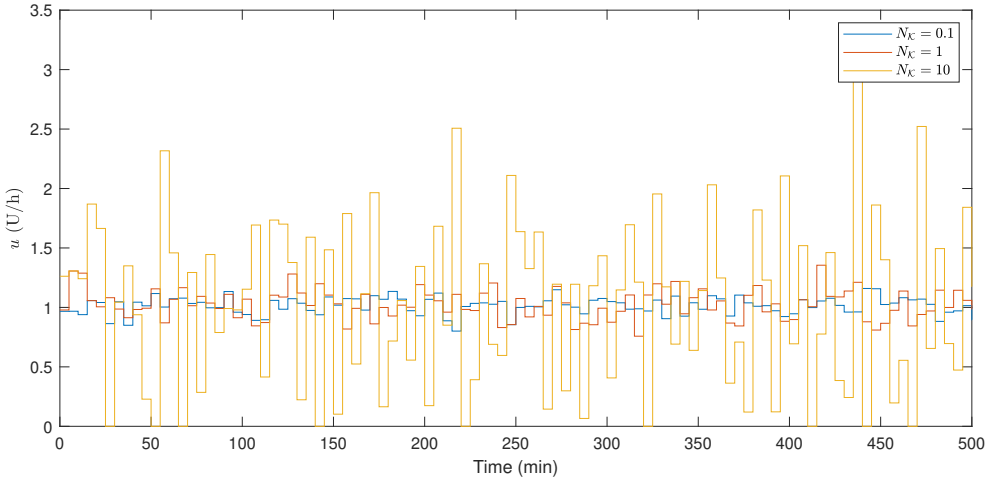

Figure 3-2: Comparative plots of PID controller response to a perturbed measurement output y_{CGM} of Patient 14 for different values of $N_{D,\mathcal{K}}$.

Parameter	Value	Unit
K_p	0.006	U/h/(mg/dL)
τ_I	459	min
τ_D	114	min
$N_{D,\mathcal{K}}$	1	min^{-1}

Table 3-4: Chosen parameter values of PID controller (3-3).

Bearing in mind that patient safety is of priority, we adopt a conservative approach by considering the lowest K_P value from Table 3-3. The controller gain of $K_P = 0.006$ is thus chosen, and is deemed enough to yield a stable response across all the virtual patients. The final step of the PID controller parameterization procedure is to determine a

suitable value for the derivative filter constant $N_{D,\mathcal{K}}$. Considerations on balancing the trade-off between noise attenuation and controller response performance is required. Three values ($N_{D,\mathcal{K}} = 0.1, N_{D,\mathcal{K}} = 1, N_{D,\mathcal{K}} = 10$) were experimented on the controller, with the other parameters assigned to the same values (see Table 3-4). A pseudo-random binary signal was added to the glucose measurement output variable y_{CGM} of Patient 14 during which it is in steady state. The effects of the signal on the resulting control action for the three derivative filter constant values are illustrated in Figure 3-2. From the figure, we can clearly see that there is a significant difference in noise attentuation effect between $N_{D,\mathcal{K}} = 1$ and $N_{D,\mathcal{K}} = 10$. Compared to $N_{D,\mathcal{K}} = 0.1$ on the other hand, we are unable to observe a significant difference. Based on the performance trade-off considerations, a higher filter constant between the latter two is therefore preferred and we finalise the controller parameter design with $N_{D,\mathcal{K}} = 1$.

3-2-2 Prediction Model Parameterization

State-space Formulation

We have established earlier to frame the inner-loop control system as a linear one. The goal is to identify a suitable linear model using the black-box approach, and treat the non-linear glucose-insulin dynamics of the patient, as well as that of the inner-loop system $\mathcal{M}$ as unknowns. To understand the relationship between the realized linear model and $\mathcal{M}$, we first formulate a discrete-time nonlinear mathematical representation of the latter:

$$\begin{aligned} \Xi(k+1) &= f_{\Xi}(\Xi(k), g(k), d(k), k) \\ \begin{bmatrix} y(k) \\ u(k) \end{bmatrix} &= f_{\mathcal{M}}(\Xi(k), g(k), v(k)) \end{aligned} \tag{3-11}$$

where $\Xi \in \mathbb{R}^{N_\Xi}$ denotes the state variables of the inner-loop system $\mathcal{M}$ of dimension N_Ξ, $g \in \mathbb{R}$ represents the control signal of the outer-loop controller, $u \in \mathbb{R}_{\geq 0}$ the rate of insulin infusion that directly controls $\mathcal{G}$, $d \in \mathbb{R}_{\geq 0}$ the rate of food intake, $v \in \mathbb{R}$ the measurement noise and finally $y \in \mathbb{R}_{\geq 0}$, the subcutaneous glucose concentration, also known as the sensor glucose (SG) or sensor glucose level (SGL).

Assuming that the system is in a state of equilibrium at the desired operating point ($g = \overline{g},\ y = \overline{y},\ d = 0$) during a pasting period. Using the first-order Taylor series approximation approach, the deterministic parts of model (3-11) is linearized around ($\overline{g},\ \overline{y}$), resulting in

$$\begin{aligned} \Xi(k+1) &= f_{\Xi}(\overline{\Xi}, \overline{g}, 0, 0) + A_{\mathcal{M}}\ \tilde{\Xi}(k) + B_{\mathcal{M}}\ \tilde{g}(k) + B_{\mathcal{M},d}\ d(k) \\ \begin{bmatrix} y(k) \\ u(k) \end{bmatrix} &= f_{\mathcal{M}}(\overline{\xi}(k), \overline{g}(k)) + C_{\mathcal{M}}\ \tilde{\Xi}(k) + D_{\mathcal{M}}\ \tilde{g}(k) \end{aligned} \tag{3-12}$$

where $A_{\mathcal{M}} \in \mathbb{R}^{N_\Xi \times N_\Xi}$, $B_{\mathcal{M}} \in \mathbb{R}^{N_\Xi \times 1}$, $C_{\mathcal{M}} \in \mathbb{R}^{2 \times N_\Xi}$, $D_{\mathcal{M}} \in \mathbb{R}^2$ and $B_{\mathcal{M},d} \in \mathbb{R}^{N_\Xi \times 1}$ are the matrices governing the linearized dynamics of (3-11), with $\overline{\Xi}$ denoting the corresponding

equilibrium state values at the given operating point. $\tilde{g}$ and $\tilde{y}$ represents the deviation from $\overline{g}$ and $\overline{y}$:

$$\tilde{g} = g - \overline{g}, \quad \tilde{y} = y - \overline{y}.$$

Using the knowledge that y is subjected to reference tracking, when a disturbance is completely rejected, $y = g$ at steady state. Hence, at any time instant k, we treat the values of both operating point values as equal to one another ($\overline{g} = \overline{y}$). Having formulated model (3-12), we now consider augmenting the model to suit the practical needs required of the desired prediction model, assuming that the augmented model can capture the dynamics to a sufficient degree of accuracy. We aim to reduce the parameter space of the prediction model and other complexities associated with the during the model identification process. Regarding meals, by accounting for the impediments surrounding the modelling of BG response to CHO intakes, as well as the meal bolus action which will be explained later, we therefore consider a prediction model with insulin infusion as the sole exogenous input. A standalone model describing only the linearized dynamics without the meal intake component is thus conceived, described by

$$\begin{aligned} \xi(k+1) &= A_M\ \xi(k) + B_M\ \tilde{g}(k) \\ \begin{bmatrix} \tilde{y}(k) \\ u_{\mathcal{K}}(k) \end{bmatrix} &= C_M\ \xi(k) + D_M\ \tilde{g}(k) \end{aligned} \tag{3-13}$$

where $\xi \in \mathbb{R}^{N_M}$ represents the state vector of the linear system model, $A_M \in \mathbb{R}^{N_M \times N_M}$, $B_M \in \mathbb{R}^{N_M \times 1}$, $C_M \in \mathbb{R}^{2 \times N_M}$, $D_M \in \mathbb{R}^2$ are the state-space matrices of the latter. Having omitted the bolus insulin component u_{bolus} from the model, this leaves with only the insulin corrections from the PID controller, u_K as the control action that is regulated by the reference governor in the overall control architecture. We denote this inner-loop system model (3-13) that corresponds only to g as M.

For the sake of comprehensivity, we also consider a scenario where the model corresponding to CHO intake is included, which mirrors the control architecture scheme presented in Fig. 3-1. Model (3-13) can be then be extended to

$$\begin{aligned} \xi(k+1) &= \overbrace{\begin{bmatrix} A_M & 0 \\ 0 & A_{M_d} \end{bmatrix}}^{A_{\tilde{\mathcal{M}}}}\ \xi(k) + \overbrace{\begin{bmatrix} B_M \\ 0 \end{bmatrix}}^{B_{\tilde{\mathcal{M}}}}\ \tilde{g}(k) + \overbrace{\begin{bmatrix} 0 \\ B_{M_d} \end{bmatrix}}^{B_{\tilde{\mathcal{M}},d}}\ \tilde{g}(k) \\ \begin{bmatrix} \tilde{y}(k) \\ u_{\mathcal{K}}(k) \end{bmatrix} &= \underbrace{\begin{bmatrix} C_M & C_{M_d} \end{bmatrix}}_{C_{\tilde{\mathcal{M}}}}\ \xi(k) + \underbrace{\begin{bmatrix} D_M & D_{M_d} \end{bmatrix}}_{D_{\tilde{\mathcal{M}}}}\ \tilde{g}(k) \end{aligned} \tag{3-14}$$

where $A_{M_d} \in \mathbb{R}^{N_{M_d} \times N_{M_d}}$, $B_{M_d} \in \mathbb{R}^{N_{M_d} \times 1}$, $C_{M_d} \in \mathbb{R}^{2 \times N_{M_d}}$, $D_{M_d} \in \mathbb{R}^2$ are the state matrices corresponding to the linear model M_d. The latter forms a secondary sub-system of the overall inner-loop model, with d as its input variable and have a dimensionality of N_{M_d} . The resulting model described in (3-14) represents the *linearized* inner-loop system model $\tilde{\mathcal{M}}$, which is a parallel concatenation of M and M_d, with $A_{\tilde{\mathcal{M}}}$, $B_{\tilde{\mathcal{M}}}$, $C_{\tilde{\mathcal{M}}}$, $D_{\tilde{\mathcal{M}}}$ and $B_{\tilde{\mathcal{M}},d}$ being its state-space matrices with a dimensionality of

$$N_{\tilde{\mathcal{M}}} = N_M + N_{M_d}.$$

Model Formulation and Individualisation

Having defined the relevant state-space models, the next step is to mathematically derive the inner-loop model $\tilde{\mathcal{M}}$, particularly M, which requires understanding the relationship between the outputs of the inner-loop model and its input. The delays associated with subcutaneous sensing from the CGM and insulin onset must also be taken into account and corrected before applying model identification. Similar to before, the derivation of M_d is also be treated.

Let τ_y, τ_u and τ_d denote the delays associated with the CGM measurements, insulin effect and meal disturbance respectively relative to the actual blood glucose level (BGL). We have τ_{uy}, which denotes the observed delay in the output measurements with respect to input, calculated by taking the sum of the insulin effect and sensor delays:

$$\tau_{uy} = \tau_u + \tau_y.$$

Likewise with the observed delayed between the uncontrollable input and output measurement, we have

$$\tau_{dy} = \tau_d + \tau_y.$$

In discrete-time, we denote the respective delays when expressed in terms of time samples as n_y, n_u, n_d, n_{uy} and n_{dy}, all of which correspond to the delays represented by their subscripts. The time sample delays are obtained by multiplying the respective delays by a factor of $\frac{1}{T_s}$. Next, we express the relationship between the outputs y and u and the inputs g and d using the symbols denoting the models $\tilde{\mathcal{M}}$, M and M_d:

$$\begin{bmatrix} y \\ u \end{bmatrix} = \underbrace{\begin{bmatrix} M & M_d \end{bmatrix}}_{\tilde{\mathcal{M}}} \begin{bmatrix} g \\ d \end{bmatrix} \tag{3-15}$$

We can further subdivide $\tilde{\mathcal{M}}$ into four parts, with M and M_d each comprising of a sub-model describing the relationship between each input and output:

$$\tilde{\mathcal{M}} = \begin{bmatrix} M_y & M_{d,y} \\ M_u & M_{d,u} \end{bmatrix} \tag{3-16}$$

where M_y refers to the closed loop system from g to y

$$M_y = z^{-n_{uy}} M_{y0}. \tag{3-17}$$

M_{y0} describes the dynamical relationship between g and y in the absence of delay between the two channels, which can be described analytically by

$$M_{y0} = \frac{\mathcal{K} G_u}{1 + z^{-(n_{uy}+1)} \mathcal{K} G_u}. \tag{3-18}$$

G_u and G_d refers to the linearized open-loop description of the plant's sub-systems from u to y and d to y respectively. Substituting eq. (3-18) into (3-17) yields

$$M_y = \frac{z^{-n_{uy}}\mathcal{K}G_u}{1 + z^{-(n_{uy}+1)}\mathcal{K}G_u} \tag{3-19}$$

Furthermore, using the derivations from Appendix B, we get

$$M_u = \mathcal{K}\left(1 - z^{-1}M_y\right), \tag{3-20a}$$

$$M_{d,y} = z^{-n_{dy}}G_d\ (1 - M_y), \tag{3-20b}$$

$$M_{d,u} = -z^{-(n_{dy}+1)}G_d M_u \tag{3-20c}$$

Returning to the original objective, we can now mathematically express the control system based on model (3-13) as

$$\begin{bmatrix} \tilde{y} \\ u_{\mathcal{K}} \end{bmatrix} = \underbrace{\begin{bmatrix} M_y \\ \mathcal{K}\left(1 - z^{-1}M_y\right) \end{bmatrix}}_{M} \tilde{g}, \tag{3-21}$$

where we treat M as an equivalence to the perceived inner-loop system model $\tilde{\mathcal{M}}$. To realize a suitable parameterization for M, we seek to identify the model parameters of M_{y0} with a reduced order and dimensionality of $N_{M_{y0}} = 2$ with the following state-space matrices:

$$\begin{aligned} A_{My0} &= \begin{bmatrix} a_{11} & a_{12} \\ a_{21} & a_{22} \end{bmatrix} \in \mathbb{R}^{2\times 2}, \quad B_{My0} = \gamma_B \begin{bmatrix} b_1 \\ b_2 \end{bmatrix} \in \mathbb{R}^2, \\ C_{My0} &= \begin{bmatrix} c_1 & c_2 \end{bmatrix} \in \mathbb{R}^{1\times 2}, \quad D_{My0} = 0 \end{aligned} \tag{3-22}$$

where $a_{11} \in \mathbb{R}$, $a_{12} \in \mathbb{R}$, $a_{21} \in \mathbb{R}$, $a_{22} \in \mathbb{R}$, $b_1 \in \mathbb{R}$, $b_2 \in \mathbb{R}$ are scalar parameters to be identified. In the initial stage, we treat the scaling factor of the input matrix as $\gamma_B = 1$.

Identifying the Model

The main goal of the system identification step is to identify a satisfactory set of parameters for model 3-18 that can be globally employed. All identified models and their associated parameters are obtained using the MATLAB *System Identification* toolbox. To obtain a suitable dataset, the first step is to establish an inner-loop system configuration with the PID controller, initialized with the parameters given in Table 3-4. For each numerical simulation performed on an *in silico* subject, the inner-loop system is first stabilised such as the BGL of the virtual patient lies around the desired BG reference point $y_{\text{ref}} = 110$ mg/dL. We aim to linearize the model around this value such that $\overline{y} = y_{\text{ref}} = 110$ mg/dL. Next, we feed a signal corresponding to 80 mg/dL as the reference tracking target for the inner-loop system. This value is chosen since it represents the lower limit of the tight BG target range as defined in Table 2-1. After a suitable dataset was obtained and augmenting to account for delays,

using a sample size of 150 from the obtained data, we use it to identify a state-space model of dimensionality 2 for each of the ten *in silico* patients. The validation results of the identified state-space models are presented in Figure 3-3.

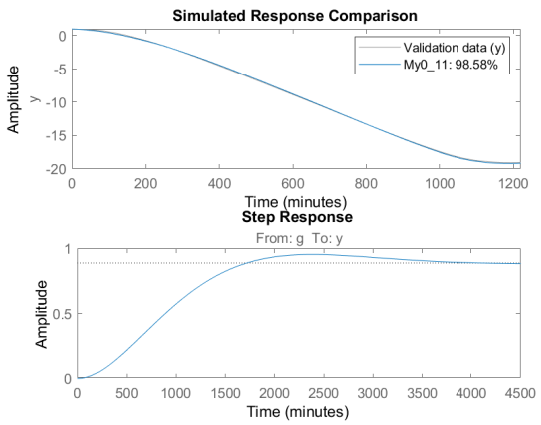

(a) Patient 11

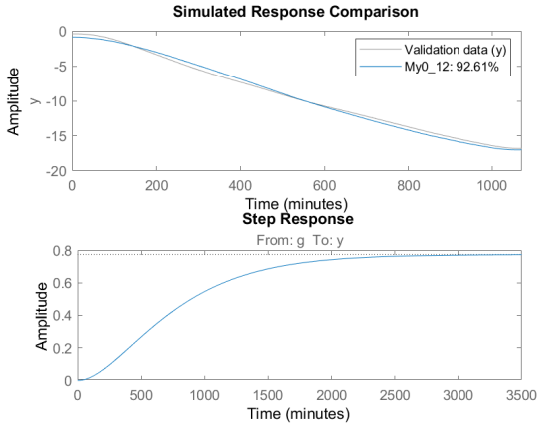

(b) Patient 12

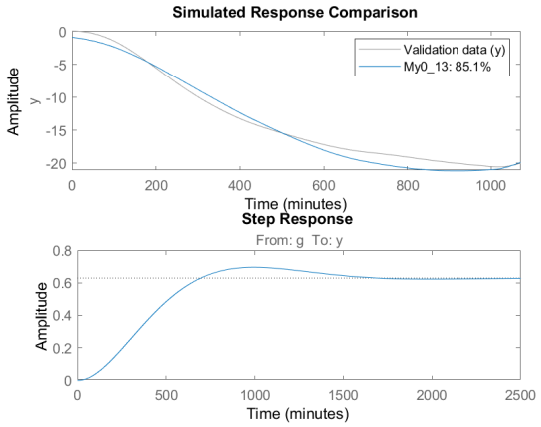

(c) Patient 13

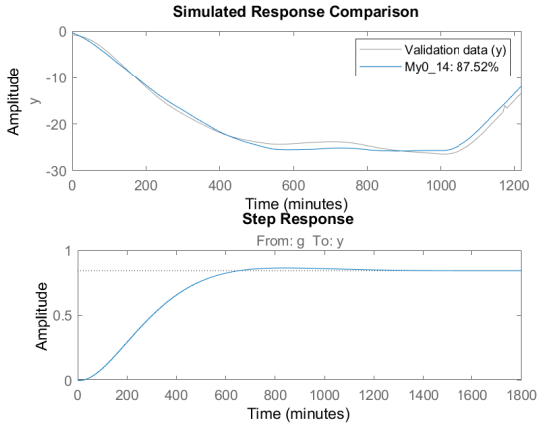

(d) Patient 14

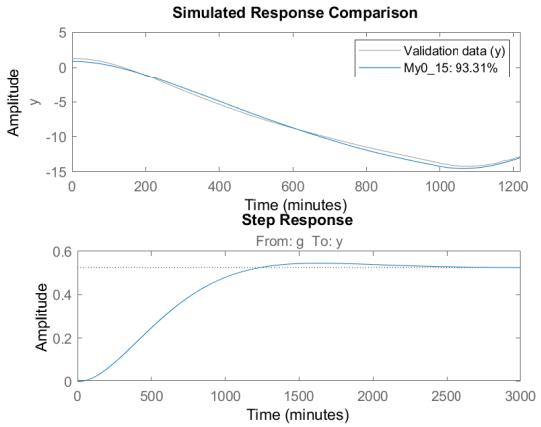

(e) Patient 15

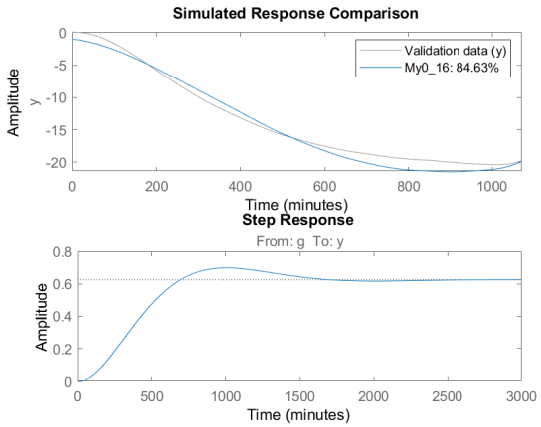

(f) Patient 16

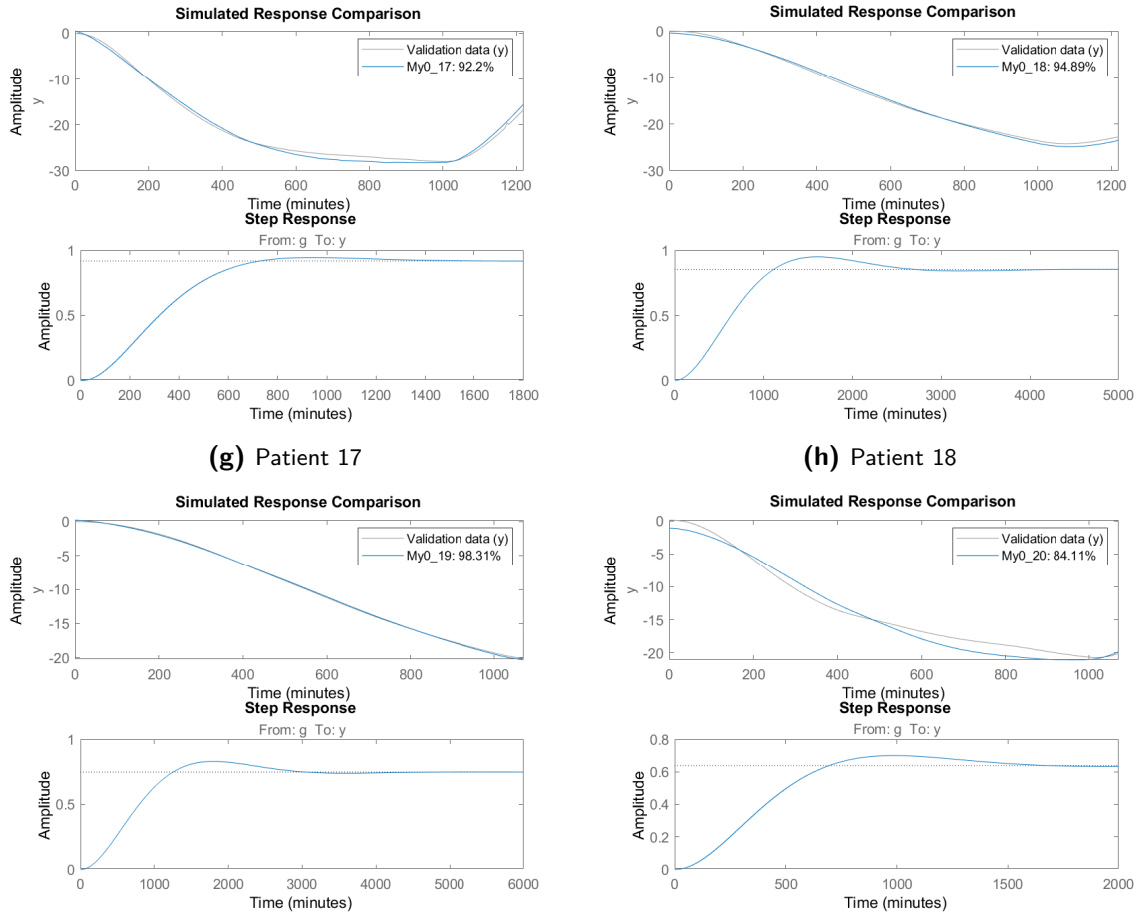

(g) Patient 17 **(h)** Patient 18

(i) Patient 19 **(j)** Patient 20

Figure 3-3: Validation (top) and step (bottom) plot of identified model for each adult virtual patient.

With the parameters of model (3-22) known, we then derive a state-space model for the inner-loop system M using the relation given in (3-21). Using the obtained parameters of models (3-10b) and (3-22), the final state-space of M, when expressed in its minimal realization form, is then given by

$$\begin{aligned}
\xi(k+1) &= \underbrace{\begin{bmatrix} A_{M_{y0}} & 0 & B_{M_{y0}} & 0 & 0 \\ 0 & 0 & 0 & 0 & 0 \\ 0 & I_{n_{\tau_{uy}}-1} & 0 & 0 & 0 \\ 0 & 0 & 0 & A_{\mathcal{K}} & B_{\mathcal{K}} \\ C_{M_{y0}} & 0 & 0 & 0 & 0 \end{bmatrix}}_{A_M} \xi(k) + \underbrace{\begin{bmatrix} 0 \\ 1 \\ 0 \\ -B_{\mathcal{K}} \\ D_{M_{y0}} \end{bmatrix}}_{B_M} \tilde{g}(k) \\
\begin{bmatrix} \tilde{y}(k) \\ u_K(k) \end{bmatrix} &= \underbrace{\begin{bmatrix} C_{M_{y0}} & 0 & 0 & 0 & 0 \\ 0 & 0 & 0 & C_{\mathcal{K}} & -D_{\mathcal{K}} \end{bmatrix}}_{C_M} \xi(k) + \underbrace{\begin{bmatrix} D_{M_{y0}} \\ D_{\mathcal{K}} \end{bmatrix}}_{D_M} \tilde{g}(k)
\end{aligned} \tag{3-23}$$

We can express N_M as a sum of the dimensionalities of M_{y0} and $\mathcal{K}$, as well as the delay $n_{\tau_{uy}}$

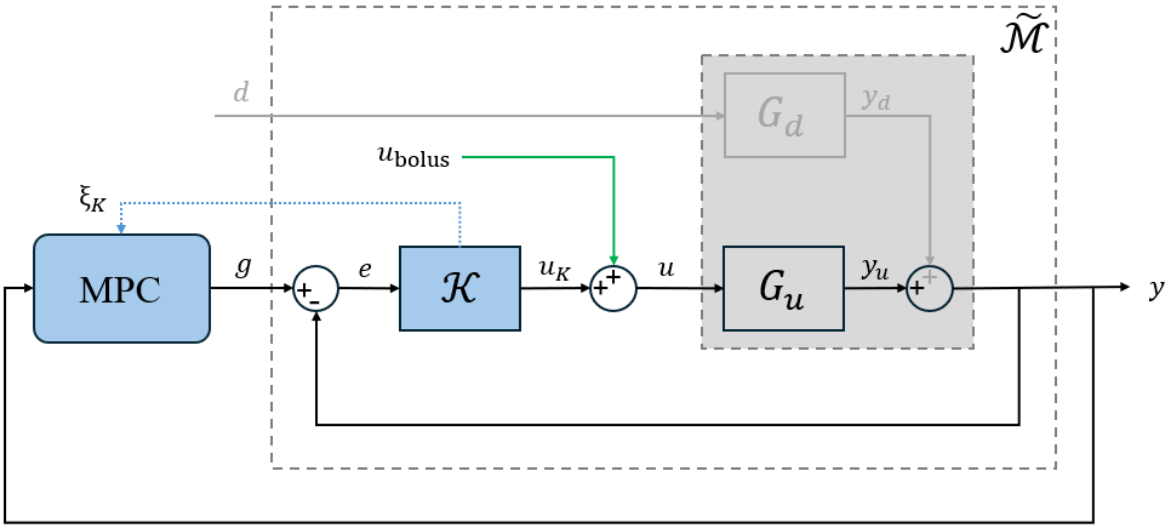

Figure 3-5: Block diagram of the *linear* control architecture, including the contributions of d. Since the latter is omitted in the MPC control scheme, the blocks and notations corresponding to it are given a faded depiction.

and also the delay contribution of z^{-1} in eq. (3-20a):

$$N_M = N_{M_{y0}} + N_{\mathcal{K}} + n_{\tau_{uy}} + 1 \tag{3-24}$$

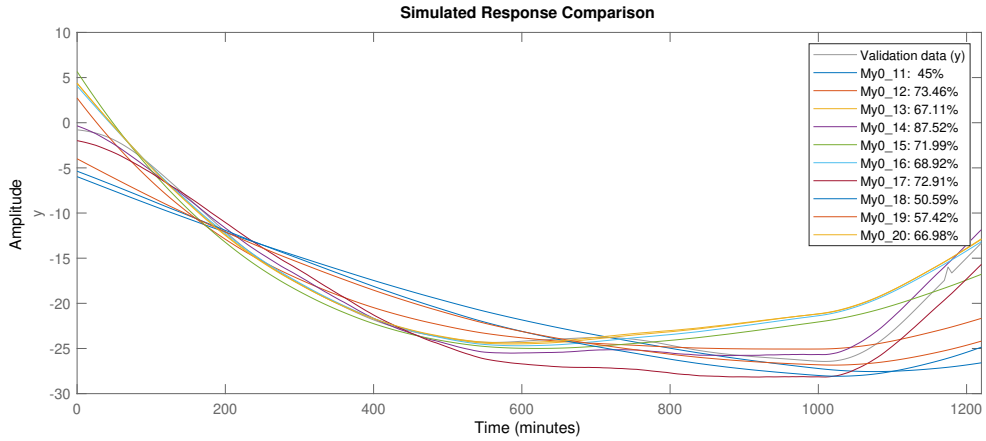

Figure 3-4: Comparative validation plots of all patient models with respect to the validation data of Patient 14.

We select one of the 10 patient models that is to be globally employed by the MPC. When comparing the validation fit for each model to the data used to train a model for Patient 14, we see from 3-4 that among all the identified models, the model corresponding to Patient 13 (`My0_13`) which has a validation fit of 67.11%, was closest to the average validation fit of 66.19% across the all the trained models. With this observation, we thus select the model

parameters corresponding to Patient 13 for the final model design of M_{y0}. The parameter values for model (3-22) are summarised in Table 3-5a.

State Estimator Design

To estimate the staes of the model M, we employ a Luenburger observer with a gain matrix

$$L = \begin{bmatrix} L_{y0} & 0 \end{bmatrix} \in \mathbb{R}^{1 \times N_M} \tag{3-25a}$$

where

$$L_{y0} = \begin{bmatrix} l_1 & l_2 \end{bmatrix} \in \mathbb{R}^{1 \times 2} \tag{3-25b}$$

In the design consideration of L, we consider a balanced trade-off between the estimation error response time and overshoot. Using the MATLAB command '`place`', L_{y0} was fined-tuned using the desired the pole location values of the estimation error response model, ranging between 10 and 25 times faster than those of M_{y0}. The chosen values for l_1 and l_2 are those listed in Table 3-5b.

Parameter	Value	Unit
a_{12}	9.9677×10^{-1}	-
a_{12}	6.6098×10^{-3}	-
a_{21}	4.7205×10^{-2}	-
a_{22}	9.8039×10^{-1}	-
b_1	-4.1482×10^{-7}	-
b_2	-2.7051×10^{-4}	-
c_1	-1.3147×10^{2}	-
c_2	2.1180×10^{-1}	-

(a) Parameters of model (3-22)

Parameter	Value	Unit
l_1	3.9013×10^{-3}	-
l_2	8.5236×10^{-2}	-

(b) Parameters of L_{y0} in (3-25b)

Parameter	Value	Unit
$N_{M_{y0}}$	2	-
$N_{\mathcal{K}}$	2	-
N_M	10	-
$N_{\tilde{M}}$	10	-

(c) Dimentionality value

Parameter	Value	Unit
n_{τ_y}	2	-
n_{τ_u}	3	-
$n_{\tau_{uy}}$	5	-

(d) Time delay (sample) values

Table 3-5: Parameter and constant values from Section 3-2-2

With all the primary parameterization contributions discussed in Sections 3-2-1 and 3-2-2 established, we can thus conceive a realizable inner-loop system control architecture illustrated in Figure 3-5 for the final controller design.

3-2-3 Safety Regulation Unit

In the proposed control paradigm, the Safety Regulation Unit (SRU) is tasked with the dynamic regulation of insulin saturation, insulin bolus delivery prior to meals, as well as the

switching logic between the SP-MPC and Z-MPC. The goal is to establish a safe form of control tailored to individual patients, so as to minimize the occurrence of hypoglycaemia and glycaemic variations during fasting or overnight periods.

IOB Formulation

Computing the estimated insulin-on-board (IOB) in absolute terms refer to the approximated amount of actual active insulin in the patient's body. From a control design perspective however, incorporating the IOB in insulin saturation constraints involves calculating the quantity in terms of insulin delivery rates at specific time instances, denoted by u_{IOB}. We do not include the basal insulin component in the u_{IOB}, only corrections above the the set-point or basal insulin rate. Since the insulin bolus, which is assumed to be administered within one sample time interval of T_s minutes, is delivered in a significant amount compared to automated insulin corrections made during non-meal consumption periods by the PID controller, we treat the estimated u_{IOB} as a sum of two contributing quantities:

$$u_{\text{IOB}} = u_{\text{IOB},\mathcal{K}} + u_{\text{IOB,bolus}} \tag{3-26}$$

The first component $u_{\text{IOB},\mathcal{K}}$, relates to the insulin corrections made by the PID controller from the patient-specific insulin set-point rate u_{sp}. All negative insulin delivery deviations from u_{sp} at every time step are assigned as 0. $u_{\text{IOB,bolus}}$ on the other hand represents the IOB contribution derived from bolus insulin corrections u_{bolus} delivered to the patient on top of u_{sp}, based on calculations made by the bolus insulin calculator described in eq. (3-2-3).

We start by defining the IOB decay curve function [88] as

$$\theta(n,\mathcal{T}) = \begin{cases} \dfrac{1-b_{\text{IOB}}}{1-a_{\text{IOB}}} \cos\left(\arccos(a_{\text{IOB}}) \left(\dfrac{n}{\frac{60\mathcal{T}}{T_s}}\right)^{c_{\text{IOB}}}\right) + \dfrac{b_{\text{IOB}}-a_{\text{IOB}}}{1-a_{\text{IOB}}} & \text{for } 0 \le n \le \frac{60\mathcal{T}}{T_s} \\ 0 & \text{otherwise} \end{cases} \tag{3-27}$$

where $n \in \mathbb{Z}$ refer to the number of time samples since the corresponding insulin correction was infused into the body, and $\mathcal{T}$ the decay curve length expressed in hours (h). The parameter constants of (3-27) are assigned with the following values:

$$a_{\text{IOB}} = 0.995, \quad b_{\text{IOB}} = 0.04, \quad c_{\text{IOB}} = 0.84.$$

Subsequently, at every time step k, we define a vector of IOB fraction values based on eq. (3-27) for the past 8 h corresponding to basal insulin corrections

$$\boldsymbol{\Theta}_{\mathcal{K}}(k) = \begin{bmatrix} \theta(1, \mathcal{T}_{\mathcal{K}}(y_{\text{CGM}}(k))) \\ \theta(2, \mathcal{T}_{\mathcal{K}}(y_{\text{CGM}}(k))) \\ \vdots \\ \theta(N_{\boldsymbol{\Theta}_{\mathcal{K}}}, \mathcal{T}_{\mathcal{K}}(y_{\text{CGM}}(k))) \end{bmatrix} \in \mathbb{R}^{N_{\boldsymbol{\Theta}_{\mathcal{K}}}} \tag{3-28}$$

with a length of

$$N_{\boldsymbol{\Theta}_{\mathcal{K}}} = \frac{480}{T_s},$$

and the bolus insulin corrections for the past $\mathcal{T}_{\text{bolus}}$ h

$$\boldsymbol{\Theta}_{\text{bolus}} = \begin{bmatrix} \theta(1, \mathcal{T}_{\text{bolus}}) \\ \theta(2, \mathcal{T}_{\text{bolus}}) \\ \vdots \\ \theta(N_{\boldsymbol{\Theta}_{\text{bolus}}}, \mathcal{T}_{\text{bolus}}) \end{bmatrix} \in \mathbb{R}^{N_{\boldsymbol{\Theta}_{\text{bolus}}}} \tag{3-29}$$

with a length of $N_{\boldsymbol{\Theta}_{\text{bolus}}} = \dfrac{60\ \mathcal{T}_{\text{bolus}}}{T_s}$, where $\mathcal{T}_{\text{bolus}}$ refers to the estimated bolus insulin active time. As part of the novelty in this thesis, we define $\mathcal{T}_{\text{bolus}}$ as a subject-specific parameter, instead of a fixed value of 4 as used in [88].

Similarly to before, we have a vector of the past automated insulin correction delivery rates

$$\tilde{\mathbf{u}}_{\text{K}}(k) = \begin{bmatrix} \max(0, u_{\mathcal{K}}(k-1) - u_{\text{sp}}(k)) \\ \max(0, u_{\mathcal{K}}(k-2) - u_{\text{sp}}(k)) \\ \vdots \\ \max(0, u_{\mathcal{K}}(k - N_{\boldsymbol{\Theta}_{\mathcal{K}}}) - u_{\text{sp}}(k)) \end{bmatrix} \in \mathbb{R}^{N_{\boldsymbol{\Theta}_{\mathcal{K}}}} \tag{3-30}$$

and that of the bolus insulin

$$\mathbf{u}_{\text{bolus}}(k) = \begin{bmatrix} u_{\text{bolus}}(k-1) \\ u_{\text{bolus}}(k-2) \\ \vdots \\ u_{\text{bolus}}(k - N_{\boldsymbol{\Theta}_{\text{bolus}}}) \end{bmatrix} \in \mathbb{R}^{N_{\boldsymbol{\Theta}_{\text{bolus}}}}. \tag{3-31}$$

The length of the IOB curve for automated insulin corrections used is not fixed, but rather, it depends on the last SG measurement y_{CGM}:

$$\mathcal{T}_{\mathcal{K}}(y_{\text{CGM}}) = \max\left[\min\left(-\frac{y_{\text{CGM}}}{30} + 12,\ 8\right), 2\right] \tag{3-32}$$

The final IOB insulin rate can thus be estimated using the expression

$$u_{\text{IOB}}(k, y_{\text{CGM}}) = \underbrace{\boldsymbol{\Theta}_{\mathcal{K}}^{\top}\ \tilde{\mathbf{u}}_{\mathcal{K}}}_{u_{\text{IOB},\mathcal{K}}} + \underbrace{\boldsymbol{\Theta}_{\text{bolus}}^{\top}\ \mathbf{u}_{\text{bolus}}}_{u_{\text{IOB,bolus}}} \tag{3-33}$$

Insulin Limits

During fasting periods, the nominal insulin limit at time instant k is expressed mathematically as

$$u_{\max,0}(k) = \begin{cases} \max\left(0, 12 + \frac{y_{\text{CGM}}(k) - y_{\text{ref}}}{\text{CF}} \times \frac{60}{T_s} - u_{\text{IOB}}\right) + u_{\text{sp}}(k) & \text{if } y_{\text{CGM}} < y_{\text{ref}} \\ \max\left(0, \frac{y_{\text{CGM}}(k) - y_{\text{ref}}}{\text{CF}} \times \frac{60}{T_s} - u_{\text{IOB}}\right) + u_{\text{sp}}(k) & \text{otherwise} \end{cases} \tag{3-34}$$

in which $\frac{60}{T_s}$ serves as a conversion factor. During this period, u_{sp} is of the same value as the subject-specific basal insulin rate, u_{basal}. A feature in (3-34) that differs starkly from the safe

insulin constraint as defined in (2-37) is the addition of 12 U/h of insulin to the insulin limit when the SG is below the nominal reference value y_{ref} of 110 mg/dL. The introduction of this modification stems from an observation that with constraint (2-37), the MPC is prevented from delivering any insulin corrections when an overshoot is predicted as long as the SGL is below the glucose reference y_{sp}. Through trial and error, the value of 12 was chosen such that it is sufficiently high enough for the controller to curb overshoot, without significant insulin over-delivery. However, when the SG exceeds y_{ref}, constraint (2-37) becomes active for safety reasons.

During post-bolusing and postprandial periods, a different set of insulin constraints as well as its set-point reference value differs from (3-34), with the latter not always equal to u_{basal} for an announced meal scenario. Before we delve into the algorithmic details, we first define the duration parameters (in time steps) using the previously explained parameters relating to the insulin, CGM sensor delays and bolus insulin active time, by the expressions

$$n_{\mathcal{T}_0} = n_{\tau_u} - 1, \quad n_{\mathcal{T}_1} = \frac{120}{T_s} + n_{\tau_y}, \quad n_{\mathcal{T}_2} = \frac{60}{T_s}\mathcal{T}_{\text{bolus}} + n_{\tau_y} \tag{3-35}$$

For any announced or known meal time instance k_{meal}, we define the two time sets $\mathcal{P}_1$ and $\mathcal{P}_2$, which can be mathematically express in mathematical terms as

$$\mathcal{P}_1(k_{\text{meal}}) = \{k \in \mathbb{Z} \mid k_{\text{meal}} - n_{\mathcal{T}_0} \leq k < k_{\text{meal}} + n_{\mathcal{T}_1}\} \tag{3-36a}$$

and

$$\mathcal{P}_2(k_{\text{meal}}) = \{k \in \mathbb{Z} \mid k_{\text{meal}} + n_{\mathcal{T}_1} \leq k < k_{\text{meal}} + n_{\mathcal{T}_2}\} \tag{3-36b}$$

Whenever a meal is 'announced', if the concurrent time step k has reached the time at which the meal bolus for the newly announced meal is given, the parameter k_{meal} is updated with the corresponding meal time.

We define the insulin limits as

$$u_{\max}(k) = \begin{cases} u_{\text{sp}}(k) & \text{if } k \in \mathcal{P}_1 \\ u_{\max,2}(k) & \text{if } k \in \mathcal{P}_2 \\ u_{\max,0}(k) & \text{otherwise} \end{cases} \tag{3-37}$$

where

$$u_{\max,2}(k) = \max\left(0, \frac{y_{\text{CGM}}(k) - \zeta_{\text{upper}}(k)}{\text{CF}} \times \frac{60}{T_s} - u_{\text{IOB}}(k)\right) + u_{\text{sp}}(k) \tag{3-38}$$

The employment of the constraint $u_{\max} = u_{\text{sp}}$ in (3-37) when concurrent time lies within $\mathcal{P}_1$ is adapted from the practice adopted by Gondhalekar *et al.* [88] in which the AP controller cannot deliver any insulin that goes above the basal rate within 2 h after the delivery of insulin based on the recommendations by endocrinologists. We extended this 2 h period (denoted by $\mathcal{P}_1$) by $n_{\mathcal{T}_0} + n_y$ time steps since the delays stemming from insulin effect on BG and subcutaneous CGM measurements need to be accounted for. Instead of having the set-point

insulin value fixed at the insulin basal rate, we introduce the attenuation factors γ_1 and γ_2 to the basal rate during the $\mathcal{P}_1$ and $\mathcal{P}_2$ time periods respectively, resulting in

$$u_{\text{sp},1} = \max\left(0, \min\left(\gamma_1\ u_{\text{basal}} - \frac{\text{CHO} - \overline{\text{CHO}}}{\text{CR}(n_{\mathcal{T}_1} - n_{\mathcal{T}_0})} \times \frac{60}{T_s}, u_{\text{basal}}\right)\right), \tag{3-39a}$$

$$u_{\text{sp},2} = \gamma_2\ u_{\text{basal}}. \tag{3-39b}$$

The set-point reference value for the different time periods in an announced meal scenarios is therefore given by

$$u_{\text{sp}}(k) = \begin{cases} u_{\text{sp},1} & \text{if } k \in \mathcal{P}_1(k_{\text{meal}}) \\ u_{\text{sp},2} & \text{if } k \in \mathcal{P}_2(k_{\text{meal}}) \\ u_{\text{basal}} & \text{otherwise} \end{cases} \tag{3-40}$$

$\overline{\text{CHO}}$ denotes the normalised CHO amount, or the average CHO consumption for a meal. The value for this quantity is not always fixed, and will be defined later in Chapter 4. The introduction of the second component of (3-39a) considers the common practice of using a fixed, estimated TDD value based on average CHO consumption, which does not frequently change with different total meal sizes for each day. Based on intuition, since a larger than usual meal size requires larger insulin boluses, this "excess" insulin needs to be compensated with less insulin delivery in the $\mathcal{P}_1$ period, which could alleviate the risk of hypoglycaemia. The attenuating factors γ_1 and γ_2 are introduced to further mitigate hypoglycaemia after a meal bolus is given for an announced meal. Since the pharmacokinetics in relation to a CHO intake differs for every patient, we define γ_1 and γ_2 as subject-specific parameters.

Bolus Calculation

Using the patient's pre-determined carbohydrate-to-insulin ratio (CR) using rule (2-21b) and (2-37), the final calculated meal bolus that is to be delivered across one sampling time is given by

$$u_{\text{bolus}}(k) = \max\left(0, \left\{\frac{\text{CHO}}{\text{CR}} + \frac{y_{\text{CGM}}(k) - y_{\text{sp}}(k)}{\text{CF}}\right\} \times \frac{60}{T_s} - u_{\text{IOB}}(k)\right), \tag{3-41}$$

Insulin bolus corrections are given to the patient on top of the basal insulin rate delivered by the PID controller. During the time interval when insulin bolus is infused into the patient, the insulin delivered by the controller cannot exceed u_{basal}. As seen in eq. (3-2-3), the term from (3-34) is incorporated in addition to the standard bolus calculation represented by the first term. As a safety measure, a decreased insulin bolus amount is expected for the same meal size when $y_{\text{CGM}} < y_{\text{ref}}$ or if an announced meal intake occurs before the end of the $\mathcal{P}_2$ period corresponding to the last announced meal intake time so as to prevent over insulin delivery. On the other hand when $y_{\text{CGM}} > y_{\text{ref}}$, a larger insulin bolus is supplied to the patient to compensate for the increase in peak BG following a meal consumption.

Safety Regulation Scheme

Details on how insulin limits are defined have been extensively covered in earlier parts of this section. For every meal that is "announced", Safety Regulation Unit follows the protocol defined in Algorithm 1 to regulate the insulin limits, and Algorithm 2 for the switching MPC scheme. The switching MPC scheme works in two ways. The first pertains to the switching mechanism during the day when the Z-MPC is nominally deployed. When the SGL falls below the threshold of $y_{\text{ref}}^{(\text{lower})} = 100$ mg/dL, this will trigger the SP-MPC to activate until $y_{\text{CGM}} > 105$ mg/dL, or when a meal bolus dose for the next meal occuring at $k_{\text{meal,new}}$ is issued to the patient. The second way involves triggering mechanism occurs from midnight to 06:00. Also during this period, a shorter prediction and control horizon time is employed ($N_p = 6$,$N_c = 6$), compared to the nominal settings ($N_p = 15$,$N_c = 10$). The choice of having the SP-MPC to operate during overnight periods is motivated by the fact that there is less expected glycaemic variations, such as meals and other activities. In addition, overnight periods are considered the most ideal time to estimate the basal insulin rate to achieve the given y_{ref}, thereby exploiting the functionality of the inner-loop PID controller. Having said, BG variations can still occur, which would be less effective with the Z-MPC if BG remains within the zonal target range. The employment of the SP-MPC is expected to correct any deviation from y_{ref} in a more active fashion than the Z-MPC. The choice of using shorter prediction and control time horizons settings stems from model-plant mismatch considerations. With an SP-MPC, we expect a more aggressive control action around y_{ref}. The use of shorter prediction and control horizon steps attempts to address the shortcomings associated with potential miscalculated insulin deliveries. It is also useful to consider real-life scenarios when the patient is asleep and low glucose variability is expected. The purpose of steps 2.1 to 2.4 is to account for the possibility of a $\mathcal{P}_2$ that overlaps with the time period after midnight. As long as $\mathcal{P}_2$ is still 'active', the AP will continue employing the Z-MPC. The underlying assumption is that $\mathcal{P}_2$ does not overlap with any time instant beyond 06:00 the next day, and that dinner is consumed before midnight.

Algorithm 1: Pre- and Post-prandial Insulin Safety Scheme for an Announced Meal

1. **initialize** Meal bolus time k_{bolus} for current meal occurring at k_{meal}
   $k_{\text{bolus}} \leftarrow k_{\text{meal}} - n_{\tau_u}$;
2. **initialize** Meal bolus time $k_{\text{bolus,new}}$ for next meal occurring at $k_{\text{meal,new}}$
   $k_{\text{bolus,new}} \leftarrow k_{\text{meal,new}} - n_{\tau_u}$;
3. **for** $k = k_{\text{bolus}}, k_{\text{bolus}} + 1, \ldots, k_{\text{meal}} + n_{\mathcal{T}_2} - 1$ **do**
   - 3.1 **if** $k = k_{\text{bolus}}$ **then**
     $u_{\max}(k) \leftarrow u_{\text{basal}} + u_{\text{bolus}}(k)$;
   - 3.2 **elseif** $k_{\text{bolus}} + 1 \leq k < k_{\text{meal}} + n_{\mathcal{T}_1}$; **then**
     $u_{\max}(k) \leftarrow u_{\text{sp},1}$; (See eq. (3-39a))
   - 3.3 **else**
     - 3.3.1 $u_{\max}(k) \leftarrow u_{\max,2}(k)$; (See eq. (3-38))
     - 3.3.2 **if** $k = k_{\text{bolus,new}} - 1$ **do**
       exit for loop
     - 3.3.3 **end if**
   - 3.4 **end if**
   - 3.5 **continue** experiment
4. **end for**

Algorithm 2: MPC Switching Safety Scheme

while $k < \frac{1440}{T_s}\ N_{\text{days}}$ **do**
1. $k' \leftarrow k \pmod{\frac{1440}{T_s}}$
2. **if** $0 \leq k' < \frac{360}{T_s}$ **then**
   - 2.1 **update** parameters using last (dinner) meal time k_{meal} from previous day
     $$k_{\text{last}} \leftarrow k_{\text{meal}} + n_{\mathcal{T}_2};$$
     $$k'_{\text{last}} \leftarrow k_{\text{last}} \pmod{\frac{1440}{T_s}};$$
   - 2.2 **if** $0 < k'_{\text{last}} < \frac{360}{T_s}$ **then**
     - 2.2.1 **if** $k' \geq k'_{\text{last}}$ **then**
       MPC $\leftarrow$ 'Set-point';
       $N_p \leftarrow 6$;
       $N_c \leftarrow 6$;
     - 2.2.2 **else**
       MPC $\leftarrow$ 'Zone';
       $N_p \leftarrow 15$;
       $N_c \leftarrow 10$;
     - 2.2.3 **end if**
   - 2.3 **else**
     MPC $\leftarrow$ 'Set-point';
     $N_p \leftarrow 6$;
     $N_c \leftarrow 6$;
   - 2.4 **end if**
3. **else**
   - 3.1 MPC $\leftarrow$ MPC;
     $N_p \leftarrow 15$;
     $N_c \leftarrow 10$;
   - 3.2 **if** $y_{\text{CGM}} < 100$ mg/dL; **then**
     MPC $\leftarrow$ 'Set-point';
   - 3.3 **elseif** $y_{\text{CGM}} > 105$ mg/dL **then**
     MPC $\leftarrow$ 'Zone';
   - 3.4 **end if**
4. **end if**
5. **continue** experiment

end while

3-2-4 Model Predictive Control

Problem Formulation

First, let us consider

$$\tilde{\mathbf{g}} = \{\tilde{g}(k),\ \tilde{g}(k+1),\ \cdots,\ \tilde{g}(k+N_p-1)\} \in \mathbb{R}^{N_p}$$

as the set of decision variables in the MPC optimisation problem starting from time instant k, with a prediction horizon N_p and control horizon N_c.

The SP-MPC problem is described as follows:

$$\min_{\tilde{\mathbf{g}}} \quad \sum_{i=n_{\tau_{uy}}+1}^{Np+n_{\tau_{uy}}} \left\{ J_{y_+}(i) + J_{y_-}(i) + J_{(\Delta y)_+}(i) \right\} + \sum_{i=0}^{Np-1} \left\{ J_{u_+}(i) + J_{u_-}(i) + J_{\Delta u}(i) \right\} + Q_\epsilon \, \epsilon^2 \tag{3-42a}$$

$$\text{s.t.} \quad J_{y_+}(i) = Q_{y_+}(i) \, || \max(y(k+i) - y_{\text{sp}}(k+i), 0)||^2, \quad i \in \mathbb{Z}_y \tag{3-42b}$$

$$J_{y_-}(i) = Q_{y_-}(i) \, || \min(y(k+i) - y_{\text{sp}}(k+i), 0)||^2, \quad i \in \mathbb{Z}_y \tag{3-42c}$$

$$J_{u_+}(i) = Q_{u_+}(i) \, || \max(u(k+i) - u_{\text{sp}}(k+i), 0)||^2, \quad i \in \mathbb{Z}_u \tag{3-42d}$$

$$J_{u_-}(i) = Q_{u_-}(i) \, || \min(u(k+i) - u_{\text{sp}}(k+i), 0)||^2, \quad i \in \mathbb{Z}_u \tag{3-42e}$$

$$J_{(\Delta y)_+}(i) = Q_{(\Delta y)_+}(i) \, || \max(y(k+i) - y(k+i-1), 0)||^2, \quad i \in \mathbb{Z}_y \tag{3-42f}$$

$$J_{\Delta u}(i) = Q_{\Delta u}(i) \, ||(u(k+i) - u(k+i-1))||^2, \quad i \in \mathbb{Z}_y \tag{3-42g}$$

$$y(k+i) = \mathbf{M}_y(\xi(k+i), \tilde{g}(i - \tau_{uy} - 1)) + \overline{y} \quad i \in \mathbb{Z}_y \tag{3-42h}$$

$$u(k+i) = \mathbf{M}_u(\xi(k+i), \tilde{g}(i)) \quad i \in \mathbb{Z}_u \tag{3-42i}$$

$$g(k+i) = g(k+N_c-1), \quad i \in \overline{\mathbb{Z}}_g \tag{3-42j}$$

$$u_{\min} - V_u \, \epsilon \leq u(k+i) \leq u_{\max}(k) + V_u \, \epsilon, \quad i \in \mathbb{Z}_u \tag{3-42k}$$

$$\Delta u_{\min} - V_{\Delta u} \, \epsilon \leq u(k+i) - u(k+i-1) \leq \Delta u_{\max}(k) + V_{\Delta u} \, \epsilon, \quad i \in \mathbb{Z}_u \tag{3-42l}$$

$$\tilde{g}_{\min}(k) \leq \tilde{g}(k+i) \leq \tilde{g}_{\max}(k), \quad i \in \mathbb{Z}_g \tag{3-42m}$$

$$(3\text{-}37), (3\text{-}43)\text{–}(3\text{-}46) \tag{3-42n}$$

$$(3\text{-}47) \tag{3-42o}$$

where

$$\begin{aligned}
\mathbb{Z}_y &= \{n_{\tau_{uy}} + 1, n_{\tau_{uy}} + 2, \cdots, N_p + n_{\tau_{uy}}\}, \\
\mathbb{Z}_u &= \{0, 1, \cdots N_p - 1\}, \\
\mathbb{Z}_g &= \{0, 1, \cdots N_c - 1\}, \\
\overline{\mathbb{Z}}_g &= \{N_c, N_c + 1, \cdots N_p - 1\}
\end{aligned}$$

denote the sets of horizon time steps. The definitions of the non-negative weights denoted as Q are as defined in Table 2-5. V_u and $V_\Delta u$ are non-negative scalars that account for the violation factor with respect to u and Δu.

Theoretically, given that soft constraints are enforced in (3-42k), the constraint (3-42m) would at first glance seem redundant. We need to take into account the factor of increasing computation efficiency from an engineering perspective, especially when numerical errors associated with the employment of an optimisation software is concerned. The introduction of (3-42m) seeks to minimize constraint violations in (3-42k). Given that we have access to the state values of the PID controller $\xi_\mathcal{K}$, and accurate information on the model describing the relationship between g and $u_\mathcal{K}$, we can easily compute the limits in constraint (3-42m) by

$$\tilde{g}_{\min}(k) = D_K^{-1} \ (u_{\max} - C_K \ \xi_\mathcal{K}(k)) \tag{3-43a}$$

and

$$\tilde{g}_{\max}(k) = D_K^{-1} \ (u_{\min} - C_K \ \xi_{\mathcal{K}}(k)) \tag{3-43b}$$

respectively. Since insulin cannot be removed from the body, we have

$$u_{\min} = 0. \tag{3-44}$$

We employ a static set of constraints used by Garcia-Tirado *et al.* [82] on $\Delta u_{\min}$ and $\Delta u_{\max}$, given by

$$\Delta u_{\min} = -3, \tag{3-45a}$$

$$\Delta u_{\max} = 3. \tag{3-45b}$$

At every time step k, the corresponding states $\xi(k)$ are initialised using estimated state values, computed in the previous time step by the Luenberger observer:

$$\hat{\xi}(k) = A_M \ \hat{\xi}(k-1) + B_M \ g(k-1) + L \ (y(k-1) - \hat{y}(k-1)) \tag{3-46}$$

The state values in (3-46) that corresponds to $\xi_{\mathcal{K}}$ are manually updated using model (3-10b) with the latest measurements of y_{CGM}.

The time-varying set-point reference trajectory is given by

$$y_{\text{sp}}(k+i) = y_{\text{ref}} + (y_{\text{CGM}}(k) - y_{\text{ref}}) \ \exp\left(-\frac{i - n_{\tau_{uy}}}{\tau_{\text{sp}}}\right) \tag{3-47}$$

for $i \in \mathbb{Z}_y$. In eq. (3-47), y_{ref} refers to the nominal reference value of 110 mg/dL as previously defined and τ_{sp} is a time constant represented in time samples, used to symmetrically modulate the rate by which the patient's BG approaches y_{ref} from above and below. To account for changes in N_p, we define τ_{sp} as a function of the prediction horizon:

$$\tau_{\text{sp}} = \gamma_{\tau_{\text{sp}}} \ N_p, \tag{3-48}$$

where $\gamma_{\tau_{\text{sp}}}$ acts as a modulating factor to the size of τ_{sp}.

For the Z-MPC, the problem is formulated as follows:

$$\min_{\mathbf{g}} \quad \sum_{i=n_{\tau_{uy}}+1}^{Np+n_{\tau_{uy}}} \left\{ J_{\zeta_+}(i) + J_{\zeta_-}(i) + J_{(\Delta y)_+}(i) \right\} + \sum_{i=0}^{Np-1} \left\{ J_{u_+}(i) + J_{u_-}(i) + J_{\Delta u}(i) \right\} + Q_\epsilon \ \epsilon^2 \tag{3-49a}$$

$$\text{s.t.} \quad J_{\zeta_+}(i) = Q_{\zeta_+}(i) \ ||\max(y(k+i) - \zeta(k+i), 0)||^2, \qquad i \in \mathbb{Z}_y \tag{3-49b}$$

$$J_{\zeta_-}(i) = Q_{\zeta_-}(i) \ ||\min(y(k+i) - \zeta(k+i), 0)||^2, \qquad i \in \mathbb{Z}_y \tag{3-49c}$$

$$\zeta(k+i) = \begin{cases} \min(y(k+i), \zeta_{\text{upper}}(k)) & \text{if } y(k+i) > \zeta_{\text{upper}}(k) \\ \max(y(k+i), \zeta_{\text{lower}}(k)) & \text{if } y(k+i) < \zeta_{\text{lower}}(k) \\ y(k+i) & \text{otherwise,} \end{cases} \quad i \in \mathbb{Z}_y \tag{3-49d}$$

$$\text{(3-42d)–(3-42n), (3-50a)–(3-50b)} \tag{3-49e}$$

While the Z-MPC problem closely resembles that of the SP-MPC problem as defined earlier, one stark difference lies with the way that SG deviations are penalised. Rather than a single set-point reference tracking value defined for a particular horizon step, an artificial decision variable ζ is introduced in the optimisation problem. The optimum value of ζ at each horizon step is dependent on the predicted glucose value y and the respective zonal bounds of the target zonal target, as described in constraint (3-49d). Instead of assigning a static set of lower (ζ_{lower}) and upper (ζ_{upper}) bounds for the target zone, we adopt the same underlying principle behind the formulation of (2-35) in [146], which avoids penalising glucose deviations from the reference point or in this case, the upper bound of the zonal range during a certain time period of time after a meal consumption. The bounds are described by the expressions

$$\zeta_{\text{upper}}(k) = \begin{cases} \max\left(y_{\text{ref}}^{(\text{upper})}, y_{\text{CGM}}(k)\right) & \text{if } k \in \mathcal{P}_1(k_{\text{meal}}) \\ \max\left(y_{\text{ref}}^{(\text{upper})}, \min\left(y_{\text{CGM}}(k), \zeta_{\text{upper}}(k-1)\right)\right) & \text{if } k \in \mathcal{P}_1(k_{\text{meal}}) \\ y_{\text{ref}}^{(\text{upper})} & \text{otherwise} \end{cases} \tag{3-50a}$$

and

$$\zeta_{\text{lower}}(k) = \begin{cases} \zeta_{\text{upper}}(k) - \Delta\zeta & \text{if } k \in \mathcal{P}_2(k_{\text{meal}}) \\ y_{\text{ref}}^{(\text{lower})} & \text{otherwise,} \end{cases} \tag{3-50b}$$

where $\Delta\zeta$ refers to the zonal range of the Z-MPC when time $k \in \mathcal{P}_1(k_{\text{meal}})$, for a given announced meal time k_{meal}. $y^{(\text{upper})}$ and $y^{(\text{lower})}$ denote the nominal upper and lower bounds of the target zone respectively, utilised by the Z-MPC. In this thesis work, we assign the parameters in (3-50) with the following values: $y^{(\text{upper})} = 130$, $y^{(\text{min})} = 100$ and $\Delta\zeta = 5$.

Weight design

Various weight adaptation strategies have been proposed in the literature, however, among those that employed a static cost function weight approach, few have considered a glycaemic zone-dependent weight design. The consideration behind this approach lies with the differences in priority for the different glycaemic zones. When BG is above the acceptable limit $y_{\text{ref}}^{(\text{upper})}$, the ratio between positive glucose deviations from the reference point and that of the insulin will be significantly higher than within the target range. If the same set of weights are used, this means that when BGLs are high, for instance after a meal consumption, the penalisation on insulin delivery becomes increasingly less significant, which could result in over-insulin delivery due to delayed glucose response that are not sufficiently account by the prediction model. In other words, the employment of the same set weights across all BGL ranges could lead to an over-aggressive control action and potentially hypoglycaemia. As such, a set of different BG zonal regions are introduced where the same penalising weight parameter can be assigned with different values. For the SP-MPC, the different ranges are defined as follows:

- **Range 1 (SP-MPC)**: $y_{\text{CGM}} < y_{\text{ref}}^{(\text{lower})}$
- **Range 2a (SP-MPC)**: $y_{\text{ref}}^{(\text{lower})} \leq y_{\text{CGM}} < y_{\text{ref}}$
- **Range 2b (SP-MPC)**: $y_{\text{ref}} \leq y_{\text{CGM}} \leq y_{\text{ref}}^{(\text{upper})}$

- **Range 3 (SP-MPC)**: $y_{\text{CGM}} > y_{\text{ref}}^{(\text{upper})}$

and for the Z-MPC:

- **Range 1 (Z-MPC)**: $y_{\text{CGM}} < \zeta_{\text{lower}}$
- **Range 2 (Z-MPC)**: $\zeta_{\text{lower}} \leq y_{\text{CGM}} \leq \zeta_{\text{upper}}$
- **Range 3 (Z-MPC)**: $y_{\text{CGM}} > \zeta_{\text{upper}}$

Unlike the those of the SP-MPC, the range categories defined for the Z-MPC are time-varying, especially during post-prandial periods where the bounds are dependent on y_{CGM}. However, during fasting, overnight or unannounced meal scenarios, they follow the same ranges as the SP-MPC, given the conditions in eq. (3-50). The final weights assigned to the SP-MPC and Z-MPC controllers for each defined CGM range are as shown in Tables 3-6 and 3-7 respectively.

For the SP-MPC, we defined two sub-regions, Range 2a and 2b that exists within what is considered the safe glucose range. The main difference between the two lies with the assigned weights pertaining to glucose deviations. The underlying reason behind this distinction pertains to the management of over and undershoots. When BGL is above the nominal reference, we want to penalise negative glucose deviations more than positive, with the goal of mitigating undershoot, and vice-versa for the case of a BGL that is below the nominal reference with overshoots. We intentionally assigned a higher Q_{y_+}/Q_{y_-} ratio for Range 2a compared to that of Q_{y_-}/Q_{y_+} for Range 2b. This is due to the SP-MPC serving as a contingency MPC in the control scheme when BG falls into Range 1. Since the Z-MPC is less ineffective in dealing with overshoots due the employment of a quiescent target zone, we prioritise the reduction of overshoots when BG is below y_{ref}, more so than with undershoots when BG approaches the nominal reference point from above, considering that there are safety measures in place such as the IOB constraints to manage the latter.

Parameter	**Range 1 (SP-MPC)**	**Range 2a (SP-MPC)**	**Range 2b (SP-MPC)**	**Range 3 (SP-MPC)**
Q_{y+}	10	5	0.5	0.01
Q_{y-}	1	0.1	1	0.5
$Q_{(\Delta y)_+}$	10	10	10	1
Q_{u_+}	1	1	1	1
Q_{u_-}	0.1	1	1	1
$Q_{\Delta u}$	10	10	10	100
Q_ϵ	10^5	10^5	10^5	10^5

Table 3-6: Nominal weights of the Set-point MPC for different y_{CGM} (SGL) ranges

Parameter	Range 1 (Z-MPC)	Range 2 (Z-MPC)	Range 3 (Z-MPC)
$Q_{\zeta+}$	0.1	10	0.1
$Q_{\zeta-}$	1	1	10
$Q_{(\Delta y)_+}$	1	50	1
Q_{u_+}	10	100	10
Q_{u_-}	1	10	10
$Q_{\Delta u}$	10	10	100
Q_{ϵ}	10^5	10^5	10^5

Table 3-7: Nominal weights of the Zone MPC for different y_{CGM} (SGL) ranges

3-3 Performance-Driven Parameter Tuning

To this end, contributions of the lower-layer control architecture has been detailed. The final part of the proposed paradigm pertains to the tuning of selected parameters that have been previously defined in Section 3-2. The performance-driven parameter tuning proposed here utilises BO in two stages: the first to tune clinical-related parameters, and the second a controller-related and a prediction model parameter. The to-be-tuned parameters in the first and second stage of the tuning process are first defined in vector form $\mathbf{w} \in \mathcal{W}$ and $\mathbf{o} \in \mathcal{O}$ respectively, where $\mathcal{W}$ and $\mathcal{O}$ refer to the admissible domains of $\mathbf{w}$ and $\mathbf{o}$. Each parameter vector is treated as set of decision variables in the optimisation problem that yields a performance cost $J_{\mathbf{w}}$ for $\mathbf{w}$ and $J_{\mathbf{o}}$ for $\mathbf{o}$. At every iteration evaluation, the performance costs are computed from the dataset $\mathbf{y}$ containing 288 glucose measurements of y_{CGM}, which is equivalent to an entire day (1440 min or 24 h). Each BO iteration occurs once at the same time instance on each day. Evaluation takes place one time step before the first meal bolus dose for breakfast is released to the patient.

In the Stage 1 BO tuning framework, we consider four parameters: γ_1 and γ_2 , the CR as well as $\mathcal{T}_{\mathrm{bolus}}$. γ_1 and γ_2 (see eq. (3-39)) act as attenuating factors that reduce the set-point insulin delivery rate u_{sp} during post-prandial periods $\mathcal{P}_1$ and $\mathcal{P}_2$ respectively so as to manage hypoglycaemia. In addition to its effect on the IOB (u_{IOB}), the bolus insulin decay length $\mathcal{T}_{\mathrm{bolus}}$ (see eq. (3-29)) influences the length of the time period that defines $\mathcal{P}_2$. We define the parameter vector for the Stage 1 BO tuning scheme as

$$\mathbf{w} = \begin{bmatrix} \mathbf{w}(1) & \mathbf{w}(2) & \mathbf{w}(3) & \mathbf{w}(4) \end{bmatrix}^\top \tag{3-51a}$$

where each vector element represents a parameter:

$$\mathbf{w}(1) \equiv \gamma_1,\ \mathbf{w}(2) \equiv \gamma_2,\ \mathbf{w}(3) \equiv \mathrm{CR},\ \mathbf{w}(1) \equiv \mathcal{T}_{\mathrm{bolus}}. \tag{3-51b}$$

In the Stage 2 BO tuning framework, we consider two parameters: γ_B, which represents the input gain scaling factor (see eq. (3-22)), and $\gamma_{\tau_{\mathrm{sp}}}$ which relates to the length of τ_{sp} (see (3-48)) that is responsible for modulating the set-point tracking trajectory in the SP-MPC. We therefore define the parameter vector for the Stage 2 BO tuning scheme as

$$\mathbf{o} = \begin{bmatrix} \mathbf{o}(1) & \mathbf{o}(2) \end{bmatrix}^\top \tag{3-52a}$$

where the vector elements represent the following parameters:

$$\mathbf{o}(1) \equiv \gamma_B, \ \mathbf{o}(2) \equiv \gamma_{\tau_{\text{sp}}} \tag{3-52b}$$

Next, under the hierarchical architecture of 3-5, we define the respective control design problems as

$$\min_{\mathbf{w} \in \mathcal{W}} \ J_{\mathbf{w}}(\mathbf{y}; \mathbf{w}) \tag{3-53a}$$

and

$$\min_{\mathbf{o} \in \mathcal{O}} \ J_{\mathbf{o}}(\mathbf{y}; \mathbf{o}), \tag{3-53b}$$

where

$$J_{\mathbf{w}}(\mathbf{y}; \mathbf{w}) = \sqrt{\frac{1}{N_{\mathbf{y}_\mathbf{w}}} \sum_{k=1}^{N_{\mathbf{y}_\mathbf{w}}} (\mathbf{y}(k) - y_{\text{ref}})^2} + \overline{y}_{\text{peak}} + \exp(\min(95 - y_{\min}, 12)) \tag{3-54}$$

and

$$\begin{aligned} J_{\mathbf{o}}(\mathbf{y}; \mathbf{o}) = &\sqrt{\frac{1}{289 - N_{\mathbf{y}_\mathbf{o}}} \sum_{k=N_{\mathbf{y}_\mathbf{o}}}^{288} \left\{ \beta_{\mathbf{o}} \max\left(\mathbf{y}(k) - y_{\text{ref}}, 0\right) + \min\left(\mathbf{y}(k) - y_{\text{ref}}, 0\right) \right\}^2} \\ &- y_{\min} + \exp(\min(95 - y_{\min}, 12)). \end{aligned} \tag{3-55}$$

$N_{\mathbf{y}_\mathbf{w}}$ denotes the index of the dataset $\mathbf{y}$ that corresponds to the final real time step at which the glucose deviation error is accounted for in the performance cost, while $\overline{y}_{\text{peak}}$ refers to the average recorded peak BG corresponding to all the announced meals taken during the 24-h recorded period. $y_{\min}$ is the minimum recorded SGL in the dataset $\mathbf{y}$. $N_{\mathbf{y}_\mathbf{o}}$ denotes the index of the dataset $\mathbf{y}$ that corresponds to the first real time step at which the glucose deviation error is accounted for in the performance cost, while $\beta_{\mathbf{o}}$ is a penalisation factor on positive glucose deviations in the dataset $\mathbf{y}$. In this thesis work, we define the parameters as $\beta_{\mathbf{o}} = 20$, $N_{\mathbf{y}_\mathbf{w}} = 228$ and $N_{\mathbf{y}_\mathbf{o}} = 227$.

Given that $J_{\mathbf{w}}$ and $J_{\mathbf{o}}$ cannot be analytically computed using $\mathbf{w}$ and $\mathbf{o}$, we treat the cost functions of both optimisation problems as those given in a black-box oracle form. The design problems (3-53a) and (3-53b) are solved through the BO strategy outlined in Algorithms 3a and 3b respectively. First, $\mathbf{w}$ and $\mathbf{o}$ are assigned with the respective initial (nominal) parameter vectors defined in the first rows of Table 3-8. The corresponding performance costs of $\mathbf{w}_0$ and $\mathbf{o}_0$, denoted by ($J_{\mathbf{w}_0}$ and $J_{\mathbf{o}_0}$) are assumed to be known. The tuning schemes for Stages 1 and 2 begin by initializing the training sets $\mathcal{D}_{\mathbf{w}}$ and $\mathcal{D}_{\mathbf{o}}$ using $\{\mathbf{w}_0, J_{\mathbf{w}_0}\}$ and $\{\mathbf{o}_0, J_{\mathbf{o}_0}\}$ respectively. We define $N_{\text{w}}^{(\text{ini})} = 2$ and $N_{\text{o}}^{(\text{ini})} = 1$, since there are only 2 training parameter vectors of $\mathbf{w}$ and 1 of $\mathbf{o}$ to perform the experiment with in the initial stage, in order evaluate their respective performance costs which are not yet known. $\mathcal{D}_{\mathbf{w}}$ and $\mathcal{D}_{\mathbf{o}}$ are

augmented after each iteration. After the initial number of iterations are performed, the resulting $\mathcal{D}_{\mathbf{w}}$ and $\mathcal{D}_{\mathbf{o}}$ are then each used to train a Gaussian Process (GP)-based surrogate model that generates an approximated cost, denoted by $\hat{J}_{\mathbf{w}}(\mathbf{y};\mathbf{w})$ and $\hat{J}_{\mathbf{o}}(\mathbf{y};\mathbf{o})$ respectively. We will not treat the details on how the approximated costs are computed with the surrogate models in this section. Interest readers may refer to the reader [159] for further details.

In the optimisation phase, the design parameters that are to be tested in the next iteration are chosen by minimizing the acquisition functions $\alpha_{\mathbf{w}}(\mathbf{w}|\mathcal{D}_{\mathbf{w}})$ and $\alpha_{\mathbf{o}}(\mathbf{o}|\mathcal{D}_{\mathbf{o}})$, both of which are constructed using the mean and variance properties of the respective GPs. In both stages of the BO tuning frameworks, we use the *Lower Confidence Bound* (LCB) acquisition functions, such that the next design parameters for a given iteration i, are selected by solving the optimisation problems

$$\mathbf{w}_{i+1} = \arg\min_{\mathbf{w}\in\mathcal{W}_i} \ \alpha_{\mathbf{w}}(\mathbf{w}|\mathcal{D}_{\mathbf{w}}) \tag{3-56a}$$

$$\mathbf{o}_{i+1} = \arg\min_{\mathbf{o}\in\mathcal{O}_i} \ \alpha_{\mathbf{o}}(\mathbf{o}|\mathcal{D}_{\mathbf{o}}) \tag{3-56b}$$

Since the proposed BO approach is adopted without any probabilistic safety-critical constraints, the iteration-based constrained domains $\mathcal{W}_i$ and $\mathcal{O}_i$ are defined and enforced in (3-56) at every iteration. $\mathcal{W}_i$ and $\mathcal{O}_i$ are each constrained by a pair of lower and upper limits based on known information or intuition about the physical effects that $\mathbf{w}$ and $\mathbf{o}$ have on BG. The constrained domains are defined as

$$\mathcal{W}_i = \left\{\mathbf{w}\in\mathbb{R}^4 \mid \mathbf{w}_{i,\min} \le \mathbf{w} \le \mathbf{w}_{i,\max}\right\} \tag{3-57a}$$

and

$$\mathcal{O}_i = \left\{\mathbf{o}\in\mathbb{R}^2 \mid \mathbf{o}_{i,\min} \le \mathbf{o} \le \mathbf{o}_{i,\max}\right\}, \tag{3-57b}$$

where

$$\mathbf{w}_{i,\min} = \begin{bmatrix}0.4 & 0.4 & \min(0.9\ \mathbf{w}_{i,\mathrm{opt}}(3), 0.9\ \mathrm{CR}_0) & \mathcal{T}_{\mathrm{bolus},0} - 0.5\end{bmatrix}^\top \tag{3-58a}$$

$$\mathbf{w}_{\max} = \begin{bmatrix}1 & 1 & \max(1.1\ \mathbf{w}_{i,\mathrm{opt}}(3), 1.1\ \mathrm{CR}_0) & \mathcal{T}_{\mathrm{bolus},0} + 0.5\end{bmatrix}^\top \tag{3-58b}$$

and

$$\mathbf{o}_{\min} = \begin{bmatrix}0.5 & \min(0.5, 0.9\ \mathbf{o}_{i,\mathrm{opt}}(2))\end{bmatrix}^\top \tag{3-59a}$$

$$\mathbf{o}_{\max} = \begin{bmatrix}2 & \max(2, 1.5\ \mathbf{o}_{i,\mathrm{opt}}(2))\end{bmatrix}.^\top \tag{3-59b}$$

Since the CR has the biggest impact on BG, a conservative tuning approach to the latter is required as a preventive measure against hypoglycaemia. According to [140], the CR is tuned incrementally by a margin between 10% and 25% of its initial value in real-life settings where commercially-available automated insulin delivery (AID) devices are utilised. We thus adopt a similar approach in (3-58), where we allow the limits of $\mathbf{w}(3)$ to be augmented by a 10% margin of the optimum parameter $\mathbf{w}_{i,\mathrm{opt}}(3)$ that corresponds to the best objective $J_{\mathbf{w}_{i,\mathrm{opt}}}$ at iteration i.

The tuning algorithms of $\mathbf{w}$ and $\mathbf{o}$ continue until a total number $N_{\text{days,w}}$ and $N_{\text{days,o}}$ iterations is achieved for the former and latter parameters.

Parameter Vector	$\mathbf{w}(1)$	$\mathbf{w}(2)$	$\mathbf{w}(3)$	$\mathbf{w}(4)$
$\mathbf{w}_0^{(r)}$	1	1	CR_0	$\mathcal{T}_{\text{bolus},0}$
$\mathbf{w}_1^{(r)}$	1	1	$0.9\ \text{CR}_0$	$\mathcal{T}_{\text{bolus},0}$
$\mathbf{w}_2^{(r)}$	1	1	$1.1\ \text{CR}_0$	$\mathcal{T}_{\text{bolus},0}$

(a) Stage 1 BO tuning parameter set

Parameter Vector	$\mathbf{o}(1)$	$\mathbf{o}(2)$
$\mathbf{o}_0^{(r)}$	1	0.5
$\mathbf{o}_1^{(r)}$	1	0.7

(b) Stage 2 BO tuning parameter set

Table 3-8: Initial and training parameter vectors used in Stage 1 (top) and Stage 2 (bottom) BO parameter tuning for a run r. CR_0 represents the empirically calculated patient-specific CR using eq. (2-21b), and $\mathcal{T}_{\text{bolus},0}$ refers to the nominal insulin bolus decay length that is *a priori*-determined.

Algorithm 3a: Bayesian Optimisation with constrained domain (Stage 1)

1. **initialize** parameters vs performance set for run r
$$\mathcal{D}_{\mathbf{w}}^{(r)} \leftarrow \{\mathbf{w}_0^{(r)}, J_{\mathbf{w}_0}^{(r)}\};$$
2. **for** $i = 1, 2, \ldots, N_{\mathbf{w}}^{(\text{ini})}$ **do**
   2.1 based on $\mathbf{w}_i^{(r)}$, **perform** experiment and **measure** performance cost $J_{\mathbf{w}_i}^{(r)}$;
   2.2 **augment** the training set $\mathcal{D}_{\mathbf{w}}^{(r)} \leftarrow \mathcal{D}_{\mathbf{w}}^{(r)} \cup \{\mathbf{w}_i^{(r)}, J_{\mathbf{w}_i}^{(r)}\}$;
3. **end for**
4. **for** $i = N_{\mathbf{w}}^{(\text{ini})}, N_{\mathbf{w}}^{(\text{ini})} + 1, \ldots, N_{\text{days},\mathbf{w}} - 1$ **do**
   4.1 based on the data $\mathcal{D}_{\mathbf{w}}^{(r)}$, train a GP approximating $\hat{J}_{\mathbf{w}}^{(r)}$
   4.2 based on the GP, **define acquisition function** $\alpha_{\mathbf{w}}(\mathbf{w}|\mathcal{D}_{\mathbf{w}})$;
   4.3 **update** domain $\mathcal{W}_i$;
   4.4 **compute** next parameters as
$$\mathbf{w}_{i+1}^{(r)} \leftarrow \arg\min_{\mathbf{w}\in\mathcal{W}_i}\ \alpha_{\mathbf{w}}(\mathbf{w}|\mathcal{D}_{\mathbf{w}});$$
   4.5 **perform** experiment and **measure** performance cost $J_{\mathbf{w}_{i+1}}^{(r)}$;
   4.6 **augment** the training set $\mathcal{D}_{\mathbf{w}}^{(r)} \leftarrow \mathcal{D}_{\mathbf{w}}^{(r)} \cup \{\mathbf{w}_{i+1}^{(r)}, J_{\mathbf{w}_{i+1}}^{(r)}\}$;
5. **end for**
6. **update** γ_1, γ_2, CR, $\mathcal{T}_{\text{bolus}}$ based on found optimum parameter vector of $\mathbf{w}$

Algorithm 3b: Bayesian Optimisation with constrained domain (Stage 2)

1. **initialize** parameters vs performance set for run r
$$\mathcal{D}_{\mathbf{o}}^{(r)} \leftarrow \{\mathbf{o}_0^{(r)}, J_{\mathbf{o}_0}^{(r)}\};$$

2. **for** $i = 1, 2, \ldots, N_{\mathbf{o}}^{(\text{ini})}$ **do**
   - 2.1 based on $\mathbf{o}_i^{(r)}$, **perform** experiment and **measure** performance cost $J_{\mathbf{o}_i}^{(r)}$;
   - 2.2 **augment** the training set $\mathcal{D}_{\mathbf{o}}^{(r)} \leftarrow \mathcal{D}_{\mathbf{o}}^{(r)} \cup \{\mathbf{o}_i^{(r)}, J_{\mathbf{o}_i}^{(r)}\}$;

3. **end for**
4. **for** $i = N_{\mathbf{o}}^{(\text{ini})}, N_{\mathbf{o}}^{(\text{ini})} + 1, \ldots, N_{\text{days},\mathbf{o}} - 1$ **do**
   - 4.1 based on the data $\mathcal{D}_{\mathbf{o}}^{(r)}$, train a GP approximating $\hat{J}_{\mathbf{o}}^{(r)}$
   - 4.2 based on the GP, **define acquisition function** $\alpha_{\mathbf{o}}(\mathbf{o}|\mathcal{D}_{\mathbf{o}})$;
   - 4.3 **update** domain $\mathcal{O}_i$;
   - 4.4 **compute** next parameters as
   $$\mathbf{o}_{i+1}^{(r)} \leftarrow \arg\min_{\mathbf{o}\in\mathcal{O}_i} \ \alpha_{\mathbf{o}}(\mathbf{o}|\mathcal{D}_{\mathbf{o}});$$
   - 4.5 **perform** experiment and **measure** performance cost $J_{\mathbf{o}_{i+1}}^{(r)}$;
   - 4.6 **augment** the training set $\mathcal{D}_{\mathbf{o}}^{(r)} \leftarrow \mathcal{D}_{\mathbf{o}}^{(r)} \cup \{\mathbf{o}_{i+1}^{(r)}, J_{\mathbf{o}_{i+1}}^{(r)}\}$;

5. **end for**
6. **compute** γ_B, $\gamma_{\tau_{\text{sp}}}$ based on found optimum parameter vector of $\mathbf{o}$

Chapter 4

Performance and Results

The overall design scheme of the proposed control system has been introduced in Chapter 3. Implementing these blueprints is the next and final phase of this thesis, in order to effectively verify the efficacy of the control design. This process is carried out by means of an *in silico* simulation of three virtual patients. In Section 4-1, we first assess the performance of a zone model predictive control (Z-MPC)-only and set-point tracking model predictive control (SP-MPC)-only control strategy, using a single-meal scenario on Patient 14. We then carry out a full evaluation of the two-stage Bayesian Optimisation (BO) tuning frameworks for which the results are reported in Section 4-2. Finally in Section 4-3, the optimised artificial pancreas (AP) controller is put to test in scenarios that mimic real-life scenarios.

4-1 Analysis of MPC Design Choices

In Section 3-2, we have extensively discussed the significance of introducing certain novel features in the control architecture, as well as the underlying reason behind the adaptation of some policy features found in the literature to the proposed control design. In order to reinforce the motivations behind our proposal, we will attempt to systematically verify the benefits of the incorporated features and make a comparative performance analysis.

First, we test the performance for a single announced meal scenario with a carbohydrates (CHO) intake size of 70 g, which is the defined average meal size $\overline{\text{CHO}}$. In the following experiments, the performances of a standalone Z-MPC and SP-MPC are evaluated. The goals for each of the experiments are as follows:

- Experiment 1a: Evaluate the performance impact of introducing $Q_{(\Delta y)_+}$ in the Z-MPC, using static zonal bounds;
- Experiment 1b: Evaluate the performance impact of introducing $Q_{(\Delta y)_+}$ in the SP-MPC, using a fixed, constant set-point tracking trajectory;

- Experiment 2a: Verify the effectiveness of employing time-varying zonal bounds in the Z-MPC, by evaluating the oscillatory performance;
- Experiment 2b: Verify the effectiveness of employing a time-varying set-point tracking trajectory in the SP-MPC, by evaluating the oscillatory performance.

We perform experiments using both standalone model predictive control (MPC)s, as well as the proposed switching MPC strategy to evaluate their respective performances for an unannounced meal scenario, with the following aims:

- Experiment 3a: Compare the performance between Z-MPC and SP-MPC for an unannounced meal size of 40 g CHO;
- Experiment 3b: Compare the performance between Z-MPC and SP-MPC for an unannounced meal size of 70 g CHO;
- Experiment 4a: Verify the benefits of the proposed switching MPC strategy for an unannounced meal size of 40 g CHO;
- Experiment 4b: Verify the benefits of the proposed switching MPC strategy for an unannounced meal size of 70 g CHO.

The final performance (Experiment 5) analysis of this section pertains to the introduction of proportional insulin limits that depend on the relative size of the ingested CHO relative to CHO = 70 g during the first time period $\mathcal{P}_1$, as defined by the second term of (3-39a).

4-1-1 Performance in Announced Meal Scenario

Experiment 1

In this experiment, the static lower and upper bounds of the zonal target range are defined according to their nominal values $\zeta_{\text{lower}} = y_{\text{ref}}^{(\text{lower})}$ and $\zeta_{\text{upper}} = y_{\text{ref}}^{(\text{upper})}$ as defined in Section 3-2-4. When comparing Figures 4-1a and 4-1b, we can clearly see the impact of introducing $Q_{(\Delta y)_+}$ in the Z-MPC on the overshoot performance inside the zonal range, while no observable difference can be noted for the SP-MPC. Bearing in mind that when the sensor glucose level (SGL) is within the zonal range, glucose deviations from the reference point are not penalised and the Z-MPC would steer the input signal back to the reference value in order to minimize insulin deviations that partly account for the cost function of the Z-MPC, unless there is a predicted excursion of y into the glucose range above and below ζ_{upper} and ζ_{lower} respectively. As seen in Figure 4-1a, when the time is at approximately 725 min, a small amount of insulin correction is made for the Z-MPC without $Q_{(\Delta y)_+}$ as the sensor glucose (SG) approaches ζ_{upper}. It is apparent that with a non-zero $Q_{(\Delta y)_+}$, apart from the positive change in blood glucose (BG) inside the zonal target range, even an anticipated increase in the SG before it reaches the zonal range from below the lower bound can be effectively penalised. From experiments 1, it can thus be established that $Q_{(\Delta y)_+}$ is particularly useful and needed when a Z-MPC is employed, and is not as significant with the SP-MPC, since glucose deviations can be effectively penalised from a single reference tracking value. For the subsequent experiment, we therefore employ the glucose increase penalisation weight $Q_{(\Delta y)_+}$ in the MPCs.

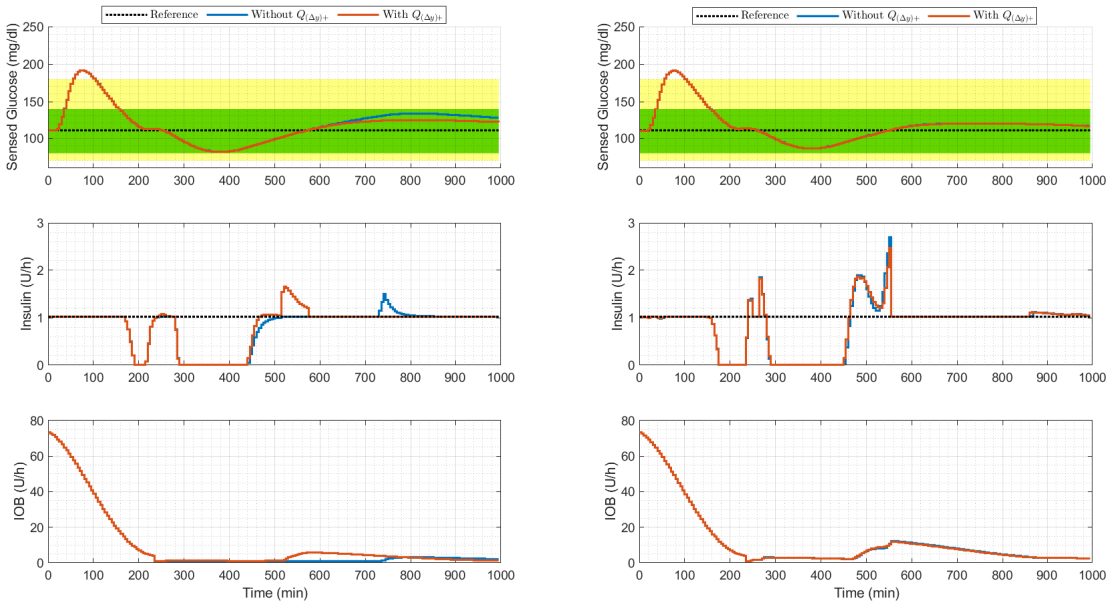

(a) Zone MPC **(b)** Set-point tracking MPC

Figure 4-1: Post-prandial performance analysis of AP controller with vs without $Q_{(\Delta y)_+}$ in the respective single MPC strategies during a 70 g CHO announced meal scenario.

Experiment 2

Next, we compare the performance when a varying zonal range, and set-point tracking value feature based on (3-50) and (3-47) respectively are introduced in the Z-MPC and SP-MPC. The varying zonal range applies only to post-prandial periods when meals are announced, as is the case in this set-up, while the reference set-point trajectory value is independent of the latter. Similar to the observations from Experiments 1, the improved performance is more apparent with the Z-MPC compared to the SP-MPC. The noticeable difference is more pronounced from Figure 4-2a that the subject, when using the Z-MPC with varying zone feature, experiences not only a reduction in undershoot from post-prandial glucose recovery, but also overshoot during a BG rebound compared to with fixed zonal bounds. In contrast to the SP-MPC, the varying set-point feature only improved undershoot by a small margin, albeit a more improved overshoot performance compared to using a fixed set-point value, as seen in 4-2b. By means of a general comparison of all the SG profiles in Figure 4-2, the Z-MPC with varying set-point appears to yield the best performance among the four configurations for an announced meal scenario. We observe that the insulin delivery profile when dealing with the undershoot differs starkly for the latter compared to the other three configurations, with a much reduced insulin suspension time required, and hence likelihood of a high overshoot and potential risk of hyperglycaemia [88]. We thus incorporate the varying zonal bounds and set-point tracking features in the main framework of the AP architecture.

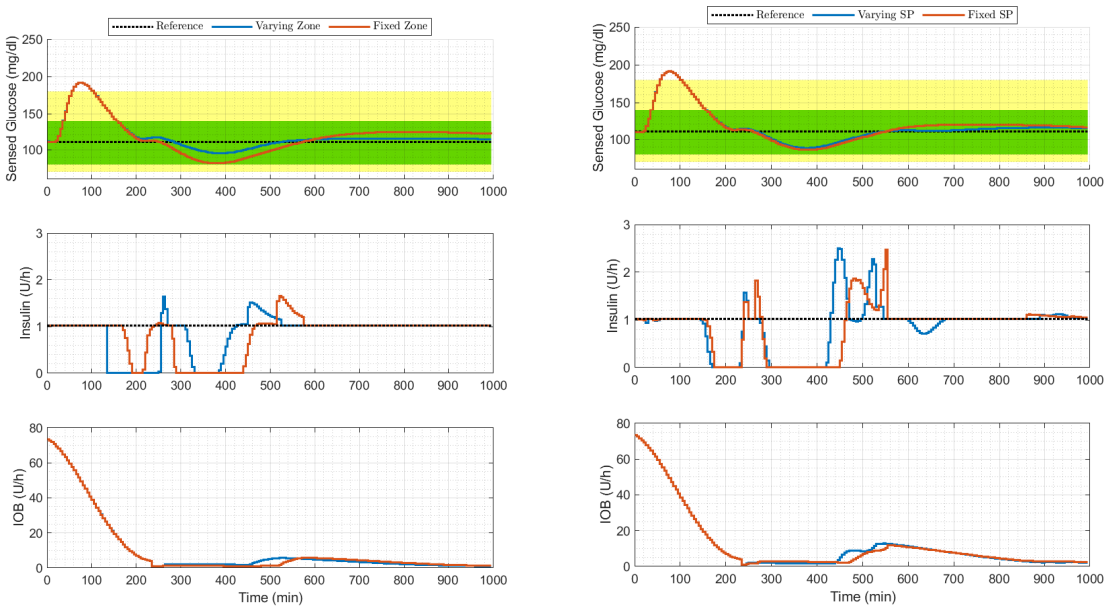

(a) Zone MPC **(b)** Set-point tracking MPC

Figure 4-2: Post-prandial performance analysis of AP controller with varying zonal bound or set-point tracking values vs fixed values employed in the respective single MPC strategies, during a 70 g CHO announced meal scenario.

4-1-2 Performance in Unannounced Meal Scenario

Experiment 3

For this experiment, we first test the controller in a scenario with 40 g CHO intake, a size that corresponds approximately to a slightly large snack. Based on intuition, patients are most likely to forget or fail to 'announce' their CHO consumption size when a snack is consumed. Moreover, we want to verify how the effective the AP controller can perform using only automated insulin corrections when a smaller meal size is consumed, which can possibly obviate the need for meal announcement in such a scenario. Subsequently, we assess the AP controller's response to an unannounced CHO consumption corresponding to the same size as those used in the previous experiments. A peak BG value stood slightly below 200 mg/dL as seen in Figure 4-3a when both settings when Z-MPC and SP-MPC are individually employed. It is obvious that the SP-MPC outperforms the Z-MPC by a significant margin, with little to no observable undershoot during the post-prandial period with the former as opposed to the latter. This observation can be attributed to two factors. First, the SP-MPC's early detection of an increased negative SG deviation from its set-point value enables a suspension of insulin infusion to occur 60 min (1 h) earlier than a reduced insulin delivery action for the Z-MPC. The second lies with the absence of the time-varying zonal bounds in unaanounced meal scenarios. The zonal variation mechanism is activated only when meals are announced while the time-varying set point feature of the SP-MPC is active throughout the simulation. In the unannounced 70 g CHO scenario, the peak blood glucose level (BGL) values reach

slightly above 250 mg/dL for both MPC strategies, significantly higher than those in the announced meal scenario as exemplified in Experiment 2. Moreover, a larger undershoot is observed for both the Z-MPC and the SP-MPC. One can infer that the large excursion into the hyperglycaemic range makes the control strategy without meal bolusing for an average or large meal size unfeasible.

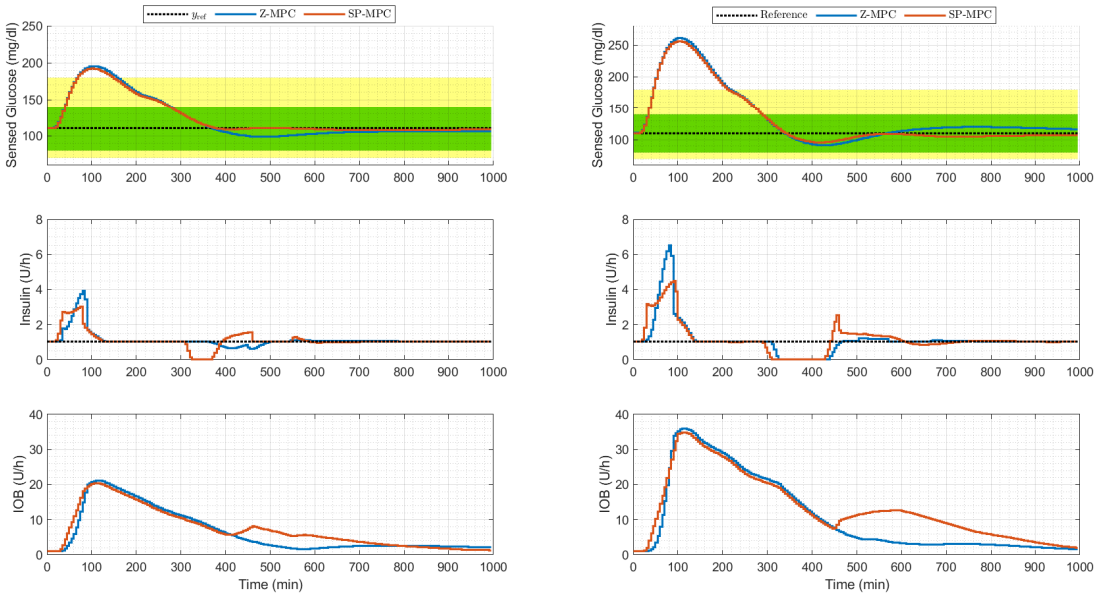

(a) 40 g CHO intake **(b)** 70 g CHO intake

Figure 4-3: Post-prandial performance analysis of Z-MPC only vs SP-MPC only strategy for two different unannounced CHO sizes.

Experiment 4

Having examined the capabilities of both the SP-MPC and Z-MPC- only strategies, the performance of the proposed switching MPC scheme forms the next focus of the experiments. The same unannounced meal protocols from Experiment 3 are repeated. We see from Figure 4-4 that for the unannounced 40 g CHO scenario, the switching MPC configuration handles the glucose rebounce effect better than the Z-MPC-only strategy, despite the Z-MPC being deployed for most periods until the switching criteria is met. Moreover, no observable overshoot occurred using the switching MPC strategy when a 70 g CHO is consumed without meal bolusing, which follows the response profile of the SP-MPC-only strategy.

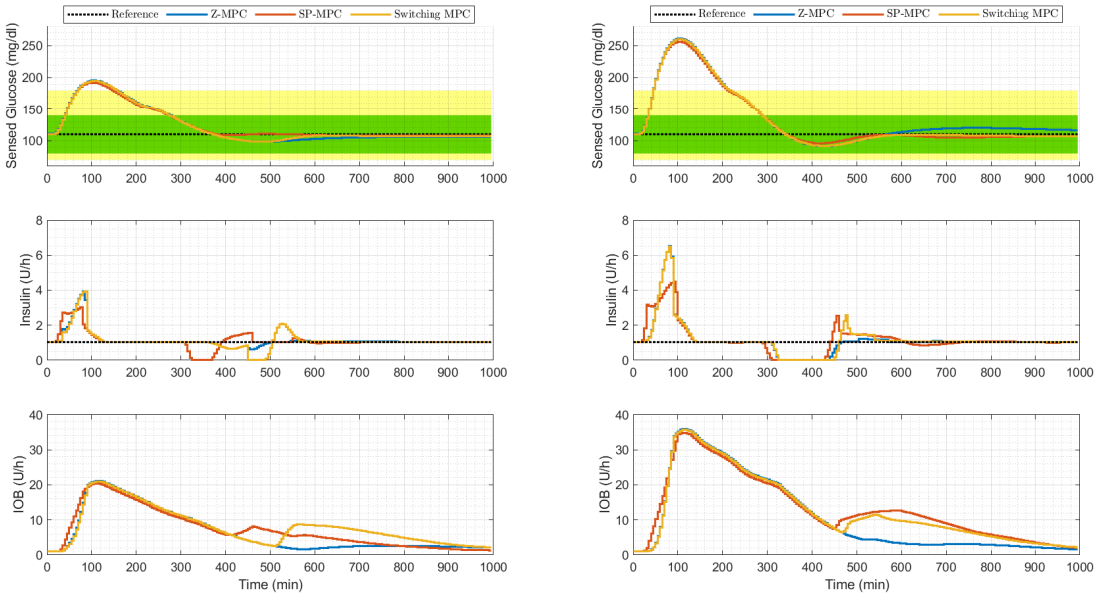

(a) 40 g CHO intake **(b)** 70 g CHO intake

Figure 4-4: Post-prandial performance analysis of the proposed switching MPC-strategy vs Z-MPC only and SP-MPC only strategy during two independent unannounced meal scenarios.

Experiment 5

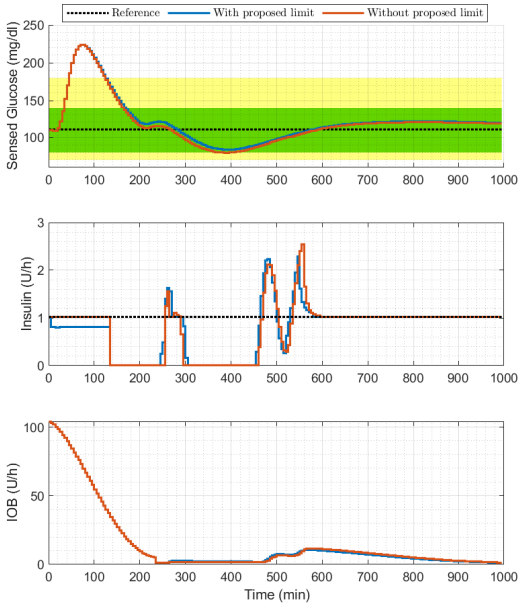

Figure 4-5: Performance analysis of proposed controller with proportional insulin limits dependent on announced CHO size vs without, during a 100 g CHO announced meal scenario.

Having demonstrated the efficacy of the switching MPC strategy from previous experiments, a final test is performed using the latter to demonstrate the effectiveness of the insulin limit proposed in eq. (3-39a). A significantly larger CHO meal size of 100 g is fed to the virtual Patient 14, and compared to when the nominal CHO amount is taken. A imposition of a tighter post-prandial insulin limit can be observed from the start of the simulation when meal bolus is given to the virtual patient, till approximately 130 min after the meal consumption as depicted in Figure 4-5. A slightly reduced undershoot is observed, caused by the reduction of basal insulin.

4-2 Performance Analysis of Bayesian Optimisation Tuning

In this section, the performance of the proposed tuning method outlined in Section 3-3 is evaluated on three different adult *in silico* patients. In addition to Patient 14, which has been extensively used in this thesis as a baseline to design the basic functions of the AP, Patients 12 and 15 will also be also undergo the same performance evaluation. Throughout the rest of this chapter, we assume that the basal rate u_{basal} for each subject required to achieve a reference glucose value of $y_{\text{ref}} = 110$ mg/dL is *a priori* known. The empirically-calculated correction factor (CF) is fixed as well, based on the prior knowledge on total daily insulin dose (TDD) value TDD_0 (see Table 4-1). In addition, no additive noise is included in the continuous glucose monitor (CGM) measurements so as to facilitate the goal of this study.

We conduct an experiment that resembles a regular person's meal routine, which comprises of breakfast, lunch and dinner. For the experiment, certain assumptions are considered, which is key to capturing a quality objective cost for the tuning algorithm. First, the initial conditions of the patient are treated the same at the start of every BO iteration, which includes the starting value of y_{CGM}. This is because, when the initial conditions of the patient vary, the extent by which performance variations corresponding to a given decision variable set might overshadow the performance difference caused by a change in the decision variables, depending on the sensitivity of the performance cost with respect to the tuning parameter. It is thus imperative to ensure that each iteration of evaluation is subjected to same if not similar conditions.

For each stage of the BO tuning scheme, we employ a strict meal consumption protocol in which each virtual patient are given 3 meals, consisting of breakfast, lunch and dinner that are taken at 07:30, 13:00 and 19:00 respectively on every day until the stopping criterion, that is the maximum number of iterations, is met. Each meal size is the same, containing of 70 g of CHO content. All meals are subjected to announcements with the correct meal bolus supplied to the patients according to the carbohydrate-to-insulin ratio (CR) value ($\mathbf{w}(3)$) determined by the BO algorithm. All *glycaemic* performances of the AP controller corresponding to any set of parameter vectors (i.e. $\mathbf{w}, \mathbf{o}$) are evaluated using the same meal protocol, across a 48-h period starting from 06:00 in the morning.

To effectively assess the performance of the BO tuning scheme, the experiment is repeated with Algorithms 3a and 3b until 10 experimental runs are completed ($r \in \{1, 2, \cdots, 10\}$). In the first stage, the optimum parameters for a run r, is denoted by $\mathbf{w}_{\text{opt}}^{(r)}$. The reader should take note that the tuning paradigm does not follow one in which a run r from the first stage directly precedes the run of the same index in the second stage. After completing the first

10 runs of experiments, the parameter vector $\mathbf{w}$ deployed for the following stage of tuning is then selected among the pool of 10 optimum parameter vectors, based on their corresponding glycaemic performance summarised in Tables 4-2. The selected parameter vector from the first stage of tuning is denoted by $\mathbf{w}^*$. Likewise for the variables subjected to parameter tuning in the second stage, we use $\mathbf{o}_{\text{opt}}^{(r)}$ to denote the optimum parameter vector for the run r, whose corresponding 48-h glycemic performance is summarised in Table 4-2, and $\mathbf{o}^*$ for the selected tuned parameter vector corresponding to the individual subjects.

With each patient, we conduct a total of 15 iterations (15 days, excluding the dataset $\{\mathbf{w}_0^{(r)}, J_{\mathbf{w}_0}^{(r)}\}$) in the first stage for a particular run r. In the subsequent tuning stage (Stage 2), 14 iterations (14 days) are performed in a single run, also excluding iteration 0 to which dataset $\{\mathbf{o}_0^{(r)}, J_{\mathbf{o}_0}^{(r)}\}$ corresponds. The number of iterations for each stage was chosen using practical knowledge on a human eating and lifestyle habits. Since in reality, a patient is unable to be consume the same amounts of food and maintaining a strict eating routine for extended periods of time, the number of iterations and thus the total experimental duration are crucial. We therefore consider a simulation period that lasts approximately two weeks long for both stages in each run, spanning 28 days. The initial parameters required to initialize the CF, CR and active insulin bolus time $\mathcal{T}_{\text{bolus}}$ are summarised in Table 4-1.

Patient	CR_0 (g CHO/(mg/dL))	TDD_0 (U)	$\mathcal{T}_{\text{bolus},0}$ (h)
12	11.851	57.869	5
14	11.503	33.808	4.5
15	8.5004	68.316	5.5

Table 4-1: Initial and training parameter sets for BO parameter tuning.

4-2-1 Stage 1: Clinical-related Parameters

Based on the general trend of the curves in Figure 4-6, we see that the mean minimum value of $J_{\mathbf{w}}$ decreases after each iteration for all three patients. The reduction in mean cost after 15 iterations differs greatly among the patients. The mean minimum cost appears to be converging for Patients 12 and Patients 14, whereas for Patient 15, a steady-decrease in the minimum cost is still evident. This observation can be related to inferences from the glycaemic performance results summarised in Table 4-2. From the 48-h simulation protocol, we can see that even with the nominal parameters $\mathbf{w}_0$ employed, a substantially high time-in-range (TIR) of 98.43% in the wider target range ($\in [80, 140]$ mg/dL) is already observed for Patient 12. While the TIR ($\in [80, 140]$ mg/dL) for Patient 14 is comparable to Patient 15 which is lower than that of Patient 12, the recorded mean BG is far lower than Patient 15's, achieving an average value of 127.79 mg/dL in contrast to the 146.87 mg/dL for Patient 15, implying that the AP controller tailored to Patient 14 is operating at much closer to its optimum performance compared to that of Patient 15. For both Patients 14 and 15, we can infer an improvement in the TIR both in the tight ($\in [80, 140]$ mg/dL) and wide ($\in [70, 180]$ mg/dL) target ranges across the 10 runs. Moreover, the observed improvement in glycaemic performance is generally correlated to the BO final cost obtained for both Patients 14 and 15.

The line of reasoning that was used to account for the performance observations for Patients 14

and 15 does not however, apply to Patient 12. Despite already achieving a rather high TIR, we would still expect an improvement in the tight TIR. Instead, we notice that the wide TIR for the mentioned BG target range slightly worsened in 8 of the optimum parameter vector candidates, with the exception of $\mathbf{w}_{\text{opt}}^{(4)}$. One can refer to Figure 4-7a to seek an adequate explanation for this observation. It is clear that in the first 24-h period, the improved performance of the AP controller where a distinctive decrease in BGL is evident, resulting in the increase in the tight TIR (BG $\in [80, 140]$ mg/dL) as reported in Figure 4-2a, which on the positive note, follows the expected correlation with the achieved BO cost. After the 24-h period, a larger mean peak BGL occurs after the consumption of breakfast compared to when $\mathbf{w} = \mathbf{w}_0$. By referring to the insulin delivery profile, we can see that before insulin bolus (sharp peak) is delivered, there is a stark contrast in the profile of the mean insulin delivery between approximately 04:30 and the time instant right before insulin bolus is taken for breakfast. In the initial settings where insulin delivery returns to the basal rate, the mean insulin delivery rate continues to be far below than the latter when $\mathbf{w}_{\text{opt}}$ is employed. As explained in Section 3-2, the AP controller switches to the SP-MPC mode after midnight (00:00) or after the $\mathcal{P}_2$ period relative to the dinner consumption time. The cause of the prolonged the insulin suspension action could be attributed to the set-point tracking decay nature of the SP-MPC. Noting that the minimum BG is generally lower for the optimal parameter vectors whose control performance had a poorer standard TIR than for the initial, we infer that an excessive penalisation on negative glucose deviation could have occurred, in spite of the presence of an exponential decay varying set-point tracking feature. Despite a larger insulin bolus dose (refer to the IOB plot) fed to the subject, the latter is unable to sufficiently compensate for the lack of automated insulin corrections from before. After approximately 15:00 on the second day, we observe that the mean SGL is lower for the tuned AP, if not, the same as the initial settings. Having said, achieving a lower minimum BG does not necessarily worsen glycaemic performance, as exemplified by the performance corresponding to $\mathbf{w}_{\text{opt}}^{(4)}$, in which the recorded minimum BG of 99.24 mg/dL is lower than the 101.20 mg/dL of $\mathbf{w}_0$. In addition, the increased tight TIR demonstrates the effectiveness of the Stage 1 BO tuning scheme.

Determining $\mathbf{w}^*$

To assign a suitable parameter vector $\mathbf{w}^*$, we refer back to the performance metric results in Table 4-2. We seek the parameter vector among the the pool of $\mathbf{w}_{\text{opt}}$ candidates that yields the lowest BO cost. In the BO cost function $J_{\mathbf{w}}$ (see (3-54)), a barrier-penalty function is introduced to penalise the cost function if the minimum glucose value falls below 95 mg/dL as a safety measure. In this regard, we select the $\mathbf{w}_{\text{opt}}$ candidate achieves the best BO performance, and also with a minimum BG that is greater than or equals to 95 mg/dL. We thus assign the parameter vectors $\mathbf{w}_{\text{opt}}^{(3)}$ (Patient 14) and $\mathbf{w}_{\text{opt}}^{(2)}$ (Patient 15) as the values of $\mathbf{w}^*$ for Patient 14 and 15 respectively. For Patient 12, a different approach is taken. The parameter vector $\mathbf{w}_{\text{opt}}^{(4)}$ (Patient 12) is selected owing to its glycaemic performance result. The values for $\mathbf{w}^*$ corresponding to each subject are presented in Table 4-3a.

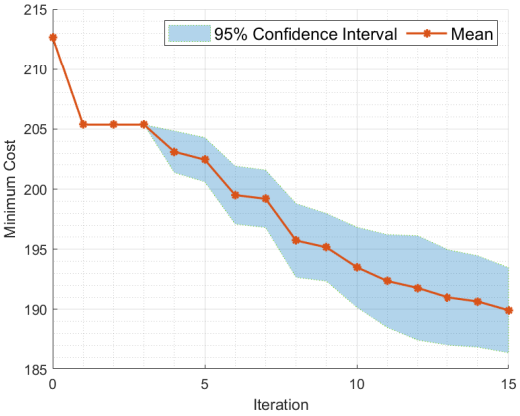

(a) Patient 12

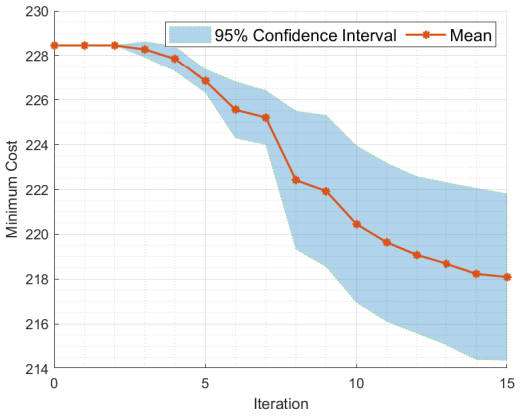

(b) Patient 14

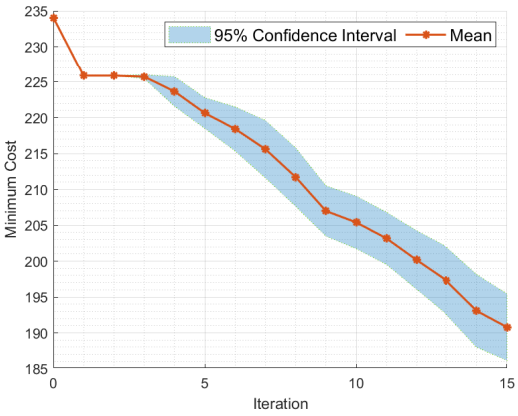

(c) Patient 15

Figure 4-6: *In silico* performance analysis of minimum performance cost after each iteration for the first stage of BO tuning.

$\mathbf{w}$	**BO Cost**	**TIR (%)** $\in [70, 180]$ mg/dL	**TIR (%)** $\in [80, 140]$ mg/dL	**Mean ± Std Deviation BG (mg/dL)**	**Min BG (mg/dL)**	**Max BG (mg/dL)**
$\mathbf{w}_0$	212.66	98.43	51.74	136.58 ± 26.91	99.58	182.62
$\mathbf{w}_{\text{opt}}^{(1)}$	191.30	96.01	54.86	132.87 ± 27.29	95.42	189.52
$\mathbf{w}_{\text{opt}}^{(2)}$	196.79	96.01	52.95	135.14 ± 27.28	97.33	189.76
$\mathbf{w}_{\text{opt}}^{(3)}$	189.13	96.88	55.38	132.32 ± 26.59	95.60	186.76
$\mathbf{w}_{\text{opt}}^{(4)}$	197.95	100.00	56.08	132.96 ± 24.26	99.64	174.96
$\mathbf{w}_{\text{opt}}^{(5)}$	180.94	97.40	58.33	129.68 ± 25.99	94.23	185.13
$\mathbf{w}_{\text{opt}}^{(6)}$	186.70	96.18	56.25	131.70 ± 26.89	94.78	188.33
$\mathbf{w}_{\text{opt}}^{(7)}$	194.79	95.66	55.04	132.81 ± 27.73	94.63	190.86
$\mathbf{w}_{\text{opt}}^{(8)}$	192.24	95.49	54.69	132.92 ± 27.98	94.34	192.04
$\mathbf{w}_{\text{opt}}^{(9)}$	186.18	97.22	56.77	131.10 ± 26.17	95.53	185.65
$\mathbf{w}_{\text{opt}}^{(10)}$	183.20	97.74	56.42	131.15 ± 25.56	95.68	184.15
Mean $(\mathbf{w}_{\text{opt}})$	**189.92**	**96.86**	**55.68**	$\mathbf{132.27 \pm 26.58}$	**95.71**	**186.71**

(a) Patient 12

$\mathbf{w}$	**BO Cost**	**TIR (%)** $\in [70, 180]$ mg/dL	**TIR (%)** $\in [80, 140]$ mg/dL	**Mean ± Std Deviation BG (mg/dL)**	**Min BG (mg/dL)**	**Max BG (mg/dL)**
$\mathbf{w}_0$	228.46	91.32	75.17	127.79 ± 26.10	101.20	192.98
$\mathbf{w}_{\text{opt}}^{(1)}$	224.84	95.31	77.43	123.66 ± 25.55	94.23	188.24
$\mathbf{w}_{\text{opt}}^{(2)}$	215.40	97.57	78.82	125.00 ± 22.55	99.24	184.04
$\mathbf{w}_{\text{opt}}^{(3)}$	212.77	97.74	79.51	122.35 ± 23.31	96.30	183.96
$\mathbf{w}_{\text{opt}}^{(4)}$	224.68	93.58	76.74	124.55 ± 25.97	96.79	190.05
$\mathbf{w}_{\text{opt}}^{(5)}$	225.09	94.62	77.08	124.19 ± 25.75	95.31	189.01
$\mathbf{w}_{\text{opt}}^{(6)}$	213.43	97.05	80.03	122.71 ± 23.48	94.14	184.38
$\mathbf{w}_{\text{opt}}^{(7)}$	215.36	98.44	79.86	121.10 ± 23.60	93.69	184.87
$\mathbf{w}_{\text{opt}}^{(8)}$	224.86	93.23	76.74	124.77 ± 25.93	96.44	189.52
$\mathbf{w}_{\text{opt}}^{(9)}$	214.08	97.22	79.51	122.86 ± 23.36	97.28	183.64
$\mathbf{w}_{\text{opt}}^{(10)}$	210.40	100	80.73	120.03 ± 22.73	94.41	179.45
Mean $(\mathbf{w}_{\text{opt}})$	**218.09**	**96.48**	**78.65**	$\mathbf{123.12 \pm 24.22}$	**95.78**	**185.72**

(b) Patient 14

$\mathbf{w}$	**BO Cost**	**TIR (%)** $\in [70, 180]$ mg/dL	**TIR (%)** $\in [80, 140]$ mg/dL	**Mean ± Std Deviation BG (mg/dL)**	**Min BG (mg/dL)**	**Max BG (mg/dL)**
$\mathbf{w}_0$	234.06	91.84	34.72	146.87 ± 26.07	105.36	193.49
$\mathbf{w}_{\text{opt}}^{(1)}$	192.69	99.13	68.92	128.89 ± 21.50	95.30	181.13
$\mathbf{w}_{\text{opt}}^{(2)}$	182.72	100.00	76.39	124.73 ± 19.74	95.16	178.13
$\mathbf{w}_{\text{opt}}^{(3)}$	185.54	100.00	73.79	126.14 ± 20.66	94.69	179.26
$\mathbf{w}_{\text{opt}}^{(4)}$	184.07	100.00	75.17	125.68 ± 19.62	96.76	177.90
$\mathbf{w}_{\text{opt}}^{(5)}$	183.81	100.00	75.52	125.24 ± 19.88	95.31	178.44
$\mathbf{w}_{\text{opt}}^{(6)}$	186.85	100.00	71.53	127.53 ± 20.41	96.14	178.68
$\mathbf{w}_{\text{opt}}^{(7)}$	193.64	100.00	68.75	129.38 ± 20.77	97.60	179.51
$\mathbf{w}_{\text{opt}}^{(8)}$	193.00	99.13	68.75	129.05 ± 21.52	95.42	181.14
$\mathbf{w}_{\text{opt}}^{(9)}$	202.47	98.26	69.10	132.87 ± 23.80	95.17	185.03
$\mathbf{w}_{\text{opt}}^{(10)}$	203.11	98.44	68.52	133.75 ± 23.05	97.46	183.19
Mean $(\mathbf{w}_{\text{opt}})$	**190.79**	**99.50**	**70.23**	$\mathbf{128.33 \pm 21.09}$	**95.89**	**180.24**

(c) Patient 15

Table 4-2: *In silico* results corresponding to the 10 optimum parameter vectors of $\mathbf{w}_{\text{opt}}$ and the initial settings $\mathbf{w}_0$. BO cost is evaluated during the tuning process prior to the 48-h protocol.

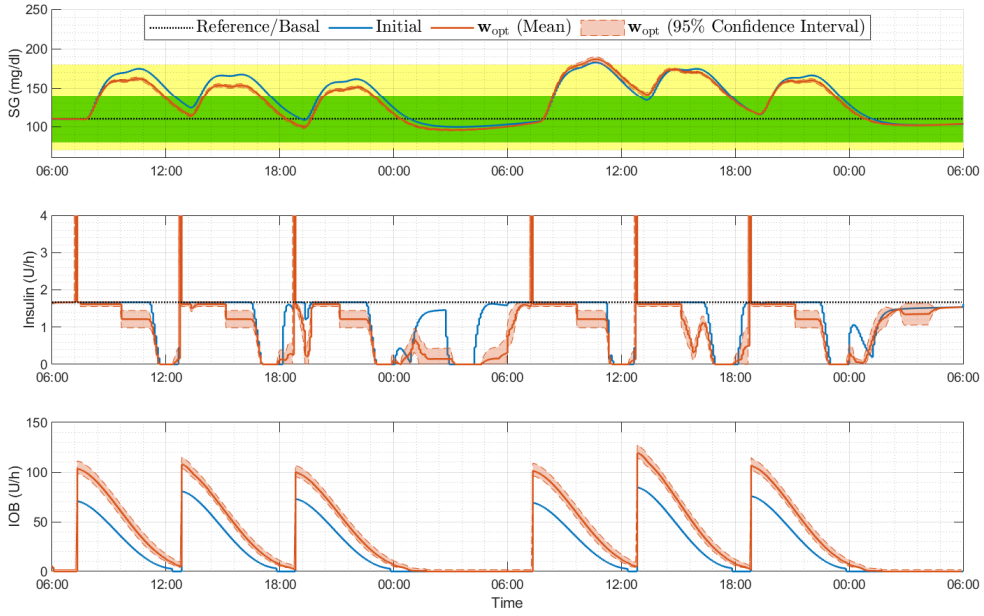

(a) Patient 12

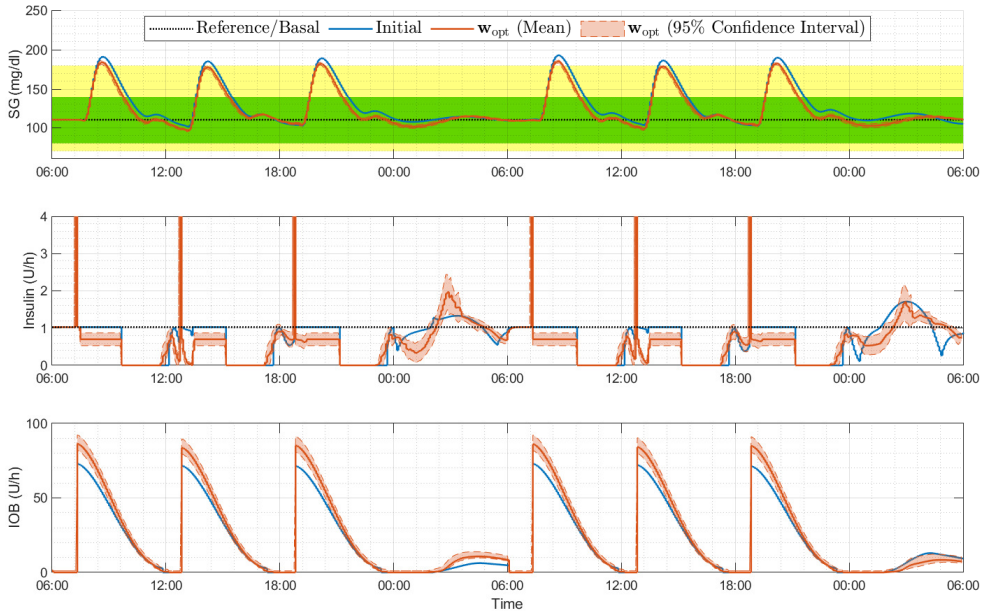

(b) Patient 14

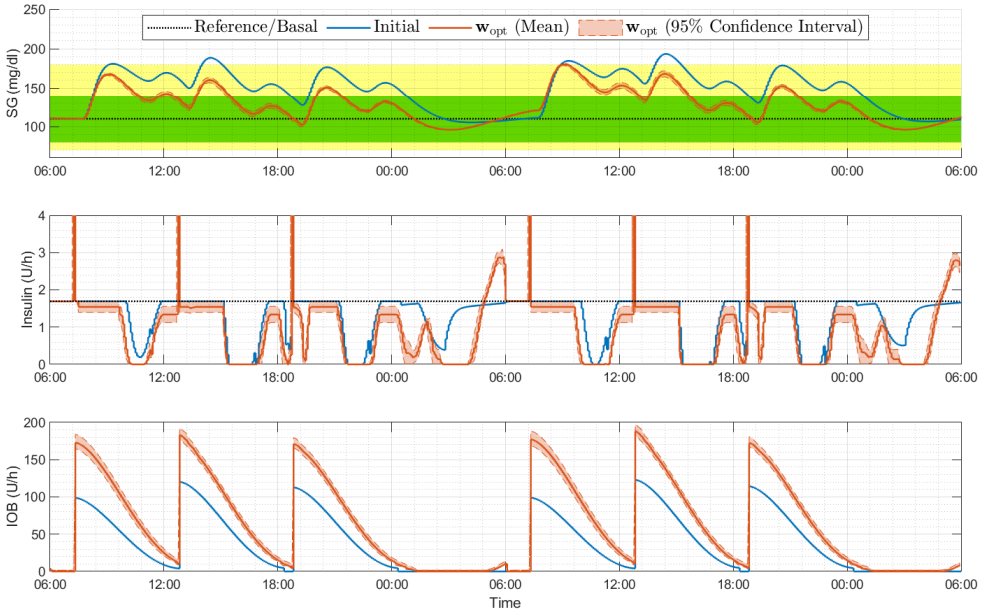

(c) Patient 15

Figure 4-7: *In-silico* performance analysis for all three virtual patients when initial parameter settings $(\mathbf{w}, \mathbf{o}) = (\mathbf{w}_0, \mathbf{o}_0)$ are used vs tuned parameters after BO Stage 1 tuning $(\mathbf{w}, \mathbf{o}) = (\mathbf{w}_{\text{opt}}, \mathbf{o}_0)$, across a 48-h time span starting from 6 am. The ensemble means and 95% confidence intervals of the SG, insulin delivery rate u and IOB u_{IOB} across the 10 runs for each subject using $\mathbf{w} = \mathbf{w}_{\text{opt}}$ (see Table 4-2) are presented.

4-2-2 Stage 2: Tuning of Model and Control-related parameters

For this tuning strategy, we will only present an analysis involving Patients 14 and 15. During the experimentation process, the algorithm failed to reach a satisfactory solution for Patient 12. The Stage 2 BO tuning framework aims to minimize potential overshoot overnight or before the intake of breakfast the next day, as well as the total glucose deviation from y_{ref}. We can infer a slow BG insulin pharmacokinetics of Patient 12 based on the glucose response profile in Figure 4-7a, which would render any tuning of the parameters γ_B and $\gamma_{\tau_{\text{sp}}}$ ineffective with the current experimental setup.

At the start of the tuning process, having initialized the parameters γ_1, γ_2, CR as well as $\mathcal{T}_{\text{bolus}}$ using subjects' respective $\mathbf{w}^*$, we repeat Algorithm 3b on both Patients 14 and 15 with the same meal 48-h meal protocol as before with the same number of runs. For Patient 14, a satisfactory result is observed, with the mean minimum cost appearing to properly converge in 8 iterations as shown in 4-8a. We see that the 95% confidence interval appears to have converged fully within 8 iterations. For Patient 15 on the other hand, similar to the results depicted in Fig. 4-6c, the mean minimum cost decreases after every of the 13 iterations, but without an observed convergence trend. This suggests that more iterations are needed to be performed on the subject. The performance of an extended iteration tuning paradigm are addressed in Section 4-3. Using the objective model function plots as shown in Figures 4-9

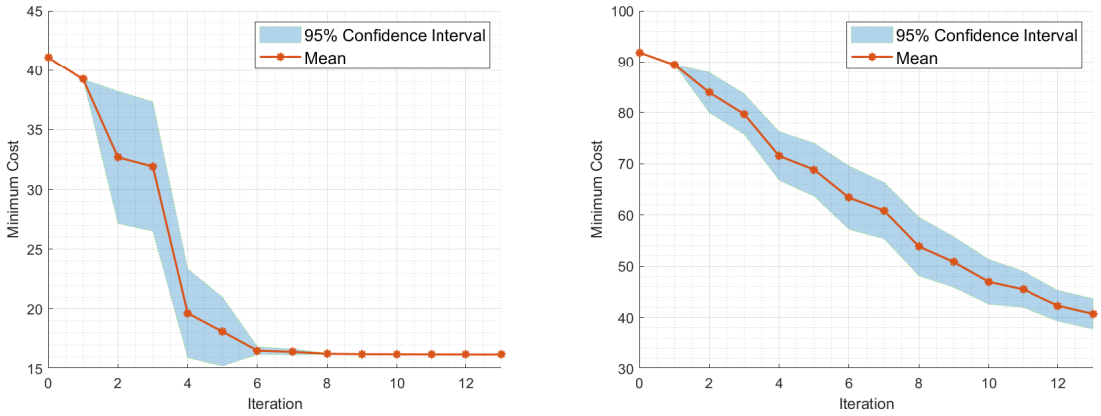

(a) Patient 14 **(b)** Patient 15

Figure 4-8: Minimum cost performance vs iterations for Stage 1 BO tuning.

and 4-10, we see that for patient 14, the plots corresponding to the worse performing run (Run 6) and the best performing run (Run 3). The observed points in Run 6 for Patient 14 is seen to be modelled accurately to a larger degree, compared to in Run 10 for Patient 15, where the objective function model is not well fitted to the observed points. When a set of observed points is modelled correctly, a smaller BO minimum cost function can be achieved, as exemplified by the objective function plot in Run 4 for Patient 15 as opposed to Run 10. This could account for the lack of confidence interval convergence for Patient 15.

Here, we will select the parameters of $\mathbf{o}^*$ based on the performance of the AP controller after 13 iterations of the Stage 2 BO tuning process. As shown in Table 4-4, for both Patients 14 and 15, we observe that there is an observable improvement in the glycameic performance, including the TIR and mean BG for all the runs. We see that the minimum blood glucose remains approximately the same if not, improved which is key to reducing hypoglycaemic risks.

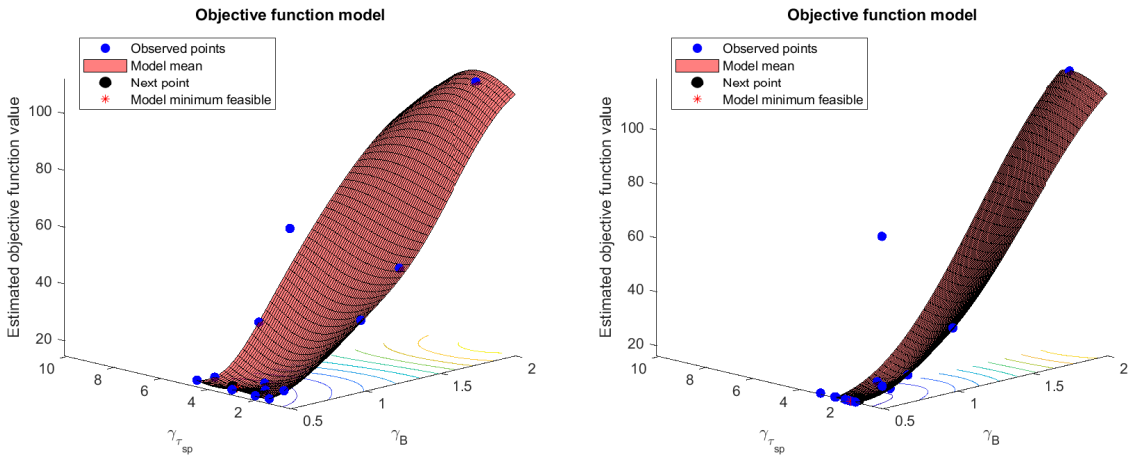

(a) Run 3 **(b)** Run 6

Figure 4-9: Objective function model plot after 13 iterations for Patient 14.

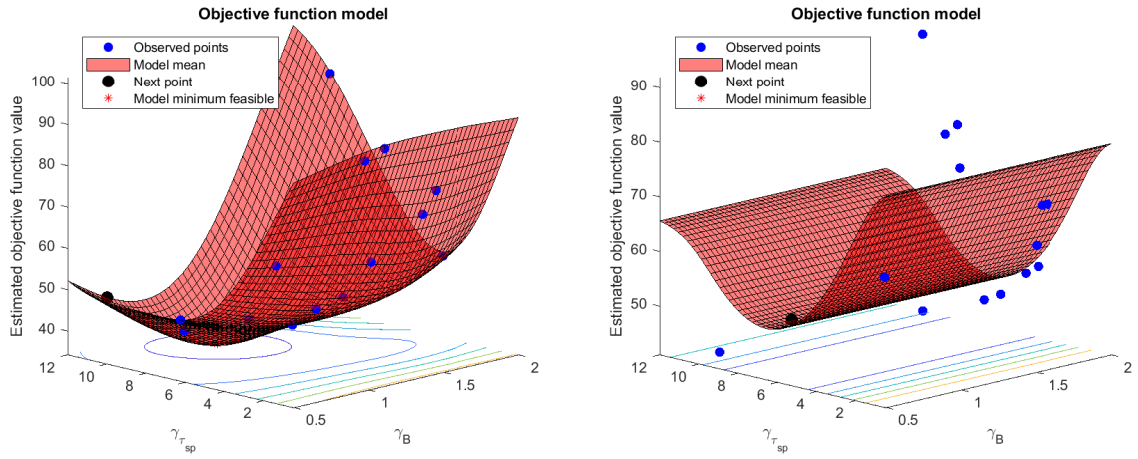

(a) Run 4 **(b)** Run 10

Figure 4-10: Objective function model plot after 13 iterations for Patient 15.

Furthermore, the improved performance can be observed graphically from the BG profile depicted in Figure 4-11. Paying attention to the overnight period starting from 00:00 to the time when the SG begins to rapidly increase as a result of breakfast consumption, we can clearly see that undershoot is effectively eliminated for Patient 14 based on Figure 4-11a. A less aggressive control action is also observed. For Patient 15, a significant decrease in overshoot at the time when the BGL starts to increase demonstrates the effectiveness of the tuning strategy. This improvement in performance can be attributed to the increase in value of the scaling factor $\gamma_{\tau_{\text{sp}}}$ and thus the parameter τ_{sp}. With increased τ_{sp}, this means that rapid increase in BG is reduced due to a slower convergence trajectory across the time horizon.

For the selection of parameter vector $\mathbf{o}^*$, a different approach from that of $\mathbf{w}^*$ is used. Since the best performing parameter vector in the previous tuning stage was used, we adopt a more realistic approach, one that would yield a performance that is closest to the mean value. We therefore select $\mathbf{o}_{\text{opt}}^{(1)}$ (Patient 14) and $\mathbf{o}_{\text{opt}}^{(6)}$ (Patient 15) as the parameter vectors of $\mathbf{o}^*$ for the respective subject. We assign the initial parameter vector $\mathbf{o}_0$ as the parameter vector for Patient 12 for the subsequent *in silico* evaluations described in Section 4-3. The final values of $\mathbf{w}^*$ and $\mathbf{o}^*$ employed in the AP controller for each virtual patient is summarised in Table 4-3.

Patient	$\mathbf{w}(1)$	$\mathbf{w}(2)$	$\mathbf{w}(3)$	$\mathbf{w}(4)$
12	0.9883	0.5412	9.0206	6.1498
14	0.4893	0.7250	9.0735	4.5117
15	0.9931	0.7022	4.4827	6.2988

(a) Vector element values of $\mathbf{w}^*$.

Patient	$\mathbf{o}(1)$	$\mathbf{o}(2)$
12	1	0.5
14	0.6349	2.770
15	1.9967	10.111

(b) Vector element values of $\mathbf{o}^*$.

Table 4-3: Final parameter vector after the dual-stage BO parameter tuning process.

$\mathbf{o}$	**BO Cost**	**TIR (%)** $\in [70, 180]$ mg/dL	**TIR (%)** $\in [80, 140]$ mg/dL	**Mean ± Std Deviation BG (mg/dL)**	**Min BG (mg/dL)**	**Max BG (mg/dL)**
$\mathbf{o}_0$	41.08	97.74	79.51	122.35 ± 23.31	96.30	183.96
$\mathbf{o}_{\text{opt}}^{(1)}$	16.19	98.09	79.86	121.56 ± 23.50	96.50	181.84
$\mathbf{o}_{\text{opt}}^{(2)}$	16.30	98.09	79.86	121.40 ± 23.46	96.50	181.78
$\mathbf{o}_{\text{opt}}^{(3)}$	16.07	97.92	79.86	121.68 ± 23.51	96.51	182.06
$\mathbf{o}_{\text{opt}}^{(4)}$	16.16	98.09	79.86	121.52 ± 23.46	96.52	181.79
$\mathbf{o}_{\text{opt}}^{(5)}$	16.29	98.09	79.86	121.53 ± 23.53	96.50	181.87
$\mathbf{o}_{\text{opt}}^{(6)}$	16.25	98.09	79.86	121.41 ± 23.43	96.52	181.74
$\mathbf{o}_{\text{opt}}^{(7)}$	16.20	98.09	79.86	121.48 ± 23.46	96.51	181.76
$\mathbf{o}_{\text{opt}}^{(8)}$	16.14	98.09	79.86	121.59 ± 23.47	96.53	182.08
$\mathbf{o}_{\text{opt}}^{(9)}$	16.11	97.92	79.86	121.64 ± 23.51	96.50	182.00
$\mathbf{o}_{\text{opt}}^{(10)}$	16.19	97.92	79.86	121.65 ± 23.55	96.50	182.02
Mean $(\mathbf{o}_{\text{opt}})$	**16.19**	**98.04**	**79.86**	$\mathbf{121.55 \pm 23.49}$	**96.50**	**181.89**

(a) Patient 14

$\mathbf{o}$	**BO Cost**	**TIR (%)** $\in [70, 180]$ mg/dL	**TIR (%)** $\in [80, 140]$ mg/dL	**Mean ± Std Deviation BG (mg/dL)**	**Min BG (mg/dL)**	**Max BG (mg/dL)**
$\mathbf{o}_0$	91.87	100.00	76.39	124.73 ± 19.74	95.16	178.13
$\mathbf{o}_{\text{opt}}^{(1)}$	36.37	100.00	78.47	123.65 ± 19.00	95.34	170.78
$\mathbf{o}_{\text{opt}}^{(2)}$	35.46	100.00	78.82	123.61 ± 18.96	95.18	170.28
$\mathbf{o}_{\text{opt}}^{(3)}$	41.59	100.00	78.30	123.61 ± 19.27	95.08	172.34
$\mathbf{o}_{\text{opt}}^{(4)}$	38.25	100.00	78.47	123.71 ± 19.08	95.36	171.29
$\mathbf{o}_{\text{opt}}^{(5)}$	52.96	100.00	77.60	123.86 ± 19.35	95.16	173.72
$\mathbf{o}_{\text{opt}}^{(6)}$	41.10	100.00	78.30	123.60 ± 19.27	95.07	172.28
$\mathbf{o}_{\text{opt}}^{(7)}$	41.11	100.00	78.30	123.60 ± 19.26	95.08	172.27
$\mathbf{o}_{\text{opt}}^{(8)}$	40.12	100.00	78.30	123.61 ± 19.24	95.15	172.10
$\mathbf{o}_{\text{opt}}^{(9)}$	38.99	100.00	78.13	123.72 ± 19.13	95.31	171.58
$\mathbf{o}_{\text{opt}}^{(10)}$	41.08	100.00	78.30	123.60 ± 19.27	95.07	172.28
Mean $(\mathbf{o}_{\text{opt}})$	**40.70**	**100.00**	**78.30**	$\mathbf{123.66 \pm 19.18}$	**95.18**	**171.89**

(b) Patient 15

Table 4-4: *In silico* results corresponding to the 10 optimum parameter vectors of $\mathbf{o}_{\text{opt}}$ and the initial settings $\mathbf{o}_0$. BO cost is evaluated during the tuning process prior to the 48-h protocol

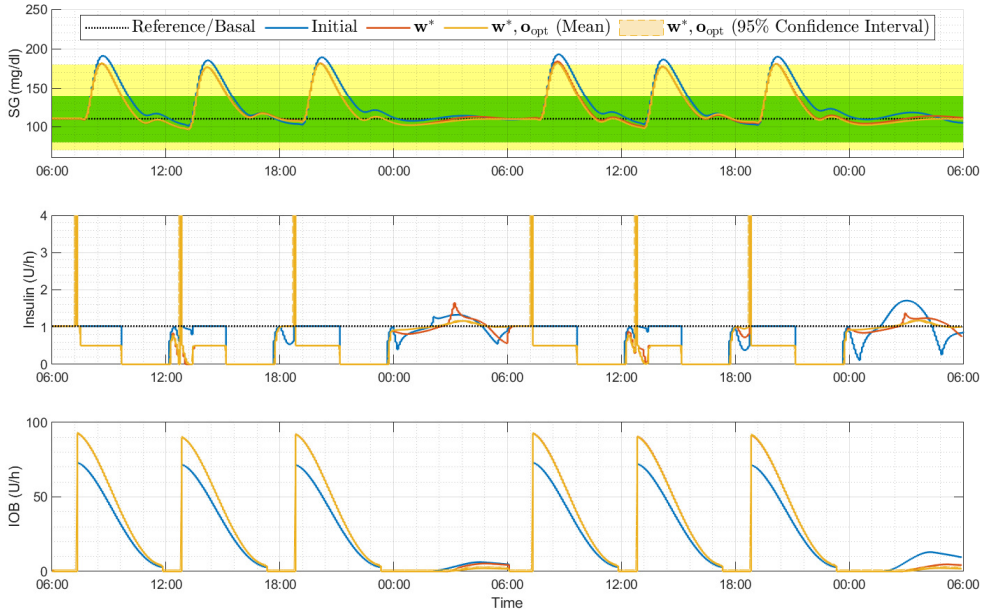

(a) Patient 14

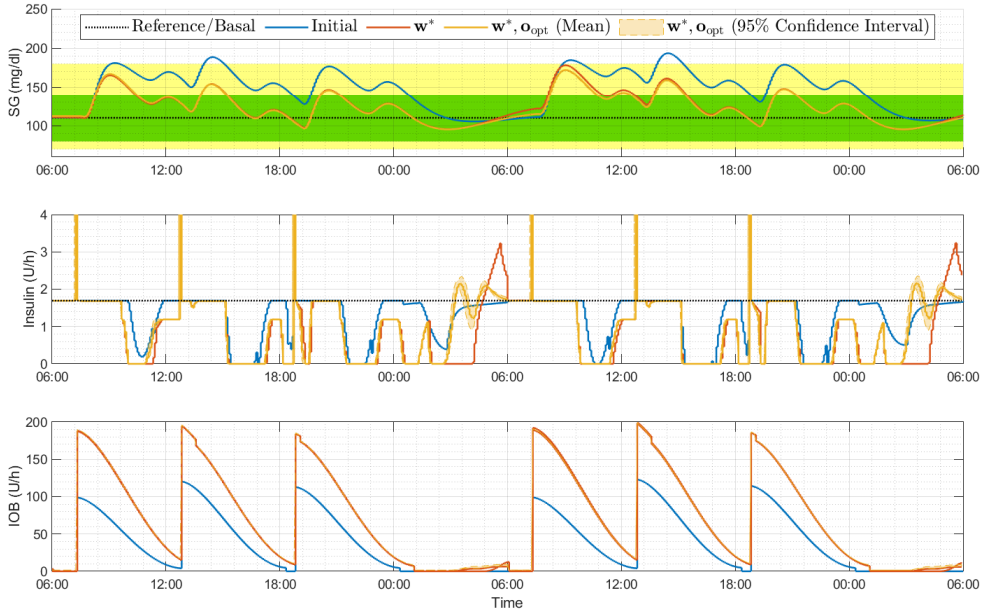

(b) Patient 15

Figure 4-11: *In-silico* performance analysis for all three virtual patients when initial parameter settings $(\mathbf{w}, \mathbf{o}) = (\mathbf{w}_0, \mathbf{o}_0)$ are used vs after Stage 1 BO tuning settings $(\mathbf{w}, \mathbf{o}) = (\mathbf{w}^*, \mathbf{o}_0)$ vs after Stage 2 BO tuning settings $(\mathbf{w}, \mathbf{o}) = (\mathbf{w}^*, \mathbf{o}_{\text{opt}})$, across a 48-h time span starting from 6 am. The ensemble means and 95% confidence intervals of the SG, insulin delivery rate u and insulin-on-board (IOB) u_{IOB} corresponding to $\mathbf{o}_{\text{opt}}$ across the 10 runs (see Table 4-4) are presented.

4-3 Performance Analysis of Tuned Controller in Different Meal Scenarios

Having undergone the tuning processes described, the goal of this section is to analyze and validate the proposed controller design under a different set of experimental protocols. The performance of the experiments are evaluated over a 48-h duration starting from 06:00 like in the previous section. A different set of meal sizes are now considered, as well as the meal times. We follow the meal protocols used by Shi *et al.* [163] in terms of the meal times and sizes and well as meal bolusing settings. The reason for adopting the chosen meal protocols lies with the authors' work being based on a development of the state-of-the-art zone MPC developed by Gondhalekar *et al.* [88], which was reviewed earlier in Section 2-3. The aim is to compare the performance of the tuned controller with the those in [163]. Four experimental protocols are considered for the performance evaluation:

- **Protocol A**: Announced meals with meal boluses calculated according to the 100% of the actual meal sizes
- **Protocol B**: Announced meals, with meal boluses calculated according to the 130% of the actual meal sizes (Over-bolus)
- **Protocol C**: Announced meals, with meal boluses are calculated according to the 70% of the actual meal sizes (Under-bolus)
- **Protocol D**: Unannounced with no meal boluses given

For each experimental protocol, three meals with meal sizes 50 g CHO (breakfast), 75 g CHO (lunch), and 75 g CHO (dinner) are taken at 08:00, 12:00 and 19:00 respectively. A general observation from the results presented in 4-2 lies with the dominance of glucose response by meal boluses particularly for a fully bolused meal, which poses the greatest impact on the TIR. The effect of closed-loop control in terms of improvements in glucose regulation is therefore limited to the ability for the artifical pancreas system (APS) to mitigate hypoglycaemic risks and overnight glucose oscillations or overshoots. In the presented results, we consider Protocol D to properly evaluate the performance of a fully-automated closed-loop system rather than a hybrid one. The implementation of Protocol C seeks to assess the ability for the closed-loop system to compensate for the lack of insulin bolus resulting from under-bolused meals, while Protocol B demands a more onerous task from the closed-loop system in relation to the prevention of hypoglycaemia, in the event that meals are over-bolused.

The performance for each patient after the 48-h simulation period are assessed according to the standard performance metrics from Table (2-1) (except for the glucose coefficient of variation). The low and high blood glucose indices (LBGI/HBGI) from eq. (2-29) are utilised in the performance evaluation, which follows that of [88] so as to provide a basis for future quantitative comparisons.

Performance analysis in Protocol A settings

We see from Table 4-5 that the TIR results in the Protocol A experimental scenario for each patient are comparable to those in Tables 4-2a and 4-4. While both the TIR in the wider

target range and the minimum BG for Patients 14 and 15 are observed to be lower compared to the last meal protocol, this is expected since there is a slightly larger intake of lunch and dinner CHO. A similar observation can be made with regards to the minimum BG recorded for Patients 12. Moreover, the TIR and minimum BG values for all three patients are still within the acceptable range ($> 90\%$ TIR and **Min BG** $\gtrapprox 95$ mg/dL). A notable observation relating to Patient 14 can be made in relation to the its overnight glucose profile. Between 00:00 and 06:00 during which the SP-MPC is activated, there is an occurrence of BG rebound despite the minimum BG over the given period not crossing below the reference value of 110 mg/dL. This stems from the prior insulin suspension sometime after 21:00, which coincides with the $\mathcal{P}_2$ period. Insulin suspension action is initiated as a result of the tight zonal bound ($\Delta\zeta = 5$ mg/dL) during this period (see eq. (3-49d)), whose bounds are dependent on the last measured SG. Having said, the AP is swift in reacting to the rebound as seen by the increased insulin delivery overnight. However, there appears to be a subtle overly aggressive insulin reduction in response to the decrease in BGL after the overshoot until 06:00 which is when controller switches from the Z-MPC to Z-MPC mode. Nevertheless, one can conclude that the AP performance for Protocol A fulfills the minimum expected requirements for all the tested subjects.

Performance analysis in Protocol B settings

For the comparative analysis between the other experimental protocols and with A, we first examine the case of meal over-bolusing in Protocol B, in which an increased TIR (both tight and wide ranges) and time-above-range (TAR), as well as a reduction in maximum BG are expected. The AP controller is expected to prevent any episodes of hypoglycaemia. Numerical results show that these expectations are met for all but Patient 14. Similar to the other subjects, Patient 14 experiences a larger TIR in the wider range compared to in Protocol A (99.13% vs 94.44%), but suffers in performance (75.17% vs 78.99) in the tight TIR range. A minor episode of hypoglycaemia is reported, with a time-below-range (TBR) of 0.87%, whereas no hypoglycaemia episodes occured. One can pinpoint to high insulin sensitivity and insuliin-glucose response time for Patient 14 compared to the other two patients as a contributing factor to the occurence of hypoglycaemia. As shown in Figure 4-12b, The AP controller appears to have maximised insulin suspension before the hypoglycaemic occurence, but the action is insufficient to counteract against the excess insulin delivered from meal bolusing. A similar observation can be made for the AP controller when tested on the other two patients.

It is worth noting that hypoglycaemia is only seen after lunch. The minimum BG after dinner is higher than the last value. This is due to the second term in eq. (3-2-3), which account for the difference between the SG at the time of meal bolusing and the 110 mg/dL reference. Less insulin bolus is given to the subject when the SG is less than the reference value. One significant positive takeaway based on the observed glucose profile of Patient 14, as shown in Figure 4-12b, lies with the AP controller's ability to avoid an overshoot. When comparing the overnight overshoot response of Protocol B with that when the meal protocol of Section 4-2 as seen in Figure 4-11a, we would expect the likelihood of an overshoot to be higher in the former case than the latter since the starting point of the BG rebound is lower and hence a greater negative deviation from the reference point. However, we see that the AP is effective in preventing an overshoot in Protocol B, thus demonstrating the efficacy

of the BO-tuned parameter $\gamma_{\tau_{sp}}$. Similarly, no significant difference in overshoot is observed for Patient 15, which was previously shown likely to experience an overshoot at the time of breakfast consumption the next day, compared to Protocol A. Therefore through Protocol B, the results reinforced the effectiveness of the BO tuning strategy of the parameter vector $\mathbf{o}$ in handling overnight overshoots.

Performance analysis in Protocol C settings

Numerical results show a lower TIR ($\in [80, 140]$) in Protocol C compared to Protocol A for all the tested subjects, with Patient 14 experiencing the worst difference (49.48% vs 78.99 %). A similar observation can be made for the TIR ($\in [70, 180]$) on Patient 14, with the reported TIR ($\in [70, 180]$) being lowest (86.46%) among the three subjects. The AP demonstrated an effective performance on Patient 12, who did not suffer any deterioration in the TIR ($\in [70, 180]$) as it remains at 100%. Also for the same patient, little undershoot was observed as Patient 12 achieved a minimum BG value of 106.05 mg/dL, higher than those in protocols A and B, as the BG converges relatively smoothly to the reference point during the overnight period. There is also little overshoot for patients 14 and 15, who have recorded minimum BG values of 109.96 and 109.90 mg/dL respectively that are comparable to that of Patient 12. The BG of Patients 12 and 15 manage to reach close to if not, cross the reference point by the time dinner consumption starts taking effect on the SG. This is not the case with Patient 14, whose BG value is substantially higher compared to the other two patients at that time instant, leading to a higher maximum BG.

Performance analysis in Protocol D settings

In this meal protocol, the overall glycaemic performance is significantly poorer for all three patients, with Patient 14 attaining the lowest TIR in the tight range among the lot, with a recorded value of 65.28%, while Patient 15 has the worst performing TIR in the tight target range (35.93%). Having said, the risk of hypoglycaemia is not compromised for Patients 12 and 15, with their recorded BGLs attaining a minimum BG that is higher than when the correct insulin bolus dose is supplemented (98.42 vs 89.86 mg/dL for Patient 12 and 98.42 vs 89.86 mg/dL Patient 15). One could also to refer their respective LBGI values to arrive at the same conclusion with respect to the hypoglycaemic risks. On the other hand, Patient 14 experienced a worse minimum BG, achieving having a value (85.80 vs 95.12 mg/dL). We can however see the impact that the IOB has on alleviating hypoglycaemic risks by referring to the insulin delivery profile shown in Fig. 4-12. For instance with Patient 12, we see that when the effect of breakfast consumption on the SG becomes apparent, after approximately 15 min (3 time samples) later, there is a gradual decrease in insulin delivered, which follows the trend of the IOB curve.

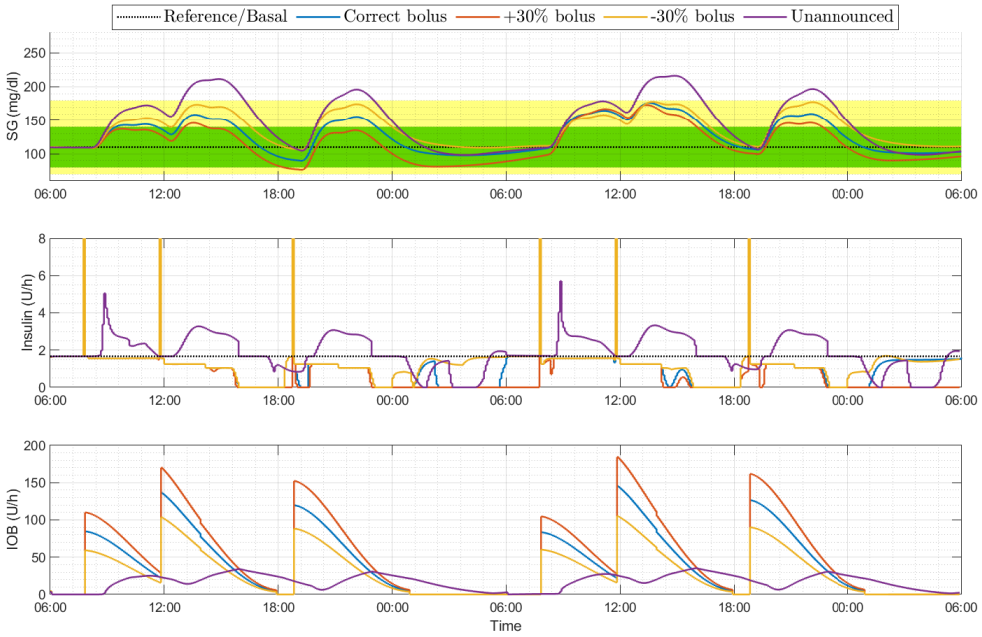

(a) Patient 12

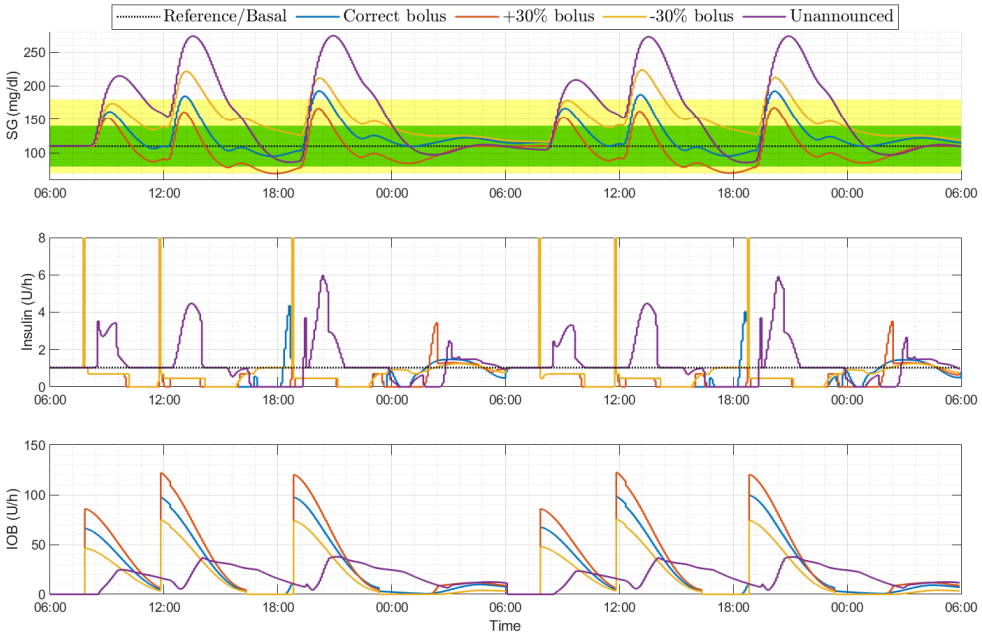

(b) Patient 14

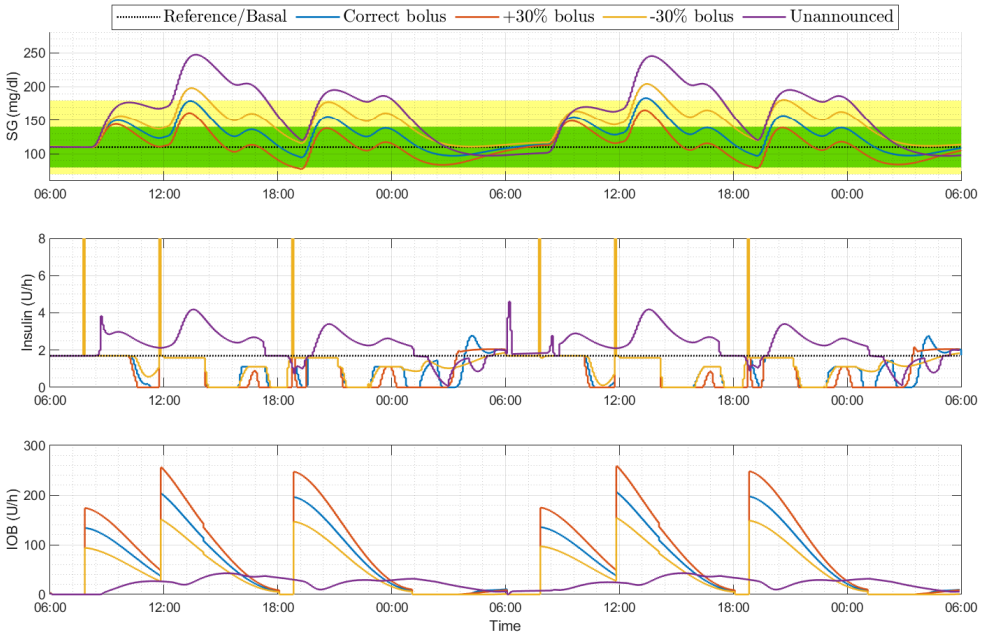

(c) Patient 15

Figure 4-12: *In silico* visual analysis comparing the performances among the different experimental protocols used in Section 4-3, across a 48-h time span starting from 6 am.

Metrics	Protocol A	Protocol B	Protocol C	Protocol D
TIR (%) $\in [80, 140]$ mg/dL	61.29	76.22	51.91	46.88
TIR (%) $\in [70, 180]$ mg/dL	100.00	100.00	100.00	76.74
TBR (%) < 70 mg/dL	0.00	0.00	0.00	0.00
TBR (%) < 54 mg/dL	0.00	0.00	0.00	0.00
TAR (%) > 180 mg/dL	0.00	0.00	0.00	23.26
TAR (%) > 250 mg/dL	0.00	0.00	0.00	0.00
Mean $\pm$ SD BG (mg/dL)	127.58 ± 24.43	117.06 ± 26.47	137.63 ± 24.06	147.21 ± 37.99
Min BG (mg/dL)	89.86	76.47	106.05	98.42
Max BG (mg/dL)	176.35	173.15	177.83	216.24
LBGI	0.01	0.31	0.00	<0.01
HBGI	4.03	2.84	5.71	9.08

(a) Patient 12

Metric	Protocol A	Protocol B	Protocol C	Protocol D
TIR (%) $\in [80, 140]$ mg/dL	78.99	75.17	49.48	48.79
TIR (%) $\in [70, 180]$ mg/dL	94.44	99.13	86.46	65.28
TBR (%) < 70 mg/dL	0.00	0.87	0.00	0.00
TBR (%) < 54 mg/dL	0.00	0.00	0.00	0.00
TAR (%) > 180 mg/dL	5.56	0.00	13.54	34.72
TAR (%) > 250 mg/dL	0.00	0.00	0.00	11.11
Mean ± SD BG (mg/dL)	125.11 ± 23.70	105.21 ± 23.70	146.94 ± 27.74	157.55 ± 58.09
Min BG (mg/dL)	95.11	69.65	109.96	85.80
Max BG (mg/dL)	192.72	167.63	223.80	274.22
LBGI	< 0.01	0.7	0.00	0.05
HBGI	3.40	1.42	7.81	13.40

(b) Patient 14

Metric	Protocol A	Protocol B	Protocol C	Protocol D
TIR (%) $\in [80, 140]$ mg/dL	75.69	87.33	42.01	35.93
TIR (%) $\in [70, 180]$ mg/dL	98.96	100.00	92.36	65.80
TBR (%) < 70 mg/dL	0.00	0.00	0.00	0.00
TBR (%) < 54 mg/dL	0.00	0.00	0.00	0.00
TAR (%) > 180 mg/dL	1.04	0.00	7.64	34.20
TAR (%) > 250 mg/dL	0.00	0.00	0.00	0.00
Mean ± SD BG (mg/dL)	127.03 ± 21.29	112.51 ± 20.12	144.03 ± 24.75	159.26 ± 42.73
Min BG (mg/dL)	94.94	77.73	109.90	97.02
Max BG (mg/dL)	183.48	165.53	204.28	247.09
LBGI	<0.01	0.22	0.00	<0.01
HBGI	3.60	1.67	7.09	12.38

(c) Patient 15

Table 4-5: *In silico* results of all four protocol experimental settings performed on each of the three virtual patients, across a 48-h time span starting from 6 am.

Performance evaluation after augmentation of $Q_{\zeta+}$ for Range 3 (Z-MPC)

Previously, we adopted a conservative approach to the penalising weight $Q_{\zeta+}$ in the glucose range when $y_{\text{CGM}} > \zeta_{\text{upper}}$, where $Q_{\zeta+} = 0.1$. With the expectation of improving the glycaemic performance by means of reducing the maximum BG during post-prandial periods, an attempt is made to increase $Q_{\zeta+}$ by a factor of 10 to $Q_{\zeta+} = 1$ in order to penalize positive

glucose deviations from the zonal upper bound by a higher magnitude. Augmenting $Q_{\zeta+}$ would eventually reduce the ratio $Q_{\zeta+} : Q_{\zeta-}$ for Range 3 (Z-MPC) to 0.1. The main intention is to penalise positive glucose deviations especially during unannounced meal scenarios, while keeping $Q_{\zeta-} > Q_{\zeta+}$ given the importance of hypoglycaemia prevention. To evaluate the performance of the augmented controller, the experiment protocols A to D are repeated like before, with the numerical results presented in Table 4-6c. The most pronounced difference in glycaemic performance is observed for Protocol D. All three subjects experienced an improvement in the TIR (both $\in [80, 140]$ and $\in [70, 180]$), especially for Patient 15, in which the new TIR is increased significantly from 65.80% to 75.00 %. In addition, the minimum BG for Patient 14, which was the only one of the three subjects that had a lower minimum BG in Protocol D than in Protocol A, now has an improved value (91.09% vs 85.80%) and also a reduced LBGI value (0.05 vs 0.02) and thereby reducing its hypoglycaemic risk. Having said, the minimum BG for Patient 12 in Protocol D decreased from 98.42 to 94.53 mg/dL, however based on the LBGI, the increased risk of hypoglycaemia is relatively low and hence insignificant. The results for the other protocols were comparable to before, and even though the weight augmentation did not significantly improve the performance for Protocols A to C, it is not an important factor to consider so long as the performances in announced meal scenarios are not significantly compromised.

The underlying reason behind the improvement in glycaemic performance is due to the delivery of insulin in a more active fashion and conservative manner subsequently. As shown in Figure 4-13, a sharp increase in insulin is delivered for all subjects as soon as the AP senses an sharply increasing glucose values. After a few time samples later, insulin delivery gradually decreases due to the rapid rise in the IOB. The AP controller is also shown to be capable of timely suspending insulin delivery for the case of Patient 14 between one to two hours before 18:00 when it anticipates that the SG would fall below $\zeta_{\text{lower}} = 100$ mg/dL.

Metrics	Protocol A	Protocol B	Protocol C	Protocol D
TIR (%) $\in [80, 140]$ mg/dL	61.29 (61.29)	76.22 (76.22)	51.74 (51.91)	48.79 (46.88)
TIR (%) $\in [70, 180]$ mg/dL	100.00 (100.00)	100.00 (100.00)	100.00 (100.00)	78.82 (76.74)
TBR (%) < 70 mg/dL	0.00 (0.00)	0.00 (0.00)	0.00 (0.00)	0.00 (0.00)
TBR (%) < 54 mg/dL	0.00 (0.00)	0.00 (0.00)	0.00 (0.00)	0.00 (0.00)
TAR (%) > 180 mg/dL	0.00 (0.00)	0.00 (0.00)	0.00 (0.00)	21.18 (23.26)
TAR (%) > 250 mg/dL	0.00 (0.00)	0.00 (0.00)	0.00 (0.00)	0.00 (0.00)
Mean ± SD BG (mg/dL)	127.54 ± 24.38 (127.58 ± 24.43)	117.11 ± 26.47 (117.06 ± 26.47)	137.71 ± 24.07 (137.63 ± 24.06)	143.85 ± 37.62 (147.21 ± 37.99)
Min BG (mg/dL)	90.00 (89.86)	76.59 (76.47)	106.21 (106.05)	94.53 (98.42)
Max BG (mg/dL)	176.05 (176.35)	173.16 (173.15)	177.88 (177.83)	213.93 (216.24)
LBGI	0.01 (0.01)	0.30 (0.31)	0.00 (0.00)	0.01 (<0.01)
HBGI	4.02 (4.03)	2.85 (2.84)	5.73 (5.71)	8.38 (9.08)

(a) Patient 12

Metrics	Protocol A	Protocol B	Protocol C	Protocol D
TIR (%) $\in [80, 140]$ mg/dL	79.17 (78.99)	75.17 (75.17)	51.39 (49.48)	49.65 (48.79)
TIR (%) $\in [70, 180]$ mg/dL	94.44 (94.44)	99.13 (99.13)	87.15 (86.46)	67.71 (65.28)
TBR (%) < 70 mg/dL	0.00 (0.00)	0.87 (0.87)	0.00 (0.00)	0.00 (0.00)
TBR (%) < 54 mg/dL	0.00 (0.00)	0.00 (0.00)	0.00 (0.00)	0.00 (0.00)
TAR (%) > 180 mg/dL	5.56 (5.56)	0.00 (0.00)	12.85 (13.54)	32.29 (34.72)
TAR (%) > 250 mg/dL	0.00 (0.00)	0.00 (0.00)	0.00 (0.00)	9.03 (11.11)
Mean ± SD BG (mg/dL)	125.06 ± 23.71 (125.11 ± 23.70)	105.16 ± 23.67 (105.21 ± 23.70)	145.72 ± 27.49 (146.94 ± 27.74)	154.79 ± 55.21 (157.55 ± 58.09)
Min BG (mg/dL)	95.12 (95.11)	69.65 (69.65)	109.34 (109.96)	91.09 (85.80)
Max BG (mg/dL)	192.72 (192.72)	167.63 (167.63)	222.13 (223.80)	272.06 (274.22)
LBGI	<0.01 (< 0.01)	0.72 (0.7)	0.00 (0.00)	0.02 (0.05)
HBGI	3.40 (3.40)	1.42 (1.42)	7.53 (7.81)	12.39 (13.40)

(b) Patient 14

Metrics	Protocol A	Protocol B	Protocol C	Protocol D
TIR (%) $\in [80, 140]$ mg/dL	75.17 (75.69)	87.15 (87.33)	40.97 (42.01)	38.72 (35.93)
TIR (%) $\in [70, 180]$ mg/dL	98.61 (98.96)	100.00 (100.00)	91.84 (92.36)	75.00 (65.80)
TBR (%) < 70 mg/dL	0.00 (0.00)	0.00 (0.00)	0.00 (0.00)	0.00 (0.00)
TBR (%) < 54 mg/dL	0.00 (0.00)	0.00 (0.00)	0.00 (0.00)	0.00 (0.00)
TAR (%) > 180 mg/dL	1.39 (1.04)	0.00 (0.00)	8.16 (7.64)	25.00 (34.20)
TAR (%) > 250 mg/dL	0.00 (0.00)	0.00 (0.00)	0.00 (0.00)	0.00 (0.00)
Mean ± SD BG (mg/dL)	127.24 ± 21.37 (127.03 ± 21.29)	112.76 ± 20.25 (112.51 ± 20.12)	145.87 ± 24.23 (144.03 ± 24.75)	154.10 ± 40.04 (159.26 ± 42.73)
Min BG (mg/dL)	95.09 (94.94)	77.88 (77.73)	111.67 (109.90)	97.22 (97.02)
Max BG (mg/dL)	183.48 (183.48)	165.54 (165.53)	206.78 (204.28)	242.17 (247.09)
LBGI	<0.01 (<0.01)	0.22 (0.22)	0.00 (0.00)	<0.01 (<0.01)
HBGI	3.64 (3.60)	1.71 (1.67)	7.44 (7.09)	10.86 (12.38)

(c) Patient 15

Table 4-6: *In silico* results of all four protocol experimental settings performed on each of the three virtual patients after the augmentation of $Q_{\zeta+}$, across a 48-h time span starting from 6 am. Results in brackets refer to those before augmenting $Q_{\zeta+}$, as presented in Table 4-5.

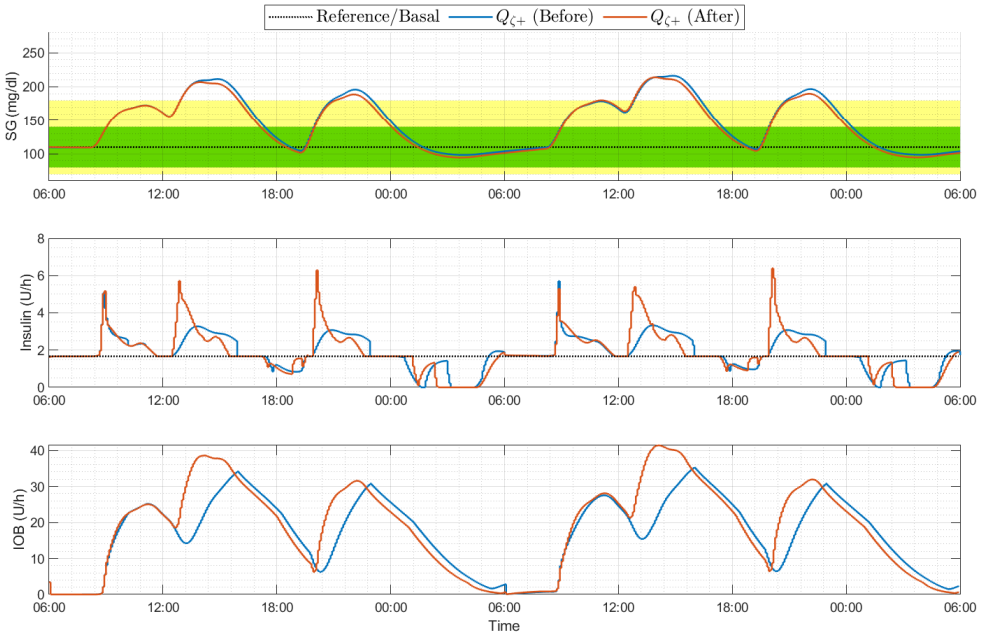

(a) Patient 12

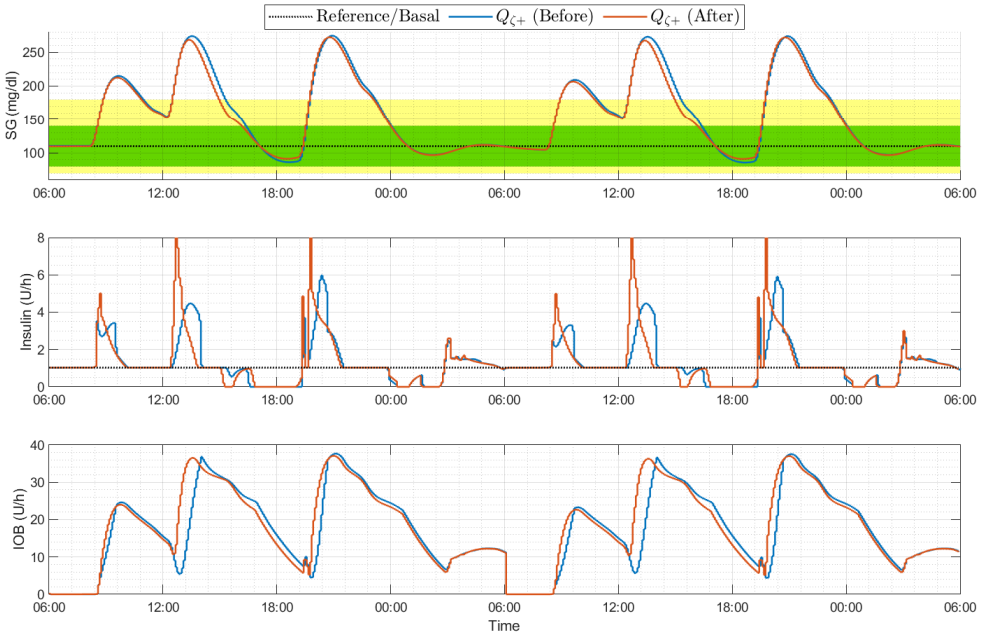

(b) Patient 14

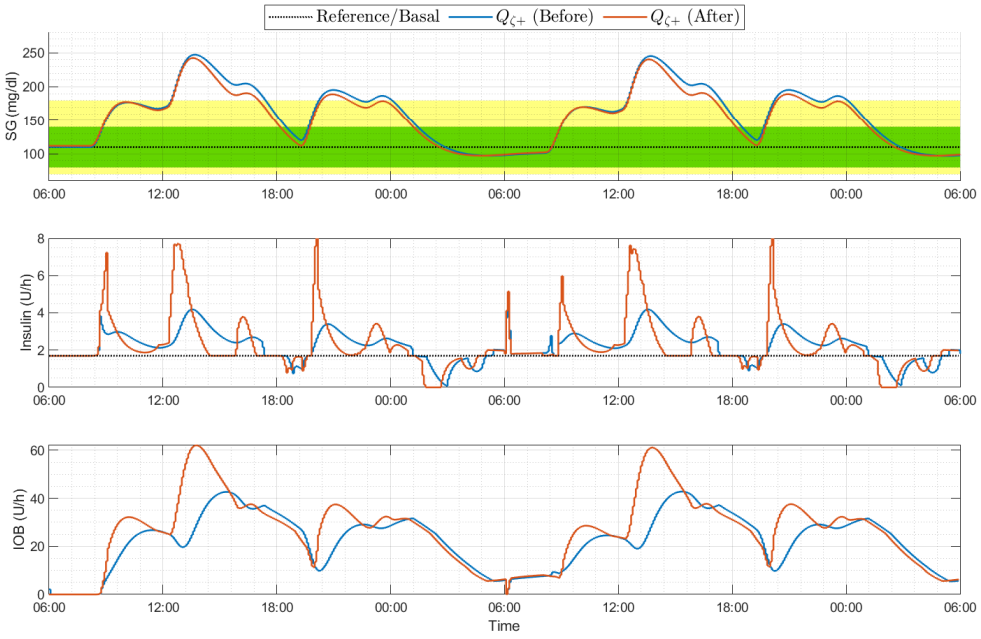

(c) Patient 15

Figure 4-13: *In silico* performance visual analysis for Protocol D (unannounced meals) when $Q_{\zeta+} = 0.1$ (before augmentation) vs $Q_{\zeta+} = 1$ (after augmentation) for Range 3 (Z-MPC), across a 48-h time span starting from 6 am.

Performance comparison with baseline controller

Metric	Proposed	Shi *et al.* [163]
TIR (%) $\in [70, 180]$ mg/dL	97.7	90.6
TBR (%) < 70 mg/dL	0.0%	0.0%
Mean BG (mg/dL)	126.61	129.2

(a) Correctly announced meal (100%)

Metric	Proposed	Shi *et al.* [163]
TIR (%) $\in [70, 180]$ mg/dL	99.71	95.4
TBR (%) < 70 mg/dL	0.29	0.0
Mean BG (mg/dL)	111.7	129.2

(b) Incorrectly announced meal (130%)

Metric	Proposed	Shi *et al.* [163]
TIR (%) $\in [80, 180]$ mg/dL	93.0	83.1
TBR (%) < 70 mg/dL	0.0	0.0
Mean BG (mg/dL)	143.1	141.8

(c) Incorrectly announced meal (70%)

Metric	Proposed	Shi *et al.* [163]
TIR (%) $\in [70, 180]$ mg/dL	73.8	70.5%
TBR (%) < 70 mg/dL	0.0	0.0
Mean BG (mg/dL)	150.91	153.8

(d) Unannounced meals (0%)

Table 4-7: Performance comparison with adaptive Z-MPC strategy proposed in [163]. The percentages in brackets denote the fractions of correctly calculated insulin boluses that were delivered to the subjects for a given meal size.

Here, we compare the results obtained from the proposed method after augmenting $Q_{\zeta+}$, with *in silico* results of the baseline controller in the literature [163], which employs a Z-MPC controller scheme with added modifications to the velocity-dependent weight adaptation from the works of Gondhalekar *et al.* [88]. The results are summarised in Table 4-7, in which the mean of each key performance metric across the three *in silico* patients are reported. One should take note that the results reported in [163] were obtained using a 100-adult subject cohort of the UVA/Padova simulator with the same meal times and sizes, but across a 24-h period instead of the 48-h employed in this work.

For the fully announced meals (100%), the result obtained outperformed that of the baseline controller in all aspects of listed performance metrics. The same applies for unannounced meals. While the TIR ($\in [70, 180]$ mg/dL) achieved with the proposed strategy for both the miscalculated-bolus meals (130% and 70%) are greater than those of the baseline, a slightly higher mean BG is reported for under-bolused meals (143.1 vs 141.8 mg/dL), and TBR (< 70 mg/dL) for over-bolused meals (0.29% vs 0.0%). The differences in mean BG and TBR for under- and over-bolused meals respectively are however subtle, and one may consider based on the current results, that the proposed controller outperforms the baseline.

Performance evaluation for an extended number of BO iterations

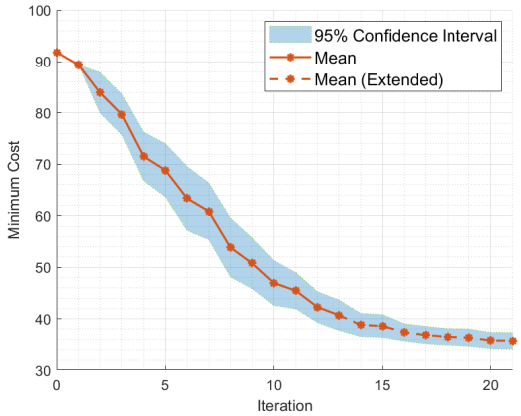

Figure 4-14: Extended minimum cost performance after each iteration in the Stage 2 BO tuning scheme for Patient 15. Refer to Figure 4-6c for non-extended plot.

The number of iterations was extended by 8 and continued from the previous 10 runs for Patient 15. After close examination of 4-10, we noticed that $\gamma_{\tau_{\text{sp}}}$ dominates the performance cost as using observation from Run 10. As shown in 4-10a, results from Run 4 in the first 13 iterations demonstrate the potential of achieving further reduction in the performance cost with a changing γ_B, but only at higher values of $\gamma_{\tau_{\text{sp}}}$. We therefore augment the search space upper limit that ensures τ_{sp} does not exceed a value of 12, while keeping the limits of the first tuning variable γ_B the same. We see that with increased variation in the search space for γ_B, the a lower minimum cost can still be achieved, with both the iteration mean and 95% confidence interval managing to converge to a sufficient minimum within 21 iterations.

Chapter 5

Discussion

In this research, we have explored the possibility of employing a proportional-integral-derivative (PID) controller with global (non-subject specific) parameters as an inner-loop system controller, whose reference value is regulated by a reference governor, that is the model predictive control (MPC), under *in silico* environments on three patients with distinctive glycaemic profiles. Based on the results gathered from Chapter 4, there are several aspects of the controller performance and the approach to the control problem that merit a discussion.

BO Performance Cost Function

The evaluation of the performance costs in both Stage 1 and Stage 2 Bayesian Optimisation (BO) tuning schemes were conducted in a 24-h scenario starting from approximately steady-state initial conditions of the first day. Based on visual observation on only the first 24-h of sensor glucose (SG) profiles depicted in Figure 4-7, it is clear that the defined BO objective function for the Stage 1 tuning is effective in achieving a lower average blood glucose (BG), and thus a higher time-in-range (TIR) while satisfying the conditions related to the minimum BG. The results of all three subjects fell within or close to the CVGA Zone A (see 2-1a) in which the minimum BG has to exceed 90 mg/dL while the maximum BG must be less than or equal to 180 mg/dL. The extend of reduction in the average BG is limited by the exponential penalty barrier term in the cost function to prevent an excessively low minimum BG value. Initial conditions play a significant role in influencing the peak post-pranidal BG, as exemplified by Patients 12 and 15. For both patients, one can visually estimate using Figure 4-7 that the average BG on the second day is higher than the first, which is attributed to the increasing glucose trend at the time of breakfast consumption. A significant BG rebound effect in response to the negative glucose deviation from the closest glucose target point led to a compromise in TIR ($\in [70, 180]$ mg dL) and maximum BG for the overall 48-h period (See 4-2, which was not accounted for in evaluation process during the Stage 1 BO tuning process. Moreover, there is a limitation on the extent to which insulin suspension can cause a sufficient reaction to negative glucose deviations from the desired set-point or range. Given that insulin delivery cannot go below 0, the rate at which BG rises would depend

on the insulin sensitivity and other underlying glucose response factors of the patient. The observation made suggests a need to augment the barrier penalty term in the cost function, by increasing the acceptable minimum BG threshold, which was set at 95 mg/dL in this research work.

Selection and Tuning of $\mathbf{w}^*$

Due to practical considerations on the patient's safety and lifestyle, the number of iterations that can be performed on an actual patient is limited. In Section 4-2, we saw that for Patients 12 and 14, despite an improvement in the minimum cost of $J_{\mathbf{w}}$ after 15 iterations, there were no signs of a converging confidence interval. In a separate finding that is not reported in this work, attempts were made to extend the number of iterations for all the existing runs for Patients 12 and 15, with in some of the runs, there was a tendency for the BO algorithm to be trapped in a certain sub-region of the feasible search space, particularly relating to the carbohydrate-to-insulin ratio (CR) parameter which has the most influence on the post-prandial peak BG. There are several factors that could have caused this occurrence. While the initial purpose of introducing γ_1 and γ_2 as attenuating factors to the insulin set-point lies with them serving as a contingency against anticipated hypoglycaemia, their roles could be expanded by contributing to a reduction in feasible search space of CR. What this means is that the reduced insulin delivered during the $\mathcal{P}_1$ and $\mathcal{P}_2$ expands room for more bolus supplements (via a reduced CR) that would facilitate the increased curbing of the post-prandial peak BG value, which mimics the concept of insulin "compensation". However, if the CR is not sufficiently low and both γ_1 amd γ_2 values are too low, it would result in a higher mean BG. Similarly, if γ_1 amd γ_2 are not sufficiently low when CR is reduced to the extent that a violation of the minimum BG threshold occurs, the BO algorithm would perceive any reduction in the CR relative to the last CR that yielded the latest minimum performance cost as an unfeasible means of reducing the cost, thus rendering the BO unable to find an improved solution. Moreover, there also exists the possibility that the initial estimations of $\mathcal{T}_{\text{bolus}}$ are inaccurate, with the constraint imposed on the search space relating to $\mathcal{T}_{\text{bolus}}$ having an inhibiting effect on the performance cost, or none at all. A reduction in the size or reformulation of the parameter search approach for $\mathbf{w}$ could yield an improved outcome in the Stage 1 BO-tuning scheme.

Selection and Tuning of $\mathbf{o}^*$

With a smaller number of tuning parameters for $\mathbf{o}^*$ in the Stage 2 BO-tuning scheme than $\mathbf{w}^*$, one would expect the BO algorithm to perform better in the search for the optimum solution. We can argue that this assumption holds true in the case of Patient 14, and partially with 15. Due to the relatively high insulin sensitivity and glucose response, we observe that a larger impact can be made by the artificial pancreas (AP) controller overnight on the SG of Patient 14. This could explain the reason for the full or near convergence in both the mean and the confidence interval across the ten runs after the given initial number of iterations. One can validate the claim on the effectiveness of the BO tuning of $\mathbf{o}$ for Patient 14 by examining the optimum solutions for each of the runs for the subject in Table 5-1, specifically $\mathbf{o}(1)$, which has a dominant influence on the performance cost $J_{\mathbf{o}}$ based on the visual analysis in Figure 4-9. We can see that despite the hard constraints imposed on $\mathbf{o}(1)$ between 0.5 and 2,

only in Runs 2 and 6 were the corresponding $\mathbf{o}_{\text{opt}}(1)$ were of close proximity to the lower limit of 0.5. Moreover, based on the reported BO costs in Table 4-6c, $\mathbf{o}_{\text{opt}}^{(3)}$ (Run 3) and $\mathbf{o}_{\text{opt}}^{(9)}$ (Run 9) with $\mathbf{o}_{\text{opt}}(1)$ values of 0.7189 and 0.6976 respectively achieved the two lowest minimum costs, thus validating the aforementioned claim.

Run	$\mathbf{o}(1)$	$\mathbf{o}(2)$
1	0.6349	2.771
2	0.5020	1.998
3	0.7189	2.994
4	0.5657	1.752
5	0.6556	3.592
6	0.5002	1.643
7	0.5581	1.957
8	0.6041	1.833
9	0.6976	2.999
10	0.7509	4.494

Table 5-1: $\mathbf{o}_{\text{opt}}$ values corresponding to each Stage 2 BO-tuning run for Patients 14 after 13 iterations.

Run	$\mathbf{o}(1)$	$\mathbf{o}(2)$
1	1.1332	11.998
2	1.1808	11.999
3	1.2441	11.439
4	1.1604	12.000
5	1.9609	11.999
6	1.1115	12.000
7	1.9990	11.998
8	1.1951	11.999
9	1.1482	11.321
10	1.9982	11.995

Table 5-2: $\mathbf{o}_{\text{opt}}$ values corresponding to each Stage 2 BO tuning run for Patients 15 after 22 iterations.

The limitations of the Stage 2 BO tuning of $\mathbf{o}$ were found to be more apparent for patients with slower insulin-glucose metabolism response. From the analysis in Section 4-2, we learned that $\gamma_{\tau_{\text{sp}}}$ has a dominant influence on $J_{\mathbf{o}}$ and that γ_B is relatively insensitive at low values of the former for Patient 15. Apart from the effect that $\gamma_{\tau_{\text{sp}}}$ has on $J_{\mathbf{o}}$ for the given subject, a high $\gamma_{\tau_{\text{sp}}}$ which in turn means a high τ_{sp}, can be detrimental when $y_{\text{CGM}} > y_{\text{ref}}$ while the set-point tracking model predictive control (SP-MPC) is active. Given that τ_{sp} is symmetric for both positive and negative deviations, this causes an overly-aggressive reduction in insulin delivery by the AP as BG approaches y_{ref} from above, which explains the slight rebound during Protocol C between approximately 04:30 till 06:00 when the SP-MPC is active as shown in Figure 4-12c. One takeaway from this observation lies with the necessity of employing a set of asymmetric τ_{sp} parameters, as utilised by Boiroux *et al.* [27], where the defined

exponential-decay-trajectories for the set-point reference across the prediction horizon are defined differently defined when $y_{\mathrm{CGM}} \geq y_{\mathrm{ref}}$ and $y_{\mathrm{CGM}} < y_{\mathrm{ref}}$. However, when $\gamma_{\tau_{\mathrm{sp}}}$ was constrained to an upper limit of 12 during the extended iteration process, we see an improvement in the minimum cost as explained in the extended performance analysis in Section 4-3. We can infer from Table 5-2 that the algorithm was effective in tuning the optimum value of $\mathbf{o}(1)$ for Patient 15, where $\mathbf{o}_{\mathrm{opt}}(1)$ lies in the region of $1.1 \lessapprox \mathbf{o}_{\mathrm{opt}}(1) \lessapprox 1.3$. This can be validated by an analysis of the minimum feasible point in Figure 4-10a. With Patient 12, the tuning scheme was ineffective as the insulin-glucose response of the subject was by far the slowest among the three patients, which results in an insensitive performance cost with respect to $\mathbf{o}$.

Chapter 6

Conclusion and Future Work

6-1 General Conclusion

In this thesis research, we have presented an efficient formulation of a novel control framework to better manage glycaemic control in Type-1 diabetes mellitus (T1DM). The lower-layer control architecture which is paired with an upper layer dual-stage parameter tuning scheme using Bayesian Optimisation (BO), demonstrated its ability to improve performance using standard glycaemic performance metric, when compared to an established baseline control strategy [163].

Before answering the research question, we first revisit the major contributions of this thesis work. In this step, we will relate the corresponding results to the prior findings from the literature, as an attempt to close the research gap. Subsequently, the extent to which the achieved outcomes of the thesis work have met the objectives outlined in Section 1-2 are assessed before finally arriving at a conclusive answer to the research question.

The main contributions of the thesis are as follows:

- **Dual-loop (inner and outer) controller architecture**
  We exploited the knowledge gained from our literature survey on the extensive use of the proportional-integral-derivative (PID) and model predictive control (MPC) as established control approaches for artificial pancreas (AP) designs. The proposed architecture moves away from the common AP practice in T1DM, in which either an MPC or PID controller is employed in the control paradigm. Instead of a prediction model that is based on the patient's pharmacokinetics, we considered identifying the model structure of a stable inner-loop control system. In addition, the employment of the PID controller as the inner-loop and parameterizing it using the Skogestad half-rule [164] facilitates an efficient formulation of the inner-loop control architecture. In spite of inter-subject variability, the global use of a selected model that was identified using *in silico* data from a chosen subject, was successful, with the MPC being able to effectively manage overshoots in post-prandial periods for subjects with a fasting insulin-glucose

metabolism, especially with the set-point tracking model predictive control (SP-MPC) as demonstrated in Chapter 4. The dual-loop approach also facilitates increased local linearity, allowing for the employment of a reduced-order state-space model which can be identified using a data-driven fashion. In addition to reduced a computation effort, a reduced-order model enabled an employment of a Luenberger observer which is considered to be more straightforward in implementation compared to a Kalman Filter, which contributes to increased implementation efficiency.

- **Safety Regulation Scheme that includes a switching MPC mechanism**
  The employment of the zone MPC has its benefits which have been treated extensively in the literature. However, it is susceptible to an overshoot if blood glucose (BG) rises too quickly from below the target zone, even which the penalty weight $Q_{(\Delta y)+}$ is unable to effectively counteract. The possible pitfall with the employment of the zone MPC alone is also shared by Lee *et al.* [122], who highlighted possible concerns on sluggish response to hyperglycaemic excursions due to the existence of a quiescent zone. Findings from the state-of-the-art zone MPC works in the literature show that no other zone MPC approach or controller have been utilised in conjuncture with the zone MPC to treat glycaemic variations contributed by the utilisation of a quiescent zone. The switching MPC mechanism allows for improved overshoot performance by employing the set-point MPC when BG falls below the BG target range, as shown in preliminary results in Section 4-1. In addition, the Safety Regulation Unit (SRU) facilitates a dynamical regulation in the insulin limit especially during post-prandial periods for announced meal scenarios, as an improved contingency against possible hypoglycemia.

- **Tuning of insulin reference attenuating factors and the insulin decay length**
  In Chapter 5, we discussed the relevance of insulin attenuating factors γ_1 and γ_2 and their relationships with carbohydrate-to-insulin ratio (CR) in influencing post-prandial glucose response upon the consumption of an announced meal. The tuning of these three variables as part of the Stage 1 BO tuning process presents an open door to opportunities in peak BG reduction efforts, so as to increase time-in-range (TIR) without compromising on hypoglycaemia risks. The insulin decay length, in particular the one that corresponds to a insulin bolus intake ($\mathcal{T}_{\text{bolus}}$), have been reported in the literature as a subject-specific parameter, with significant inter-subject variability within populations of T1DM patients. However, long-term adaptation or tuning efforts on this parameter is absent to the best of our knowledge. The inclusion of $\mathcal{T}_{\text{bolus}}$ in the tuning framework provides a chance to evaluate its impact on glycaemic performance improvements.

- **BO framework that follows the Identification for Control (I4C) philosophy**
  In the Stage 2 BO tuning framework, we attempt to augment the input matrix gain γ_B of the reduced state-space model as part of the goal of model personalisation. This is in view of the practical challenges surrounding a thorough individualised model parameter identification process, which has warranted the use of clinical parameters such as the total daily insulin dose (TDD) to determine the input gain value. The tuning of γ_B using BO follows the principle of I4C [85], but in this context we took inspiration from Piga *et al.* where we treat γ_B as a design parameter that is used to minimize the BO performance cost $J_{\mathbf{o}}$. The latter is defined by the amount of glucose deviation from the desired value y_{ref} during overnight periods, particular positive ones which typically correspond to overshoots. The design parameter set was extended to include $\gamma_{\tau_{\text{sp}}}$ as a

means of individualised control. Based on the *in silico* performance analysis for Patient 14, the proposed framework demonstrated its ability to reduce overshoot or oscillatory responses in the event of a significant negative deviation from y_{ref}.

Based on the outcomes of the main contributions, we arrive at the general conclusion of this thesis research by aligning them with the four defined objectives:

- *Assess the effectiveness of a dual-loop control scheme with limited adaptation of its inner-loop system parameter settings*
  Due to safety and practical reasons, a full model-parameter adaptation of the inner-loop control system is not feasible. Instead, a conservative approach is employed to the tuning approach of the PID controller parameters offline, such that the dual-loop controller is sufficiently safe to apply on all the tested subjects. The tuning of $\gamma_{\tau_{\text{sp}}}$ has shown to be efficient, as it does not require augmenting the state and output matrices of the prediction model, which would have required a redesign of the observer gain. Given the results assessed using the key performance metrics, the dual-loop control scheme is deemed to be largely effective in achieving the expected glycaemic performance.

- *Determine alternative measures to increasing the TIR without compromising on patient safety*
  Via the introduction of γ_1 and γ_2, we managed to allow the feedforward bolus calculator to deliver more insulin bolus during announced meals with a reduced CR, thereby a reduction of peak BG, which would eventually lead to an expected higher TIR. The presence of exponential penalty barrier terms in the BO cost functions ensures that the minimum BG is not violated, thus enforcing patient safety by preventing an increase in the time-below-range (TBR).

- *Validate the applicability of the Identification for Control (I4C) approach in T1DM treatment*
  With the exception of Patient 12, we managed to successfully use the Stage 2 BO tuning framework, the scaling factor γ_B for the input matrix gain is carefully tuned in order to achieve a better overshoot and undershoot performance during overnight periods for Patient 14. We arrived at a similar conclusion with Patient 15, when an augmentation to the $\gamma_{\tau_{\text{sp}}}$ upper limit was applied during an extend run of iterations. We hypothesize that with an increase in the minimum BG threshold for Patient 12 and thus the post-prandial undershoot, we might be able to apply the Stage 2 BO tuning framework to the subject. Based on the final results to the optimum γ_B for Patients 14 and Patients 15, assuming that the TDD of the patient is an accurate indicator of the relative model gain. Given that the initial model gain ($\gamma_B = 1$) corresponds to that of Patient 13, who had an *a priori*-known TDD value of 56.423 U. One would expect the γ_B for Patient 14 to be greater than 1 due to its higher insulin sensiivity and overall lower TDD value, and less than 1 for Patient 15 using the same reasoning. The differences in the results, based on Tables 5-1 and 5-2, asserts the underlying belief behind the I4C ideology, that the best performing model for control may not be the one with the fewest prediction errors, but rather the one that yields the best result on the actual system when used in a closed-loop setting, with the corresponding model-based controller [149], in this case, the MPC .

- *Evaluate the robustness of the AP controller under miscalculated meal bolusing and unannounced meal scenarios*
  In Section 4-3, the numerical results and performance analysis conducted show that the AP controller is able to achieve greater TIR in the event of an over-bolused meal without significantly compromising on the TBR, while in an under-bolused meal setting, the TIR suffered in performance, however hypoglycaemic risks are absent for all three patients, all of whom achieved an LBGI score of 0. In unannounced meal scenarios, it was expected that glycaemic performance was the worst among the three considered meal scenarios. Most important, no hypoglycaemic episodes were observed, which can be attributed to the employment of the set-point MPC, in addition to the zone MPC. The utilisation of the set-point MPC facilitates a more proactive role in insulin suspension as well as overshoot mitigation in the event of a significant BG rebound. We can therefore conclude that the proposed AP control strategy is sufficiently robust against non-ideal, uncertain meal scenarios.

By achieving all of the four aforementioned goals, we can finally answer the stated research question:

Can a dual-loop control scheme supported by an iterative Bayesian Optimisation parameter tuning framework yield a satisfactory glycaemic performance in T1DM?

In spite of the possible significant model-plant mismatch due to the global use of model parameters and limited parameter adaptation, we have thus far demonstrated from our thesis research that the dual-loop control scheme, in which the PID controller serves as the inner-loop controller and the MPC the outer-loop, yielded a highly satisfactory glycaemic performance, especially when paired with an upper-layer BO-based parameter tuning framework. We concluded our findings using numerical results defined by performance metrics that have been well-established by the international consensus. The applicability of this novel approach paves way for greater opportunities in the research domain of T1DM.

6-2 Recommendations for Future Work

We have covered the limitations of this thesis work in various parts of this thesis work. Future studies that can

- **Enlarge the number of tested subjects** During the build-up to this thesis work, we only considered 10 *in silico* patients of the UVa/Padova virtual metabolic simulation, in which only three of them have been subjected to performance evaluation analysis. In addition to the remaining subjects of the adult cohort, the proposed strategy can be applied to cohorts of virtual adolescents and children subjects to further validate the performance of the control scheme.
- **Safe and Constrained Bayeesian Optimisation**
  In this thesis work, the adopted BO problem was implemented using the built-in MATLAB function `bayesopt` which does not incorporate probabilistic constraints, and rely

only on a constrained domain. The limitations of this approach are apparent, which include ineffective learning of parameters that are to be evaluated in each iteration, which increases the probability of a sub-optimal solution within a given maximum number of iterations. We can consider the safe BO strategy proposed by Khosravi and colleagues [110], who employed the algorithm in a data-driven approach to model the performance of a closed-loop system with respect to controller gain parameters. In addition to a safety penalty in the cost function, such as the exponential barrier term proposed in this work, we can further enforce safety by the addition of safety-critical constraints like Gaussian Process (GP)s, or through the modification of the acquisition function, which has been attempted in a T1DM context as exemplified by the works of Krishnamoorthy *et al.* [118, 119].

- **Improved control personalisation**
  We learned from our research that the insulin and glucose pharmacokinetics vary greatly for different subjects. Factors accounting for these differences can be related to insulin sensitivity, gastric emptying or glucose absorption among others. One can introduce a diurnal, periodic nominal set-point (y_{ref}) and $\zeta_{\text{lower}}, \zeta_{\text{upper}}$ range such as the example in [87] to better manage BG rebound from larger meal intakes, or positive glucose deviation penalisation. Moreover, we can consider taking inspiration from the concept of *glucose velocity*-dependent adaptive weights proposed by Gondhalekar [88] and Shi *et al.*[163] in shaping our asymmetric MPC cost function weights, so as to better manage glucose penalisations.

Appendix A

Supplementary materials for Chapter 2

A-1 Glossary

Definition	Glucose	Insulin
Absolute mass	Q	M
Mass per unit body mass	q	m
Concentration	C	C
Flux Rate / Input	R	R
Volume per unit body mass	V	V

Table A-1: Symbol definition of glucose-insulin simulation model discussed in Section 2-1.

Distributed refers to the quantity per unit patient mass (kg). The definitions are derived from [53, 54, 134].

A-1-1 State Variables

- $Q_{\text{sto},s}$: Solid glucose mass in the stomach [mg]
- $Q_{\text{sto},l}$: Liquid glucose mass in the stomach [mg]
- Q_{gut} : Glucose mass in the intestines [mg]
- q_{pla} : Distributed glucose mass in plasma [mg/kg]
- q_{tis} : Distributed glucose mass in tissue [mg/kg]
- m_{pla} : Distributed insulin amount in plasma [pmol/kg]
- $C_{m_{\text{inter}}}$: Interstitial insulin concentration in liver / Insulin action on glucose concentration [pmol/L]

- $C_{m_{\text{liv}}}$: Insulin concentration (action) in liver [pmol/L]
- $C_{m_{\text{liv,delay}}}$: Delayed insulin concentration signal (action) in liver [pmol/L]
- m_{liv}: Distributed insulin amount in liver [pmol/kg]
- $m_{\mathbf{sc},1}$: Distributed amount of non-monomeric insulin in subcutaneous space [pmol/kg]
- $m_{\mathbf{sc},2}$: Distributed amount of monomeric insulin in subcutaneous space [pmol/kg]
- $q_{\mathbf{sc}}$: Distributed amount of glucose in subcutaneous space [mg/kg]

A-1-2 Model Parameters and Process Variables

Flux Processes

- $R_{\mathbf{U},\text{dep}}$: Insulin-dependent glucose utilization rate [mg/kg/min]
- $R_{\mathbf{U},\text{indep}}$: Insulin-independent glucose utilization rate (erythrocytes) [mg/kg/min]
- $R_{\mathbf{GA}}$: Glucose appearance rate in plasma [mg/kg/min]
- $R_{\mathbf{EGP}}$: Endogenous glucose production rate [mg/kg/min]
- $R_{\mathbf{E}}$: Glucose renal excretion rate [mg/kg/min]
- $R_{\mathbf{IA}}$: Insulin appearance rate [pmol/kg/min]

Glucose Kinetics

- k_{q1}: Rate parameter associated with q_{pla} [min^{-1}]
- k_{q2}: Rate parameter associated with q_{tis} [min^{-1}]
- V_q: Distribution volume of glucose [L/kg]

Insulin Kinetics

- V_m: Distribution volume of insulin [dL/kg]
- k_{m1}: Rate constant of insulin transportation from liver to plasma [min^{-1}]
- k_{m2}: Rate constant of insulin transportation from plasma to liver [min^{-1}]
- k_{m3}: Rate of insulin degradation in the liver [min^{-1}]
- k_{m4}: Rate constant of insulin degradation in the periphery [min^{-1}]

Glucose Appearance (GA)

- W_{body}: Patient body mass (weight) [kg]
- Q_{total}: Total glucose present in the stomach at the start of meal and ingested glucose during meal [mg]
- Q_{sto}: Sum of liquid and solid glucose present in the stomach [mg]
- $k_{\mathbf{GA}1}$ Glucose (Q) absorption rate constant in small intestine [min^{-1}]
- $k'_{\mathbf{GA}1}$: Fraction of intestinal absorption which appears in plasma [-]
- $k_{\mathbf{GA}2}$: Glucose grinding rate constant in stomach [min^{-1}]
- $k_{\mathbf{GA}3}$: Gastric emptying time-varying rate parameter in stomach (Q_{sto} dependent) [min^{-1}]
- $\overline{k}_{\mathbf{GA}3}$: Maximum $k_{\mathbf{GA}3}$ [min^{-1}]
- $\underline{k}_{\mathbf{GA}3}$: Minimum $k_{\mathbf{GA}3}$ [min^{-1}]
- $k_{\mathbf{GA}3\downarrow}$: Rate of decrease parameter of $k_{\mathbf{GA}3}$ to $\underline{k}_{\mathbf{GA}3}$ [mg^{-1}]
- $k'_{\mathbf{GA}3\downarrow}$: Fraction of dose by which $k_{\mathbf{GA}3}$ decreases at a rate of $\frac{\overline{k}_{\mathbf{GA}3}-\underline{k}_{\mathbf{GA}3}}{2}$ [-]
- $k_{\mathbf{GA}3\uparrow}$: Rate of increase parameter of $k_{\mathbf{GA}3}$ to $\overline{k}_{\mathbf{GA}3}$ [mg^{-1}]
- $k'_{\mathbf{GA}3\uparrow}$: Fraction of dose by which $k_{\mathbf{GA}3}$ increases at a rate of $\frac{\overline{k}_{\mathbf{GA}3}-\underline{k}_{\mathbf{GA}3}}{2}$ [-]

EGP

- $k_{\mathbf{EPG}1}$: Extrapolated R_{EGP} at zero glucose and insulin [mg/kg/min]
- $k_{\mathbf{EPG}2}$: Parameter of liver glucose effectiveness [min^{-1}]
- $k_{\mathbf{EPG}3}$: Parameter governing amplitude of insulin action on the liver [mg/kg/min per pmol/L]
- $k_{\mathbf{EGP}m}$: Rate parameter accounting for the delay between insulin signal and insulin action [min^{-1}]

Glucose Utilization (U)

- $k_{\mathbf{U}1}$: Lower bound of glucose transportation rate limit to cells [mg/kg/min]
- $k_{\mathbf{U}2}$: Gradient of glucose transportation rate limit to cells with respect to $C_{m_{\text{inter}}}$ [mg/kg/min per pmol/L]
- $k_{\mathbf{U}3}$: Michaelis constant [195] [mg/kg]
- $k_{\mathbf{U}m}$: Rate constant of insulin action on the peripheral glucose utilization [min^{-1}]

- $C_{m_{\text{pla}},\text{b}}$: Parameter constant denoting basal insulin concentration in plasma [pmol/L]
- $k_{f_{\text{risk}},1}$: Parameter constant in blood glucose risk function [-]
- $k_{f_{\text{risk}},2}$: Parameter constant in blood glucose risk function [-]
- $\underline{C}_{q_{\text{pla}}}$: Plasma glucose concentration hypoglycemia threshold [mg/dL]

Insulin Appearance (IA)

- $k_{m_{\mathbf{sc1}}}$: Rate constant of non-monomeric insulin absorption in subcutaneous tissue [min^{-1}]
- $k_{m_{\mathbf{sc2}}}$: Rate constant of monomeric insulin absorption subcutaneous tissue [min^{-1}]
- $k_{m_{\mathbf{sc3}}}$: Rate constant of insulin dissociation in subcutaneous tissue [min^{-1}]
- $k_{q_{\mathbf{sc}}}$: Rate parameter accounting for the delay between sensed and actual blood glucose [min^{-1}]

Renal Excretion (E)

- $k_{\mathbf{E}1}$: Glomerular filtration rate [min^{-1}]
- $k_{\mathbf{E}2}$: Renal threshold of glucose [mg/kg]

A-1-3 Input and Output variables

Input

- $R_{m_{\text{in}}}$: (Distributed) Exogenous insulin infusion rate [pmol/kg/min]
- $R_{Q_{\text{in}}}$: Rate of ingested glucose [mg/min]

Output

- $C_{q_{\mathbf{sc}}}$: Glucose concentration in subcutaneous tissue [mg/dL]

Symbol Notation Equivalency

Chap. 2	[53, 54]	Chap. 2	[53, 54]	Chap. 2	[53, 54]
k_{q1}	k_1	k_{q2}	k_2		
k_{m1}	m_1	k_{m2}	m_2	k_{m3}	m_3
k_{m4}	m_4				
$k_{\mathbf{EPG}1}$	k_{p1}	$k_{\mathbf{EPG}2}$	k_{p2}	$k_{\mathbf{EPG}3}$	k_{p3}
$k_{\mathbf{EPG}m}$	k_i				
$k_{\mathbf{E}1}$	k_{e1}	$k_{\mathbf{E}2}$	k_{e2}		
$k_{\mathbf{GA}1}$	k_{abs}	$k'_{\mathbf{GA}1}$	f	$k_{\mathbf{GA}2}$	k_{gri}
$k_{\mathbf{GA}3}$	k_{empt}	$\bar{k}_{\mathbf{GA}3}$	$k_{\max}$	$\underline{k}_{\mathbf{GA}3}$	$k_{\min}$
$k_{\mathbf{GA}3\uparrow}$	β	$k_{\mathbf{GA}3\downarrow}$	α		
$k'_{\mathbf{GA}3\uparrow}$	c	$k'_{\mathbf{GA}3\downarrow}$	b		
$k_{\mathbf{U}1}$	V_{m0}	$k_{\mathbf{U}2}$	V_{mx}	$k_{\mathbf{U}3}$	K_{m0}
$k_{\mathbf{U}m}$	p_{2U}				
$k_{f_{\text{risk}},1}$	r_1	$k_{f_{\text{risk}},2}$	r_2		
$k_{m_{\mathbf{sc}}1}$	k_{a1}	$k_{m_{\mathbf{sc}}2}$	k_{a2}	$k_{m_{\mathbf{sc}}3}$	k_d
$k_{q_{\mathbf{sc}}}$	$\frac{1}{T_s}$				
V_q	V_G	V_m	V_I	W_{body}	BW
$Q_{\text{sto},s}$	Q_{sto1}	$Q_{\text{sto},l}$	Q_{sto2}	Q_{sto}	Q_{sto}
Q_{gut}	Q_{gut}	Q_{total}	D		
$C_{q_{\text{pla}}}$	G	$C_{q_{\text{pla}},\text{b}}$	G_b	$C_{m_{\text{inter}}}$	X
$C_{m_{\text{liv}}}$	I_1/I'	$C_{m_{\text{liv,delay}}}$	I_d/X^L	$C_{m_{\text{pla}}}$	I
$C_{m_{\text{pla}},\text{b}}$	I_b	$C_{q_{\mathbf{sc}}}$	G_{s}		
q_{pla}	G_p	q_{tis}	G_t	q_{sc}	—
m_{pla}	I_p	m_{liv}	I_l		
$m_{\mathbf{sc},1}$	I_{sc1}	$m_{\mathbf{sc},2}$	I_{sc2}		
$R_{\mathbf{U},\text{dep}}$	U_{id}	$R_{\mathbf{U},\text{indep}}$	U_{ii}	$R_{\mathbf{GA}}$	Ra
$R_{\mathbf{EGP}}$	EGP	$R_{\mathbf{E}}$	E	$R_{\mathbf{IA}}$	R_{ai}
$R_{Q_{\text{in}}}$	$D \cdot \delta$	$R_{m_{\text{in}}}$	IIR		

Table A-2: Symbol chart from Section 2-1 denoting the equivalent notations used in [53, 54].

A-2 Insulin Guide

This section aims to impart readers with additional knowledge or reference about the various insulin types, their characteristics, with examples of commercially available insulin that may differ in strength, based on the information provided by the American Diabetes Association (ADA) [13] and the Centre for Diabetes and Care (CDC) [72, 73].

A-2-1 Insulin Characteristics

Insulin has three characteristics:

- **Onset** — The length of time before insulin reaches the bloodstream and begins lowering blood glucose.

- **Peak time** — The time during which insulin is at maximum strength in terms of lowering blood glucose.
- **Duration** — The length of time for which insulin continues to lower blood glucose.

A summary of the insulin types based on the three characteristics described can be found in Table A-3.

Insulin Type	Onset	Peak Time	Duration
Rapid-acting	15 minutes	1 hour	2 to 4 hours
Regular/Short-acting	30 minutes	2 to 3 hours	3 to 6 hours
Intermediate-acting	2 to 4 hours	4 to 12 hours	12 to 18 hours
Long-acting	2 hours	None	Up to 24 hours
Ultra-long acting	6 hours	None	36 hours or longer
Rapid-acting (inhaled)	10 to 15 minutes	30 minutes	3 hours
Premixed	5 to 60 minutes	Peaks vary	10 to 16 hours

Table A-3: Characteristics of the different insulin types.

Examples of the various insulin types are as follows [13]:

- Rapid-acting insulin: Insulin aspart (Fiasp, NovoLog), insulin glulisine (Apidra), and insulin lispro (Admelog, Humalog, Lyumjev)
- Regular or short-acting insulin: Human Regular (Humulin R, Novolin R, Velosulin R)
- Intermediate-acting insulin: NPH (Humulin N, Novolin N, ReliOn)
- Long-acting insulin: degludec (Tresiba), detemir (Levemir), and glargine (Basaglar, Lantus)
- Ultra long-acting insulin: glargine U-300 (Toujeo)
- Rapid-acting (inhaled): Technosphere insulin-inhalation system (Afrezza)
- Premixed: Afrezza

Appendix B

Supplementary materials for Chapter 3

Using the knowledge that

$$u(k) = \mathcal{K} * e(k) \tag{B-1a}$$

and

$$\begin{aligned} y(k + n_{\tau_y}) &= G_u * u(k - n_{\tau_u}) \\ y(k) &= G_u * u(k - n_{\tau_{uy}}), \end{aligned} \tag{B-1b}$$

the error

$$e(k) = g(k) - y(k-1) \tag{B-2}$$

can be used to derive y in terms of g by

$$\begin{aligned} y(k) &= g(k+1) - e(k+1) \\ \mathcal{K} * y(k) &= \mathcal{K} * g(k+1) - \underbrace{\mathcal{K} * e(k+1)}_{u(k+1)} \\ \mathcal{K}G_u * y(k) &= \mathcal{K}G_u * g(k+1) - y(k+1+n_{\tau_{uy}}) \\ z^{-(n_{\tau_{uy}}+1)}\mathcal{K}G_u * y(k) &= \mathcal{K}Gz^{-n_{\tau_{uy}}} * g(k) - y(k) \\ y(k) &= \underbrace{\frac{z^{-n_{\tau_{uy}}}\mathcal{K}G_u}{1 + z^{-(n_{\tau_{uy}}+1)}\mathcal{K}G_u}}_{M_y} * g(k) \end{aligned} \tag{B-3}$$

By means of substituting (B-1a) and (B-3), into

$$u(k) = \mathcal{K} * (g(k) - y(k-1)), \tag{B-4a}$$

u can be expressed in terms of g by

$$\begin{aligned} u(k) &= \mathcal{K} * (g(k) - M_y * g(k-1)) \\ &= \underbrace{\mathcal{K}\left(1 - z^{-1}M_y\right)}_{M_u} * g(k). \end{aligned} \tag{B-4b}$$

Considering that food intake is now taken into account in the model, not only are y and u dependent on g but also d. For y, this gives

$$\begin{aligned}
y(k+n_{\tau_y}) &= G_u * u(k-n_{\tau_u}) + G_d * d(k-n_{\tau_d}) \\
y(k) &= G_u\mathcal{K} * e(k-n_{\tau_{uy}}) + G_d * d(k-n_{\tau_{dy}}) \\
&= G_u\mathcal{K} * \big(g(k-n_{\tau_{uy}}) - y(k-n_{\tau_{uy}}-1)\big) + G_d * d(k-n_{\tau_{dy}}) \\
&= \frac{G_u\mathcal{K}}{1+z^{-(n_{\tau_{uy}}+1)}G_u\mathcal{K}} * g(k-n_{\tau_{uy}}) + \frac{G_d}{1+z^{-(n_{\tau_{uy}}+1)}G_u\mathcal{K}} * d(k-n_{\tau_{dy}}) \\
&= \frac{z^{-n_{\tau_{uy}}}G_u\mathcal{K}}{1+z^{-(n_{\tau_{uy}}+1)}G_u\mathcal{K}} * g(k) + \frac{G_d}{1+z^{-(n_{\tau_{uy}}+1)}G_u\mathcal{K}} * d(k-n_{\tau_{dy}}) \\
&= M_y * g(k) + \underbrace{z^{-n_{\tau_{dy}}}G_d(1-M_y)}_{M_{d,y}} * d(k)
\end{aligned} \tag{B-5}$$

Similarly for u, by substituting (B-3) and (B-5) into (B-4a) from before, this yields

$$\begin{aligned}
u(k) &= \mathcal{K} * (g(k) - y(k-1)) \\
&= \mathcal{K} * \Big(g(k) - M_y * g(k-1) - G_d(1-M_y) * d(k-n_{\tau_{dy}}-1)\Big) \\
&= \mathcal{K}\left(1 - z^{-1}M_y\right) * g(k) - z^{-(n_{\tau_{dy}}+1)}\mathcal{K}G_d\,(1-M_y) * d(k) \\
&= M_u * g(k) \underbrace{-z^{-(n_{\tau_{dy}}+1)}G_dM_u}_{M_{d,u}} * d(k)
\end{aligned} \tag{B-6}$$

Bibliography

[1] P. Abuin, P.S. Rivadeneira, A. Ferramosca, and A.H. González. Artificial pancreas under stable pulsatile MPC: Improving the closed-loop performance. *Journal of Process Control*, 92:246–260, 2020.

[2] Pablo Abuin, Antonio Ferramosca, Chiara Toffanin, Lalo Magni, and Alejandro H. Gonzalez. Artificial pancreas under periodic mpc for trajectory tracking: handling circadian variability of insulin sensitivity. *IFAC-PapersOnLine*, 55(16):196–201, 2022. 18th IFAC Workshop on Control Applications of Optimization CAO 2022.

[3] United States Food & Drug Administration. FDA approves first automated insulin delivery device for type 1 diabetes. https://www.fda.gov/news-events/press-announcements/fda-approves-first-automated-insulin-delivery-device-type-1-diabetes. Accessed: 2024-06-10.

[4] United States Food & Drug Administration. FDA approves first automated insulin delivery device for type 1 diabetes. https://www.fda.gov/medical-devices/recently-approved-devices/minimed-780g-system-p160017s091. Accessed: 2024-06-10.

[5] United States Food & Drug Administration. FDA authorizes first interoperable, automated insulin dosing controller designed to allow more choices for patients looking to customize their individual diabetes management device system. https://www.fda.gov/news-events/press-announcements/fda-authorizes-first-interoperable-automated-insulin-dosing-controller-designed-allo
Accessed: 2024-06-10.

[6] United States Food & Drug Administration. FDA Clears New Insulin Pump and Algorithm-Based Software to Support Enhanced Automatic Insulin Delivery. https://www.fda.gov/news-events/press-announcements/fda-clears-new-insulin-pump-and-algorithm-based-software-support-enhanced-automatic-
Accessed: 2024-06-10.

[7] Eleonora M. Aiello, Jordan E. Pinsker, Eva Vargas, Hazhir Teymourian, Farshad Tehrani, Mei Mei Church, Lori M. Laffel, III Francis J. Doyle, Mary-Elizabeth Patti, Joseph Wang, and Eyal Dassau. Clinical Evaluation of a Novel Insulin Immunosensor. *Journal of Diabetes Science and Technology*, 17(4):1038–1048, 2022. PMID: 35118893.

[8] Eleonora M. Aiello, Kelilah L. Wolkowicz, Jordan E. Pinsker, Eyal Dassau, and Francis J. Doyle III. A novel model-based estimator for real-time prediction of insulin-on-board. *Chemical Engineering Science*, 267:118321, 2023.

[9] Eleonora Maria Aiello, Mehrad Jaloli, and Marzia Cescon. Model predictive control (mpc) of an artificial pancreas with data-driven learning of multi-step-ahead blood glucose predictors. *Control Engineering Practice*, 144:105810, 2024.

[10] American Diabetes Association. Table 1—Système International (SI) units for plasma, serum, or blood concentrations. *Diabetes Care*, 21(12):2206–2206, 12 1998.

[11] American Diabetes Association Professional Practice Committee. 6. Glycemic Targets: Standards of Medical Care in Diabetes—2022. *Diabetes Care*, 45(Supplement 1):S83–S96, 12 2021.

[12] American Diabetes Association. eAG/A1C Conversion Calculator. https://professional.diabetes.org/glucose_calc. Accessed: 2024-05-16.

[13] American Diabetes Association. Insulin Basics. http://https://diabetes.org/health-wellness/medication/insulin-basics. Accessed: 2024-04-04.

[14] American Diabetes Association. Postprandial Blood Glucose. *Diabetes Care*, 24(4):775–778, 04 2001.

[15] American Diabetes Association. Standards of Medical Care in Diabetes—2014. *Diabetes Care*, 37(Supplement 1):S14–S80, 12 2013.

[16] Eran Atlas, Revital Nimri, Shahar Miller, Eli A. Grunberg, and Moshe Phillip. MD-Logic Artificial Pancreas System: A pilot study in adults with type 1 diabetes. *Diabetes Care*, 33(5):1072–1076, 02 2010.

[17] Bansal, Somil and Calandra, Roberto and Xiao, Ted and Levine, Sergey and Tomlin, Claire J. Goal-driven dynamics learning via bayesian optimization. In *2017 IEEE 56th Annual Conference on Decision and Control (CDC)*, pages 5168–5173, 2017.

[18] Tadej Battelino, Thomas Danne, Richard M. Bergenstal, Stephanie A. Amiel, Roy Beck, Torben Biester, Emanuele Bosi, Bruce A. Buckingham, William T. Cefalu, Kelly L. Close, Claudio Cobelli, Eyal Dassau, J. Hans DeVries, Kim C. Donaghue, Klemen Dovc, Francis J. Doyle III, Satish Garg, George Grunberger, Simon Heller, Lutz Heinemann, Irl B. Hirsch, Roman Hovorka, Weiping Jia, Olga Kordonouri, Boris Kovatchev, Aaron Kowalski, Lori Laffel, Brian Levine, Alexander Mayorov, Chantal Mathieu, Helen R. Murphy, Revital Nimri, Kirsten Nørgaard, Christopher G. Parkin, Eric Renard, David Rodbard, Banshi Saboo, Desmond Schatz, Keaton Stoner, Tatsuiko Urakami, Stuart A. Weinzimer, and Moshe Phillip. Clinical Targets for Continuous Glucose Monitoring Data Interpretation: Recommendations From the International Consensus on Time in Range. *Diabetes Care*, 42(8):1593–1603, 06 2019.

[19] Roy W. Beck, Richard M. Bergenstal, Peiyao Cheng, Craig Kollman, Anders L. Carlson, Mary L. Johnson, and David Rodbard. The Relationships Between Time in Range, Hyperglycemia Metrics, and HbA1c. *Journal of Diabetes Science and Technology*, 13(4):614–626, 2019. PMID: 30636519.

[20] B. Wayne Bequette. Algorithms for a closed-loop artificial pancreas: The case for model predictive control. *Journal of Diabetes Science and Technology*, 7(6):1632–1643, 2013. PMID: 24351190.

[21] Richard M. Bergenstal, Satish Garg, Stuart A. Weinzimer, Bruce A. Buckingham, Bruce W. Bode, William V. Tamborlane, and Francine R. Kaufman. Safety of a Hybrid Closed-Loop Insulin Delivery System in Patients With Type 1 Diabetes. *JAMA*, 316(13):1407–1408, 10 2016.

[22] Richard M Bergenstal, Revital Nimri, Roy W Beck, Amy Criego, Lori Laffel, Desmond Schatz, Tadej Battelino, Thomas Danne, Stuart A Weinzimer, Judy Sibayan, Mary L Johnson, Ryan J Bailey, Peter Calhoun, Anders Carlson, Elvira Isganaitis, Rachel Bello, Anastasia Albanese-O'Neill, Klemen Dovc, Torben Biester, Kate Weyman, Korey Hood, and Moshe Phillip. A comparison of two hybrid closed-loop systems in adolescents and young adults with type 1 diabetes (FLAIR): a multicentre, randomised, crossover trial. *The Lancet Diabetes & Endocrinogy*, 397(10270):208–219, 2021.

[23] R N Bergman, Y Z Ider, C R Bowden, and C Cobelli. Quantitative estimation of insulin sensitivity. *American Journal of Physiology-Endocrinology and Metabolism*, 236(6):E667, 1979. PMID: 443421.

[24] Arthur Bertachi, Lyvia Biagi, Aleix Beneyto, and Josep Vehí. Dynamic Rule-Based Algorithm to Tune Insulin-on-Board Constraints for a Hybrid Artificial Pancreas System. *Journal of Healthcare Engineering*, 2020:1414597, 2020.

[25] Mads Bisgaard Bengtsen and Niels Møller. Mini-review: Glucagon responses in type 1 diabetes – a matter of complexity. *Physiological Reports*, 9(16):e15009, 2021.

[26] Dimitri Boiroux, Vladimír Bátora, Morten Hagdrup, Sabrina Lyngbye Wendt, Niels Kjølstad Poulsen, Henrik Madsen, and John Bagterp Jørgensen. Adaptive model predictive control for a dual-hormone artificial pancreas. *Journal of Process Control*, 68:105–117, 2018.

[27] Dimitri Boiroux, Anne Katrine Duun-Henriksen, Signe Schmidt, Kirsten Nørgaard, Niels Kjølstad Poulsen, Henrik Madsen, and John Bagterp Jørgensen. Adaptive control in an artificial pancreas for people with type 1 diabetes. *Control Engineering Practice*, 58:332–342, 2017.

[28] Victor W. Bolie. Coefficients of normal blood glucose regulation. *Journal of Applied Physiology*, 16(5):783–788, 1961. PMID: 13870789.

[29] Marc D. Breton, Lauren G. Kanapka, Roy W. Beck, Laya Ekhlaspour, Gregory P. Forlenza, Eda Cengiz, Melissa Schoelwer, Katrina J. Ruedy, Emily Jost, Lori Carria, Emma Emory, Liana J. Hsu, Mary Oliveri, Craig C. Kollman, Betsy B. Dokken, Stuart A. Weinzimer, Mark D. DeBoer, Bruce A. Buckingham, Daniel Cherñavvsky, and

R. Paul Wadwa. A randomized trial of closed-loop control in children with type 1 diabetes. *New England Journal of Medicine*, 383(9):836–845, 2020.

[30] Sue Brown, Dan Raghinaru, Emma Emory, and Boris Kovatchev. First Look at Control-IQ: A New-Generation Automated Insulin Delivery System. *Diabetes Care*, 41(12):2634–2636, 10 2018.

[31] Sue A. Brown, Gregory P. Forlenza, Bruce W. Bode, Jordan E. Pinsker, Carol J. Levy, Amy B. Criego, David W. Hansen, Irl B. Hirsch, Anders L. Carlson, Richard M. Bergenstal, Jennifer L. Sherr, Sanjeev N. Mehta, Lori M. Laffel, Viral N. Shah, Anuj Bhargava, Ruth S. Weinstock, Sarah A. Macleish, Daniel J. Desalvo, Thomas C. Jones, Grazia Aleppo, Bruce A. Buckingham, and Trang T. Ly. Multicenter trial of a tubeless, on-body automated insulin delivery system with customizable glycemic targets in pediatric and adult participants with type 1 diabetes. *Diabetes Care*, 44(7):1630–1640, 2021.

[32] Sue A. Brown, Boris P. Kovatchev, Marc D. Breton, Stacey M. Anderson, Patrick Keith-Hynes, Stephen D. Patek, Boyi Jiang, Najib Ben Brahim, Paul Vereshchetin, Daniela Bruttomesso, Angelo Avogaro, Simone Del Favero, Federico Boscari, Silvia Galasso, Roberto Visentin, Marco Monaro, and Claudio Cobelli. Multinight "Bedside" Closed-Loop Control for Patients with Type 1 Diabetes. *Diabetes Technology & Therapeutics*, 17(3):203–209, 2015. PMID: 25594434.

[33] Sue A. Brown, Boris P. Kovatchev, Dan Raghinaru, John W. Lum, Bruce A. Buckingham, Yogish C. Kudva, Lori M. Laffel, Carol J. Levy, Jordan E. Pinsker, R. Paul Wadwa, Eyal Dassau, Francis J. Doyle, Stacey M. Anderson, Mei Mei Church, Vikash Dadlani, Laya Ekhlaspour, Gregory P. Forlenza, Elvira Isganaitis, David W. Lam, Craig Kollman, and Roy W. Beck. Six-Month Randomized, Multicenter Trial of Closed-Loop Control in Type 1 Diabetes. *New England Journal of Medicine*, 381(18):1707–1717, 10 2019.

[34] Bruce A. Buckingham, Mark P. Christiansen, Gregory P. Forlenza, R. Paul Wadwa, Thomas A. Peyser, Joon Bok Lee, Jason O'Connor, Eyal Dassau, Lauren M. Huyett, Jennifer E. Layne, and Trang T. Ly. Performance of the omnipod personalized model predictive control algorithm with meal bolus challenges in adults with type 1 diabetes. *Diabetes Technology & Therapeutics*, 20(9):585–595, 2018. PMID: 30070928.

[35] Bruce A. Buckingham, Gregory P. Forlenza, Jordan E. Pinsker, Mark P. Christiansen, R. Paul Wadwa, Jennifer Schneider, Thomas A. Peyser, Eyal Dassau, Joon Bok Lee, Jason O'Connor, Jennifer E. Layne, and Trang T. Ly. Safety and feasibility of the omnipod hybrid closed-loop system in adult, adolescent, and pediatric patients with type 1 diabetes using a personalized model predictive control algorithm. *Diabetes Technology & Therapeutics*, 20(4):257–262, 2018. PMID: 29431513.

[36] Deheng Cai, Wei Liu, Linong Ji, and Dawei Shi. Bayesian optimization assisted meal bolus decision based on gaussian processes learning and risk-sensitive control. *Control Engineering Practice*, 114:104881, 2021.

[37] Zhixing Cao, Ravi Gondhalekar, Eyal Dassau, and Francis J. Doyle. Extremum Seeking Control for Personalized Zone Adaptation in Model Predictive Control for Type 1 Diabetes. *IEEE Transactions on Biomedical Engineering*, 65(8):1859–1870, 2018.

[38] Anders L. Carlson, Jennifer L. Sherr, Dorothy I. Shulman, Satish K. Garg, Rodica Pop-Busui, Bruce W. Bode, David R. Lilenquist, Ron L. Brazg, Kevin B. Kaiserman, Mark S. Kipnes, James R. Thrasher, John H. Chip Reed, Robert H. Slover, Athena Philis-Tsimikas, Mark Christiansen, Benyamin Grosman, Anirban Roy, Melissa Vella, Richard A.M. Jonkers, Xiaoxiao Chen, John Shin, Toni L. Cordero, Scott W. Lee, Andrew S. Rhinehart, and Robert A. and Vigersky. Safety and Glycemic Outcomes During the MiniMed™ Advanced Hybrid Closed-Loop System Pivotal Trial in Adolescents and Adults with Type 1 Diabetes. *Diabetes Technology & Therapeutics*, 24(3):178–189, 2022. PMID: 34694909.

[39] Luz E. Castellanos, Courtney A. Balliro, Jordan S. Sherwood, Rabab Jafri, Mallory A. Hillard, Evelyn Greaux, Rajendranath Selagamsetty, Hui Zheng, Firas H. El-Khatib, Edward R. Damiano, and Steven J. Russell. Performance of the Insulin-Only iLet Bionic Pancreas and the Bihormonal iLet Using Dasiglucagon in Adults With Type 1 Diabetes in a Home-Use Setting. *Diabetes Care*, 44(6):e118–e120, 06 2021.

[40] A Castillo, M F Villa-Tamayo, E Pryor, J Garcia-Tirado, P Colmegna, and M Breton. Deep Neural Network Architectures for an Embedded MPC Implementation: Application to an Automated Insulin Delivery System. In *22nd IFAC World Congress*, 7 2023.

[41] Marzia Cescon and Eric Renard. Adaptive subspace-based prediction of T1DM glycemia. In *2011 50th IEEE Conference on Decision and Control and European Control Conference*, pages 5164–5169, 2011.

[42] Jianwei Chen, Kezhi Li, Pau Herrero, Taiyu Zhu, and Pantelis Georgiou. Dilated recurrent neural network for short-time prediction of glucose concentration. In *KHD@ IJCAI*, pages 69–73, 2018.

[43] Ana Chico, Jesús Moreno-Fernández, Diego Fernández-García, and Eva Solá. The Hybrid Closed-Loop System Tandem t:slim X2™ with Control-IQ Technology: Expert Recommendations for Better Management and Optimization. *Diabetes Therapy*, 15(1):281–295, 2024.

[44] Ali Cinar. Artificial pancreas systems: An introduction to the special issue. *IEEE Control Systems Magazine*, 38(1):26–29, 2018.

[45] Claudio Cobelli, Chiara Dalla Man, Giovanni Sparacino, Lalo Magni, Giuseppe De Nicolao, and Boris P. Kovatchev. Diabetes: Models, signals, and control. *IEEE Reviews in Biomedical Engineering*, 2:54–96, 2009.

[46] Claudio Cobelli, Chiara Dalla Man, Giovanni Sparacino, Lalo Magni, Giuseppe De Nicolao, and Boris P. Kovatchev. Diabetes: Models, signals, and control. *IEEE Reviews in Biomedical Engineering*, 2:54–96, 2009.

[47] Claudio Cobelli and Chiara Dalla Man. Minimal and maximal models to quantitate glucose metabolism: Tools to measure, to simulate and to run in silico clinical trials. *Journal of Diabetes Science and Technology*, 16(5):1270–1298, 2022. PMID: 34032128.

[48] Claudio Cobelli, Eric Renard, Boris P. Kovatchev, Patrick Keith-Hynes, Najib Ben Brahim, Jérôme Place, Simone Del Favero, Marc Breton, Anne Farret, Daniela Bruttomesso, Eyal Dassau, Howard Zisser, III Doyle, Francis J., Stephen D. Patek, and Angelo Avogaro. Pilot Studies of Wearable Outpatient Artificial Pancreas in Type 1 Diabetes. *Diabetes Care*, 35(9):e65–e67, 08 2012.

[49] Olivia J. Collyns, Renee A. Meier, Zara L. Betts, Denis S.H. Chan, Chris Frampton, Carla M. Frewen, Niranjala M. Hewapathirana, Shirley D. Jones, Anirban Roy, Benyamin Grosman, Natalie Kurtz, John Shin, Robert A. Vigersky, Benjamin J. Wheeler, and Martin I. de Bock. Improved Glycemic Outcomes With Medtronic MiniMed Advanced Hybrid Closed-Loop Delivery: Results From a Randomized Crossover Trial Comparing Automated Insulin Delivery With Predictive Low Glucose Suspend in People With Type 1 Diabetes. *Diabetes Care*, 44(4):969–975, 02 2021.

[50] P. Colmegna and R.S. Sánchez Peña. Analysis of three t1dm simulation models for evaluating robust closed-loop controllers. *Computer Methods and Programs in Biomedicine*, 113(1):371–382, 2014.

[51] Patricio Colmegna, Ricardo S. Sánchez Peña, Ravi Gondhalekar, Eyal Dassau, and Francis J. Doyle III. Reducing risks in type 1 diabetes using H_∞ control. *IEEE Transactions on Biomedical Engineering*, 61(12):2939–2947, 2014.

[52] Chiara Dalla Man, Michael Camilleri, and Claudio Cobelli. A system model of oral glucose absorption: Validation on gold standard data. *IEEE Transactions on Biomedical Engineering*, 53(12):2472–2478, 12 2006.

[53] Chiara Dalla Man, Francesco Micheletto, Dayu Lv, Marc Breton, Boris Kovatchev, and Claudio Cobelli. The UVA/PADOVA type 1 diabetes simulator: New features. *Journal of Diabetes Science and Technology*, 8(1):26–34, 2014.

[54] Chiara Dalla Man, Robert A. Rizza, and Claudio Cobelli. Meal simulation model of the glucose-insulin system. *IEEE Transactions on Biomedical Engineering*, 54(10):1740–1749, 10 2007.

[55] Thomas Danne, Revital Nimri, Tadej Battelino, Richard M. Bergenstal, Kelly L. Close, J. Hans DeVries, Satish Garg, Lutz Heinemann, Irl Hirsch, Stephanie A. Amiel, Roy Beck, Emanuele Bosi, Bruce Buckingham, Claudio Cobelli, Eyal Dassau, Francis J. Doyle III, Simon Heller, Roman Hovorka, Weiping Jia, Tim Jones, Olga Kordonouri, Boris Kovatchev, Aaron Kowalski, Lori Laffel, David Maahs, Helen R. Murphy, Kirsten Nørgaard, Christopher G. Parkin, Eric Renard, Banshi Saboo, Mauro Scharf, William V. Tamborlane, Stuart A. Weinzimer, and Moshe Phillip. International Consensus on Use of Continuous Glucose Monitoring. *Diabetes Care*, 40(12):1631–1640, 11 2017.

[56] Eyal Dassau, Sue A. Brown, Ananda Basu, Jordan E. Pinsker, Yogish C. Kudva, Ravi Gondhalekar, Steve Patek, Dayu Lv, Michele Schiavon, Joon Bok Lee, Chiara Dalla Man, Ling Hinshaw, Kristin Castorino, Ashwini Mallad, Vikash Dadlani, Shelly K. McCrady-Spitzer, Molly McElwee-Malloy, Christian A. Wakeman, Wendy C. Bevier, Paige K. Bradley, Boris Kovatchev, Claudio Cobelli, Howard C. Zisser, and

Francis J. Doyle III. Adjustment of Open-Loop Settings to Improve Closed-Loop Results in Type 1 Diabetes: A Multicenter Randomized Trial. *The Journal of Clinical Endocrinology & Metabolism*, 100(10):3878–3886, 10 2015.

[57] Eyal Dassau, Jordan E. Pinsker, Yogish C. Kudva, Sue A. Brown, Ravi Gondhalekar, Chiara Dalla Man, Steve Patek, Michele Schiavon, Vikash Dadlani, Isuru Dasanayake, Mei Mei Church, Rickey E. Carter, Wendy C. Bevier, Lauren M. Huyett, Jonathan Hughes, Stacey Anderson, Dayu Lv, Elaine Schertz, Emma Emory, Shelly K. McCrady-Spitzer, Tyler Jean, Paige K. Bradley, Ling Hinshaw, Alejandro J. Laguna Sanz, Ananda Basu, Boris Kovatchev, Claudio Cobelli, and Francis J. Doyle III. Twelve-Week 24/7 Ambulatory Artificial Pancreas With Weekly Adaptation of Insulin Delivery Settings: Effect on Hemoglobin A1c and Hypoglycemia. *Diabetes Care*, 40(12):1719–1726, 10 2017.

[58] Paul C. Davidson, Harry R. Hebblewhite, Robert D. Steed, and Bruce W. Bode. Analysis of guidelines for basal-bolus insulin dosing: Basal insulin, correction factor, and carbohydrate-to-insulin ratio. *Endocrine Practice*, 14(9):1095–1101, 2008.

[59] S. Del Favero, J. Place, J. Kropff, M. Messori, P. Keith-Hynes, R. Visentin, M. Monaro, S. Galasso, F. Boscari, C. Toffanin, F. Di Palma, G. Lanzola, S. Scarpellini, A. Farret, B. Kovatchev, A. Avogaro, D. Bruttomesso, L. Magni, J. H. DeVries, C. Cobelli, E. Renard, and on behalf of the AP@home Consortium. Multicenter outpatient dinner/overnight reduction of hypoglycemia and increased time of glucose in target with a wearable artificial pancreas using modular model predictive control in adults with type 1 diabetes. *Diabetes, Obesity and Metabolism*, 17(5):468–476, 2015.

[60] Simone Del Favero, Federico Boscari, Mirko Messori, Ivana Rabbone, Riccardo Bonfanti, Alberto Sabbion, Dario Iafusco, Riccardo Schiaffini, Roberto Visentin, Roberta Calore, Yenny Leal Moncada, Silvia Galasso, Alfonso Galderisi, Valeria Vallone, Federico Di Palma, Eleonora Losiouk, Giordano Lanzola, Davide Tinti, Andrea Rigamonti, Marco Marigliano, Angela Zanfardino, Novella Rapini, Angelo Avogaro, Daniel Chernavvsky, Lalo Magni, Claudio Cobelli, and Daniela Bruttomesso. Randomized Summer Camp Crossover Trial in 5- to 9-Year-Old Children: Outpatient Wearable Artificial Pancreas Is Feasible and Safe. *Diabetes Care*, 39(7):1180–1185, 03 2016.

[61] Francis J. Doyle III, Lauren M. Huyett, Joon Bok Lee, Howard C. Zisser, and Eyal Dassau. Closed-Loop Artificial Pancreas Systems: Engineering the Algorithms. *Diabetes Care*, 37(5):1191–1197, 04 2014.

[62] Decio L Eizirik, Florian Szymczak, and Roberto Mallone. Why does the immune system destroy pancreatic β-cells but not α-cells in type 1 diabetes? *Nature Reviews Endocrinology*, 19(7):425–434, 2023.

[63] Firas H El-Khatib, Courtney Balliro, Mallory A Hillard, Kendra L Magyar, Laya Ekhlaspour, Manasi Sinha, Debbie Mondesir, Aryan Esmaeili, Celia Hartigan, Michael J Thompson, Samir Malkani, J Paul Lock, David M Harlan, Paula Clinton, Eliana Frank, Darrell M Wilson, Daniel DeSalvo, Lisa Norlander, Trang Ly, Bruce A Buckingham, Jamie Diner, Milana Dezube, Laura A Young, April Goley, M Sue Kirkman, John B Buse, Hui Zheng, Rajendranath R Selagamsetty, Edward R Damiano, and Steven J

Russell. Home use of a bihormonal bionic pancreas versus insulin pump therapy in adults with type 1 diabetes: a multicentre randomised crossover trial. *The Lancet*, 389(10067):369–380, 1 2017.

[64] Firas H. El-Khatib, John Jiang, and Edward R. Damiano. Adaptive closed-loop control provides blood-glucose regulation using dual subcutaneous insulin and glucagon infusion in diabetic swine. *Journal of Diabetes Science and Technology*, 1(2):181–192, 2007. PMID: 19888405.

[65] Firas H. El-Khatib, Steven J. Russell, Kendra L. Magyar, Manasi Sinha, Katherine McKeon, David M. Nathan, and Edward R. Damiano. Autonomous and Continuous Adaptation of a Bihormonal Bionic Pancreas in Adults and Adolescents With Type 1 Diabetes. *The Journal of Clinical Endocrinology & Metabolism*, 99(5):1701–1711, 05 2014.

[66] Firas H. El-Khatib, Steven J. Russell, David M. Nathan, Robert G. Sutherlin, and Edward R. Damiano. A Bihormonal Closed-Loop Artificial Pancreas for Type 1 Diabetes. *Science Translational Medicine*, 2(27):27ra27–27ra27, 2010.

[67] Christian Ellingsen, Eyal Dassau, Howard Zisser, Benyamin Grosman, Matthew W. Percival, Lois Jovanovič, and Francis J. Doyle III. Safety constraints in an artificial pancreatic β cell: An implementation of model predictive control with insulin on board. *Journal of Diabetes Science and Technology*, 3(3):536–544, 2009. PMID: 20144293.

[68] Alaa A. Embaby, Zaki Nossair, and Hesham Badr. Adaptive nonlinear model predictive control algorithm for blood glucose regulation in type 1 diabetic patients. In *2020 2nd Novel Intelligent and Leading Emerging Sciences Conference (NILES)*, pages 109–115, 2020.

[69] Meriyan Eren-Oruklu, Ali Cinar, Derrick K. Rollins, and Lauretta Quinn. Adaptive system identification for estimating future glucose concentrations and hypoglycemia alarms. *Automatica*, 48(8):1892–1897, 2012.

[70] Andrea Facchinetti. Continuous Glucose Monitoring Sensors: Past, Present and Future Algorithmic Challenges. *Sensors*, 16(12):2093, 2016.

[71] Daniel A. Finan, Cesar C. Palerm, Francis J. Doyle III, Dale E. Seborg, Howard Zisser, Wendy C. Bevier, and Lois Jovanovič. Effect of input excitation on the quality of empirical dynamic models for type 1 diabetes. *AIChE Journal*, 55(5):1135–1146, 2009.

[72] Centre for Diabetes Control and Prevention. Insulin Basics. https://www.cdc.gov/diabetes/basics/type-1-4-ways-to-take-insulin.html. Accessed: 2024-04-04.

[73] Centre for Diabetes Control and Prevention. Insulin Basics. https://diabetes.org/health-wellness/medication/insulin-basics. Accessed: 2024-04-04.

[74] National Institute for Health and Care Excellence. Type 1 diabetes in adults: diagnosis and management. https://www.nice.org.uk/guidance/ng17/ifp/chapter/having-your-blood-glucose-checked-hba1c. Accessed: 2024-04-09.

[75] Gregory P. Forlenza, Bruce A. Buckingham, Sue A. Brown, Bruce W. Bode, Carol J. Levy, Amy B. Criego, R. Paul Wadwa, Erin C. Cobry, Robert J. Slover, Laurel H. Messer, Cari Berget, Susan McCoy, Laya Ekhlaspour, Ryan S. Kingman, Mary K. Voelmle, Jennifer Boyd, Grenye O'Malley, Aimee Grieme, Kaisa Kivilaid, Krista Kleve, Bonnie Dumais, Todd Vienneau, Lauren M. Huyett, Joon Bok Lee, Jason O'Connor, Eric Benjamin, and Trang T. Ly. First Outpatient Evaluation of a Tubeless Automated Insulin Delivery System with Customizable Glucose Targets in Children and Adults with Type 1 Diabetes. *Diabetes Technology & Therapeutics*, 23(6):410–424, 2021. PMID: 33325779.

[76] Gregory P. Forlenza, Bruce A. Buckingham, Mark P. Christiansen, R. Paul Wadwa, Thomas A. Peyser, Joon Bok Lee, Jason O'Connor, Eyal Dassau, Lauren M. Huyett, Jennifer E. Layne, and Trang T. Ly. Performance of Omnipod Personalized Model Predictive Control Algorithm with Moderate Intensity Exercise in Adults with Type 1 Diabetes. *Diabetes Technology & Therapeutics*, 21(5):265–272, 2019. PMID: 30925077.

[77] Gregory P. Forlenza, Sunil Deshpande, Trang T. Ly, Daniel P. Howsmon, Faye Cameron, Nihat Baysal, Eric Mauritzen, Tatiana Marcal, Lindsey Towers, B. Wayne Bequette, Lauren M. Huyett, Jordan E. Pinsker, Ravi Gondhalekar, III Doyle, Francis J., David M. Maahs, Bruce A. Buckingham, and Eyal Dassau. Application of Zone Model Predictive Control Artificial Pancreas During Extended Use of Infusion Set and Sensor: A Randomized Crossover-Controlled Home-Use Trial. *Diabetes Care*, 40(8):1096–1102, 06 2017.

[78] Gregory P. Forlenza, Laya Ekhlaspour, Marc Breton, David M. Maahs, R. Paul Wadwa, Mark DeBoer, Laurel H. Messer, Marissa Town, Jennifer Pinnata, Geoff Kruse, Bruce A. Buckingham, and Daniel Cherñavvsky. Successful at-home use of the tandem control-iq artificial pancreas system in young children during a randomized controlled trial. *Diabetes Technology & Therapeutics*, 21(4):159–169, 2019. PMID: 30888835.

[79] Gregory P. Forlenza, Orit Pinhas-Hamiel, David R. Liljenquist, Dorothy I. Shulman, Timothy S. Bailey, Bruce W. Bode, Michael A. Wood, Bruce A. Buckingham, Kevin B. Kaiserman, John Shin, Suiying Huang, Scott W. Lee, and Francine R. Kaufman. Safety evaluation of the minimed 670g system in children 7–13 years of age with type 1 diabetes. *Diabetes Technology & Therapeutics*, 21(1):11–19, 2019. PMID: 30585770.

[80] Jonas Freiburghaus, Aïcha Rizzotti, and Fabrizio Albertetti. A deep learning approach for blood glucose prediction of type 1 diabetes. In *Proceedings of the Proceedings of the 5th International Workshop on Knowledge Discovery in Healthcare Data co-located with 24th European Conference on Artificial Intelligence (ECAI 2020), 29-30 August 2020, Santiago de Compostela, Spain*. 29-30 August 2020, 2020.

[81] Jose Garcia-Tirado, John P. Corbett, Dimitri Boiroux, John Bagterp Jørgensen, and Marc D. Breton. Closed-loop control with unannounced exercise for adults with type 1 diabetes using the Ensemble Model Predictive Control. *Journal of Process Control*, 80:202–210, 2019.

[82] Jose Garcia-Tirado, Dayu Lv, John P. Corbett, Patricio Colmegna, and Marc D. Breton. Advanced hybrid artificial pancreas system improves on unannounced meal response -

in silico comparison to currently available system. *Computer Methods and Programs in Biomedicine*, 211:106401, 2021.

[83] Jose Garcia-Tirado, Christian Zuluaga-Bedoya, and Marc D. Breton. Identifiability analysis of three control-oriented models for use in artificial pancreas systems. *Journal of Diabetes Science and Technology*, 12(5):937–952, 2018. PMID: 30095007.

[84] Satish K. Garg, Stuart A. Weinzimer, William V. Tamborlane, Bruce A. Buckingham, Bruce W. Bode, Timothy S. Bailey, Ronald L. Brazg, Jacob Ilany, Robert H. Slover, Stacey M. Anderson, Richard M. Bergenstal, Benyamin Grosman, Anirban Roy, Toni L. Cordero, John Shin, Scott W. Lee, and Francine R. Kaufman. Glucose outcomes with the in-home use of a hybrid closed-loop insulin delivery system in adolescents and adults with type 1 diabetes. *Diabetes Technology & Therapeutics*, 19(3):155–163, 2017. PMID: 28134564.

[85] M. Gevers. Identification for Control: From the Early Achievements to the Revival of Experiment Design. In *Proceedings of the 44th IEEE Conference on Decision and Control*, pages 12–12, 2005.

[86] Ravi Gondhalekar, Eyal Dassau, and Francis J. Doyle. Velocity-weighting to prevent controller-induced hypoglycemia in MPC of an artificial pancreas to treat T1DM. In *2015 American Control Conference (ACC)*, pages 1635–1640, 2015.

[87] Ravi Gondhalekar, Eyal Dassau, and Francis J. Doyle. Periodic zone-mpc with asymmetric costs for outpatient-ready safety of an artificial pancreas to treat type 1 diabetes. *Automatica*, 71:237–246, 2016.

[88] Ravi Gondhalekar, Eyal Dassau, and Francis J. Doyle. Velocity-weighting & velocity-penalty MPC of an artificial pancreas: Improved safety & performance. *Automatica*, 91:105–117, 2018.

[89] Ravi Gondhalekar, Eyal Dassau, Howard C. Zisser, and Francis J. Doyle III. Periodic-Zone Model Predictive Control for Diurnal Closed-Loop Operation of an Artificial Pancreas. *Journal of Diabetes Science and Technology*, 7(6):1446–1460, 2013. PMID: 24351171.

[90] Stewart Greenhill, Santu Rana, Sunil Gupta, Pratibha Vellanki, and Svetha Venkatesh. Bayesian Optimization for Adaptive Experimental Design: A Review. *IEEE Access*, 8:13937–13948, 2020.

[91] Gabriel A. Gregory, Thomas I.G. Robinson, Sarah E. Linklater, Fei Wang, Stephen Colagiuri, Carine de Beaufort, Kim C. Donaghue, Dianna J. Magliano, Jayanthi Maniam, Trevor J. Orchard, Priyanka Rai, and Graham D. Ogle. Global incidence, prevalence, and mortality of type 1 diabetes in 2021 with projection to 2040: a modelling study. *The Lancet Diabetes & Endocrinology*, 10(10):741–760, 10 2022.

[92] JJ Grimm, W Berger, and J Ruiz. Functional insulin therapy: patient education and algorithms. *Diabetes & Metabolism*, 28(4 Pt 2):2S15—2S18, September 2002.

[93] Benyamin Grosman, Eyal Dassau, Howard C. Zisser, Lois Jovanovič, and Francis J. Doyle III. Zone model predictive control: A strategy to minimize hyper- and hypoglycemic events. *Journal of Diabetes Science and Technology*, 4(4):961–975, 2010. PMID: 20663463.

[94] Benyamin Grosman, Neha Parikh, Anirban Roy, Louis Lintereur, Robert Vigersky, Ohad Cohen, and Andrew Rhinehart. In Silico Evaluation of the Medtronic 780G System While Using the GS3 and Its Calibration-Free Successor, the G4S Sensor. *Annals of Biomedical Engineering*, 51(1):211–224, 2023.

[95] Benyamin Grosman, Anirban Roy, Louis Lintereur, Kamuran Turksoy, Andrea Benedetti, Toni L. Cordero, Robert A. Vigersky, Jennifer McVean, Andrew S. Rhinehart, and Ohad Cohen. A Peek Under the Hood: Explaining the MiniMed™ 780G Algorithm with Meal Detection Technology. *Diabetes Technology & Therapeutics*, 26(S3):17–23, 2024. PMID: 38377324.

[96] Bionic Pancreas Research Group. Multicenter, Randomized Trial of a Bionic Pancreas in Type 1 Diabetes. *New England Journal of Medicine*, 387(13):1161–1172, 2022.

[97] George Grunberger, Yehuda Handelsman, ZacharyT Bloomgarden, Vivian A. Fonseca, Alan J. Garber, Richard A. Haas, Victor L. Roberts, and Guillermo E. Umpierrez. American Association of Clinical Endocrinologists And American College of Endocrinology 2018 Position Statement On Integration of Insulin Pumps And Continuous Glucose Monitoring In Patients With Diabetes Mellitus. *Endocrine Practice*, 24(3):302–308, 2018.

[98] R. Hovorka. Continuous glucose monitoring and closed-loop systems. *Diabetic Medicine*, 23(1):1–12, 2006.

[99] Roman Hovorka, Valentina Canonico, Ludovic J. Chassin, Ulrich Haueter, Massimo Massi-Benedetti, Marco Orsini Federici, Thomas R. Pieber, Helga C. Schaller, Lukas Schaupp, Thomas Vering, and Malgorzata E. Wilinska. Nonlinear model predictive control of glucose concentration in subjects with type 1 diabetes. *Physiological Measurement*, 25(4):905 – 920, 2004.

[100] Roman Hovorka, Fariba Shojaee-Moradie, Paul V. Carroll, Ludovic J. Chassin, Ian J. Gowrie, Nicola C. Jackson, Romulus S. Tudor, A. Margot Umpleby, and Richard H. Jones. Partitioning glucose distribution/transport, disposal, and endogenous production during IVGTT. *American Journal of Physiology-Endocrinology and Metabolism*, 282(5):E992–E1007, 2002. PMID: 11934663.

[101] J. D. Hoyos, M. F. Villa-Tamayo, C. E. Builes-Montaño, A. Ramirez-Rincón, J. L. Godoy, J. Garcia-Tirado, and P. S. Rivadeneira. Identifiability of control-oriented glucose-insulin linear models: Review and analysis. *IEEE Access*, 9:69173–69188, 2021.

[102] Colleen S. Hughes, Stephen D. Patek, Marc D. Breton, and Boris P. Kovatchev. Hypoglycemia Prevention via Pump Attenuation and Red-Yellow-Green "Traffic" Lights Using Continuous Glucose Monitoring and Insulin Pump Data. *Journal of Diabetes Science and Technology*, 4(5):1146–1155, 2010. PMID: 20920434.

[103] Lauren M. Huyett, Eyal Dassau, Howard C. Zisser, and Francis J. Doyle III. Design and evaluation of a robust pid controller for a fully implantable artificial pancreas. *Industrial & Engineering Chemistry Research*, 54(42):10311–10321, 2015. PMID: 26538805.

[104] Lauren M. Huyett, Trang T. Ly, Gregory P. Forlenza, Suzette Reuschel-DiVirgilio, Laurel H. Messer, R. Paul Wadwa, Ravi Gondhalekar, Francis J. Doyle, Jordan E. Pinsker, David M. Maahs, Bruce A. Buckingham, and Eyal Dassau. Outpatient closed-loop control with unannounced moderate exercise in adolescents using zone model predictive control. *Diabetes Technology & Therapeutics*, 19(6):331–339, 2017. PMID: 28459617.

[105] Insulet. Insulet Announces FDA Clearance of its Omnipod® 5 Automated Insulin Delivery System, First Tubeless System with Smartphone Control. https://investor.insulet.com/news/news-details/2022/Insulet-Announces-FDA-Clearance-of-its-Omnipod-5-Automated-Insulin-Delivery-System-F default.aspx. Accessed: 2024-06-10.

[106] Elvira Isganaitis, Dan Raghinaru, Louise Ambler-Osborn, Jordan E. Pinsker, Bruce A. Buckingham, R. Paul Wadwa, Laya Ekhlaspour, Yogish C. Kudva, Carol J. Levy, Gregory P. Forlenza, Roy W. Beck, Craig Kollman, John W. Lum, Sue A. Brown, Lori M. Laffel, , Boris Kovatchev, Stacey Anderson, Emma Emory, Mary Voelmle, Katie Conshafter, Kim Morris, Mary Oliveri, Linda Gondor-Fredrick, Harry Mitchell, Kayla Calvo, Christian Wakeman, Marc Breton, Emily Flint, Kenny Kim, Lindsay Roethke, Mei Mei Church, Camille Andre, Molly Piper, David Lam, Grenye O'Malley, Camilla Levister, Selassie Ogyaadu, Jessica Lovett, Vinaya Simha, Vikash Dadlani, Shelly McCrady-Spitzer, Corey Reid, Kanchan Kumari, Greg Forlenza, G. Todd Alonso, Robert Slover, Emily Jost, Laurel Messer, Cari Berget, Lindsey Towers, Alex Rossick-Solis, Tali Jacobson, Marissa Town, Ideen Tabatabai, Jordan Keller, Evalina Salas, Francis Doyle, Eyal Dassau, Samantha Passman, Tiffany Campos, Carlos Murphy, Nandan Patibandla, Sarah Borgman, Guillermo Arreaza-Rubín, Neal Green, Boris Kovatchev, Sue Brown, Stacey Anderson, Marc Breton, Lori Laffel, Jordan Pinsker, Carol Levy, R. Paul Wadwa, Bruce Buckingham, Francis Doyle, Eric Renard, Claudio Cobelli, Yves Reznik, Guillermo Arreaza-Rubín, John Lum, Roy Beck, Robert Janicek, Deanna Gabrielson, Steven H. Belle, Jessica Castle, Jennifer Green, Laurent Legault, Steven M. Willi, Carol Wysham, and Thomas Eggerman. Closed-Loop Insulin Therapy Improves Glycemic Control in Adolescents and Young Adults: Outcomes from the International Diabetes Closed-Loop Trial. *Diabetes Technology & Therapeutics*, 23(5):342–349, 2021. PMID: 33216667.

[107] Andrej Janež, Cristian Guja, Asimina Mitrakou, Nebojsa Lalic, Tsvetalina Tankova, Adam G. Czupryniak, Leszek amd Tabák, Martin Prazny, Emil Martinka, and Lea Smircic-Duvnjak. Insulin Therapy in Adults with Type 1 Diabetes Mellitus: a Narrative Review. *Diabetes Therapy*, 11, 2020.

[108] N. Jeandidier, J.-P. Riveline, N. Tubiana-Rufi, A. Vambergue, B. Catargi, V. Melki, G. Charpentier, and B. Guerci. Treatment of diabetes mellitus using an external insulin pump in clinical practice. *Diabetes & Metabolism*, 34(4, Supplement 1):425–438, 2008. External insulin pump therapy in diabetes.

[109] Su Lim Kang, Yoo Na Hwang, Ji Yean Kwon, and Sung Min Kim. Effectiveness and safety of a model predictive control (MPC) algorithm for an artificial pancreas system in outpatients with type 1 diabetes (T1D): systematic review and meta-analysis. *Diabetology & Metabolic Syndrome*, 14(1):187, 2022.

[110] Mohammad Khosravi, Varsha N. Behrunani, Piotr Myszkorowski, Roy S. Smith, Alisa Rupenyan, and John Lygeros. Performance-Driven Cascade Controller Tuning With Bayesian Optimization. *IEEE Transactions on Industrial Electronics*, 69(1):1032–1042, 2022.

[111] Boris Kovatchev, Stacey M. Anderson, Dan Raghinaru, Yogish C. Kudva, Lori M. Laffel, Carol Levy, Jordan E. Pinsker, R. Paul Wadwa, Bruce Buckingham, III Doyle, Francis J., Sue A. Brown, Mei Mei Church, Vikash Dadlani, Eyal Dassau, Laya Ekhlaspour, Gregory P. Forlenza, Elvira Isganaitis, David W. Lam, John Lum, Roy W. Beck, and iDCL Study Group. Randomized Controlled Trial of Mobile Closed-Loop Control. *Diabetes Care*, 43(3):607–615, 01 2020.

[112] Boris Kovatchev, Marc Breton, Chiara Dalla Man, and Claudio Cobelli. *In Silico* Preclinical Trials: A Proof of Concept in Closed-Loop Control of Type 1 Diabetes. *Journal of diabetes science and technology*, 3:44–55, 02 2009.

[113] Boris P Kovatchev. Diabetes Technology: Markers, Monitoring, Assessment, and Control of Blood Glucose Fluctuations in Diabetes. *Scientifica*, 2012:283821, 2012.

[114] Boris P. Kovatchev, William L. Clarke, Marc Breton, Kenneth Brayman, and Anthony McCall. Quantifying Temporal Glucose Variability in Diabetes via Continuous Glucose Monitoring: Mathematical Methods and Clinical Application. *Diabetes Technology & Therapeutics*, 7(6):849–862, 2005. PMID: 16386091.

[115] Boris P. Kovatchev, Eric Renard, Claudio Cobelli, Howard C. Zisser, Patrick Keith-Hynes, Stacey M. Anderson, Sue A. Brown, Daniel R. Chernavvsky, Marc D. Breton, Anne Farret, Marie-Josée Pelletier, Jérôme Place, Daniela Bruttomesso, Simone Del Favero, Roberto Visentin, Alessio Filippi, Rachele Scotton, Angelo Avogaro, and III Doyle, Francis J. Feasibility of Outpatient Fully Integrated Closed-Loop Control: First studies of wearable artificial pancreas. *Diabetes Care*, 36(7):1851–1858, 06 2013.

[116] Boris P. Kovatchev, Eric Renard, Claudio Cobelli, Howard C. Zisser, Patrick Keith-Hynes, Stacey M. Anderson, Sue A. Brown, Daniel R. Chernavvsky, Marc D. Breton, Lloyd B. Mize, Anne Farret, Jérôme Place, Daniela Bruttomesso, Simone Del Favero, Federico Boscari, Silvia Galasso, Angelo Avogaro, Lalo Magni, Federico Di Palma, Chiara Toffanin, Mirko Messori, Eyal Dassau, and III Doyle, Francis J. Safety of Outpatient Closed-Loop Control: First Randomized Crossover Trials of a Wearable Artificial Pancreas. *Diabetes Care*, 37(7):1789–1796, 06 2014.

[117] Dinesh Krishnamoorthy. On Tuning Parameterized Control Policies Online for Safety-Critical Systems – Applied to Biomedical Systems. In *22nd IFAC World Congress*, Yokohoma, Japan, 7 2023.

[118] Dinesh Krishnamoorthy and Francis J Doyle. Safe Bayesian optimization using interior-point methods—Applied to personalized insulin dose guidance. *IEEE Control Systems Letters*, 6:2834–2839, 2022.

[119] Dinesh Krishnamoorthy and Francis J. Doyle III. Safe and Personalized Meal Bolus Calculator for Type-1 Diabetes Using Bayesian Optimization. *IEEE Transactions on Biomedical Engineering*, 70(5):1481–1492, 2023.

[120] Davida Kruger, Alex Kass, Jacqueline Lonier, Jeremy Pettus, Philip Raskin, Maamoun Salam, Subbulaxmi Trikudanathan, Keren Zhou, Steven J. Russell, Edward R. Damiano, Firas H. El-Khatib, Katrina J. Ruedy, Courtney Balliro, Zoey Li, Martin Chase Marak, Peter Calhoun, and Roy W. Beck. A Multicenter Randomized Trial Evaluating the Insulin-Only Configuration of the Bionic Pancreas in Adults with Type 1 Diabetes. *Diabetes Technology & Therapeutics*, 24(10):697–711, 2022. PMID: 36173236.

[121] Srinivas Laxminarayan, Jaques Reifman, and Garry M. Steil. Use of a Food and Drug Administration-Approved Type 1 Diabetes Mellitus Simulator to Evaluate and Optimize a Proportional-Integral-Derivative Controller. *Journal of Diabetes Science and Technology*, 6(6):1401–1412, 2012. PMID: 23294787.

[122] Joon Bok Lee, Eyal Dassau, Ravi Gondhalekar, Dale E Seborg, Jordan E Pinsker, and Francis J I I I Doyle. Enhanced Model Predictive Control (eMPC) Strategy for Automated Glucose Control. *Industrial & Engineering Chemistry Research*, 55(46):11857–11868, 11 2016.

[123] Joon Bok Lee, Eyal Dassau, Dale E. Seborg, and Francis J. Doyle. Model-based personalization scheme of an artificial pancreas for type 1 diabetes applications. In *2013 American Control Conference*, pages 2911–2916, 2013.

[124] Seunghyun Lee, Jiwon Kim, Sung Woon Park, Sang-Man Jin, and Sung-Min Park. Toward a Fully Automated Artificial Pancreas System Using a Bioinspired Reinforcement Learning Design: In Silico Validation. *IEEE Journal of Biomedical and Health Informatics*, 25(2):536–546, 2021.

[125] Jessica Lin, Normy N. Razak, Christopher G. Pretty, Aaron Le Compte, Paul Docherty, Jacquelyn D. Parente, Geoffrey M. Shaw, Christopher E. Hann, and J. Geoffrey Chase. A physiological Intensive Control Insulin-Nutrition-Glucose (ICING) model validated in critically ill patients. *Computer Methods and Programs in Biomedicine*, 102(2):192–205, 2010. Glucose Modelling: Selected extended papers from the 7th IFAC Symposium on Modelling and Control in Biomedical Systems.

[126] Trang T. Ly, Anirban Roy, Benyamin Grosman, John Shin, Alex Campbell, Salman Monirabbasi, Bradley Liang, Rie von Eyben, Satya Shanmugham, Paula Clinton, and Bruce A. Buckingham. Day and Night Closed-Loop Control Using the Integrated Medtronic Hybrid Closed-Loop System in Type 1 Diabetes at Diabetes Camp. *Diabetes Care*, 38(7):1205–1211, 06 2015.

[127] Trang T. Ly, Stuart A. Weinzimer, David M. Maahs, Jennifer L. Sherr, Anirban Roy, Benyamin Grosman, Martin Cantwell, Natalie Kurtz, Lori Carria, Laurel Messer, Rie von Eyben, and Bruce A. Buckingham. Automated hybrid closed-loop control with a proportional-integral-derivative based system in adolescents and adults with type 1 diabetes: individualizing settings for optimal performance. *Pediatric Diabetes*, 18(5):348–355, 2016.

[128] Nicolas Magdelaine, Lucy Chaillous, Isabelle Guilhem, Jean-Yves Poirier, Michel Krempf, Claude H. Moog, and Eric Le Carpentier. A long-term model of the glucose–insulin dynamics of type 1 diabetes. *IEEE Transactions on Biomedical Engineering*, 62(6):1546–1552, 2015.

[129] L. Magni, D.M. Raimondo, C. Dalla Man, G. De Nicolao, B. Kovatchev, and C. Cobelli. Model predictive control of glucose concentration in type i diabetic patients: An in silico trial. *Biomedical Signal Processing and Control*, 4(4):338–346, 2009. Special Issue on Biomedical Systems, Signals and Control Extended Selected papers from the IFAC World Congress, Seoul, July 2008.

[130] Lalo Magni. Model predictive control of type 1 diabetes. *IFAC Proceedings Volumes*, 45(17):99–106, 2012. 4th IFAC Conference on Nonlinear Model Predictive Control.

[131] Lalo Magni, Marco Forgione, Chiara Toffanin, Chiara Dalla Man, Boris Kovatchev, Giuseppe De Nicolao, and Claudio Cobelli. Run-to-run tuning of model predictive control for type 1 diabetes subjects: In silico trial. *Journal of Diabetes Science and Technology*, 3(5):1091–1098, 2009. PMID: 20144422.

[132] Lalo Magni, Davide M. Raimondo, Luca Bossi, Chiara Dalla Man, Giuseppe De Nicolao, Boris Kovatchev, and Claudio Cobelli. Model predictive control of type 1 diabetes: An in silico trial. *Journal of Diabetes Science and Technology*, 1(6):804–812, 2007. PMID: 19885152.

[133] Lalo Magni, Davide M. Raimondo, Chiara Dalla Man, Marc Breton, Stephen Patek, Giuseppe De Nicolao, Claudio Cobelli, and Boris P. Kovatchev. Evaluating the Efficacy of Closed-Loop Glucose Regulation via Control-Variability Grid Analysis. *Journal of Diabetes Science and Technology*, 2(4):630–635, 2008. PMID: 19885239.

[134] Chiara Dalla Man, Davide M. Raimondo, Robert A. Rizza, and Claudio Cobelli. Gim, simulation software of meal glucose—insulin model. *Journal of Diabetes Science and Technology*, 1(3):323–330, 2007. PMID: 19885087.

[135] Chiara Dalla Man, Giana Toffolo, Claudio Cobelli, and Robert A. Rizza. A Model of Glucose Production During a Meal. *Proceedings of the 28th IEEE*, 08 2006.

[136] Gianni Marchetti, Massimiliano Barolo, Lois Jovanovic, Howard Zisser, and Dale E. Seborg. An improved pid switching control strategy for type 1 diabetes. *IEEE Transactions on Biomedical Engineering*, 55(3):857–865, 2008.

[137] Gianni Marchetti, Massimiliano Barolo, Lois Jovanovič, Howard Zisser, and Dale E. Seborg. A feedforward–feedback glucose control strategy for type 1 diabetes mellitus. *Journal of Process Control*, 18(2):149–162, 2008.

[138] Cynthia R. Marling and Razvan C. Bunescu. The ohiot1dm dataset for blood glucose level prediction. In *KDH@IJCAI*, 2018.

[139] Cynthia R. Marling and Razvan C. Bunescu. The ohiot1dm dataset for blood glucose level prediction: Update 2020. In *CEUR workshop proceedings, 2675*, pages 71–74, 2020.

[140] Laurel H. Messer, Cari Berget, and Gregory P. Forlenza. A Clinical Guide to Advanced Diabetes Devices and Closed-Loop Systems Using the CARES Paradigm. *Diabetes Technology & Therapeutics*, 21(8):462–469, 2019. PMID: 31140878.

[141] Laurel H. Messer and Marc D. Breton. Therapy Settings Associated with Optimal Outcomes for t:slim X2 with Control-IQ Technology in Real-World Clinical Care. *Diabetes Technology & Therapeutics*, 25(12):877–882, 2023. PMID: 37751154.

[142] Laurel H. Messer, Bruce A. Buckingham, Fran Cogen, Mark Daniels, Greg Forlenza, Rabab Z. Jafri, Nelly Mauras, Andrew Muir, R. Paul Wadwa, Perrin C. White, Steven J. Russell, Edward R. Damiano, Firas H. El-Khatib, Katrina J. Ruedy, Courtney A. Balliro, Zoey Li, Martin Chase Marak, Peter Calhoun, and Roy W. Beck. Positive Impact of the Bionic Pancreas on Diabetes Control in Youth 6–17 Years Old with Type 1 Diabetes: A Multicenter Randomized Trial. *Diabetes Technology & Therapeutics*, 24(10):712–725, 2022. PMID: 36173237.

[143] Armaan Nallicheri, Katherine M Mahoney, Hanna A Gutow, Natalie Bellini, and Diana Isaacs. Review of Automated Insulin Delivery systems for Type 1 Diabetes and Associated Time in Range Outcomes. *touchREVIEWS in Endocrinology*, 18(1):27, 2022.

[144] Gianluca Nucci and Claudio Cobelli. Models of subcutaneous insulin kinetics. a critical review. *Computer Methods and Programs in Biomedicine*, 62(3):249–257, 2000.

[145] Katherine Ogurtsova, Leonor Guariguata, Noël C. Barengo, Paz Lopez Doriga Ruiz, Julian W. Sacre, Suvi Karuranga, Hong Sun, Edward J. Boyko, and Dianna J. Magliano. IDF diabetes Atlas: Global estimates of undiagnosed diabetes in adults for 2021. *Diabetes Research and Clinical Practice*, 183, 1 2022.

[146] S. D. Patek, L. Magni, E. Dassau, C. Karvetski, C. Toffanin, G. De Nicolao, S. Del Favero, M. Breton, C. Dalla Man, E. Renard, H. Zisser, F. J. Doyle, III, C. Cobelli, and B. P. Kovatchev. Modular Closed-Loop Control of Diabetes. *IEEE Transactions on Biomedical Engineering*, 59(11):2986–2999, 2012.

[147] Stephen D. Patek, Dayu Lv, Edward A. Ortiz, Colleen Hughes-Karvetski, Sandip Kulkarni, Qian Zhang, and Marc D. Breton. *Empirical Representation of Blood Glucose Variability in a Compartmental Model*, pages 133–157. Springer International Publishing, Cham, 2016.

[148] M. Phillip, R. Nimri, R. M. Bergenstal, K. Barnard-Kelly, T. Danne, R. Hovorka, B. Kovatchev, L. H. Messer, C. G. Parkin, L. Ambler-Osborn, S. A. Amiel, L. Bally, R. W. Beck, S. Biester, T. Biester, J. E. Blanchette, E. Bosi, C. K. Boughton, M. D. Breton, S. A. Brown, B. A. Buckingham, A. Cai, A. Carlson, J. R. Castle, P. Choudhary, K. L. Close, C. Cobelli, A. Criego, E. A. Davis, C. d. Beaufort, M. d. Bock, D. J. DeSalvo, J. H. DeVries, K. Dovč, F. J. Doyle, L. Ekhlaspour, N. F. Shvalb, G. P. Forlenza, G. Gallen, S. K. Garg, D. C. Gershenoff, L. Gönder-Frederick, A. Haidar, S. Hartnell, L. Heinemann, S. Heller, I. B. Hirsch, K. K. Hood, D. Isaacs, D. C. Klonoff, O. Kordonouri, A. J. Kowalski, L. Laffel, J. Lawton, R. Lal, L. Leelarathna, D. M. Maahs, H. R. Murphy, K. Nørgaard, D. N. O'Neal, S. M. Oser, T. K. Oser, É. Renard, M. C. Riddell, D. Rodbard, S. Russell, D. Schatz, V. N. Shah, J. Sherr, G. D. Simonson, R. P.

Wadwa, C. Ward, S. A. Weinzimer, E. G. Wilmot, and T. Battelino. Consensus recommendations for the use of automated insulin delivery technologies in clinical practice. *Endocrine Reviews*, 44:254–280, 2022.

[149] Dario Piga, Marco Forgione, Simone Formentin, and Alberto Bemporad. Performance-oriented model learning for data-driven mpc design. *IEEE Control Systems Letters*, 3(3):577–582, 2019.

[150] Jordan E. Pinsker, Joon Bok Lee, Eyal Dassau, Dale E. Seborg, Paige K. Bradley, Ravi Gondhalekar, Wendy C. Bevier, Lauren Huyett, Howard C. Zisser, and Francis J. Doyle III. Randomized Crossover Comparison of Personalized MPC and PID Control Algorithms for the Artificial Pancreas. *Diabetes Care*, 39(7):1135–1142, 02 2016.

[151] Marcello Pompa, Simona Panunzi, Alessandro Borri, and Andrea De Gaetano. A comparison among three maximal mathematical models of the glucose-insulin system. *PloS one*, 16(9):e0257789, 2021.

[152] Jessica L. Ruiz, Jennifer L. Sherr, Eda Cengiz, Lori Carria, Anirban Roy, Gayane Voskanyan, William V. Tamborlane, and Stuart A. Weinzimer. Effect of insulin feedback on closed-loop glucose control: A crossover study. *Journal of Diabetes Science and Technology*, 6(5):1123–1130, 2012. PMID: 23063039.

[153] Ava S. Runge, Lynn Kennedy, Adam S. Brown, Abigail E. Dove, Brian J. Levine, Sophie P. Koontz, Varun S. Iyengar, Sarah A. Odeh, Kelly L. Close, Irl B. Hirsch, and Richard Wood. Does Time-in-Range Matter? Perspectives From People With Diabetes on the Success of Current Therapies and the Drivers of Improved Outcomes. *Clinical Diabetes*, 36(2):112–119, 04 2018.

[154] Steven J Russell, Courtney Balliro, Magnus Ekelund, Firas El-Khatib, Tina Graungaard, Evelyn Greaux, Mallory Hillard, Rabab Z Jafri, Naveen Rathor, Raj Selagamsetty, Jordan Sherwood, and Edward R Damiano. Improvements in Glycemic Control Achieved by Altering the tmax Setting in the iLet® Bionic Pancreas When Using Fast-Acting Insulin Aspart: A Randomized Trial. *Diabetes Therapy*, 12(7):2019–2033, 2021.

[155] Steven J. Russell, Firas H. El-Khatib, David M. Nathan, Kendra L. Magyar, John Jiang, and Edward R. Damiano. Blood Glucose Control in Type 1 Diabetes With a Bihormonal Bionic Endocrine Pancreas. *Diabetes Care*, 35(11):2148–2155, 10 2012.

[156] Steven J. Russell, Firas H. El-Khatib, Manasi Sinha, Kendra L. Magyar, Katherine McKeon, Laura G. Goergen, Courtney Balliro, Mallory A. Hillard, David M. Nathan, and Edward R. Damiano. Outpatient glycemic control with a bionic pancreas in type 1 diabetes. *New England Journal of Medicine*, 371(4):313–325, 2014.

[157] Steven J Russell, Mallory A Hillard, Courtney Balliro, Kendra L Magyar, Rajendranath Selagamsetty, Manasi Sinha, Kerry Grennan, Debbie Mondesir, Laya Ekhlaspour, Hui Zheng, Edward R Damiano, and Firas H El-Khatib. Day and night glycaemic control with a bionic pancreas versus conventional insulin pump therapy in preadolescent children with type 1 diabetes: a randomised crossover trial. *The Lancet Diabetes & Endocrinology*, 4(3):233–243, 2016.

[158] D.E. Seborg, T.F. Edgar, D.A. Mellichamp, and F.J. Doyle. *Process Dynamics and Control, 4th Edition*. Wiley, 2016.

[159] Bobak Shahriari, Kevin Swersky, Ziyu Wang, Ryan P. Adams, and Nando de Freitas. Taking the human out of the loop: A review of bayesian optimization. *Proceedings of the IEEE*, 104(1):148–175, 2016.

[160] Jennifer L. Sherr, Bruce A. Buckingham, Gregory P. Forlenza, Alfonso Galderisi, Laya Ekhlaspour, R. Paul Wadwa, Lori Carria, Liana Hsu, Cari Berget, Thomas A. Peyser, Joon Bok Lee, Jason O'Connor, Bonnie Dumais, Lauren M. Huyett, Jennifer E. Layne, and Trang T. Ly. Safety and performance of the omnipod hybrid closed-loop system in adults, adolescents, and children with type 1 diabetes over 5 days under free-living conditions. *Diabetes Technology & Therapeutics*, 22(3):174–184, 2020. PMID: 31596130.

[161] Dawei Shi, Eyal Dassau, and Francis J. Doyle. A multivariate bayesian optimization framework for long-term controller adaptation in artificial pancreas. In *2018 IEEE Conference on Decision and Control (CDC)*, pages 276–283, 2018.

[162] Dawei Shi, Eyal Dassau, and Francis J. Doyle. Zone Model Predictive Control with Glucose- and Velocity-Dependent Control Penalty Adaptation for an Artificial Pancreas. In *2018 Annual American Control Conference (ACC)*, pages 3577–3582, 2018.

[163] Dawei Shi, Eyal Dassau, and Francis J. Doyle. Adaptive zone model predictive control of artificial pancreas based on glucose- and velocity-dependent control penalties. *IEEE Transactions on Biomedical Engineering*, 66(4):1045–1054, 2019.

[164] Sigurd Skogestad. Simple analytic rules for model reduction and PID controller tuning. *Journal of Process Control*, 13(4):291–309, 2003.

[165] John Thomas Sorensen. *A physiologic model of glucose metabolism in man and its use to design and assess improved insulin therapies for diabetes*. PhD thesis, Massachusetts Institute of Technology, 1985.

[166] P. Soru, G. De Nicolao, C. Toffanin, C. Dalla Man, C. Cobelli, and L. Magni. Mpc based artificial pancreas: Strategies for individualization and meal compensation. *Annual Reviews in Control*, 36(1):118–128, 2012.

[167] Garry M. Steil. Algorithms for a Closed-Loop Artificial Pancreas: The Case for Proportional-Integral-Derivative Control. *Journal of Diabetes Science and Technology*, 7(6):1621–1631, 2013. PMID: 24351189.

[168] Garry M. Steil and Gerold M. Grodsky. The Artificial Pancreas: Is it Important to Understand How the β Cell Controls Blood Glucose? *Journal of Diabetes Science and Technology*, 7(5):1359–1369, 2013. PMID: 24124965.

[169] Garry M. Steil, Cesar C. Palerm, Natalie Kurtz, Gayane Voskanyan, Anirban Roy, Sachiko Paz, and Fouad R. Kandeel. The Effect of Insulin Feedback on Closed Loop Glucose Control. *The Journal of Clinical Endocrinology & Metabolism*, 96(5):1402–1408, 05 2011.

[170] G.M Steil, A.E Panteleon, and K Rebrin. Closed-loop insulin delivery—the path to physiological glucose control. *Advanced Drug Delivery Reviews*, 56(2):125–144, 2004. Biosensing and Drug Delivery at the Microscale.

[171] Karena L. Swan, James D. Dziura, Garry M. Steil, Gayane R. Voskanyan, Kristin A. Sikes, Amy T. Steffen, Melody L. Martin, William V. Tamborlane, and Stuart A. Weinzimer. Effect of Age of Infusion Site and Type of Rapid-Acting Analog on Pharmacodynamic Parameters of Insulin Boluses in Youth With Type 1 Diabetes Receiving Insulin Pump Therapy. *Diabetes Care*, 32(2):240–244, 02 2009.

[172] Hood Thabit and Roman Hovorka. Closed-loop insulin delivery in type 1 diabetes. *Endocrinology and Metabolism Clinics of North America*, 41(1):105–117, 2012. Insulin Therapy.

[173] Andreas Thomas and Lutz Heinemann. Algorithms for automated insulin delivery: An overview. *Journal of Diabetes Science and Technology*, 16(5):1228–1238, 2022. PMID: 33955251.

[174] Tidepool. Tidepool Loop Clearance. http://www.tidepool.org/blog/tidepool-loop-has-received-fda-clearance#:~:text=We%20at%20Tidepool%20are%20thrilled,did%20it%20during%20a%20pandemic. Accessed: 2024-06-10.

[175] C Toffanin and L Magni. Personalized Constrained MPC for Glucose Regulation. In *22nd IFAC World Congress*, 7 2023.

[176] Chiara Toffanin, Eleonora Maria Aiello, Claudio Cobelli, and Lalo Magni. Hypoglycemia Prevention via Personalized Glucose-Insulin Models Identified in Free-Living Conditions. *Journal of Diabetes Science and Technology*, 13(6):1008–1016, 2019. PMID: 31645119.

[177] Chiara Toffanin, Mirko Messori, Federico Di Palma, Giuseppe De Nicolao, Claudio Cobelli, and Lalo Magni. Artificial Pancreas: Model Predictive Control Design from Clinical Experience. *Journal of Diabetes Science and Technology*, 7(6):1470–1483, 2013. PMID: 24351173.

[178] Chiara Toffanin, Roberto Visentin, Mirko Messori, Federico Di Palma, Lalo Magni, and Claudio Cobelli. Toward a Run-to-Run Adaptive Artificial Pancreas: In Silico Results. *IEEE Transactions on Biomedical Engineering*, 65(3):479–488, 2018.

[179] Chiara Toffanin, Howard Zisser, III Francis J. Doyle, and Eyal Dassau. Dynamic insulin on board: Incorporation of circadian insulin sensitivity variation. *Journal of Diabetes Science and Technology*, 7(4):928–940, 2013. PMID: 23911174.

[180] Kamuran Turksoy, Ali Cinar, et al. Adaptive Control of Artificial Pancreas Systems - A Review. *Journal of healthcare engineering*, 5:1–22, 2014.

[181] Kamuran Turksoy, Laurie Quinn, Elizabeth Littlejohn, and Ali Cinar. Multivariable Adaptive Identification and Control for Artificial Pancreas Systems. *IEEE Transactions on Biomedical Engineering*, 61(3):883–891, 2014.

[182] Klaske van Heusden, Eyal Dassau, Howard C. Zisser, Dale E. Seborg, and Francis J. Doyle III. Control-Relevant Models for Glucose Control Using A Priori Patient Characteristics. *IEEE Transactions on Biomedical Engineering*, 59(7):1839–1849, 2012.

[183] Robert A. Vigersky and Chantal McMahon. The Relationship of Hemoglobin A1C to Time-in-Range in Patients with Diabetes. *Diabetes Technology & Therapeutics*, 21(2):81–85, 2019. PMID: 30575414.

[184] John Walsh and Ruth Roberts. *Pumping Insulin, 2nd edition.* San Diego: Torrey Pines Press, 1994.

[185] John Walsh and Ruth Roberts. *Pumping Insulin, 4th edition.* San Diego: Torrey Pines Press, 2006.

[186] John Walsh, Ruth Roberts, and Timothy Bailey. Guidelines for insulin dosing in continuous subcutaneous insulin infusion using new formulas from a retrospective study of individuals with optimal glucose levels. *Journal of Diabetes Science and Technology*, 4(5):1174–1181, 2010. PMID: 20920437.

[187] Youqing Wang, Eyal Dassau, and Francis J. Doyle. Closed-loop control of artificial pancreatic β-cell in type 1 diabetes mellitus using model predictive iterative learning control. *IEEE Transactions on Biomedical Engineering*, 57(2):211–219, 2010.

[188] Stuart A. Weinzimer, Garry M. Steil, Karena L. Swan, Jim Dziura, Natalie Kurtz, and William V. Tamborlane. Fully Automated Closed-Loop Insulin Delivery Versus Semiautomated Hybrid Control in Pediatric Patients With Type 1 Diabetes Using an Artificial Pancreas. *Diabetes Care*, 31(5):934–939, 05 2008.

[189] Malgorzata E. Wilinska, Ludovic J. Chassin, Carlo L. Acerini, Janet M. Allen, David B. Dunger, and Roman Hovorka. Simulation environment to evaluate closed-loop insulin delivery systems in type 1 diabetes. *Journal of Diabetes Science and Technology*, 4(1):132–144, 2010. PMID: 20167177.

[190] Malgorzata E. Wilinska and Roman Hovorka. Simulation models for in silico testing of closed-loop glucose controllers in type 1 diabetes. *Drug Discovery Today: Disease Models*, 5(4):289–298, 2008. Animal models of addiction / Kinetic models.

[191] Malgorzata E. Wilinska and Roman Hovorka. *Simulation Models for In-Silico Evaluation of Closed-Loop Insulin Delivery Systems in Type 1 Diabetes*, pages 131–149. Springer Berlin Heidelberg, Berlin, Heidelberg, 2014.

[192] Ashenafi Zebene Woldaregay, Eirik Årsand, Ståle Walderhaug, David Albers, Lena Mamykina, Taxiarchis Botsis, and Gunnar Hartvigsen. Data-driven modeling and prediction of blood glucose dynamics: Machine learning applications in type 1 diabetes. *Artificial Intelligence in Medicine*, 98:109–134, 2019.

[193] Jinyu Xie. Simglucose v0.2.1 (2018). https://github.com/jxx123/simglucose. Accessed: 2023-07-31.

[194] T. Yamagata, A. O'Kane, A. Ayobi, D. Katz, K. Stawarz, P. Marshall, P. Flach, and R. Santos-Rodriguez. Model-based reinforcement learning for type 1 diabetes blood

glucose control. In *1st International AAI4H - Advances in Artificial Intelligence for Healthcare Workshop, AAI4H 2020*, pages 72–77, 2020.

[195] H Yki-Järvinen, A A Young, C Lamkin, and J E Foley. Kinetics of glucose disposal in whole body and across the forearm in man. *The Journal of Clinical Investigation*, 79(6):1713–1719, 6 1987.

[196] Chengxia Yu and Chunhui Zhao. Rapid model identification for online glucose prediction of new subjects with type 1 diabetes using model migration method. *IFAC Proceedings Volumes*, 47(3):2094–2099, 2014. 19th IFAC World Congress.

[197] Konstantia Zarkogianni, Eleni Litsa, Konstantinos Mitsis, Po-Yen Wu, Chanchala D. Kaddi, Chih-Wen Cheng, May D. Wang, and Konstantina S. Nikita. A review of emerging technologies for the management of diabetes mellitus. *IEEE Transactions on Biomedical Engineering*, 62(12):2735–2749, 2015.

[198] Konstantia Zarkogianni, Andriani Vazeou, Stavroula G. Mougiakakou, Aikaterini Prountzou, and Konstantina S. Nikita. An Insulin Infusion Advisory System Based on Autotuning Nonlinear Model-Predictive Control. *IEEE Transactions on Biomedical Engineering*, 58(9):2467–2477, 2011.

[199] Meng Zhang, Kevin B. Flores, and Hien T. Tran. Deep learning and regression approaches to forecasting blood glucose levels for type 1 diabetes. *Biomedical Signal Processing and Control*, 69:102923, 2021.

[200] Taiyu Zhu, Kezhi Li, Pau Herrero, and Pantelis Georgiou. Deep learning for diabetes: A systematic review. *IEEE Journal of Biomedical and Health Informatics*, 25(7):2744–2757, 2021.

Glossary

List of Acronyms

RMSE	root-mean-square error
HbA1c	glycated hemoglobin
CSII	continuous subcutaneous insulin infusion
FIT	functional insulin therapy
MPC	model predictive control
FDA	U.S. Food & Drug Administration
PID	proportional-integral-derivative
CGM	continuous glucose monitor
CF	correction factor
GP	Gaussian Process
IOB	insulin-on-board
AP	artificial pancreas
LCB	lower confidence bound
APS	artifical pancreas system
TIR	time-in-range
AID	automated insulin delivery
T1DM	Type-1 diabetes mellitus
BO	Bayesian Optimisation
BG	blood glucose
BGL	blood glucose level
TIR	time-in-range
TBR	time-below-range
TAR	time-above-range

CHO	carbohydrates
CR	carbohydrate-to-insulin ratio
TDD	total daily insulin dose
ADA	American Diabetes Association
Z-MPC	zone model predictive control
SP-MPC	set-point tracking model predictive control
SG	sensor glucose
SGL	sensor glucose level
SISO	single-input single-output